Universität Stuttgart

Institut für Wasser- und Umweltsystemmodellierung

Mitteilungen

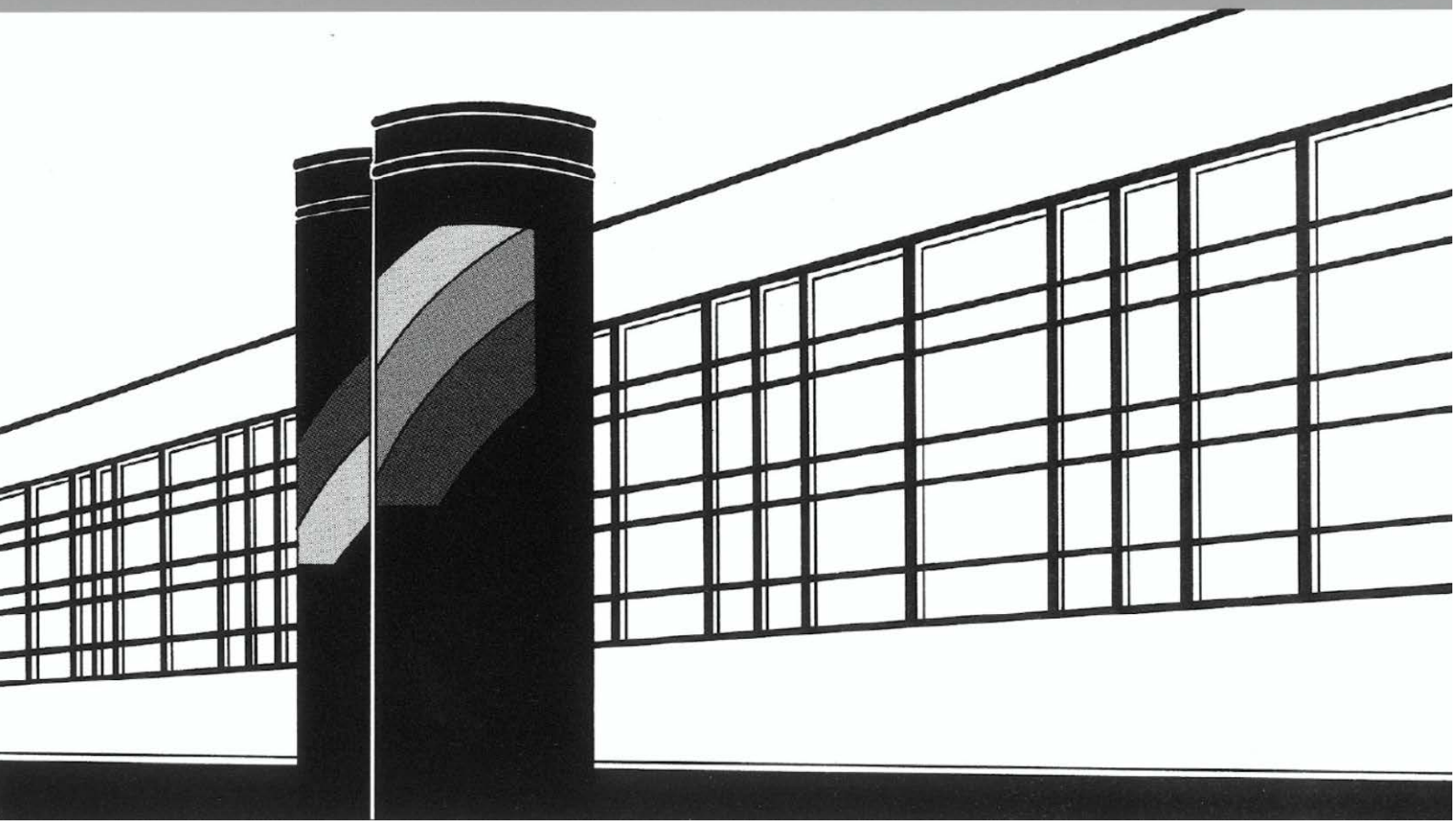

Heft 249 Simon Matthias Kleinknecht

Migration and retention of a heavy NAPL vapor and remediation of the unsaturated zone

Migration and retention of a heavy NAPL vapor and remediation of the unsaturated zone

von der Fakultät Bau- und Umweltingenieurwissenschaften der Universität Stuttgart zur Erlangung der Würde eines Doktor-Ingenieurs (Dr.-Ing.) genehmigte Abhandlung

vorgelegt von

Simon Matthias Kleinknecht

aus Öhringen

Hauptberichter:	apl. Prof. Dr.-Ing. Holger Class
Mitberichter:	Prof. Dr. rer. nat. Dr.-Ing. András Bárdossy
	Prof. Tissa Illangasekare

Tag der mündlichen Prüfung: 17.10.2016

Institut für Wasser- und Umweltsystemmodellierung
der Universität Stuttgart
2016

Heft 249

Migration and retention of a heavy NAPL vapor and remediation of the unsaturated zone

von
Dr.-Ing.
Simon Matthias Kleinknecht

Eigenverlag des Instituts für Wasser- und Umweltsystemmodellierung
der Universität Stuttgart

D93 Migration and retention of a heavy NAPL vapor and remediation of the unsaturated zone

Bibliografische Information der Deutschen Nationalbibliothek
Die Deutsche Nationalbibliothek verzeichnet diese Publikation in der Deutschen Nationalbibliografie; detaillierte bibliografische Daten sind im Internet über http://www.d-nb.de abrufbar

Simon Matthias Kleinknecht:
Migration and retention of a heavy NAPL vapor and remediation of the unsaturated zone, Universität Stuttgart. - Stuttgart: Institut für Wasser- und Umweltsystemmodellierung, 2016

(Mitteilungen Institut für Wasser- und Umweltsystemmodellierung, Universität Stuttgart: H. 249)
Zugl.: Stuttgart, Univ., Diss., 2016
ISBN 978-3-942036-53-5

NE: Institut für Wasser- und Umweltsystemmodellierung <Stuttgart>: Mitteilungen

Herausgegeben 2016 vom Eigenverlag des Instituts für Wasser- und Umweltsystem-modellierung

Druck: Document Center S. Kästl, Ostfildern

Contents

List of Figures

List of Tables

Nomenclature and Acronyms

Symbol	Meaning	Unit/Dimension
c	Concentration	$\mathrm{kg\,m^{-3}}$
d	Pore diameter	mm
$i.d.$	Inner diameter	mm
h	Piezometric head	cm
k	Intrinsic permeability	$\mathrm{m^2}$
l	Characteristic length	m
m	Mass	kg
n	van Genuchten parameter	-
$o.d.$	Outer diameter	mm
r	Recovery	%
s	Solubility	$\mathrm{g\,L^{-1}}$
u	Darcy velocity / flux	$\mathrm{m\,s^{-1}}$
v	Velocity	$\mathrm{m\,s^{-1}}$
x	Mole fraction	-
t	Time	s
D	Diffusion coefficient	$\mathrm{cm^2\,s^{-1}}$
K	Hydraulic conductivity	$\mathrm{m\,s^{-1}}$
M	Molecular weight	$\mathrm{g\,mol^{-1}}$
P	Pressure	Pa
Q	Flow rate	$\mathrm{m^3\,s^{-1}}$
R	Universal gas constant	$\mathrm{J\,mol^{-1}\,K^{-1}}$
	Retardation factor	-
Ra	Rayleigh number	-
S	Saturation	-
T	Temperature	K
V	Volume	$\mathrm{m^3}$
Greek symbols:		
α	Dispersivity	cm
	Van Genuchten parameter	$1/\mathrm{cm}$
λ	Mean-free path of gas molecules	Å
μ	Dynamic viscosity	Pa s
ϕ	Porosity	-
φ	Angle	$^\circ$
ρ	Density	$\mathrm{kg\,m^{-3}}$

Symbol	Meaning	Unit/Dimension
σ	Interfacial tension	$\mathrm{N\,m^{-1}}$
θ	Water content	$\mathrm{cm^3\,cm^{-3}}$
τ	Tortuosity	-

Indices:

b	Bulk
c	Contaminant
	Capillary
	Critical
e	Effective
g	Gas
i	Component or fluid
n	Order
nw	Non-wetting
r	Residual
s	Soil
w	Wetting
α	Phase

Acronyms:

2p2cni	2-phase 2-component non-isothermal model
BC	Boundary condition
BTC	Breakthrough curve
GC-PID	Gas chromatograph with photoionization detector
GC-TCD	Gas chromatograph with thermal conductivity detector
VME	Vapor-migration experiment
VRE	Vapor-retardation experiment
HDPE	High-density polyethylene
IC	Initial condition
MFC	Mass-flow controller
NAPL	Non-aqueous phase liquid
PDF	Probability density function
PEEK	Polyether ether ketone
PTFE	Polytetrafluoroethylene
SD	Saturation-and-drainage cycle
SRE	Spill and remediation experiment
SVE	Soil-vapor extraction
VEGAS	Research Facility for Groundwater and Subsurface Remediation
VOC	Volatile organic compound

Abstract

Subsurface contamination is a primary environmental concern in many countries around the world. The list of potential contaminants includes a wide variety of organic compounds used in industry, such as solvents and degreasers. Contaminants introduced into the unsaturated zone spread as a liquid phase; however, they can also vaporize and migrate in a gaseous state. Contaminant vapor (gas) plumes emanating from liquid sources migrate easily in the unsaturated zone. Heavy vapors preferentially migrate downward due to their greater density and, thus, pose a potential threat to underlying aquifers. Hence, an efficient and fast in-situ remediation technique is required to remove the liquid-contaminant source as well as the migrating vapor plume in the unsaturated zone. While the fate and transport of vapor plumes have attracted a great deal of attention over the past years, further investigations are necessary to improve the understanding of processes required to assess the threat to the environment.

This work addressed selected questions in this field based on the scenario of a deep unsaturated zone with an underlying aquifer (100 m below ground level). The investigations were based on 1-D (column) and 2-D (flume) experiments and results were compared with theoretical approaches and numerical simulations. The contaminant used in this work was carbon disulfide (CS_2), an industrial, non-polar solvent among many used to manufacture viscose rayon. It is highly volatile and characterized by a very high density (1.6 times the air density) in a gaseous state. The first part of this work examined two fundamental processes relevant for vapor plumes. First, density-driven vapor migration in dry porous media and second vapor retardation as a result of partitioning processes in partially water-saturated soil. The insights gained from these experiments contributed to the fundamental understanding of fate and transport of heavy NAPL-vapor plumes in the unsaturated zone. The second part of the experimental investigation explored the liquid-contaminant distribution in moist porous media and the applicability and efficiency of the in-situ remediation technique using soil-vapor extraction (SVE) after a spill.

Large-scale column experiments and numerical simulations were conducted to investigate the density-driven migration of CS_2 vapor. The experiments were conducted in large, vertical columns (i.d. = 0.109 m) of 4 m length packed with a dry porous medium. Coarse, medium, and fine glass beads were used to investigate the sensitivity of migration to permeability. The porous media were kept dry to avoid partitioning effects into pore water. Gas samples were taken along the column throughout the experiment to quantify time-and-space-dependent vapor migration. The experiments characterized the migration behavior of a heavy CS_2-vapor plume injected in the middle of the column. The vapor plume steadily migrated downward dependent on the total mass of injected CS_2 and permeability. The experiment was reproduced in a 1-D, two-phase, two-component, isothermal, numerical model. Simulation results were compared with data from the vapor-migration experiments. The results of the numerical model

satisfactorily reproduced the migration behavior observed in the experiments but suggested slightly higher velocities than those observed. History matching was performed successfully using migration velocities and concentration understanding of from the experiments.

The second set of column experiments was performed to explore retardation of CS_2 vapor in moist porous media. The experiments were conducted in columns of 2 m length packed with a porous medium. Two types of porous media, fine glass beads and Geba fine sand, were used to investigate the partitioning processes responsible for retardation. The porous media were saturated and drained to establish static water saturations as initial conditions. A slug of CS_2 vapor and the conservative tracer argon was injected at the bottom of the column followed by a nitrogen chase. Different seepage velocities, chosen based on the velocities observed in density-driven vapor-migration experiments, were applied to characterize the vapor transport and to evaluate their impact on retardation. The bottom of the column was realized as a constant-mass-flux boundary while the top was open to the surroundings, hence at constant pressure. Concentrations of CS_2 and argon were measured online at the top outlet of the column using two gas chromatographs. The temporal-moment analysis for step input was employed to evaluate the breakthrough curves and to quantify diffusion/dispersion and retardation. The experiments conducted showed a pronounced retardation of CS_2 in moist porous media as a function of porous medium and water saturation. An increase of the retardation coefficient with increasing water saturation was observed. The experimental retardation coefficient was compared to a theoretical approach taking into account the partitioning into the aqueous phase. Retardation in fine glass beads compared very well with the theoretical retardation coefficient. Retardation in Geba fine sand was stronger than predicted, probably due to the particular grain-size distribution and to the water-saturation profile. Retardation coefficients as a function of (seepage) velocity revealed only a minor dependency and suggested a slight tendency toward a reduced retardation at the highest velocity tested. These experiments demonstrated that a downward-migrating vapor plume in the unsaturated zone is retarded by partitioning processes.

An additional outcome of the experiments was that a limited mass of contaminant, if dissolved into the pore, was amenable to biodegradation. Clear evidence of biodegradation of dissolved CS_2 was found in the last series of vapor-retardation experiments.

This research improves the understanding of density-driven, advective migration and retardation of a heavy contaminant vapor in porous media on a large scale. The experimental data is available not only for future research but particularly for transfer to field situations. The experimental investigations proved that heavy vapor plumes migrate downward and thus potentially contaminate an underlying aquifer.

In the second part of this work, the in-situ remediation technique using soil-vapor extraction to remove a CS_2 spill and its vapor plume was studied. This was realized in 2-D flume experiments, conducted to examine the spill and the distribution of liquid CS_2 in moist porous media and to investigate the applicability of SVE as an efficient remediation technology. The experiments characterized the impact of the porous media, their water saturation, the CS_2 distribution, the temperature, and the soil-gas velocity on the remediation performance. The flume (1.00 x 0.70 x 0.12 m) was packed with a porous medium. Two different types, fine glass beads and Geba fine sand, were used to investigate the influence of material characteristics and dif-

ferent water saturations. A special set-up for saturation and drainage established static water saturations, hence ensured similar initial conditions for each experiment. Two different types of spills were realized which resulted in preferential pooling or a residual contaminant distribution, respectively. CS_2 distribution was found to be highly dependent on the type of spill and the porous medium determining its potential for retention by capillary forces. Two vertical wells used for clean-gas inflow and soil-vapor extraction were installed at the left-hand (inflow) and right-hand (extraction) side of the flume. Concentrations of CS_2 vapor, extraction flow rates, pressures, and temperatures were measured and recorded to quantify the contaminant removal. Different CS_2 distributions had a significant impact on the subsequent remediation employing soil-vapor extraction. The remediation of a pool required significantly more time than that for a residual distribution. Even minor increases in temperature resulted in a remarkable improvement in contaminant removal due to the low boiling point and high vapor pressure of CS_2. In addition, soil-gas velocities controlled the contaminant load in the extracted soil vapor. Lower soil-gas velocities (or extraction rates) led to a longer duration of operation despite higher contaminant loads in the soil-vapor extraction and vice versa. The experiments allowed to delineate the parameters controlling the remediation performance and to reveal first steps toward an optimization. Thus, soil-vapor extraction was proven to be an efficient technique for the remediation of a CS_2 contamination in the unsaturated zone.

In conclusion, this work contributes to the ongoing research into the fate and transport of vapor plumes in the unsaturated zone using the example of the contaminant CS_2. It provides valuable experimental data which was employed for the quantification of the processes addressed. Methods were developed and adapted to obtain and to evaluate experimental data which are available for prospective studies. The feasibility and efficiency of an in-situ remediation technique using soil-vapor extraction was demonstrated. Finally, this study provides a basis for further research into vapor migration and retardation in the unsaturated zone as well as for the dimensioning and the optimization of the in-situ remediation technique using soil-vapor extraction in a field application.

Kurzfassung

Die technologischen Entwicklungen der letzten Jahrzehnte führten zu einer starken Zunahme potenzieller Schadstoffe. Daher stellen Verunreinigungen des Untergrunds durch die Industrie für viele Länder dieser Welt eine große Herausforderung dar. Vor allem organische Verbindungen wie Lösemittel können als nichtwässrige Phase (NAPL) in die ungesättigte Bodenzone versickern und sich dort zusätzlich nach Verdampfung auch im gasförmigen Zustand ausbreiten und große Bodenvolumina kontaminieren. Schwere Schadstoffgase sinken aufgrund ihrer höheren Dichte im Vergleich zur Umgebungsluft schwerkraftgetrieben abwärts und stellen somit eine potentielle Gefahr für tieferliegende Aquifere dar. Effiziente und schnelle In-Situ-Sanierungstechnologien sind notwendig, um die flüssige Verunreinigung, aber auch die sich ausbreitenden Schadstoffgase aus dem Untergrund zu entfernen. Aufgrund dessen erlangte die Charakterisierung des Verhaltens von Schadstoffgasen in der ungesättigten Bodenzone in den vergangenen Jahren eine erhöhte Aufmerksamkeit durch die Forscherwelt. Trotz dieser Anstrengungen sind weitere Untersuchungen nötig um das physikalische Prozessverständnis zu verbessern und damit die Gefahr für die Umwelt verlässlich abschätzen und auch abwehren zu können.

Diese Dissertation konzentriert sich auf dieses Prozessverständnis und leistet damit einen Beitrag zur aktuellen Forschung auf diesem Gebiet. Die durchgeführten Untersuchungen basierten auf dem Szenario einer mächtigen, ungesättigten Bodenzone, die durch einen Aquifer, der sich in einer Tiefe von ungefähr 100 m befindet, abgegrenzt wird. Die Untersuchungen wurden in 1-D (Säule) und 2-D (Küvette) Experimenten durchgeführt und die experimentellen Ergebnisse mit theoretischen Ansätzen oder numerischen Simulationen verglichen. Die ausgewählten physikalischen Prozesse wurden am Beispiel von Schwefelkohlenstoff (CS_2), einem industriellen, unpolaren Lösemittel das unter anderem für die Produktion von Kunstseide verwendet wird, untersucht. Schwefelkohlenstoff zeichnet sich durch eine hohe Flüchtigkeit und eine hohe Gasdichte (1.6-fach höher als die Dichte der Bodenluft) aus.

Im ersten Teil dieser Arbeit wurden in Säulenexperimenten zwei fundamentale physikalische Prozesse untersucht: Erstens, die dichtegetriebene Absenkung (advektive Migration) des gasförmigen Schwefelkohlenstoffs im trockenen, porösen Medium, und zweitens, dessen Retardationsverhalten, hervorgerufen durch Partitionierungsprozesse im teilweise wassergesättigten, porösen Medium. Die Erkenntnisse, die aus diesen Experimenten gewonnen werden konnten, trugen zu einem verbesserten physikalischen Verständnis über das Verhalten von schweren Schadstoffgasen in der ungesättigten Bodenzone bei.

Im zweiten Teil der experimentellen Untersuchungen wurde das Versickerungsverhalten des flüssigen Schadstoffs im ungesättigten, porösen Medium beobachtet und im Anschluss daran die Anwendbarkeit von Bodenluftabsaugung als In-Situ-Sanierungstechnologie analysiert.

Zur Verbesserung der Kenntnisse über das Verhalten schwerer Schadstoffgaswolken im Untergrund, wurde die dichtegetriebene, advektive Absenkung von gasförmigem Schwefelkohlenstoff untersucht. Dieser Prozess wurde zunächst in großskaligen Säulenexperimenten quantifiziert und die Ergebnisse anschließend mit einem numerischen Modell verglichen. Zuerst wurden die 4 m langen, vertikalen Säulen (Innendurchmesser 0.109 m) mit einem trockenen, porösen Medium gefüllt. Quarzglaskugeln mit drei unterschiedlichen Korngrößenverteilungen (grob, mittel und fein) wurden als poröses Medium eingesetzt, jeweils mit dem Ziel, den Einfluss der Durchlässigkeit auf den Transport zu beobachten. Das poröse Medium wurde im trockenen Zustand verwendet, um mögliche Partitionierungsprozesse in das Porenwasser zu vermeiden. Die in die Mitte der Säule injizierte Schadstoffgaswolke sank gleichmäßig, abhängig von der injizierten CS_2-Gesamtmasse und der Permeabilität des Mediums, abwärts. Während der Versuche wurden entlang der Säule Gasproben entnommen um den Transport zeitlich und räumlich hochaufgelöst zu bestimmen. Der speziell entwickelte Experimentaufbau ermöglichte die Charakterisierung des Migrationsverhaltens des schweren, gasförmigen CS_2. Das Experiment wurde anschließend in einem 1-D, 2-Phasen, 2-Komponenten, isothermen, numerischen Modell nachgebildet und mithilfe eines Vergleichs der Simulationsergebnisse mit den experimentellen Daten verifiziert. Die numerischen Berechnungen konnten das in den Experimenten beobachtete Verhalten reproduzieren, sagten jedoch etwas höhere Absinkgeschwindigkeiten als die beobachteten Werte voraus. Zusätzlich wurde erfolgreich ein History matching, bei dem die Migrationsgeschwindigkeiten und Konzentrationsmessdaten der Experimente als Beobachtungspunkte eingesetzt wurden, durchgeführt.

Das Retardationsverhalten von gasförmigem CS_2 in einem ungesättigten, porösen Medium wurde in einem zweiten, speziell dafür gebauten Säulenversuchsstand untersucht. Die Versuchssäulen mit 2 m Länge wurden dazu sukzessive mit zwei unterschiedlichen Materialien (feine Quarzglaskugeln und Geba Feinsand) gepackt, um die für die Retardation des Schadstoffs verantwortlichen Partitionierungsprozesse zu analysieren. Durch Aufsättigung und anschließende Drainage konnte eine reproduzierbare stationäre Wassersättigung entlang der Säule (Anfangsbedingungen) erreicht werden. Während des Versuchs wurde ein Gemisch aus gasförmigem CS_2 und Argon (konservativer Tracer) am unteren Ende der Säule mit einem konstanten Fluss injiziert bis sich stationäre Konzentrationsverhältnisse einstellten. Anschließend wurde mit derselben Rate Stickstoff injiziert, um das Gasgemisch wiederum aus dem Porenraum auszutragen. Diese Vorgehensweise erlaubte die experimentelle Charakterisierung des Gastransports und des Retardationsverhaltens bei unterschiedlichen Fließgeschwindigkeiten. Diese wurden basierend auf den Beobachtungen während der vorherigen experimentellen Untersuchung zur dichtegetriebenen Migration ausgewählt. Mittels zweier Gaschromatographen konnten die Konzentrationen von CS_2 und Argon am oberen Auslass der Säule während der gesamten Versuchsdauer online gemessen werden. Am unteren Ende der Säule war damit eine konstante Flussrandbedingung gegeben während das obere Ende einer konstanten Druckrandbedingung (Atmosphärendruck) entsprach. Zur Auswertung der Konzentrationsdurchbruchskurven wurde die zeitliche Momentenanalyse (Temporal Moment Analysis) für konstante, punktförmige Injektion verwendet. Diese Methode erlaubte es, aus den Durchbruchskurven die Diffusion/Dispersion der beiden Gase und die Retardation von CS_2 zu bestimmen.

Die durchgeführten Experimente zeigten eine deutliche Retardation des gasförmigen CS_2 als Funktion der Eigenschaften des porösen Mediums und dessen Wassersättigung. Der ermittelte

Retardationskoeffizient nahm mit zunehmender Wassersättigung zu. Zur Bewertung der Ergebnisse wurde der experimentell bestimmte Retardationskoeffizient mit einem theoretischen Koeffizienten, der die Partitionierung in die wässrige Phase berücksichtigt, verglichen. In feinen Quarzglaskugeln spiegelte das beobachtete Retardationsverhalten die mit dem theoretischen Ansatz abgeschätzte Retardation wider. In den Experimenten mit Geba Feinsand hingegen wurde eine deutlich stärkere Retardation des CS_2 gemessen als durch den theoretischen Koeffizienten vorherbestimmt. Dies kann mit der spezifischen Korngrößenverteilung und dem entsprechenden Wassersättigungsprofil erklärt werden. Das Retardationsverhalten war weitestgehend unabhängig von den gewählten Fließgeschwindigkeiten; lediglich eine leichte Tendenz zu einer Abnahme der Retardation bei der höchsten verwendeten Geschwindigkeit konnte erahnt werden.

Die Experimente zeigten deutlich, dass eine in der ungesättigten Bodenzone gravitativ absinkende Schadstoffgaswolke durch Partitionierungsprozesse retardiert wird. Mit den durchgeführten Untersuchungen konnte somit ein relevanter Beitrag zum Verständnis von dichtegetriebener Migration und Retardation eines schweren Schadstoffgases geleistet werden. Des Weiteren stehen die experimentellen Daten für zukünftige Forschungsvorhaben und vor allem für die Übertragung der Prozesse auf die Feldskala zur Verfügung. Es wurde nicht nur nachvollzogen wie ein schweres Schadstoffgas in der ungesättigten Bodenzone absinkt und damit eine potenzielle Gefahr für einen darunterliegenden Aquifer darstellt, sondern es konnte auch eindeutig nachgewiesen werden, dass das im Porenwasser gelöste CS_2 zum mikrobiellen Abbau zur Verfügung steht, was interessante Implikationen für eine potentielle Sanierung bietet.

Der zweite Teil dieser Dissertation konzentrierte sich auf die In-Situ-Sanierung einer flüssigen CS_2-Verunreinigung und des davon ausströmenden Schadstoffgases. Dazu wurden 2-D-Küvettenexperimente durchgeführt, bei denen zuerst verschiedenartige Einträge und die damit zusammenhängenden Schadstoffverteilungen von flüssigem CS_2 in einem feuchten, porösen Medium untersucht wurden. Im Anschluss daran wurden die Verunreinigungen dann mittels Bodenluftabsaugung saniert. Ein Ziel dieser experimentellen Untersuchung war es, den Sanierungsverlauf hinsichtlich porösen Mediums, Wassersättigung, CS_2-Verteilung und Temperatur, sowie Fließgeschwindigkeit der Bodenluft zu bewerten. Dazu wurde die Küvette (1.00 x 0.70 x 0.12 m) jeweils mit einem porösen Medium (feine Quarzglaskugeln oder Geba Feinsand) gepackt, um die Abhängigkeit der Flüssigphasenverteilung von den Materialeigenschaften und der Wassersättigung zu bestimmen. Zur Einstellung der Wassersättigung (Anfangsbedingungen) durch Aufsättigung und Drainage kam ein spezieller Versuchsaufbau zum Einsatz. Die gewählte CS_2-Injektionsmethode (kontinuierlich oder intermittierend) führte, auch in Abhängigkeit der porösen Medien, die durch unterschiedliches, kapillares Rückhaltevermögen charakterisiert waren, entweder zu präferenziellem Pooling oder zu einer residualen Verteilung.

Für die Bodenluftabsaugung wurden jeweils am äußeren Rand der Küvette zwei vertikale Brunnen installiert und für die Bereitstellung von Reingas (linke Seite) und die Absaugung der kontaminierten Bodenluft (rechte Seite) verwendet. Zur Quantifizierung des Massenaustrags wurden die CS_2-Konzentrationen in der extrahierten Bodenluft, die Flussraten, die Drücke sowie die Temperaturen während der Versuche gemessen und aufgezeichnet. Es konnte gezeigt werden, dass die unterschiedlichen Schadstoffverteilungen einen signifikanten Einfluss auf die

Sanierung mittels Bodenluftabsaugung haben: Das Entfernen eines flüssigen CS_2-Pools dauerte deutlich länger als die Sanierung einer residualen Verteilung. Die Experimente zeigten weiterhin, dass aufgrund der geringen Siedetemperatur und des hohen Dampfdrucks von CS_2bereits ein geringfügiger Temperaturanstieg eine Verkürzung der Sanierungsdauer zur Folge hat. Weiterhin wurde beobachtet, dass die Fließgeschwindigkeiten die Schadstoffkonzentrationen in der abgesaugten Bodenluft kontrollieren. Langsame Fließgeschwindigkeiten (Extraktionsraten) begünstigen eine hohe Schadstoffkonzentration in der Bodenluft, führen jedoch zu einer insgesamt längeren Sanierungsdauer. Aus den Experimenten konnten die relevanten Parameter, die das Sanierungsverhalten kontrollieren, bestimmt und erste Ansätze zur Optimierung aufgezeigt werden. Die experimentellen Untersuchungen bewiesen, dass die Bodenluftabsaugung eine effiziente Technologie zur Sanierung einer CS_2-Kontamination in der ungesättigten Bodenzone darstellt.

Die wissenschaftlichen Untersuchungen, die im Rahmen dieser Dissertation am Beispiel von Schwefelkohlenstoff durchgeführt wurden, fördern das Wissen um den Forschungsschwerpunkt, der sich mit dem Verhalten von gasförmigen Schadstoffen in der ungesättigten Bodenzone und deren Umweltauswirkungen befasst. Es war möglich, repräsentative, experimentelle Daten zu erheben und diese zur Quantifizierung der relevanten physikalischen Prozesse auszuwerten. Diese neu entwickelten beziehungsweise angepassten Methoden stehen für zukünftige wissenschaftliche Arbeiten zur Verfügung. Weiterhin wurde die Anwendbarkeit und Effizienz der In-Situ-Sanierungstechnologie mit Bodenluftabsaugung experimentell nachgewiesen. Damit ist diese Dissertation nicht nur eine unabhängige Arbeit, sie bietet auch die Basis für weiterführende Forschungsvorhaben im Bereich der Migration und Retardation von gasförmigen Schadstoffen in der ungesättigten Zone, sowie für die Dimensionierung und Optimierung der Sanierungstechnologie mittels Bodenluftabsaugung im Feldeinsatz.

1. Introduction

Subsurface contamination is a major concern in industrialized as well as in developing and emerging countries. The list of potential contaminants includes a wide variety of organic compounds used in industry, such as solvents and degreasers. Contaminants introduced into the unsaturated zone migrate as a liquid phase; however, they can also vaporize and migrate in a gaseous state. In particular, vapor (gas) plumes migrate easily in the unsaturated zone (*Barber and Davis*, 1991; *Davis et al.*, 2005, 2009; *Höhener et al.*, 2006). Vapors heavier than air preferentially migrate downward, posing a potential threat to aquifers.

Humans may be exposed to hazardous contaminants directly or indirectly. Direct exposure can arise from vapor intrusion into the basements of buildings. Indirect exposure can occur when contaminants dilute into groundwater which is tapped for drinking water purposes. Governmental regulation has tightened the protection of the human health and of the environment over the past decades.

Carbon disulfide (CS_2), among many used to manufacture viscose rayon, is an industrial, non-polar solvent and a hazardous contaminant. CS_2 has been found in 139 (11.2 %) contaminated sites on the U.S. EPA National Priority List (NPL), according to *McGeough et al.* (2007). It is a dense, non-aqueous phase liquid which is highly volatile and flammable. In addition, it is characterized by a very high density (1.6 times the air density) in a gaseous state. Therefore, a thorough investigation into the contaminant CS_2 and its threat to the environment is required.

1.1. Structure of investigation

This investigation sought to explore the fate and transport of carbon disulfide (CS_2) vapor and techniques for its remediation from the unsaturated zone. It also explored the threat of CS_2 residing in the unsaturated subsurface. Hereby, the understanding of fundamental and relevant processes of vapor migration in dry porous media and retention in partially water-saturated porous media was of major importance. This investigation discusses the following central questions to assess the threat resulting from a contamination:

- How does a CS_2-vapor plume migrate in the unsaturated zone and what influence do the contaminant's properties have on its behavior?
- Do physical processes (e.g. partitioning) affect migration in porous media and what influence does water saturation have on the overall behavior?
- Does migration of vapor from a liquid CS_2 spill in the unsaturated zone pose a potential threat to underlying aquifers?

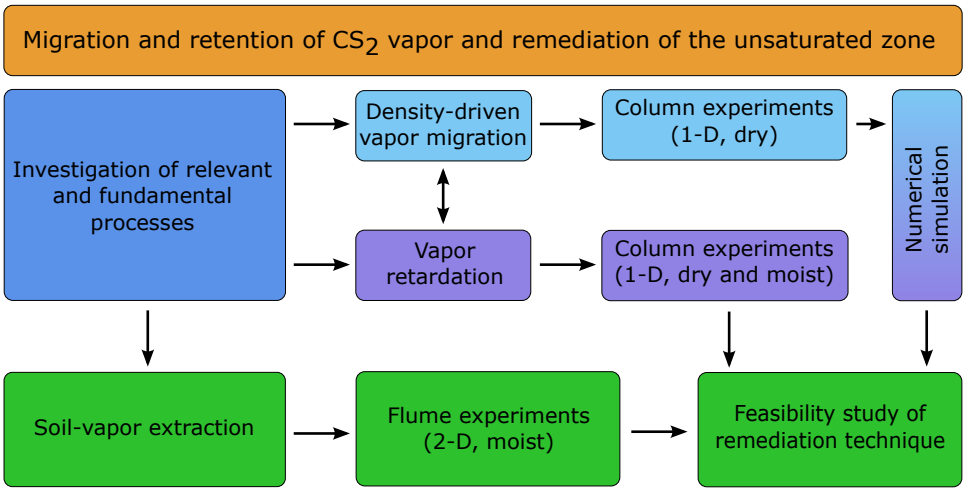

Figure 1.1. Structure of dissertation.

- Which remediation technique can be applied in the unsaturated zone to mitigate potential dangers to the environment due to migrating vapors and to remove a liquid spill?

The danger and the extent of vapor plumes emanating from liquid contaminants depend on various parameters: permeability, porosity, and soil moisture content of the porous media. These parameters influence advective and diffusive flow. The total contaminant mass directly affects the size of the vapor plume. The difference in density or molecular mass of the contaminant vapor relative to that of the soil air directly induces gravity-driven migration. While vapor pressure in conjunction with the air-contaminant interfacial area affects the vaporization speed and thus controls the velocity of plume development as well as its spatial extent, migrating vapor plumes may be retarded by sorption, dissolution, and biodegradation in the subsurface. Eventually, atmospheric pressure and temperature influence these conditions and processes.

The conditions and properties are responsible for triggering and controlling migration in the subsurface. Given the complexity of vapor transport in the unsaturated zone, this investigation therefore sought to explore density-driven vapor-plume migration within variably-permeable, dry porous media as well as retardation in partially saturated porous media under predefined boundary conditions. Hence, these processes had to be investigated in detail to provide a thorough understanding of fate and transport of CS_2 in the unsaturated zone and to provide a basis for the development and application of an efficient remediation technique of a liquid CS_2 spill. The investigation was divided into two major parts (Fig. 1.1). First, characterization of relevant and fundamental processes (blue) and, second, proof of concept for soil-vapor extraction as a remediation technique applicable in the unsaturated zone (green). The first part was subdivided into density-driven vapor migration (VME) and vapor retardation (VRE). Column experiments were conducted to investigate these processes. Numerical modeling of vapor migration greatly contributed to the knowledge gained from the experiments. The second part involved flume experiments (SRE) exploring contaminant distribution and soil-vapor extraction applied for the remediation of a CS_2 spill.

1.2. Content of investigation

Previous experimental investigations into vapor transport in the subsurface (*Bohy et al.*, 2006; *Jellali et al.*, 2003) are based on a thorough understanding of the migration and distribution of non-aqueous phase liquids (NAPL) in the unsaturated zone. This has been a subject of detailed investigations over the last decades (e.g. *Mercer and Cohen*, 1990; *Illangasekare et al.*, 1995a; *Oostrom et al.*, 2003; *Kechavarzi et al.*, 2005, 2008). *Illangasekare et al.* (1995b) found that the migration path of a liquid contaminant is highly influenced by porous-medium heterogeneities eventually responsible for saturations higher than residual saturation due to macro-scale entrapment. Trapping of a liquid NAPL in larger pores (NAPL being non-wetting with respect to water) as a result of capillary forces leads to a large interfacial area, thus raising the potential for vaporization. *Schwille et al.* (1988) stated that transport of vapor plumes must not be neglected when dealing with highly-volatile, hazardous chemicals. *Rivett et al.* (2011) emphasized that vapor transport may either lead to reduced impact on groundwater stemming from losses to the atmosphere, or increased contamination at the water table through relatively rapid, downward vapor migration.

The investigations conducted in this work were based on experiments with an emphasis on process differentiation under exactly-defined boundary conditions. Regarding migration of CS_2 vapor in the unsaturated zone, driving and retaining forces/effects were characterized and their relevance for vapor transport in porous media was explored. In the first part, two fundamental processes were investigated. First density-driven vapor migration in dry porous media and second vapor retardation as a result of partitioning processes of vapor in partially water-saturated soil. Two different sets of column experiments were designed and built to investigate both processes separately. The second part of the experimental investigation explored the contaminant distribution and in-situ remediation of liquid CS_2. A 2-D flume experiment was set up to conduct these experiments under defined initial and boundary conditions in partially water-saturated porous media.

1.2.1. Density-driven vapor migration

Large-scale column experiments

The significance of density-driven migration of gaseous compounds such as chlorinated hydrocarbons or methane during transport in the unsaturated zone has been demonstrated experimentally (*Conant et al.*, 1996; *Jellali et al.*, 2003; *Lenhard et al.*, 1995) and with simulations (*Falta et al.*, 1989; *Mendoza and Frind*, 1990a,b). The higher the density difference with respect to ambient air in the soil, the higher is the potential for upward or downward migration. *Altevogt et al.* (2003) further advanced the research on density-driven vapor transport by performing small-scale, 1-D, column experiments (length = 40 cm, i.d. = 7.7 cm) packed with air-dry sand. This made it possible for the first time to measure and interpret pressure gradients ($<$1 Pa) in the porous medium resulting from the denser-than-air vapor (Freon-113). *Jang and Aral* (2007) demonstrated in 2-D and 3-D simulations that the evaporation of a chlorinated volatile organic compound (VOC) generates vapor (around a liquid source transporting the contaminant)

that, due to the density gradient, will flow to underlying, saturated groundwater zones. A more recent study by *Cotel et al.* (2011) showed that density-driven vapor migration emanating from a liquid source affects diffusive processes in dry and moist (irreducible water saturation) porous media. These studies addressed various aspects of vapor migration both experimentally and mathematically, and demonstrated the impact of density difference on developing vapor plumes emanating from liquid sources. However, these were small-scale experimental studies that mainly concentrated on the density effects of diffusive spreading, not on migration of an established vapor plume. *Choi et al.* (2002); *Conant et al.* (1996); *Davis et al.* (2005) reported that in the field, boundary conditions are extremely difficult to delineate, let alone to control. Hence, experimental investigations into advective vapor-plume migration on a larger scale at exactly-controlled boundary conditions were necessary to further enhance the understanding of this process.

Accordingly, the objective of this study was to describe density-driven vapor migration in the subsurface quantitatively on a large scale with clearly-defined and controlled boundary conditions. This goal was achieved by conducting experiments with a large-scale column of 4 m length. Different types of porous media were used to observe the dependency of migration on permeability. Carbon disulfide (CS_2), a heavier-than-air vapor, was injected into the middle of the column to observe the plume migration. The experimental set-up was reproduced in a numerical model and simulations were compared with the developed data set from experiments.

Of course, field environments are also influenced by other factors, such as the vaporization process if the source is a liquid, fluctuations in atmospheric pressure (*Auer et al.*, 1996), and annual soil temperature (*Abbas and Al-Naseri*, 2008). In addition, winds and atmospheric conditions affect evapotranspiration and soil moisture content in the subsurface (*Liu et al.*, 2012; *Davarzani et al.*, 2014) and contaminant vapor concentrations respond to rainfall events (*Shen et al.*, 2012). While these effects may influence the potential danger for an underlying aquifer, this work focused on experiments under controlled boundary conditions to obtain a thorough process understanding. Furthermore, the porous medium was kept dry to avoid partitioning effects into pore water. This facilitated a clearly-differentiated observation of density-driven vapor migration and avoidance of any other influencing processes.

Numerical simulation

Numerical simulations are methods used to quantitatively describe physical systems and to provide knowledge of processes and understanding of a particular problem or to predict the behavior of a system under different initial and boundary conditions. They are also commonly utilized to discover problems or to resolve incomprehensibility. Therefore, values which represent the real environment/set-up are used and the system obeys the implemented physical laws controlling the processes in the simulation domain. In the end, a representation of the real situation is obtained and one can draw conclusions and gain a better understanding of the processes involved in this problem. Over the years, numerical simulation capabilities have been developed to model non-isothermal, multi-phase, multi-component processes in porous media (*Helmig and Huber*, 1998; *Class et al.*, 2002; *Class and Helmig*, 2002) and further enhanced to sophisticatedly couple model concepts of different complexity, e.g. employed to simulate

contaminant spreading in the vadose zone (*Class et al.*, 2008). Moreover, numerical simulations are employed for upscaling purposes which create additional difficulties such as the estimation of effective parameters to capture soil heterogeneities on small scales which cannot be resolved by the model (*Neuweiler et al.*, 2011).

Two simulators were used, the in-house, open-source simulator DuMu^x and Shell's Dynamo/MoReS. DuMu^x (*Flemisch et al.*, 2011, 2015) is based on *DUNE* (*Bastian et al.*, 2008a,b, 2011) and was developed by the Department of Hydromechanics and Modelling of Hydrosystems at the University of Stuttgart. Its simulation output can be visualized and evaluated using the open-source, data analysis and visualization application ParaView (*Ahrens et al.*, 2005). Dynamo/MoReS (*Por et al.*, 1989) is a proprietary software developed by Shell Global Solutions for reservoir modeling among other applications and offers extensive tools for efficient simulation work flow and history matching. The goal of the numerical modeling was to simulate the vapor-migration process observed in the large-scale column experiments. Therefore, the set-up of the experiment was reproduced employing a 1-D, two-phase, two-component, isothermal model. The process of vapor migration was first explored on a basic level.

DuMu^x was developed and is used for all kind of multi-phase, multi-component, porous-media-modeling purposes, thus the model could be set up according to the experimental set-up to meet the requirements. MoReS, however, is used and developed for all type of reservoir modeling on huge scales including water and other fluids. Hence, the first step was to validate the applicability of the model for simulating density-driven vapor migration in a dry porous medium on a scale fairly small compared to realistic scenarios. In the second step, the models had to be tested for the correct implementation of physics and fluid behavior. Afterwards, simulation results were compared with the vapor-migration experiments to verify the models. Assuming the correctness of physics involved in the model, deviations between simulation and experiments could be ascribed to an incorrect implementation of initial and boundary conditions. In the end, the models were able to successfully describe density-driven vapor migration of CS_2 and satisfactorily reproduced the experimental results. With such a validated model, future steps could include the extension to 2-D and 3-D problems and the model could be employed for modeling more-complex contamination scenarios involving the migration of vapor plumes.

1.2.2. Vapor retardation

When assessing the danger of groundwater contamination by migrating vapor plumes, retention effects on transport are of major interest. Processes such as adsorption on sand grains or partitioning to soil water are affecting density-driven migration of vapors in porous media. Vapor retardation could potentially slow down migration velocity and reduce the total contaminant mass eventually reaching, and thus endangering the groundwater.

Experimental studies (e.g. *Brusseau et al.*, 1997; *Kim et al.*, 1998) have been conducted to investigate retardation of the most common VOCs in partially saturated porous media. Experimental results have been compared with standard as well as advanced advection-dispersion models (*Popovičová and Brusseau*, 1998; *Toride et al.*, 2003). *Corley et al.* (1996) showed that low concentrations of volatile organic compounds distribute in the bulk phases (air, water and solid), adsorb

to the air-water interface, and partition into intraparticle pores in unsaturated and saturated porous media. While it has been demonstrated in experiments that the gas-water interface poses a high potential for retardation (*Brusseau et al.*, 1997), determining the size of interfacial areas and partitioning parameters in theoretical approaches is considered a challenge (*Hoff et al.*, 1993; *Kim et al.*, 1997, 1998). *Mayes et al.* (2003) stated that immobile water in pores could act as a short-term sink and as a long-term source of potential contaminants.

The effect of moisture content on vapor retention has also been described by *Cabbar and Bostanci* (2001) and *Maxfield et al.* (2005) who discovered retardation to be negatively correlated to water saturation due to preferred adsorption on the solid matrix of certain components. The latter has additionally shown the dependency of retardation on the properties of the chemical compound of interest. For instance, noble gases show no retardation behavior at all.

This component and water-saturation-dependent behavior of gas-phase retention emphasizes the necessity for a thorough investigation and quantification of retardation effects of CS_2 in unsaturated porous media. Thereby, fundamental knowledge about its potential to delay or prevent the contamination of an underlying aquifer is gained. In order to achieve this goal, experiments were designed to quantitatively characterize retardation of CS_2 on a large scale with clearly-defined and controlled boundary conditions. The experiments were conducted in vertical stainless steel columns (i.d. = 0.109 m) of 2 m length packed with fine glass beads (cf. Tab 3.2). They were carried out at dry conditions as well as at irreducible water saturation. Reproducible water saturations (initial conditions), as observed in the subsurface at a given distance above the groundwater table, were obtained by saturation with water and subsequent drainage under controlled conditions at predetermined capillary pressures. A slug of gaseous CS_2 as well as as non-retarding, conservative tracer (argon) was injected via an injection section at the bottom of the column. Effluent concentrations of CS_2 and argon were measured online at the top outlet of the column. Tensiometers installed along the column measured capillary pressures during saturation and drainage as well vapor injection. Thereby, water-saturation profiles (in-situ moisture content) of the porous media were obtained. Gas flow rates were controlled by mass-flow controllers and additionally measured by a bubble flow meter.

This experiment set-up enabled for quantification of retardation of CS_2 as a function of water saturation. Vapor-retardation experiments greatly improved the understanding of how downward-migrating CS_2 vapor is affected by partitioning processes in partially saturated porous media.

1.2.3. Spill and remediation

Contaminations by hazardous liquids demand a fast response and an efficient remediation technique to prevent further damage or threat. The feasibility and efficiency of such techniques must be explored taking into account the physicochemical properties of the contaminant and the environmental conditions. This part of the work addresses the remediation of a spill of liquid CS_2 in the unsaturated zone. The two previous investigations (vapor migration and retardation) laid the basis and provided relevant knowledge to develop a suitable remediation scheme. An efficient in-situ technique was required to remove a spill of CS_2 and at the same time prevent further contamination of the underlying aquifer. Moreover, the prevailing

boundary conditions of the unsaturated zone have to be taken into consideration. When contaminants immiscible with water spread in unsaturated porous media, water (wetting phase) is already occupying the small pores, wetting the grains, whereas air (non-wetting phase) resides in the bigger pores. From a multiphase-multicomponent perspective, the newly added liquid CS_2 behaves as wetting phase with respect to air but is considered non-wetting with respect to water. In addition to the wetting characteristics, fluid properties (such as viscosity, density and interfacial tension), spill dynamics, and geological characteristics influence the spreading of the liquid contaminant and its distribution in the subsurface. Downward percolation of CS_2 as well as rapid vaporization (due to high vapor pressure) in the unsaturated zone, and the subsequent formation of a downward-moving vapor plume pose a threat to groundwater. Therefore, after a spill a timely response and effective remediation is a necessity.

Different techniques for in-situ remediation have been developed and applied over the past decades; however innovative and contaminant-adapted methods are in demand. Selection of the most appropriate technology in terms of contaminant recovery, efficiency, and ecological impact requires a thorough understanding of the contaminated zone (hydrogeology, contaminant distribution) and the properties of the contaminant-water composition (density, surface tension, volatility). Soil-vapor extraction (SVE) appears to be the technology of choice given the contamination scenario with a highly-volatile substance such as CS_2 in residual distribution in the unsaturated zone.

The application of a soil-vapor extraction remediation involves the establishment of a stable gas-flow regime through the contaminated zone in the subsurface. Wells, installed in the unsaturated zone, extract contaminated soil air flowing from the surrounding areas in the subsurface. The contaminated air is subsequently cleaned. Provided that a stable flow regime within a certain range from the wells can be established (e.g. via sealing of the surface to prevent short circuiting of air), it is a cost-effective technology for the removal of volatile compounds such as chlorinated hydrocarbons (e.g. *Gibson et al.*, 1993). Over the years, SVE has been developed as a state-of-the-art remediation technique, nowadays often combined with thermal-energy input, e.g. steam injection (*Ochs et al.*, 2010), to enhance contaminant vaporization and mobilization (*Davis*, 1997). Latest studies (*Brusseau et al.*, 2010; *Carroll et al.*, 2012) focused on assessing mass fluxes from the vadose zone and thereby predicting time frames of operation.

The investigation presented here focuses on the demonstration of a liquid spill in the unsaturated zone and confirmation of the applicability of soil-vapor extraction as an effective remediation technique for a CS_2 spill in the unsaturated zone. The removal of CS_2 vapor from dry and moist porous media was successfully shown in the vapor-retardation column experiments. This was taken to a more realistic scenario where the contaminant resided as a liquid phase (i.e residual distribution or pool) in the unsaturated zone, from whence it had to be removed. Now, experiments were conducted in a 2-D flume to combine the investigation of a liquid spill of CS_2 into moist porous media and the subsequent remediation by means of SVE with specific emphasis on its efficiency and applicability for this particular contaminant. The spill and the subsequent migration of liquid CS_2 in the subsurface as well as the application of SVE were conducted under controlled initial and boundary conditions. In addition, the experiments were visually recorded and documented. The main objective was to provide experimental data required for the dimensioning of remediation parameters. Parameters such as

extraction flow rate and duration as a function of spill mass, hydrogeology, and vaporization dynamics of CS_2 will highly affect the efficiency in a field application.

Two-dimensional experiments were designed and conducted in a flume with dimensions of 1.00 x 0.70 x 0.12 m (L x H x W). The flume was filled with a porous medium which was water saturated and subsequently drained prior to each experiment to obtain static water saturation (similar initial conditions for each run). Tensiometers installed at the rear side of the flume monitored the drainage process and ensured similar initial conditions regarding water saturation. Fine glass beads and Geba fine sand were used as porous media. Their difference in grain-size distribution was expected to influence the migration behavior of liquid CS_2. Two different injection methods were applied to inject the spill with a predefined mass flux: either a single-port injection via one port located at the upper center of the flume or a multi-port injection using 4 ports. The first method favored pooling of liquid CS_2 on lower permeability layers while the second method caused a widespread contamination and reduced pooling.

Two vertical wells, filtered over the entire flume height, were installed at the sides. Thereby, a horizontal flow regime could be induced and controlled during the entire remediation progress. CS_2 concentrations were measured online and additionally by means of gas samples at the outlet of the flume to ensure mass balance. In order to produce proof of concept, the influence of different porous media, spill and extraction rates on efficiency of the remediation process were studied. Thus, the spill and remediation experiments helped on understanding how a liquid contaminant spreads in partially saturated porous media and which parameters affect the remediation progress.

2. Fundamentals

This chapter addresses the fundamental parameters and relationships employed in this work and which are required to understand the experimental investigations. The introduced equations and their parameters generally employ SI units if not stated otherwise. Section 3.3 of Chapter 3 Materials and Methods discusses these parameters in relation to the experimental set-ups.

2.1. Parameters of porous media

Porosity denotes the void space in a bulk volume of a porous medium which may be occupied by fluids.

$$\phi = 1 - \frac{V_s}{V_b} \tag{2.1}$$

with porosity ϕ (dimensionless), soil volume V_s (m^3), and bulk volume V_b (m^3). Theoretically, this void or pore space is available for the transport of fluids. However, it is clear that only an "effective" void space with interconnected pores is accessible for fluids. Therefore, the effective porosity is of importance for transport of fluids in porous media.

Saturation relates the volume of a fluid phase α to the pore volume of a porous medium.

$$S_\alpha = \frac{V_\alpha}{\phi V_b} \tag{2.2}$$

with saturation S_α (dimensionless), occupied volume V_α (m^3), and the general condition $\Sigma S_\alpha = 1$.

The unsaturated zone is usually treated as a two-phase system with a liquid phase (water) and a gaseous phase (humid soil air). In this case, the amount of liquid water residing in the pore space of the unsaturated zone can be quantified by the parameters water content or water saturation. Water content θ is the water-filled fraction of pore space related to the bulk volume of the porous media, thus it ranges between 0 (dry porous media) and the value of porosity ϕ (fully saturated) denoted as θ_s. Drainage of water-saturated porous media results in an amount of water trapped in small pores due to capillary forces. This amount is called irreducible water content θ_r.

The parameter water saturation S scales water content by porosity, i.e. the actual available space for fluids, hence ranging from 0 (dry) to 1 (fully saturated). The effective water saturation S_e ranges from 0 (irreducible water saturation S_r) to 1 (fully saturated).

Intrinsic permeability is a parameter of a porous medium determined by its structure and is a measure of ease for the flow of a fluid through the pore space. Permeability k is usually given in m^2 and is independent of the fluid's properties.

Hydraulic conductivity is specifically for the flow of water in a porous medium, hence dependent on its physical properties. Its relation to permeability is given by

$$K = k\frac{\mu}{\rho g} \tag{2.3}$$

with hydraulic conductivity K ($m\,s^{-1}$), permeability k (m^2), dynamic viscosity μ (Pa s), density ρ ($kg\,m^{-3}$) of water, and gravitational constant g ($m\,s^{-2}$).

Relative permeability The unsaturated zone is occupied by different fluids. These fluids may be present in different phases, e.g. the liquid phase and the gaseous phase. In multi-phase systems, the flow of a fluid in one phase (wetting) is hindered by the presence of a fluid in a second phase (non-wetting) and vice versa. This results in a fluid-dependent reduction of the intrinsic permeability and is governed by the parameter relative permeability k_r. The relative permeability of a fluid in phase α is defined as

$$k_{r,\alpha} = \frac{k_\alpha(S_\alpha)}{k} \tag{2.4}$$

with relative permeability $k_{r,\alpha}$ (dimensionless), effective permeability k_α (m^2), phase saturation S_α (dimensionless), and intrinsic permeability k. In case of a single-phase system ($S_\alpha = 1$), the relative permeability equals the intrinsic permeability k.

Capillary pressure–saturation relationship is used as a parameter in soil science to deduce the water saturation of a porous medium from its capillary pressure usually obtained from tensiometer measurements. Hence, capillary pressure is a fundamental parameter for the behavior of wetting and non-wetting fluids in porous media and accounts for the pressure discontinuity at the fluid interface in equilibrium (or relates the pressures in the two fluids, respectively).

$$P_c = P_{nw} - P_w = \frac{4\,\sigma_{w,nw}\,cos\varphi}{d} \tag{2.5}$$

with capillary pressure P_c (Pa), interfacial tension σ ($N\,m^{-1}$) of the fluid combination (w, nw), contact angle φ, and pore diameter d (m).

Considering capillarity on a macro scale leads to the relationship between the capillary pressure and the saturation of the wetting and the non-wetting fluid. The higher the saturation of the non-wetting fluid or the lower the saturation of the wetting fluid, the higher the capillary pressure which forces the wetting fluid to retreat to smaller pores. Different models have been developed to approximate this relationship for the air-water system taking into account the properties of the fluids and the porous medium.

The constrained model developed by *van Genuchten* (1980) was used for the saturation and drainage of the moist experiments.

$$S_e = \left(\frac{1}{1 + (\alpha|h|)^n} \right)^{1-\frac{1}{n}} \tag{2.6}$$

where S_e (-) is effective water saturation, h (cm H_2O) is pressure, α (1/cm), and n (-) are the van Genuchten parameters.

The water saturation can be calculated from the effective saturation with

$$S = \frac{S_e(\theta_s - \theta_r) + \theta_r}{\theta_s} \tag{2.7}$$

where S (-) is water saturation and θ_s and θ_r ($cm^3\,cm^{-3}$) are fully-saturated and irreducible water content, respectively.

2.2. Transport processes

2.2.1. Advection

Vapor/gas-phase transport in porous media generally follows Darcy's law stating that the gas-phase Darcy velocity u is directly proportional to the gradient $\frac{d}{dz}$ and the gas-phase permeability $k_{r,i}$ (*Bear*, 1972). It can be written for vertical flow of fluid i in z-direction as

$$u_i = -\frac{k_{r,i}}{\mu_i} \frac{d}{dz} \left(P_i - \rho_i g z \right) \tag{2.8}$$

where μ_i is the dynamic gas-phase viscosity and g the gravitational constant. Darcy's law is only valid for viscous flow and for regions without boundary shear flow. In case of higher velocity flow and considerable boundary shear flow, Darcy's law has to be modified using the Brinkman extension (*Brinkman*, 1949). This is not explained any further since the experiments were conducted at low velocity flow where Darcy's law is applicable.

The validity of Darcy's law can be estimated using the dimensionless Reynolds number Re (Eq. 2.9). It is used to distinguish between laminar and turbulent flow in fluid mechanics and is defined for a porous medium as

$$Re = \frac{u \rho l}{\mu} \tag{2.9}$$

with velocity u, density ρ of the fluid, a characteristic length l (for a porous medium the mean grain size, d_{50}, is used), and the fluid's dynamic viscosity μ. A Reynolds number lower than 1 (strictly 0.2) guarantees the validity of Darcy's law.

2.2.2. Diffusion

Fick's first law is used to calculate the mole flux J_M of component A in a clear fluid B in one dimension. It states that the diffusive flux is proportional to a diffusion coefficient multiplied by the mass or molar concentration gradient and is written as

$$J_A = -cD_{AB}\nabla x_A \tag{2.10}$$

where c is the concentration of the gas, D_{AB} is the binary diffusion coefficient in a clear fluid, and x_A is the mole fraction of component A. Multi-component systems are addressed using the Stefan-Maxwell equation which reduces to Fick's law for a two-component system (*Ho and Webb*, 2006).

Binary diffusion coefficient of component A in B at low density can be estimated according to the Chapman-Enskog formula.

$$D_{AB} = 1.8583 \times 10^{-3} \frac{\sqrt{T^3 \left(\frac{1}{M_A} + \frac{1}{M_B}\right)}}{p\sigma_{AB}^2 \Omega_{D,AB}} \tag{2.11}$$

with D_{AB} (cm^2 s^{-1}), temperature T (K), pressure p (atm), the Lennard-Jones parameter σ_{AB} (Å), and the collision integral $\Omega_{D,AB}$ which can be approximated with the Lennard-Jones potential. Component-specific values to determine σ_{AB} as well as $\Omega_{D,AB}$ as a function of kT/ϵ can be found in *Bird et al.* (1960).

Porous media affect diffusion of gases since space is occupied by grains and possibly by additional fluid phases. Therefore, Fick's law is often modified by the factor β to account for these deviations.

$$D_{AB}^* = \beta D_{AB} \tag{2.12}$$

while β is defined as

$$\beta = \phi S_g \tau \tag{2.13}$$

where D_{AB}^* is the effective diffusion coefficient in porous media, ϕ is the porosity, S_g the gas saturation (equal to 1 for all-gas condition), and τ is the tortuosity. According to *Millington and Quirk* (1961), tortuosity can be approximated by

$$\tau = \phi^{1/3} S_g^{7/3} \tag{2.14}$$

Knudsen diffusion Fick's law is utilized to describe ordinary (molecular) diffusion; however under certain conditions the no-slip condition at the walls or grains, crucial for the continuum-flow assumption, does not apply anymore. This occurs when the mean free path becomes the same order as the mean pore size. In this case not only the collision between molecules but also with the grains has to be taken into account. The fluid can then no longer be considered in thermodynamic equilibrium and non-continuum effects may occur. The resulting flux is denoted free-molecule or Knudsen diffusion. Since the experiments conducted in this work

employed the continuum-flow assumption, its validity was determined for the components and porous media used.

The validity of the continuum-flow assumption can be estimated using the dimensionless Knudsen number

$$Kn = \frac{\lambda}{l} \tag{2.15}$$

where λ is the mean-free-path of the molecules and l a characteristic length, in our case the mean pore size of the porous medium. *Miguel and Serrenho* (2007) classified as follows: "For a low Knudsen number ($Kn \leq 0.001$), the fluid can be regarded as a continuum. However, for higher Knudsen numbers ($0.001 < Kn \leq 0.1$) the continuum hypothesis is no longer appropriated and the gas flow is commonly referred to as the slip-flow regime." Higher values ($0.1 < Kn \leq 10$) define the transition zone to the free-molecular regime ($Kn > 10$).

The mean-free path of gas molecules λ, derived from the kinetic theory of gases according to (*Bird et al.*, 1960), is

$$\lambda = 3\frac{\mu}{\rho}\sqrt{\frac{\pi M}{8RT}} \tag{2.16}$$

with dynamic viscosity μ, density ρ, and molecular weight M. Since viscosity and density are a function of pressure and temperature, the mean-free path is dependent on absolute pressure and temperature in the porous medium.

2.2.3. Dispersion

Flow of fluids in a porous medium may vary significantly on a micro scale due to the velocity field in pores, irregularities of the pore size, flow restrictions, or dead-end pores resulting in additional spreading denoted as dispersion. These influences have to be taken into account in analytical or numerical solutions of flow in porous media. This is done by introducing the longitudinal dispersion coefficient

$$D = \beta D_{AB} + \alpha v = D^*_{AB} + \alpha v \tag{2.17}$$

with the dispersion coefficient D ($\mathrm{cm^2\,s^{-1}}$), effective binary diffusion coefficient D^*_{AB} ($\mathrm{cm^2\,s^{-1}}$) according to Eq. 2.12, gas-phase longitudinal dispersivity α (cm), and average gas velocity v ($\mathrm{cm\,s^{-1}}$). *Schulze-Makuch* (2005) reported that longitudinal dispersivity increases exponentially with the scale of measurement due to a combination of advective and diffusive processes as a compound moving through a porous medium encounters more and more heterogeneities. Hence, dispersivity is considered a scale-dependent parameter. The first term on the right-hand side of Eq. 2.17 represents the diffusive contribution dependent on the physicochemical properties of the component. The second term represents the mechanical-mixing dispersion coefficient resulting from flow through pores. Although the experiments were performed at low velocities, the contribution of mechanical mixing to the longitudinal dispersion coefficient was evaluated from the concentration breakthrough curves measured in the experiments. This work focused only on the longitudinal dispersion since transverse dispersion is far less significant, hence may be neglected. *Costanza-Robinson and Brusseau* (2002) stated that "the mechanical-mixing contribution to dispersion is conceptualized as being dependent only on the physical properties of the porous media and not on those of the compound".

2.2.4. Retardation

Vapor mass transport in a porous medium may be affected by sorption and partitioning processes. These may lead in some cases to a retardation of advective and diffusive flow depending on the component's properties. Mass transport equations consider these effects by introducing a retardation factor R_i of component i. *Brusseau et al.* (1997) defined the retardation factor (Eq. 2.18) to be the sum of various processes including adsorption and partitioning processes

$$R_i = 1 + \frac{\theta_w}{\theta_a K_H} + \frac{\rho_b K_{Dsat}}{\theta_a K_H} + \frac{K_{IA} A_{IA}}{\theta_a} \tag{2.18}$$

where θ_w is volumetric water content, θ_a is gas-filled porosity, K_H (dimensionless) is Henry's constant, K_{Dsat} ($cm^3\ g^{-1}$) is the sorption coefficient for water-saturated conditions, ρ_b ($g\,cm^{-3}$) is the dry soil bulk density, K_{IA} (cm) is the adsorption coefficient between gas and the gas-water interface and A_{IA} ($cm^2\,cm^{-3}$) is the specific surface area of the gas-water interface. The terms on the right-hand side describe retardation by the gas phase (1), partitioning into the aqueous phase (2), adsorption on the grains (3) and the last term accounts for gas-water interfacial adsorption (4).

2.2.5. One-dimensional advection-dispersion equation

Column experiments can be evaluated by comparison of concentration breakthrough curves to an advection-dispersion equation (ADE).

$$\frac{\partial c}{\partial t} + v\frac{\partial c}{\partial z} - D\frac{\partial^2 c}{\partial z^2} = 0 \tag{2.19}$$

The type of equation and its analytical solution has to be chosen according to the data as well as the initial and boundary conditions. The analytical solutions used in this work are valid for 1-D problems with a point source.

The analytical solution for a continuous injection (Heaviside function) in a semi-infinite domain is given by

$$c(z,t) = \frac{c_0}{2} erfc\left(\frac{(z - vt)}{\sqrt{4D_L t}}\right) \tag{2.20}$$

where c_0 ($kg\,m^{-3}$) represents the CS_2 flux concentration, v ($m\,s^{-1}$) is the seepage velocity, and t (s) and z (m) denote the time and location, respectively.

The analytical solution for a pulse (Dirac delta function) in a finite domain is defined as

$$c(z,t) = \frac{m}{A\phi}\frac{1}{\sqrt{4\pi D_L t}} exp\left(-\frac{(z - vt)^2}{4D_L t}\right) \tag{2.21}$$

where c ($kg\,m^{-3}$) represents the CS_2 concentration, m (kg) is the injected mass, A (m) is the cross-sectional area, ϕ (dimensionless) is the porosity, v ($m\,s^{-1}$) is the seepage velocity, and t (s) and z (m) denote the time and location, respectively.

2.3. Temporal moments

Moments are statistical measures utilized to evaluate and interpret transport in porous media such as flow of tracer in an aquifer or drawdown data from wells. Temporal moments are calculated by integration of a concentration distribution over time in comparison to spatial moments. The general temporal moment is defined as

$$m_n(x) = \int_0^\infty t^n c(x,t)\,dt \tag{2.22}$$

where $m_n(x)$ is the nth order temporal moment, c is concentration and t is time. The zeroth, first, and second moment ($m_0(x), m_1(x), m_2(x)$) represent the total response (corresponding to the mass), the mean, and the variance of the concentration distribution, respectively. For the evaluation of measurement data, it is favorable to use normalized moments.

$$M_n(x) = \frac{m_n(x)}{m_0(x)} = \frac{\int_0^\infty t^n c(x,t)\,dt}{\int_0^\infty c(x,t)\,dt} \tag{2.23}$$

The first normalized moment $M_1(x)$ is then considered the mean arrival time of the concentration distribution. The centralized (normalized) temporal moment is given by

$$\mu_n = \frac{\int_0^\infty (t - M_1)^n c(x,t)\,dt}{\int_0^\infty c(x,t)\,dt} \tag{2.24}$$

The second centralized moment μ_2 is a measure for the spreading (variance) of the mean arrival time which is linked to the physical parameter of dispersion.

2.4. Thermodynamics

This section covers the fundamentals of thermodynamics which were employed in the design, conduction and evaluation of the experiments. Physicochemical properties and constants of the compounds used in the experiments are given in the appendix A.1.

Ideal gas law is an equation of state based on the kinetic theory of gases expressing the relationship between pressure P (Pa), volume V (m^3), and temperature T (K), for a given quantity of moles n of a gas (*Ahmed*, 2007). The volume of the gas molecules is hereby insignificant compared to the total volume occupied by the gas. The relationship is expressed by

$$PV = nRT \tag{2.25}$$

where $R = 8.314\,\mathrm{J\,mol^{-1}\,K^{-1}}$ is the universal gas constant.

Peng-Robinson equation of state is an improved equation of state to correct for the non-ideality of fluids.

$$P = \frac{RT}{V_m - b} - \frac{a\alpha}{V_m^2 + 2bV_m - b^2} \tag{2.26}$$

where a and b are constants related to the critical temperature and pressure, V_m is the molar volume, and α is related to the acentric factor ω of a particular fluid (see Appendix A.1).

Dalton's law is related to the ideal gas law stating that the total gas pressure P is equal to the sum of the partial pressures P_i of the individual gases.

$$P = \sum_{i=1}^{n} P_i \tag{2.27}$$

with the partial pressure defined as $P_i = x_i P$.

Henry's law states that the amount-of-substance fraction x of a component i dissolved in the liquid phase is proportional to its partial pressure P_i in the gas phase when in equilibrium.

$$x_i = \frac{P_i}{K_{H,i}} \tag{2.28}$$

The component-dependent proportionality factor K_H is called Henry's constant and is defined in its dimensionless form as

$$K_H = \frac{c_{aq}}{c_{gas}} \tag{2.29}$$

where c_{aq} and c_{gas} are the concentration of the component in the aqueous and the gas phase, respectively. It is often approximated for components with low solubility in water as follows

$$K_H = \frac{P_{sat}}{S} \tag{2.30}$$

where P_{sat} (Pa) is the saturated vapor pressure and S the solubility limit (mol m^{-3}) in water (*Ho and Webb*, 2006).

Vapor pressure The vapor pressure P_{vap} of a liquid component in equilibrium can be approximated based on the Clausius-Clapeyron equation. Several formulas have been developed employing constants determined either by regression of experimental vapor pressure data or by calculation from critical temperature and pressure (*McGarry*, 1983). In this work, the Wagner equation was selected to calculate the vapor pressure.

$$lnP_r = \frac{1}{T_r}\left[A(1-T_r) + B(1-T_r)^{1.5} + C(1-T_r)^3 + D(1-T_r)^6\right] \tag{2.31}$$

with reduced pressure P_r defined as vapor pressure P_{vap} divided by critical pressure P_c, reduced temperature T_r and component-dependent constants A, B, C, and D (see Table A.1). Figure 2.1 shows vapor pressure over temperature of water (H_2O) and carbon disulfide (CS_2).

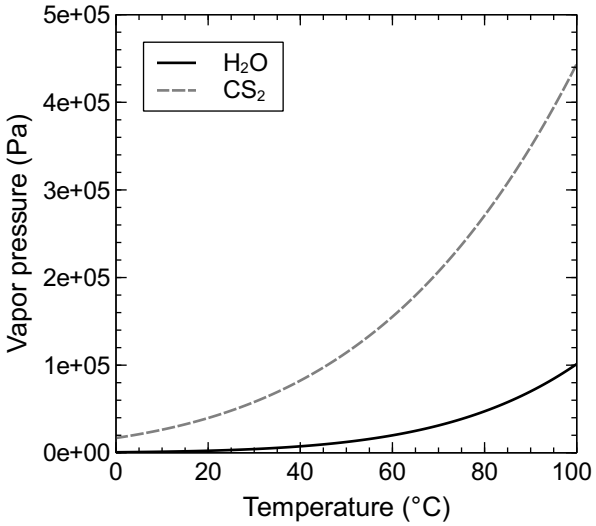

Figure 2.1. Vapor pressure as a function of temperature for the liquids water and carbon disulfide.

3. Materials and methods

3.1. Choice of materials and handling

All materials used in the experimental set-ups were chosen based on their stability with respect to the chemicals used. Custom-built parts were either made of stainless steel (1.4401 or higher), PTFE/PFA, or PEEK. They were degreased and cleaned with acetone ($(CH_3)_2CO$) prior to assembling. Only O-ring seals made of fluoropolymer were used. CS_2 is an aggressive and hazardous chemical component. Therefore, the experiments were conducted in explosion proof zones with high air ventilation and automated concentration monitoring. Volumes of liquid CS_2 greater than 30 mL were stored and transported exclusively in break-proof vessels. Laboratory personnel had to wear appropriate safety equipment such as goggles and nitrile gloves when conducting experiments and handling CS_2.

3.2. Contaminant carbon disulfide

CS_2 was chosen as the model substance since it fulfills the physicochemical requirements for density-driven vapor migration and retardation. It is highly volatile and in its gaseous state (air/nitrogen at saturated CS_2 concentration) characterized by a very high density (1.6) relative to air. Table 3.1 shows the parameters at 20 °C, 1013.15 hPa which are of relevance for these investigations. It was purchased from Sigma-Aldrich Co. LLC.

Table 3.2. Characteristic properties of the porous media used for the experiments.

Parameter	Glass beads Coarse	Glass beads Medium	Glass beads Fine	Fine sand Geba
Bulk density, kg m^{-3}	1520	1490	1420	1390
Grain size, mm	1.55 to 1.85	0.50 to 0.75	0.1 to 0.2	0.06 to 0.35
Permeability, m^2	1×10^{-9}	2×10^{-10}	1×10^{-11}	1×10^{-11}
Grain diameter d_{50}, µm	n/a	n/a	162	140
Pore diameter (median), µm	n/a	n/a	66	39
Knudsen number (CS_2)	n/a	n/a	1.51×10^{-4}	2.56×10^{-4}
van Genuchten (constrained)				
α, 1/cm	-	-	0.0193	0.0145
n	-	-	17.783	10.305
θ_s, cm^3 cm^{-3}	-	-	0.392	0.460
θ_r, cm^3 cm^{-3}	-	-	0.043	0.071

Table 3.1. Physicochemical properties of contaminant carbon disulfide (CS_2) at 20 °C and 1013.15 hPa.

Parameter	Value	Reference
CAS number	75-15-0	
Molecular weight (M_{CS2}), g mol^{-1}	76.1	*Budavari* (1996)
Density of liquid (ρ), kg m^{-3}	1263	*Budavari* (1996)
Solubility in water ($c_{w,sat}$), g L^{-1}	2.1	*Riddick et al.* (1986)
Henry coefficient (H_{cc}), dimensionless	1.04	*De Bruyn et al.* (1995)
Boiling point (T_B), °C	46.5	*Budavari* (1996)
Vapor pressure (P_{sat}), hPa	396.9	Wagner equation
Saturation concentration in gas phase ($c_{a,sat}$), kg m^{-3}	1.239	Ideal gas law
CS_2-Air vapor mixture density (ρ_{vap}), kg m^{-3}	1.971	Ideal gas law
Diffusion coefficient in air (D_{CS_2Air}), cm^2 s^{-1}	9.71×10^{-2}	Chapman-Enskog

3.3. Porous media

Sand types and initial sand preparation Four different types of porous media were used in the experiments. Well-defined porous media were obtained by applying glass beads (soda-lime glass) of different sizes (Sigmund Lindner, Warmensteinach, Germany and Sand-Schulz, Berlin-Reinickendorf, Germany) as well as a fine sand (Geba, Quarzsande GmbH, Eferding, Austria). Glass beads are available in very defined ranges of grain sizes. Their uniformity

comes from the manufacturing process and benefits reproducible and homogeneous packings and experimental conditions. Geba fine sand is a natural quartz sand having a wider grain-size distribution including smaller particles.

The vapor-migration experiments (VME) were conducted in coarse, medium, and fine glass beads. In the vapor-retardation (VRE) and the spill and remediation experiments (SRE), fine glass beads and Geba sand were used. The latter provided a capillary pressure–saturation characteristic better suitable for obtaining a moist porous medium at irreducible water saturation. Information about the materials are shown in Table 3.2 and Figure 3.1.

Grain (mean) and pore (median) diameter were determined from soil samples in the laboratory. Grain diameter d_{50} was determined from particle-size analysis (Mastersizer 2000, Malvern Instruments Ltd. Worcestershire, United Kingdom) and pore diameter was determined by mercury intrusion porosimetry (Pascal 140, Thermo Fisher Scientific, Waltham, MA, USA). The uniformity, the sphere-like shape, and the narrow grain-size distribution complicated the particle-size measurements of the medium and the coarse glass beads. Hence, no reliable values could be determined and therefore were not included in the parameter table.

The dimensionless Knudsen number (Eq. 2.15) was determined to verify the continuum-flow assumption for the component CS_2 in fine glass beads and Geba sand. Knudsen numbers of about 10^{-4} confirmed the validity of the assumption. This can be explained by relatively high permeabilities of the materials used and pressures close to ambient pressure in the experiments. Hence, no effects on flow through the porous medium due to free-molecule flow at the pore walls had to be considered.

Porosity of the dry porous media in the experiment columns or flumes was calculated with Eq. 2.1 using the densities of the porous media. The densities were determined using a pycnometer. In case of a moist porous medium, gas-effective porosity gets ideally reduced by the space occupied by pore water. Hence, gas-effective porosity is calculated with

$$\phi_{eff} = \phi(1 - S_w) \tag{3.1}$$

where S_w (dimensionless) is the water saturation of the porous medium. Dead-end pores or other flow restrictions due to the pore water might further reduce the gas-effective porosity.

Moreover, the grains were examined with a scanning electron microscope to evaluate whether intraparticle porosity or dead-end pores could possibly affect the transport and retardation behavior. Pictures showed that such effects can be neglected (see Appendix A.2).

Permeability was determined in gas-permeameter experiments and checked in-situ prior to the experiments using high-accuracy differential pressure transducer and gas mass-flow controllers. *Tidwell* (2006) defined the following equation to experimentally measure permeability in an unsaturated porous medium.

$$k = \frac{2\mu Q P_1 L}{A(P_1^2 - P_0^2)} \tag{3.2}$$

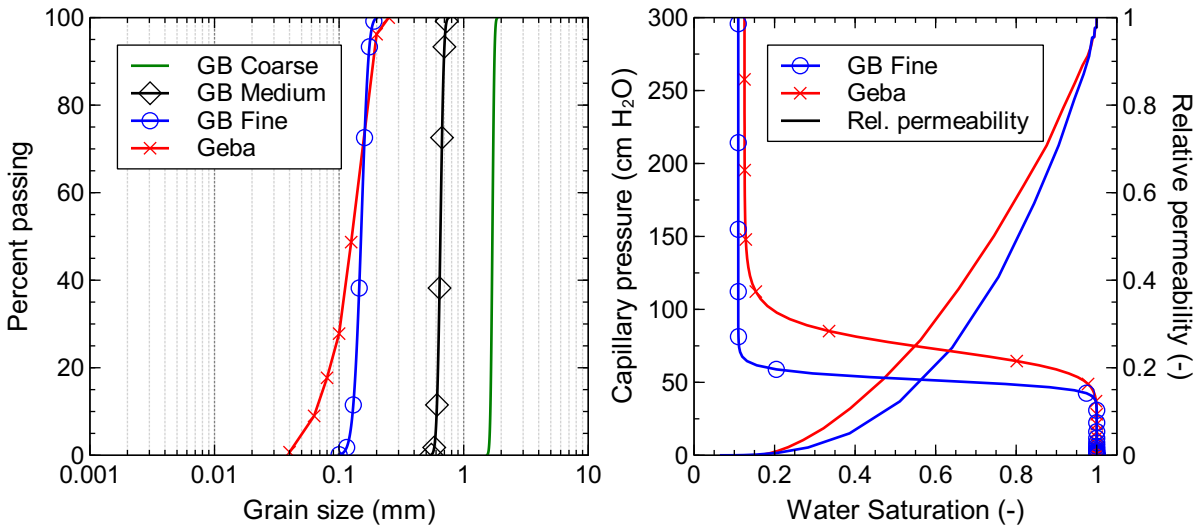

Figure 3.1. Grains-size distribution, capillary pressure–saturation relationship, and relative permeabilities (for the wetting phase) of materials used in experiments.

where k (m^2) is permeability, μ (Pa s) is the dynamic gas viscosity, L (m) is the length, and A (m^2) is the cross-sectional area of the experimental recipient. P_1 and P_0 (Pa) are the pressures at the inlet and at the outlet, respectively.

Capillary pressure–saturation relationship of the materials (Fig. 3.1) used in moist experiments was measured by means of a laboratory evaporation method utilizing the commercially-available device HYPROP (UMS GmbH, Munich, Germany). Measured retention curve data was fitted with the van-Genuchten-constrained relationship (Eq. 2.6) to obtain the material-dependent parameters.

Column-packing procedure Vapor-migration and vapor-retardation experiments (VME and VRE) were conducted in large-scale columns described in detail in Sections 4.1.2 and 4.2.2. The goal was to obtain homogeneous and reproducible sand packings. They were prepared employing the technique of dry pluviation with a custom-built sand rainer (Fig. 3.2). The design of the rainer was adopted from *Rad and Tumay* (1987) with modifications according to *Lagioia et al.* (2006). They investigated the impact parameters of sand pluviation covering the whole cross section under different conditions. Reproducible packings were checked through the relative density which is controlled by the terminal falling velocity of the sand. The terminal falling velocity is a combination of falling height (i.e. the distance from the lower diffuser screen to the point of impact), shutter porosity and diffuser sieves. The diameter of the sand rainer was chosen to fit into the stainless steel columns used for the unsaturated-zone column experiments and, thereby, to guarantee a uniform spreading across the column cross section. A pipe (HDPE, L = 70 cm, OD = 90 mm) was equipped with two diffuser screens, with a mesh opening of about 5 mm, which were set 5 cm apart and rotated by an angle of 45°. The mesh was built out of a high-grade steel (AlSl 316L) wire with 0.2 mm diameter which was fixed in

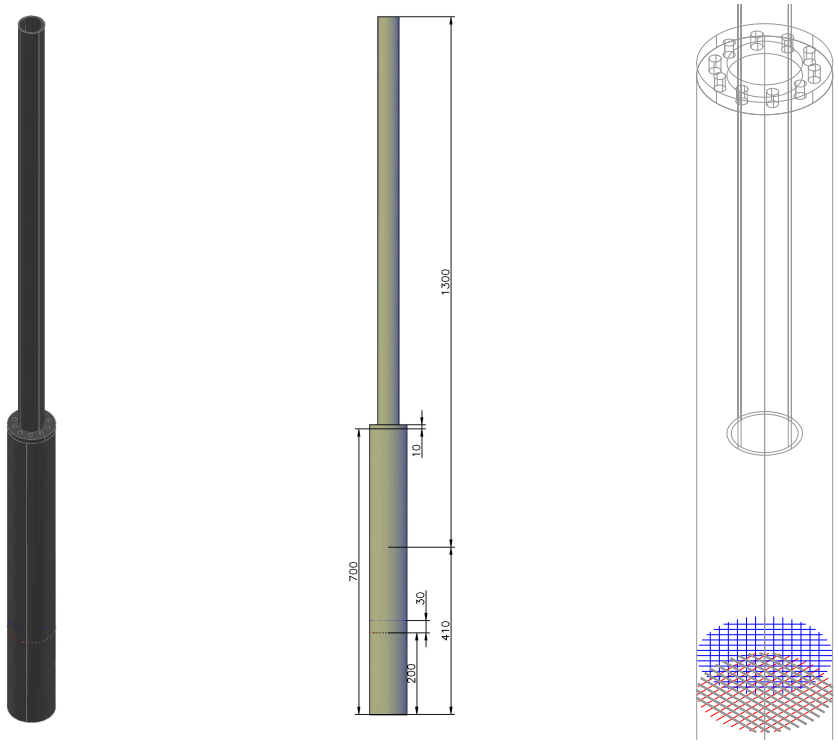

(a) Realistic view. (b) Sketch with dimensions. (c) Close-up of mesh.

Figure 3.2. Pluviation device (sand rainer) used for packing columns of vapor-migration and retardation experiments.

the pipe at distances of about 30 cm and 35 cm from the bottom. The top of the rainer tube was connected to a second HDPE tube (L = 100 cm, OD = 50 mm) and the remaining cross-sectional area was equipped with openings to allow the air to escape during the filling procedure.

The elevation of the sand rainer could be adjusted during the filling of the columns. A feed hopper with a shutter disc at its bottom was located on the top of the sand rainer. The shutter disc (perforated in a seven-hole pattern) controlled the sand mass rate. Different shutter discs with distinct porosities (open fractions of the cross-sectional area) were used to achieve similar packing densities for different grain sizes. The feed hopper was refilled throughout to maintain a constant pluviation. The sand rainer was pulled up stepwise during the filling process. The falling height was kept above the critical falling height of about 25 cm to ensure terminal falling velocity (as proposed by *Rad and Tumay* (1987)). The columns consisting of multiple column sections were filled section after section, each with an overfill of around 30 cm. This prevented additional layering of the porous medium. Prior to connecting the next column section, the overfilled column part was removed by cutting off at the junction of the two sections. The filling was continued for each section, following the same procedure. The columns were sealed with cover plates equipped with a tube fitting (SS-6M0-1-4RT, Swagelok). At the top end of the column, a perforated, stainless steel disc covered with a 50 µm screen mesh, was placed onto the porous medium, held by a stainless steel spring (power rate 4.5 N mm^{-1}, Febrotec, Halver, Germany). The remaining space was filled with glass beads (diameter of 3 mm) in order to

reduce dead volume. After the last column section was packed and sealed, porosity and pore volume were calculated from the mass balance of the material and permeability was measured.

Flume-packing procedure The spill and remediation experiments were conducted in a 2-D flume. Section 4.3.2 describes the set-up of the flume. It was again packed by means of dry pluviation with a sand rainer. In principle, the procedure was copied from the column-packing procedure. A smaller sand rainer was designed which could be introduced into the top opening of the flume. This allowed for a precise distribution of the sand and avoided loosing fractions of small particles by upward air flow and turbulence. The rainer consisted of an aluminum pipe (length of 1 m, outer diameter of 5 cm) with a mesh opening of about 5 mm attached to its bottom. It was moved continuously from one side to the other, back and forth, on a special carriage during the packing. The distance between its bottom end and the material surface in the flume was kept constant. Best possible packing results were achieved by this method. These packings however were not as reproducible as compared to the columns, mostly because of the manual moving of the carriage and due to the turnarounds. Other packing techniques, e.g. where the material rains from a carriage which moves beyond the flume opening in order to avoid turnarounds, could not be applied due to the construction of the flume. Afterwards, porosity was calculated from the material mass balance and the flume was prepared for water saturation.

Since all experiments were conducted at moist conditions, after packing the porous medium was saturated and subsequently drained. This water saturation and drainage cycle (SD) was conducted to induce settling of the porous medium. In the next step, anchoring cement (Ankermörtel 400 Ai, HeidelbergCement, Ennigerloh, Germany) was mixed and a layer of about 1 cm was placed on top of the porous medium. The final sealing consisting of silicone rubber was applied after the hydration of the cement. This guaranteed complete leak tightness and covered potential small cracks at the window or backside and in the porous medium, which could appear due to the deformation of the flume. Water was filled 1 to 2 cm high on top of the sealing to allow visual detection of possible leakages. Finally, the stainless steel top lid of the flume was installed.

3.4. Sampling and monitoring equipment

3.4.1. Pressure and temperature

Various pressure transducers (Cerabar PMP131, Endress+Hausser Messtechnik GmbH & Co. KG, Weil am Rhein, Germany) and temperature sensors (three-wire Pt100, Titec Temperaturmesstechnik GmbH, Bräunlingen, Germany) were used in the experiments. They were connected to a computer via the USB I/O module LabJack U3/U9 and RedLab TEMP, respectively. Data was recorded using the laboratory software (ProfiLab-Expert 4.0, ABACOM, Ganderkesee, Germany) for data acquisition which was customized for each experimental investigation. Ambient pressure data was provided by a close-by meteorological station run by the Department of Hydrology and Geohydrology of the university and by a pressure transducer

(APS-900/1100, Althen GmbH Mess- und Sensortechnik, Kelkheim, Germany) installed in the laboratory hall. In addition, ambient temperature was continuously measured and recorded in the laboratory and vicinity of the experiments.

3.4.2. Saturation/drainage set-up and tensiometers

Retardation of CS_2 in the columns (VRE) and remediation of a liquid spill in the flume (SRE) were investigated in moist porous media. Similar initial conditions for each experiment were guaranteed by a set-up controlling and monitoring saturation and drainage. The drainage of the porous media was realized by means of porous plates or rods exclusively permeable for water when fully saturated. This allowed for setting the water table lower than the bottom of the column or flume. Eventually, this method resulted in a water-saturation profile as observed in the unsaturated zone at a given distance from the groundwater level. The saturations followed the capillary pressure–saturation relationship (Fig. 3.1) measured in the laboratory. According to these measurements, a water level of 1 m below the bottom was sufficient to achieve irreducible water saturation in both fine glass beads and Geba fine sand.

Saturation/drainage set-up Saturation and drainage of the porous medium was realized through a porous plate (column) or rod (flume) made of recrystallized silicon carbid (water wet; Halsic-R, Morgan Advanced Materials Haldenwanger GmbH, Waldkraiburg, Germany). The silicon carbid material was characterized by a pore size of 24 µm and an air entry pressure of around 100 mbar when fully saturated. The porous plate (diameter = 100 mm, height = 8 mm) was glued into a bottom cover plate to seal the columns (VRE). The porous rods (length = 300 mm, o.d. = 30 mm, i.d. = 20 mm) were placed at the bottom of the flume (SRE). In both set-ups they were connected either to a peristaltic pump (7520-47, Masterflex, Cole-Parmer, USA) for saturation of the porous medium with de-ionized water or the drainage set-up (see Fig. 4.5 and 4.6). The drainage set-up consisted of a collection vessel placed on a scale (DE 12K1N, Kern & Sohn, Balingen, Germany) connected to a large-volume barrel to balance the vacuum. The barrel was equipped with a pressure transducer (PR23S, full span ±1 bar, Keller AG, Winterthur, Switzerland) and connected to a vacuum pump (N834.3FTE, KNF, Freiburg, Germany). The negative pressure in the vessel could be adjusted by means of a computer which controlled the vacuum pump and recorded the mass of water drained from the porous medium.

Tensiometer is an instrument which is commonly used in soil science to measure soil moisture tension in the unsaturated zone. Commercially-available types are built for field application, therefore often in larger dimensions and made from plastics to reduce costs. Custom-built tensiometers had to be designed and built to fit the specifications (dimensions and chemical stability) required for the application in the column and flume experiments. The shaft of a tensiometer consisted of a ceramic frit (length = 8 mm, o.d. = 6.5 mm, pore size = 2.5 µm, porosity = 45 %, Porous Ceramics, Soilmoisture Equipment Corp., Santa Barbara, USA) glued in a stainless steel capillary (length = 200 mm, o.d. = 6 mm, i.d. = 4 mm). A connection piece made of Plexiglas connected the shaft with a pressure transducer (PR23S, full span ±1 bar, Keller AG).

Figure 3.3. Gas chromatograph with photoionization detector combined with headspace autosampler.

The pressure transducers were connected to a data acquisition box (Labjack UE9, Meilhaus Electronic, Puchheim, Germany) running the software ProfiLab-Expert for data acquisition. Prior to installation in the experiment, the shafts with ceramic frits were saturated under vacuum with de-ionized, degassed water. Afterwards, the shafts and the pressure transducers were assembled and the tensiometers were calibrated.

Monitoring and data evaluation The capillary pressure measured by the tensiometers during drainage was converted online into effective saturation (Eq. 2.7). Water saturation was monitored at specific locations in the porous medium. This allowed for the observation of the drainage process, of the steady state, and of influences originating from gas flow or soil-vapor extraction on the water saturation. Scales were used to measure the mass of drained water from the porous medium. Thereby, the water mass balance and the mean static water saturation in the experiments were calculated.

3.4.3. Analytics

The characterization of migration, retardation, and remediation of CS_2 in the experiments was based on concentration measurements and mass balances. The physicochemical properties of CS_2 allowed its detection with photoionization detectors. Different analytical set-ups were used according to the needs of the experiment. A gas chromatograph with a photoionization detector (GC-PID HE1, Meta Messtechnische Systeme GmbH, Dresden, Germany) was utilized to measure CS_2 in-line in the experiment outflow. The oven and detector were maintained at 80 °C and nitrogen (ultra high purity) was used as carrier gas. The GC-PID could be combined with a headspace autosampler (HP 7694, Hewlett-Packard, Palo Alto, USA) shown in Fig. 3.3 to measure gas samples. Samples were obtained from the experiments by means of gas-tight micro syringes (549-0559 / 549-1187, VWR, Radnor, USA) and each sample was injected into a pre-closed 20 mL headspace vial for later analysis. In the vapor-retardation experiments, argon was used as a conservative tracer measured in-line with a gas chromatograph with thermal conductivity detector (GC-TCD, Multiple gas analyzer 8610-0270, SRI Instruments Europe GmbH, Bad Honnef, Germany). The oven and detector were maintained at 50 °C and nitrogen was

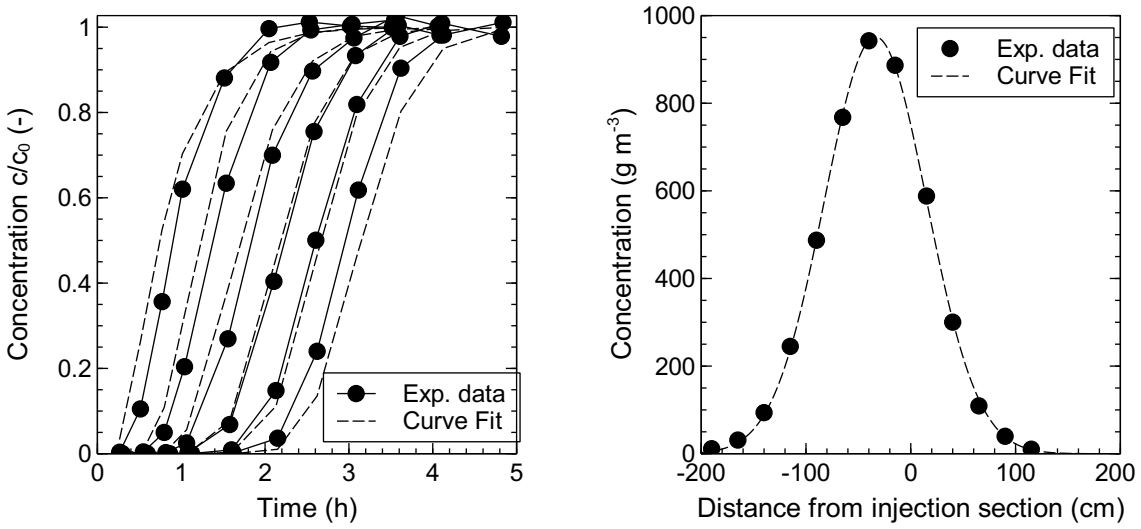

Figure 3.4. Exemplary fitting of measured concentration data of continuous injection (left-hand) and slug injection (right-hand) applied in vapor-migration experiments.

used as carrier gas. All analytical set-ups were calibrated for this specific concentration range either using a single-point calibration or a calibration obtained from concentration standards.

3.5. Data evaluation

3.5.1. Density-driven vapor migration

The data obtained from experiments were processed to quantify density-driven migration as a function of permeability. The analytical solutions described in Section 2.2.5 were used to evaluate the continuous and slug injection experiments.

Continuous injection CS_2 concentration breakthrough curves measured at the sampling ports were evaluated by fitting to the solution of the advection-dispersion equation (Eq. 2.20, point source, semi-infinite domain, Heaviside function) as shown exemplarily in Figure 3.4 (left-hand). The tool CXTfit (*Tang et al.*, 2010; *Toride et al.*, 1995) was used to facilitate the fitting and evaluation procedure. Initially, this code was developed to determine transport parameters (velocity and dispersivity) of one-dimensional solute transport during steady water flow as applied in tracer tests. The method was considered to be valid since injection pressure and flow in the experiments (at atmospheric pressure) were very small, hence compressibility effects could be neglected. Therefore, CXTfit was applicable for these experiments.

Slug injection The CS_2 concentration distribution of each time step (sampling run) was fitted to Gaussian curves using Python (Python Software Foundation, Beaverton, USA) with the modules NumPy and SciPy for statistical evaluation and data fitting. The mean (peak) of the

Gaussian curves plotted over time revealed an acceleration of the heavy vapor starting at a specific moment in time. This behavior was not expected and will be discussed in Section 5.1.1. The evaluation of the experiments was conducted in two stages. The first stage focused on constant migration and the second stage on acceleration. The velocities were obtained from the mean (peak) of the Gaussian curve fits drawn over time (distance-time graph) by fitting the constant migration (Stage 1) with a linear regression and the acceleration (Stage 2) with a fifth order polynomial. Their derivatives yielded a constant migration velocity for the first stage and a continuous velocity function for the second stage of the experiment. These were used for comparison with the numerical simulations.

Theoretical approaches are commonly used to estimate processes prior to conducting experiments or to validate experimental results. *Seely et al.* (1994) introduced two approaches which were applied and adopted in this investigation. First, the Rayleigh number (Eq. 3.3) was used to estimate the importance of density-driven advection competing with gas diffusion in the experiments. It was calculated based on experimental conditions and is defined as

$$Ra = \frac{gkH|\rho_c - \rho_\infty|}{\mu D} \tag{3.3}$$

where k (m^2) is the permeability, H (m) is the vertical spread of the vapor plume in the system, D_{eff} ($m^2\,s^{-1}$) represents the effective diffusion coefficient (*Ho and Webb*, 2006), μ (Pa s) is the dynamic gas viscosity, and ρ_c and ρ_∞ ($kg\,m^{-3}$) are the density of the contaminant vapor and the soil air, respectively. A mean density of the CS_2-vapor plume was calculated based on the injected CS_2 mass and its vertical spread H. A modification of Darcy's law was applied to compare theoretical velocities with constant migration velocities during Stage 1, expressed by

$$u = \frac{kg}{\mu}(\rho_c - \rho_\infty) \tag{3.4}$$

where u ($m\,s^{-1}$) denotes the maximum-expected Darcy velocity of the plume caused by the density difference.

The dispersion coefficient ($D = D^* + \alpha v$) was calculated from the Gaussian curves applying the analytical solution of the 1-D advection-dispersion equation (Eq. 2.21, point source, infinite domain, Dirac-delta function) introduced in Section 2.2.5. This closed solution of the Gaussian curve has its mean (peak) at $z = vt$ and the variance $2Dt$.

3.5.2. Vapor retardation

The investigation focused on obtaining a retardation factor for CS_2 vapor. Possible influences on the determined retardation factors due to experimental artifacts such as a deviation between theoretical and actual gas-effective pore volume had to be taken into consideration. Hence, for each experiment the breakthrough curve of CS_2 was related to that of argon. This ensured the independence from experimentally-induced deviations and thus allowed to quantify the influence of water saturation and migration velocity on retardation.

The data evaluation of the vapor-retardation experiments was carried out using Python with the modules NumPy and SciPy. Concentrations were normalized with respect to the steady-state concentrations ($c = c_{exp}/c_{ss}$). Mass balance was calculated from concentration data and

measured gas flow rates. Data was evaluated based on elapsed time and then correlated via flow rate, resulting from mass flux, to gas-effective pore volume. Moreover, both the slug itself and the nitrogen chase were considered which allowed for an separate evaluation of the slug front and tail (front of nitrogen chase).

Breakthrough curves were evaluated using the temporal-moment analysis (TMA, Sec. 2.3) for a step input (slug) as proposed by *Yu et al.* (1999) and *Luo et al.* (2006). The advantage of TMA "is that no underlying physical model is needed for calculating the travel times" (*Yu et al.* (1999), p. 3571), and the breakthrough curves of the CS_2-Ar mixture (slug front) as well as the N_2 chase (or slug tail) can be evaluated individually. The first two temporal moments of a BTC already reveal more than 80 % of information about the transport behavior (*Leube et al.*, 2012). Moreover, TMA can also be applied to asymmetrical BTCs resulting from non-equilibrium sorption processes during transport. *Fernàndez-Garcia et al.* (2005) encouraged the usage of the temporal-moments analysis to quantify the transport of tracers from breakthrough curves since they efficiently sample the same portion of a porous medium compared to spatial moments.

The measured BTC data had to be prepared to allow for the usage of TMA generally applied to responses from dirac input. The breakthrough curves of the step-input boundary condition (1) were transformed to a dirac-input boundary condition (2). This was achieved by using the derivative of the original step-input BTC data.

$$\frac{\partial c_1}{\partial t} = c_2 \tag{3.5}$$

This transformation then allowed for analyzing the original breakthrough curves and required adapted definitions of the temporal moments introduced in Section 2.3. The first order normalized moment M_1 representing the mean breakthrough arrival time (τ) is then defined as

$$\tau = M_1 = \frac{m_1}{m_0} = \frac{\int_0^1 t\, dc_1}{\int_0^1 dc_1}, \tag{3.6}$$

where c_1 (-) is normalized concentration of measured BTC and t (s or PV) is elapsed time. The second central moment μ_2 corresponds to the variance of travel times at the location of measurement and is given by

$$\mu_2 = \int_0^1 (t - M_1)^2\, dc_1. \tag{3.7}$$

These two moments can be used to directly infer seepage migration velocity v and dispersion coefficient D from BTC data for a one-dimensional system (*Cirpka and Kitanidis*, 2000).

$$v = \frac{z}{M_1} \tag{3.8}$$

$$D = \frac{\mu_2 v^3}{2z} \tag{3.9}$$

The dispersion coefficients obtained from experiments were compared with theoretical values (Eq. 2.12) to evaluate dependency on migration velocity.

Finally, the retardation factor R of CS_2 vapor was calculated from the ratio of the respective moments or mean breakthrough arrival time.

$$R = \frac{\tau_{CS_2}}{\tau_{Ar}} = \frac{M_{1,CS_2}}{M_{1,Ar}} \tag{3.10}$$

Hence, retardation of CS_2 in moist and dry porous media could be compared and the impact of water saturation on retardation of CS_2 could be delineated. Experimental retardation factors were compared with a theoretical factor (Eq. 2.18) composed of the contributions by various processes (terms on the right-hand side): retardation by the gas phase (1), partitioning into the aqueous phase (2), adsorption on the grains (3) and at the gas-water interface (4). In their experiments, *Brusseau et al.* (1997) used carbon dioxide (CO_2) as a tracer whose predominant source of retardation was the partitioning into the aqueous phase. The similarity of CS_2 and CO_2 regarding solubility in water and Henry constant suggests a comparable retardation behavior for CS_2. Hence, partitioning into the aqueous phase is considered the only contribution. Adsorption on grains (3) and at the gas-water interface (4) (terms on the right hand-side of Eq. 2.18) will be neglected. This then yields the adapted theoretical retardation coefficient.

$$R_{CS2} = 1 + \frac{\theta_w}{\theta_a K_H} \tag{3.11}$$

3.5.3. Spill and remediation

The spill of CS_2 was evaluated visually from pictures of the front windows taken at predefined intervals (2 and 10 min). They were post-processed for better exposure and colors (Lightroom 3.4, Adobe Systems, San Jose, USA) and converted to movies (MEncoder, The MPlayer Project). Mass balance and recovery were calculated from concentration measurements, extraction flow rates, and pressures. Flow meters were factory-calibrated for nitrogen at 20 °C and 101.325 kPa, hence flow rates had to be corrected for total pressure, temperature and density of the vapor in the outflow

$$Q_c(P, T, \rho) = Q \times K_c = Q \times \sqrt{\frac{\rho_1}{\rho_2}} \tag{3.12}$$

where Q ($m^3\,s^{-1}$) is the flow rate read from the flow meter, ρ_1 and ρ_2 ($kg\,m^{-3}$) are the densities of the gases, P (Pa) is pressure and T (K) is temperature. Index c refers to corrected flow rate, 1 refers to calibration, and 2 denotes the actual gas/condition. Density of the extracted gas mixture consisting of CS_2 vapor and water-saturated nitrogen at experiment conditions could be calculated according to the ideal gas law

$$\rho_2 = \sum \frac{P_i}{RT} M_i = \frac{P_{CS_2}}{RT} M_{CS_2} + \frac{P_{N_2}}{RT} M_{N_2} + \frac{P_w}{RT} M_w \tag{3.13}$$

where P_i (Pa) are partial pressures of CS_2, dry nitrogen, and water vapor, R ($J\,kg^{-1}\,K$) is the universal gas constant, and M_x ($kg\,mol^{-1}$) is the molecular weight of these components. Partial pressure of CS_2 was determined from concentration measurements,

$$P_{CS_2} = P_t \times \left(\frac{c_{CS_2}}{M_{CS_2}} V_m \right) \tag{3.14}$$

where P_t (Pa) is total pressure at the flow meter and V_m ($m^3\,mol^{-1}$) is the molar volume (ideal gas). Mass recovery was defined as the ratio between cumulative extracted and injected mass of CS_2, while normalized recovery was related to the total extracted mass.

4. Experiments

This chapter introduces the principal set-ups and procedures of the three experimental investigations conducted in this work to explore density-driven vapor migration, vapor retardation, and spill and remediation of liquid CS_2.

4.1. Density-driven vapor migration[1]

4.1.1. Scope

Contaminant vapor (gas) plumes emanating from liquid sources migrate easily in the unsaturated zone. Heavy vapors preferentially migrate downward due to their greater density and thus pose a potential threat to underlying aquifers. Large-scale column experiments and numerical simulations were conducted to investigate the density-driven migration of carbon disulfide (CS_2) vapor. CS_2 is highly volatile and characterized by a very high density (1.6) relative to air when in a gaseous state. The experiments (Fig. 4.1) were conducted in large, vertical columns to investigate the sensitivity of density-driven migration to permeability. Different types of glass beads were used as a porous medium. The porous media were kept dry to avoid partitioning effects into pore water. Gas samples were taken along the column throughout the experiment to quantify time-and-space-dependent vapor migration. The experiments characterized the migration behavior of a heavy CS_2-vapor plume injected in the middle of the column. The boundary installations connected to the top and bottom column outlets were open to the atmosphere, hence considered constant-pressure boundaries. Two types of injection, a continuous and a slug, were investigated: first to characterize the porous medium and delineate the boundary conditions and second to quantify density-driven vapor migration. This set-up allowed for investigating the migration of the injected vapor plume. The set-up of the experiment was reproduced in a 1-D, two-phase, two-component, isothermal, numerical model using two different simulators. Simulation results were compared with data from the vapor-migration experiments.

4.1.2. Experimental set-up

The experiment columns (length = 4 m, i.d. = 0.109 m) consisted of four custom-built column sections (stainless steel pipe 316Ti [1.4571], length = 1 m, i.d. = 0.109 m), as illustrated in Figure 4.2. The sections could be assembled in any order by means of welded flanges (8 bolts, M8)

[1] Section 3.5.1, 4.1.1 - 4.1.5, 5.1.1, and 6.1 published in Kleinknecht, S.M., H. Class, and J. Braun (2015), Density-driven migration of heavy NAPL vapor in the unsaturated zone, Vadose Zone Journal, 14(8), doi:10.2136/vzj2014.12.0173. Reprinted by Permission, ASA, CSSA, SSSA.

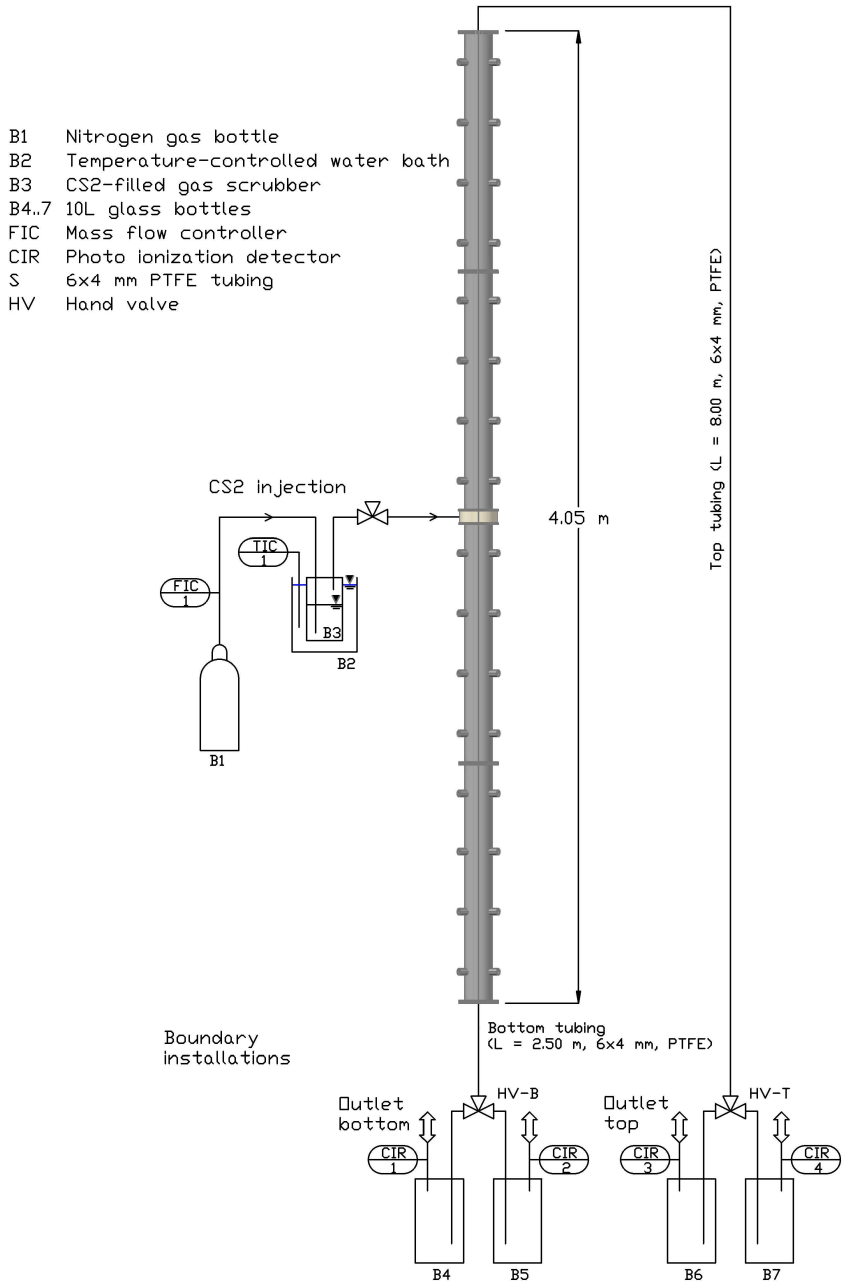

Figure 4.1. Flowchart of the vapor-migration experiment showing column, injection set-up and boundary (outlet) installations in detail (not drawn to scale).

on both ends. One of the flanges of each column section was equipped with a defined groove to hold a FPM O-ring seal (i.d. = 125 mm, width = 4 mm, 80 Shore A) ensuring gas tightness. At the bottom of the column, a perforated stainless steel disc covered with a 50 µm stainless steel screen mesh on top of a 1 cm brace ring was placed on the cover plate prior to packing. At the top end of the column, a similar disc was placed onto the porous medium, held by a stainless steel spring. The space between discs and cover plates was filled with glass beads (diam. of 3 mm) to reduce dead volume. The cover plates sealing the column were equipped with a tube fitting (SS-6M0-1-4RT, Swagelok). The materials of custom-built parts (e.g. columns, sampling ports, and injection section) were chosen based on their chemical stability (see Sec. 3.1).

Four pairs of sampling ports at a center-to-center distance of about 25 cm were welded onto the outer surface of each column section (Fig. 4.2a). They consisted of the following parts (in order): stainless steel mesh (50 µm), casing with inside thread (i.d. = 21 mm), PTFE spacer with 1 mm bore hole, septum and finally a second spacer and nut (Fig. 4.2c). In total 16 sampling ports over the entire length of the experiment column were used for concentration measurements.

A custom-built section was designed to inject the vapor (Fig. 4.3). It was installed in the center of the column in between the second and the third column section (Fig. 4.1). Machined from a PTFE rod with a CNC lathe at the workshop, it was designed as a ring (height = 50 mm, i.d. = 109 mm, o.d. = 164 mm), with the same diameter as the flanges, to fit in between two column sections. On the inside of the ring, an annular gap (height = 30 mm, diam. = 3 mm) was milled into the PTFE and two stainless steel screens made of wire mesh (50 µm supported by a 750 µm mesh) were installed in front of the annular gap. The injection section was equipped with a tube connection (1/4 ″-28G UNF inside thread) at the outside followed by a 1 mm bore hole toward the annular gap.

Vapor migration was quantified in different porous media: coarse, medium, and fine glass beads (Sec. 3.3, Materials and Methods). Glass beads were characterized by a very uniform and narrow grain-size distribution, which hence resulted in very defined and homogeneous packings.

The injection of CS_2 vapor at a constant concentration was critical to the experimental design. Therefore, CS_2 vapor was prepared prior to injection which allowed for decoupling the vaporization from the migration process. The vapor was produced by bubbling pure nitrogen gas through a gas scrubber (Fig. 4.2b) filled with liquid CS_2. This resulted in a mixture of nitrogen and CS_2 vapor. The nitrogen flow was adjusted by a mass-flow controller (EL-FLOW, $Q_{max} = 50\,mL\,min^{-1}$, Bronkhorst High-Tech B.V., Ruurlo, Netherlands) and checked prior to injection using a laboratory bubble flow meter (volume = 50 mL, 20432 Supelco, Sigma-Aldrich). A flow rate of about $Q = 1.5\,L\,h^{-1}$ ($25.0\,mL\,min^{-1}$) was applied. The gas scrubber was built from a stainless steel laboratory vessel with a volume of about 500 mL. Its lid provided an inlet and outlet 1/8 ″ fitting (SS-200-1-2RTBT, Swagelok). The inlet steel capillary (1/8 ″ AlSl 316 high-grade) ended with a stainless steel frit (porosity = 5 µm) at the bottom of the vessel. This facilitated a uniform bubbling. Thereby, CS_2 saturation concentration at given pressure and temperature (approx. $c_{Sat} = 1240\,g\,m^{-3}$, at T = 20 °C, P = 1013 hPa) was obtained. The saturation concentration of CS_2 in nitrogen strongly depends on temperature and pressure. Consequently, the scrubber was placed in a temperature-controlled water bath (Ministat 125, Huber Kältemaschinenbau GmbH, Offenburg, Germany) to guarantee a constant concentration dur-

(a) 1 m stainless steel column section.

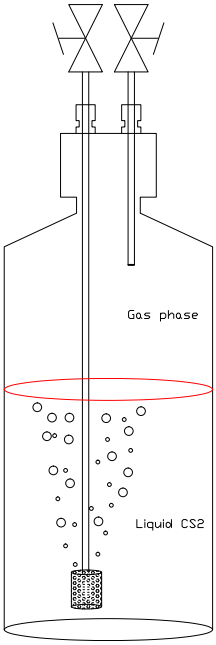

(b) CS_2 gas scrubber.

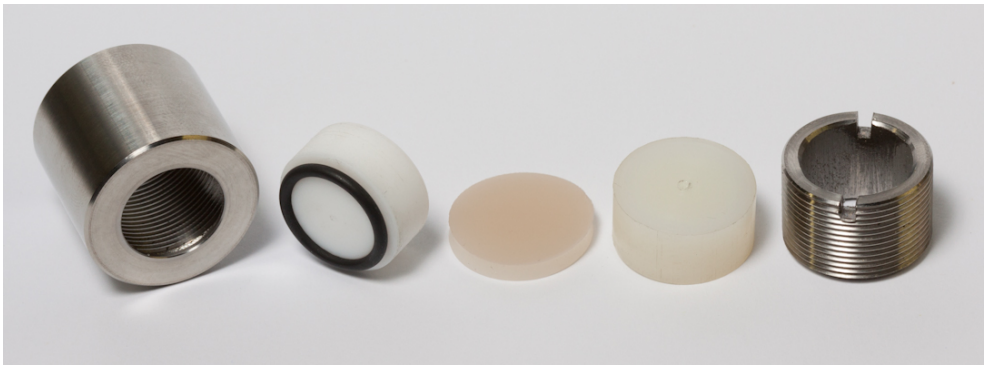

(c) Parts of the column sampling ports in assembling order.

Figure 4.2. Column section, CS_2 gas scrubber and parts of sampling port of vapor-migration experiment set-up.

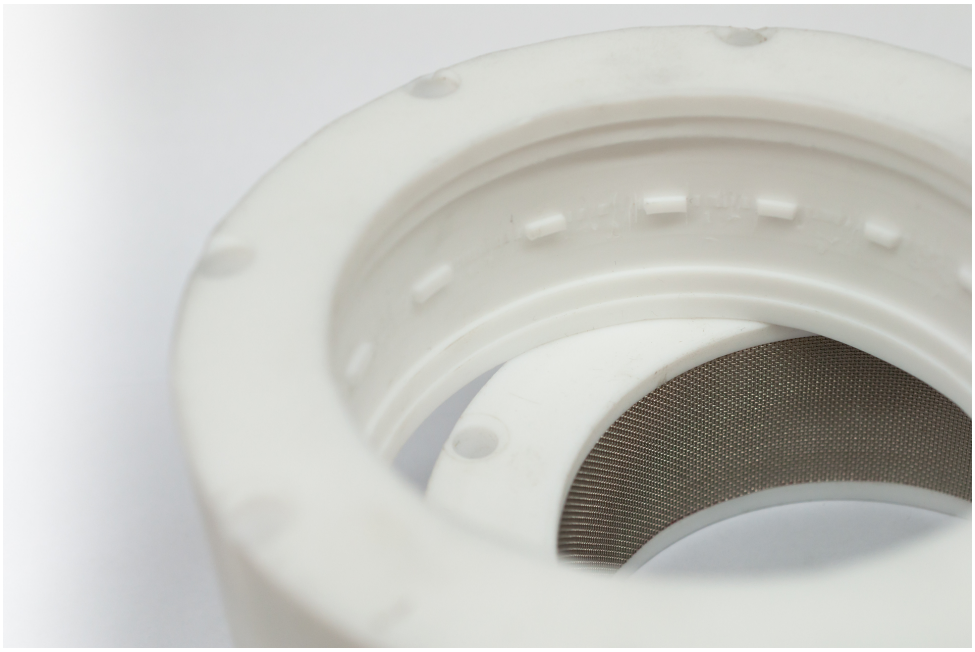

Figure 4.3. Injection section (PTFE) with stainless steel mesh in front of the annular gap (bottom) and bare section (top).

ing the injection duration of the experiments. The vapor (CS_2-N_2 mixture) then left the vessel through the outlet which was connected to the injection section using a 1/8 ″ PFA tube. A flow-through cell with a septum was installed in between to sample the injection concentration. The mass of the gas scrubber before and after the experiment was used to calculate mass rates of CS_2 (Tab. 5.2).

Experiments require well-defined boundary conditions. Hence, the top and bottom of the column were connected to boundary installations at atmospheric pressure (Fig. 4.1). This was required to observe the migration of the injected, heavier CS_2 vapor and to take into account the sensitivity due to minor pressure differences. The installations were realized by attaching PTFE tubes (o.d. = 6 mm, i.d. = 4 mm) to the outlets of the column. The tubing lengths were determined by the spatial arrangement of the column in the laboratory and were kept as short as possible (to avoid higher flow resistance) while ending at the same elevation. The tubing connected to the top and bottom of the column had a total length of 9 m and 3 m, respectively. Each tube end was connected via a T-piece with two hand ball valves to two 10 L glass bottles (Duran Group, Mainz, Germany) collecting the outflow. They were placed below the column. The bottles were sealed with a custom-built stainless steel GL 45 lid with two tube fittings (SS-6M0-1-2RTBT, Swagelok). The first fitting was used to connect a 0.5 m long tubing ending in the middle of the bottle with the hand ball valve. The second fitting was used to connect the bottle outlet to a flow-through cell equipped with a miniature photo ionization detector (PID, ZPP6018001, piD-Tech plus, Baseline-Mocon Inc., Lyons, USA and MiniPID Std, Ion Science Ltd., Cambridge, UK). All bottle outlets (other end of flow-through cells) remained open to the atmosphere, which ensured equal boundary conditions (atmospheric pressure) at the bottle

Table 4.1. Results from gas-permeameter experiments of series with coarse, medium and fine glass beads; flow rate (Q), pressure loss (Δp) and permeability (k).

Series	Parameter						
		1	2	3	4	5	6
Coarse	Q, $m^3 \times 10^{-7}\ s^{-1}$	33.33	66.67	100.00	133.33	166.67	-
	Δp, hPa	0.15	0.35	0.45	0.64	0.78	-
	k, $m^2 \times 10^{-11}$	162.49	139.28	162.49	152.34	156.24	-
Medium	Q, $m^3 \times 10^{-7}\ s^{-1}$	33.33	66.67	100.00	133.33	-	-
	Δp, hPa	1.03	2.3	3.02	3.85	-	-
	k, $m^2 \times 10^{-11}$	23.66	21.19	24.21	25.32	-	-
Fine	Q, $m^3 \times 10^{-7}\ s^{-1}$	0.96	1.89	2.83	3.39	4.70	9.37
	Δp, hPa	0.28	0.55	0.79	0.97	1.29	2.59
	k, $m^2 \times 10^{-11}$	2.49	2.56	2.65	2.60	2.70	2.68

Table 4.2. Properties of porous media (packing) in vapor-migration experiments.

Parameter	Glass beads Coarse	Glass beads Medium	Glass beads Fine
Porosity (ϕ)	0.34	0.34	0.40
Permeability (k), m^2	1.5×10^{-9}	2.4×10^{-10}	2.6×10^{-11}
System permeability (k_s), m^2	6.3×10^{-10}	3.8×10^{-10}	8.1×10^{-11}

outlet and a barometric pressure distribution inside the column.

Gas permeameter experiments were conducted after packing the columns to determine the permeability of the porous medium. Two differential pressure transducers (GMUD MP-F & GDH 200-07, Greisinger electronic GmbH, Regenstauf, Germany) with an operation range of 0.01 to 2.5 mbar and 0.01 to 200 mbar, respectively, were used. They were connected to the top and bottom sampling port of the column ($\Delta x = 3.75$ m). Various N_2 flow rates were applied and the corresponding head loss was measured. Permeability was calculated from these measurements using Eq. 3.2. Table 4.1 shows the applied gas flow rates, the measured pressure losses as well as the corresponding permeability.

Observed influences of the boundary installations (tubing) on the migration behavior required further consideration. Therefore, pseudo-permeabilities were determined from pressure loss measurements of the boundary installations (tubing, manifolds and bottles). They were used to calculate the harmonic-average permeability (*Ahmed*, 2001) of the total set-up consisting of top tubing, porous medium and bottom tubing, henceforth referred to as system permeability (Tab. 4.2).

4.1.3. Sampling and monitoring

Gas samples were taken at predefined intervals to monitor vapor migration in the column along with injection and outflow boundary conditions. Samples of 100 µL were taken from the sampling ports of the column and injected into pre-closed 20 mL headspace vials for later analysis. The small sample volume minimized disturbances of the system. The total sampled volume compared to the pore volume was approximately 0.3 %. Sampling was carried out simultaneously by two people, starting from the injection section proceeding from port to port upward and downward, respectively. Moreover, sampling personnel was trained to pull the syringe plunger as smoothly as possible to minimize disturbances. No spatial or temporal duplicate samples were taken. Hence, effects from the sampling on vapor migration, as well as sampling-induced movement can be neglected. The sampling interval was adapted to the migration velocity expected in a given porous medium.

The injection concentration was determined based on samples (volume = 100 µL) taken from the flow-through cell installed between the gas scrubber and the injection section. In addition, the bottles of the boundary installations collecting the vapor were sampled. The bottles contained around 50 boiling beads (diam. = 3 mm) in order to homogenize the gas phase by shaking the bottles prior to sampling. The photo ionization detectors were used to measure the increase of concentration in the glass bottles and to determine the point in time when switching to the spare bottle and subsequently sampling of the former one was carried out. At that point, the valve to the spare bottle was opened before the valve to the bottle in use was closed. After disconnecting the bottle, it was shaken for at least one minute. Two gas-tight syringes, a 500 µL syringe for sampling and a 10 mL syringe for purging the tube were attached to the bottle. After having purged the sampling tube with excess volume, the 500 µL gas sample was taken and injected into a 20 mL vial. Finally, the bottle was purged with air and reconnected to the boundary installations to serve as the spare bottle in the next sampling run.

Samples were analyzed by a GC-PID combined with a headspace autosampler (see Sec. 3.4.3 and Fig. 3.3). CS_2 concentrations could be measured up to saturation concentration. The calibration concentration of the GC-PID ranged from 36.4 to 1212.2 g m^{-3}. The gas calibration standards were prepared by injecting liquid CS_2 into a gas sampling tube (volume = 1000 mL, made of borosilicate glass, cf. DIN 12473-1:1976-04). After equilibration, two samples of each syringe volume 30, 50, 100, 250, 500, and 1000 µL were taken and injected into pre-closed headspace vials. Ambient temperature and atmospheric pressure were recorded during the preparation procedure.

4.1.4. Experimental procedure

Continuous injection Two series of experiments were conducted, the first in coarse and the second in medium material (glass beads). The purpose of the continuous injection was to first study migration and diffusion/dispersion of the CS_2 vapor (distribution) in a porous medium until steady state was reached. Thereby, the migration behavior and the porous medium could be characterized. These then laid the basis for the slug-injection experiments which were conducted to quantify density-driven migration of a vapor plume. The column was purged from the bottom with nitrogen (2 to 4 PV) to establish reproducible initial conditions.

The experiment was started with the continuous injection of heavy CS_2 vapor (q_{CS2} = const.). A constant nitrogen flow rate of 1.5 L h^{-1} bubbling through liquid CS_2 resulted in the injected CS_2-N_2 mixture. The injection flow rate corresponded to a unidirectional seepage velocity of about 80 cm h^{-1}. The injection was maintained until the same concentration was reached at all ports below the injection section. Once steady state had been reached, the injection was shut down and the experiment was terminated.

Slug injection Three series of experiments were conducted resulting in two experiments in coarse, three experiments in medium and two experiments in fine material (glass beads). Within each series the columns were not repacked. Comparability between experiments was ensured by applying the same injection mass flux of CS_2 vapor. It was defined by an injection duration of 1.25 h and controlled by a constant nitrogen flow rate of 1.5 L h^{-1} resulting in the injected CS_2-N_2 mixture. This configuration was chosen based on results of preceding continuous-injection experiments where migration behavior was first investigated. Utmost care was taken to control experimental/boundary conditions (CS_2 mass flux, duration of injection and top/bottom outlet installations). The column was purged from the bottom with nitrogen (2 to 4 PV) to establish reproducible initial conditions.

The experiments could be divided into two parts once the columns had been prepared. In the first part, the experiment was started with the injection of heavy CS_2 vapor (q_{CS2} = const.). The column and the injection flow were sampled every 0.25 h until shutdown of the injection ($q_{CS2} = 0$, t = 1.25 h). Thereafter in the second part, the vapor migration was only driven by the density difference between the heavy CS_2 vapor and the ambient nitrogen. The column was sampled at frequent intervals defined by the porous medium. In coarse and medium material, the sampling interval was set at 0.5 h for the first 4.0 h. Thereafter, the interval was increased to 1.0 h until the end of the experiment. In fine material, an initial sampling interval of 0.5 h was changed after 3.0 h to a 1.0 h interval. After 10.0 h a 2.0 h interval was used until the end of the experiment. The experiment was terminated when the peak of the concentration distribution passed the lowest sampling port.

For both types of injection, a slight deviation of the CS_2 mass flux between experiments was noticeable due to technically-induced temperature changes of the water bath affecting the CS_2-vapor saturation concentration.

4.1.5. Numerical model

Model description

The purpose of the numerical simulation was to model the experiments with the correct boundary conditions and to compare their results with the observed migration behavior. In addition, it was employed to understand the impact of the boundary conditions on migration. The experimental set-up (Fig. 4.1) was reproduced using a 1-D, two-phase, two-component, isothermal model (Fig. 4.4). Two different simulators were used: the in-house, open-source simulator DuMu^x and Shell's proprietary software Dynamo/MoReS. Both simulators used the fully-implicit

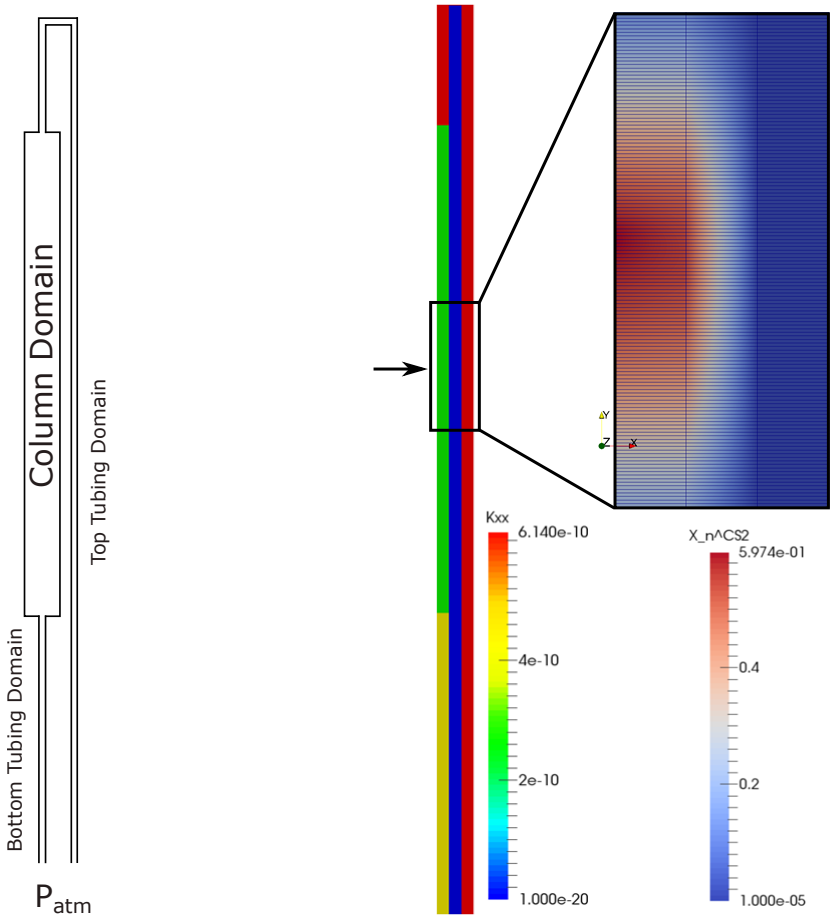

(a) Model domains.

(b) Snapshot with ongoing vapor injection and close-up showing grid cells.

Figure 4.4. 1-D model of vapor-migration experiment.

discretization scheme with the finite volume method. DuMu^x employed the ideal gas law (Eq. 2.25) and MoReS used Peng-Robinson equation of state (Eq. 2.26) to calculate fluid states. Both simulators employed Darcy's and Fick's law to calculate advective and diffusive transport, respectively.

The flow domain of the model included the porous medium of the column as well as the tubing connected to the top and bottom outlet of the column. Thus, the numerical model represented the actual experiment column as well as the experimental boundary conditions (described in Sec. 4.1.2). It consisted of three grid cells in x-direction and 1710 cells in z-direction. This resulted in a grid cell height (z-direction) of 0.5 cm. The model domain may be visualized as an upside down "U" (Fig. 4.4) consisting of two individual 1-D domains (one representing column and bottom tubing; the other one representing the top tubing) each connected via their topmost cells only. In between the two domains a barrier domain was placed and was characterized by a very low porosity and permeability, preventing any cross flow. Thus, all domain boundaries (left, right, top, front, and back) as well as the barrier domain between the two 1-D domains

Table 4.3. 1-D model specifications used for vapor-migration modeling.

Parameters	Column	Tubing	
		Bottom	Top
Length (x), m	0.1	0.1	0.1
Height (z), m	4.05	3.5	9.55
Permeability (k), m^2	Tab. 4.2	6.03×10^{-10}	6.86×10^{-10}
Porosity (ϕ)	Tab. 4.2	1.34×10^{-3}	1.34×10^{-3}
Number of grid cells in z-direction, no.	810	700	1710
Diffusion coefficient (D), $m^2\,s^{-1}$		9.71×10^{-5}	
Initial temperature (T), K		293.15	
Bottom-boundary pressure (P), bar		1.01325	

were considered no-flow (Neumann boundary). The bottom of the domain was open to the atmosphere, hence modeled as a constant-head (Dirichlet) boundary. The model was still a 1-D model even though the two vertical, parallel domains were connected via their topmost cells.

Table 4.3 shows the parameter values used in the model. The left leg consisted of the 3.50 m long bottom tubing domain followed by the 4.05 m long column domain and on top the 1.00 m long top tubing domain. The right leg represented the remaining 8.55 m of the tubing attached to the top end of the column. The tubing was implemented as a porous medium with a porosity which resulted in the same effective cross-sectional area as the tubing (inner diameter of 4 mm) used in the experiment. The permeability was calculated from experimentally-measured pressure losses of the boundary set-up of the experiment (tubing, manifolds and bottles) related to the length of the tubing. The CS_2 injection mass flux determined from the experiments was scaled to the cross-sectional area of the model.

Initially, the flow domain was saturated with nitrogen. The temperature was set to 293.15 K and the bottom boundary was at a pressure of 1.013 25 bar. The initial pressure distribution of the gas phase was calculated using the barometric formula. This was essential as a constant pressure over height would have resulted in overestimated migration velocities. The injection of CS_2 was realized by a constant mass flux into ten grid cells accounting for 5 cm of height at the appropriate location in the column domain.

The simulation output included the volumetric flux in z-direction of one grid cell in the column domain as well as the concentration of CS_2 at the positions of the sampling ports. This allowed for a direct comparison with the downward-migration velocities and the concentration data of the experiments and could be employed for sensitivity analysis and history matching purposes.

Sensitivity analysis and history matching

Sensitivity analysis Sensitivity analysis is a commonly-applied method in numerical investigations contributing to a better understanding of the processes and parameters involved.

Variation ranges for selected input parameters of interest are defined and their impact on the simulation output is being evaluated. Numerical simulations in soil science typically include parameters of porous media such as permeability and porosity in a sensitivity analysis of a model. In addition, they employ experiment or field-related parameters to complete the set.

Dynamo/MoReS's built-in tools were used to investigate the sensitivity of the simulation output to the input parameters. For this purpose, a multi-run deck was created which employed a Tornado design for handling the simulation runs. In statistics, Tornado, among others, is a commonly-used experimental designs. As *Yeten et al.* (2005) writes: "[an] experimental design method is an alternative to traditional sensitivity analysis. The basic idea behind this methodology is to vary multiple parameters at the same time so that maximum inference can be attained with minimum cost. Once the appropriate design is established and the corresponding experiments (simulations) are performed, the results can be investigated by fitting them to a response surface. This surface is usually [a function] ... which is cheap to sample. Therefore it can be used as a proxy to reservoir simulation to quantify the uncertainties." The Tornado design allowed for parameter screening by iteratively varying one parameter at a time. The worker deck (the original input file) was modified for parameter variation (Varmodels) and specification of ranges in which each parameter had to be varied. Among the parameters (multipliers) were permeability of the porous medium, porosity, diffusion coefficient of CS_2 in nitrogen, mass flux of the injected vapor mixture, injection duration, permeability of the tubing domain, length of the bottom tubing domain, and maximum time step size. They were varied, employing a symmetric triangular distribution where the lower and upper value of the range were defined as factors multiplied with the input parameters.

Observation data sets were created from experiments containing CS_2 concentrations as well as migration velocities (linear regression and fifth-order polynomial; see Fig. 5.9) which could be included into Dynamo/MoReS. The sensitivity analysis was evaluated using Pareto plots obtained from simulation runs of the Tornado design. The Pareto plots visualized the relative contribution of the variation parameters (bars) in descending order and the cumulative total (line). The plots show which of the input parameters were the most significant or to which the simulation output was most sensitive. In a second step, the parameters were weighted with uncertainties known from experimental experience. The results identify the most sensitive parameters subsequently utilized for history matching.

History matching The term history matching or inverse modeling refers to a key method in applied research where a particular numerical model is built accounting for real or experimental data. It is used to validate and/or calibrate numerical models based on the available measured data. In this work, this method was used to validate the numerical model which was developed to simulate the vapor-migration experiments and to evaluate the initial guess of the input parameters (input value).

For this purpose the DuMu^x model was combined with iTOUGH2-PEST (*Finsterle*, 2007; *Finsterle and Zhang*, 2011). iTOUGH2 provides a number of minimization algorithms for the calibration of a model against measured data. The Levenberg-Marquardt method was chosen as the minimization algorithm to find the minimum of the objective function. The PEST protocol

enables the communication between iTOUGH2 and the external application DuMu^x. Hence, these tools provide the required inverse modeling capabilities to DuMu^x.

Two separate history matching cases were performed utilizing the model introduced above. The sensitivity analysis demonstrated which parameters are principally controlling the density-driven downward migration of the heavy CS_2 vapor. The initial situation (reference simulation) was described by input parameters (permeabilities, porosity, mass flux, etc.) determined from the experimental set-up or the experiments themselves. The original values of these input parameters were denoted as input values. The history matching output suggested best match factors which had to be multiplied with the input values of the respective parameters to obtain the best match simulation. The first case (C1) involved history matching with the parameter system permeability only. The output of the simulation runs was compared with the velocity data obtained from the particular experiments. Recalling that the available data consisted of absolute concentrations measured in the experiments, the possibility that they were affected by inaccuracies of analytics, manual gas sampling and temperature/pressure changes during the experiment had to be taken into account. The migration velocities can be considered as derived observations with the advantage that they are independent from absolute concentrations.

The second case (C2) involved the parameters system permeability, porosity, and mass flux of CS_2. Two sub-cases were investigated: the first (C2a) only took into account the velocity data of the experiments whereas the second (C2b) additionally involved concentration data of CS_2 at four discrete locations in the column domain (Port +3, −1, −4, and −7; see Fig. 4.1). Comparing both sub-cases allowed to evaluate the consequence of more observation data sets on the inverse-modeling performance (direct correlations of parameters). Hence, history matching is utilized to validate the numerical model and to confirm the understanding of the physical processes involved.

Summary

- Column experiments were designed to quantify the density-driven migration of heavy CS_2 vapor in dry porous media.
- Experiment columns (length = 4 m, i.d. = 0.109 m) were packed with coarse, medium, or fine glass beads. Top and bottom column outlets were open to the atmosphere (constant pressure).
- CS_2 vapor was injected continuously and as a slug into the middle section of the column and concentrations were measured at the ports along the column throughout the experiment.
- CS_2 concentration profiles of experiments with the slug injection were fitted to Gaussian curves and compared with a 1-D ADE to quantify diffusion/dispersion and advection of the migrating CS_2 vapor.
- A numerical model was built to simulate the vapor migration and to compare the results with the experiments.

- The model was used to conduct two sensitivity analyses to determine the parameters of greatest impact on the migration.
- Two history matching cases were designed using the parameters based on the sensitivity analyses: the first case (C1) employed the parameter system permeability to match migration velocities and the second case (C2) used the parameters system permeability, porosity, and mass flux of CS_2 to match migration velocities as well as selected concentration data.

4.2. Vapor retardation

4.2.1. Scope

Retardation or retention effects on transport are of major interest when assessing the danger of groundwater contamination by migrating vapor plumes. The migration of vapor plumes due to density differences was demonstrated in the previous part of this work. Now, this part focuses on characterizing retardation effects. Processes such as adsorption on sand grains or partitioning to soil water might reduce the migration velocity and thus the total contaminant mass eventually reaching and potentially endangering the groundwater.

Experimental and numerical studies (e.g. *Brusseau et al.*, 1997; *Corley et al.*, 1996; *Kim et al.*, 1998) have been conducted in the past to investigate retardation of the most common volatile organic carbons (VOC) in unsaturated porous media. Those studies showed a contaminant mass distribution among the bulk phases (air, water and solid), the air-water interface, and intraparticle pores for unsaturated and saturated conditions. *Kim et al.* (2001, 2005) assumed that the total retardation is a sum of different phase-partitioning effects as a function of water saturation. They demonstrated experimentally that the total retardation factor of VOCs initially rises with water saturation and at some point reverts as saturation further increases. The effect of water saturation on retention has also been described by *Cabbar and Bostanci* (2001) and *Maxfield et al.* (2005) who discovered retardation to be negatively correlated to water saturation due to adsorption on the solid phase. The latter have additionally shown the dependency of retardation on the properties of the chemical compound of interest. For instance, noble gases show no retardation behavior at all.

This component and water saturation dependent behavior of gas-phase retention emphasizes the necessity for a thorough investigation and quantification of retardation effects of CS_2 in unsaturated porous media. Thereby, fundamental knowledge about its potential to delay or prevent a contamination of an underlying aquifer is gained. This goal was reached by conducting column experiments designed to quantitatively characterize retardation/retention of CS_2 on a large scale with clearly-defined and controlled boundary conditions.

4.2.2. Experimental set-up

The experiments were conducted in vertical, stainless steel columns of 2 m length with different porous media (Fig. 4.5). The experiments were carried out at dry conditions as well as at irreducible, static water saturation. Irreducible water saturations (initial conditions) were obtained by saturation of the porous medium with water and subsequent drainage under controlled conditions. A finite slug of gaseous CS_2 and a tracer was simultaneously injected via an injection section at the bottom of the column. The conservative tracer used was argon which is not affected by retardation. It has been used for this purpose in other studies e.g. *Maxfield et al.* (2005). Effluent concentrations of CS_2 and argon were measured online at the top outlet of the column. The bottom of the column was realized as a constant-mass-flux boundary while the top is open to the surroundings, hence, at constant pressure.

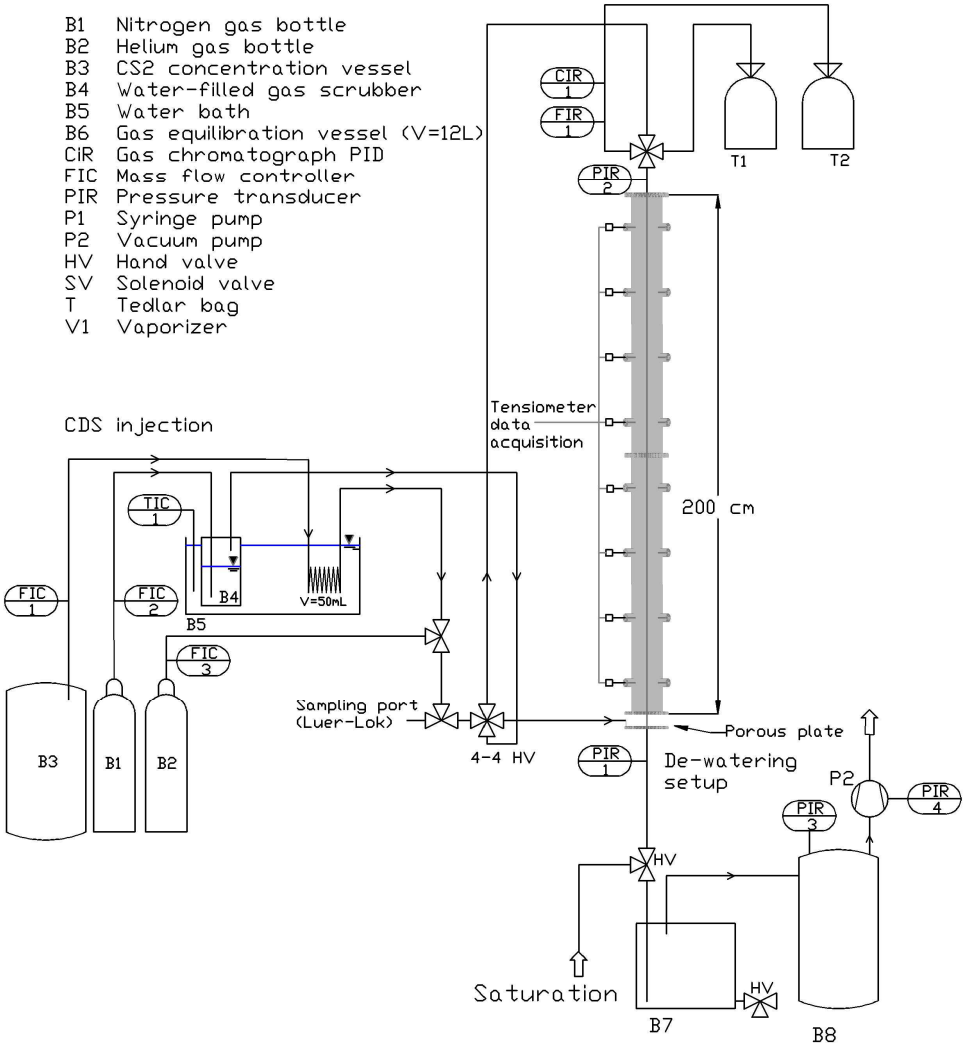

Figure 4.5. Flowchart of vapor-retardation experiment showing column, injection and saturation/drainage set-up.

The column (length = 2 m, i.d. = 0.109 m) consisted of two custom-built, 1 m long sections (Fig. 4.2a). At the bottom of the column, the injection section with a base plate was installed. Into this base plate, a porous plate made of recrystallized silicon carbid was glued to act as a suction plate for the water drainage (see Sec. 3.4.2). At the top end of the column, a perforated stainless steel disc, covered with a 50 µm stainless steel screen mesh and held by a spring, was placed onto the porous medium. The space between the disc and the cover plate was filled with glass beads (diam. of 3 mm) to reduce dead volume.

The ports of the column (Fig. 4.2a) consisted of a casing with inside thread (i.d. = 21 mm), a PTFE spacer with 8 mm bore hole, an O-ring, and a nut with a 8 mm tube connection (Swagelok) to install custom-built tensiometers to monitor the water saturation.

The custom-built injection section (Fig. 4.3) was installed at the bottom of the column (Fig. 4.5). This configuration allowed for the injection of a finite slug at a predefined mass flux and, in addition, for a controlled upward nitrogen flow stabilizing the vapor front.

The CS_2 vapor was prepared prior to injection. A predefined amount of liquid CS_2 was injected into a barrel (V = 50 L) and pressurized to an excess pressure of about 2 bar with N_2 to ensure defined vapor properties. Then the barrel was left overnight to equilibrate. The tracer argon was provided from a gas cylinder purchased from Westfalen AG, Münster, Germany. Constant mass fluxes of the injected CS_2 vapor and of the conservative tracer (argon) were critical to the experiment. Mass fluxes of argon, CS_2 vapor, and nitrogen were controlled by mass-flow controllers (EL-FLOW, Q_{max} = 3, 50, and 100 mL min^{-1}, Bronkhorst High-Tech B.V., Ruurlo, Netherlands). The resulting flow rates were checked using a bubble flow meter to account for the current ambient temperature and pressure since MFCs were calibrated for air at standard conditions (0 °C and 1013.15 hPa). Complete gas tightness of the entire set-up was ensured by using 1/8 ″ stainless steel capillaries throughout. Two 4-4 way lever operated valves (HVP 86779, Hamilton Bonaduz AG, Switzerland) allowed for flow-direction control. The inlet steel capillary loop (length = 4 m) and the scrubber were placed in a temperature-controlled water bath (Ministat 125, Huber Kältemaschinenbau GmbH, Germany) to minimize temperature-induced fluctuations during the experiments.

The slug of the gas mixture (CS_2, argon, and the carrier nitrogen) was injected and then pushed through the column using a N_2 chase at the same flow rate. Prior to injection into the column, argon (approximately Q_{Ar}/Q_{total} = 1.4 %) was added to the total flow. The mass balance was closed based on the measured flow rate, and the injection and effluent concentrations. The second objective of the nitrogen chase was to observe the recovery of the contaminant and reversibility of partitioning processes. In case of moist experiments, the gas mixture slug was humidified with ultra-pure water (RH = 100 %) to avoid a drying-up of the moist porous medium. For the preparation of the gas-mixture slug, a custom-built miniature vaporizer (ICTV, University of Stuttgart, Germany) with an ultra-low volume pump (M6, VICI AG International, Schenkon, Switzerland) was used. The nitrogen used for the chase was bubbled through a gas scrubber filled with ultra-pure water.

Vapor retardation was characterized for different porous media: fine glass beads and Geba fine sand (Tab. 3.2). Their grain-size distributions as well as capillary pressure–water saturation relationships are illustrated in Fig. 3.1. The columns were packed by dry pluviation. Porosity

and theoretical, gas-effective pore volume were calculated from the mass balance of the material and, in case of moist porous media, the remaining water content. Detailed information about the materials and packing procedure are given in Sec. 3.3 of Materials and Methods.

4.2.3. Sampling and monitoring

In the column outflow, CS_2 and argon concentration were measured to quantify retardation in dry and moist porous media. Two gas chromatographs were directly connected in-line to the column outlet. CS_2 concentrations were determined using a GC-PID and argon concentrations were determined using a GC-TCD (see Sec. 3.4.3). Single-point calibrations were conducted prior to and after each run. Measurement intervals were set depending on the flow velocity such that a high temporal resolution (0.021 to 0.065 PV) of the breakthrough curves was obtained. Prior to the start of the slug injection, the concentration of CS_2 and argon in the slug mixture was measured as a base to normalize concentrations. The water saturation was monitored using the installed tensiometers at the column ports. In addition, the column was placed on a scale to permanently monitor its weight and thus the total amount of pore water. A relative pressure transducer connected to the column inlet before the injection section was used to monitor the injection pressure. Since the top column outlet was open to the atmosphere (P_{atm}), this corresponded to the pressure loss caused by the flow through the porous medium. Temperature sensors and absolute pressure transducer continuously measured and recorded ambient and water bath temperature as well as atmospheric pressure in the vicinity of the experiment.

4.2.4. Experimental procedure

Various experiment series were conducted in two different porous media (fine glass beads and Geba fine sand) under both dry and partially saturated (moist) conditions. Within each series the columns were not repacked and no saturation-and-drainage cycle (SD) was carried out since first tests proved that the partitioning processes were fully reversible. The water saturation or total amount of pore water was monitored throughout the experiment. The slug of the gas mixture was injected with a predefined mass flux into the bottom of the 2 m long column such that it resulted in the designed migration velocity. In each series, experiments were performed with different velocities including 25, 50, 100, and 200 $cm\,h^{-1}$ (approx. 0.125, 0.25, 0.5, and 1.0 $PV\,h^{-1}$) to observe effects on retardation by kinetics. A slug of about 3.5 PV was used which corresponded to injection durations of approx. 3.5, 7, 14, and 28 h depending on the respective velocities. This ensured a residence time (plus safety factor) sufficient to attain steady-state conditions and for partitioning processes to reach equilibrium.

The experiments were conducted in four steps. In the first step, the flow rates (slug and chase) were adjusted to match the target migration velocity. In the second step, the column was flushed with nitrogen. While maintaining constant flux, the inflow was switched to the slug injection of the gas mixture in the third step. After injecting 3.5 PV it was switched back to the nitrogen chase (fourth step).

Summary

- Column experiments were designed to quantify the retardation of heavy CS_2 vapor due to partitioning effects in moist porous media.
- Experiment columns (length = 2 m, i.d. = 0.109 m) were packed with fine glass beads or Geba fine sand.
- Different water-saturation profiles in the porous media were obtained by means of saturation and subsequent drainage.
- A slug of CS_2 vapor and argon (conservative tracer) was injected at the bottom of the column (constant-flux boundary) and concentration breakthrough curves were measured at the top outlet (constant-pressure boundary).
- The temporal-moment analysis (TMA) was used to quantify diffusion and dispersion of CS_2 and argon as well as retardation of CS_2 at different seepage velocities.
- The experimental retardation coefficients of CS_2 for different water saturations were compared with a theoretical approach.

4.3. Spill and remediation

4.3.1. Scope

Contaminations by hazardous liquids demand a fast response and an efficient remediation technique to prevent further damage or threat. Various techniques have been developed in the last decades which need to be evaluated regarding feasibility and efficiency taking into account the physicochemical properties of the contaminant and the environmental conditions. Hence, this part of the work addresses the remediation of a spill of liquid CS_2 in the unsaturated zone. The technical requirements involved that it is an in-situ technique suitable for the remediation of a CS_2 spill. Moreover, the prevailing boundary conditions of the unsaturated zone have to be taken into consideration. The removal of contaminant vapor from dry and moist porous medium by a nitrogen flush was successfully shown in the vapor-retardation column experiments. Based on the column investigations, soil-vapor extraction appeared to be the method of choice. This had to be taken to a more realistic scenario where the contaminant resided as a liquid phase (i.e residual distribution or pool) in a moist porous medium, from which it had to be remediated. Therefore, two-dimensional spill and remediation experiments (SRE) were conducted. They allowed for a combined investigation of the liquid distribution of CS_2 into moist porous media at irreducible water saturation and the subsequent remediation using soil-vapor extraction (SVE). The main objective was to provide experimental data required for the dimensioning of remediation parameters such as extraction flow rate and duration as a function of spill geometry, hydrogeology, and vaporization dynamics of CS_2 which highly affect the efficiency in a field application.

The experiments were designed and conducted in a 2-D flume. A detailed description of the experimental set-up is given in the following section. The flume was filled with a porous medium which was water-saturated and subsequently drained prior to each experiment to obtain a static water saturation (similar initial conditions for each experiment). Tensiometers installed at the rear side of the flume monitored the drainage process and water saturations throughout the experiments. Fine glass beads or Geba fine sand were used as porous medium. The flume filling technique ensured homogeneous packings. However, the different grain-size distribution of the two materials and different spill types were expected to influence the distribution of CS_2.

The sequence of the experiment was to first observe the spreading of liquid, dyed CS_2 in a homogeneous porous medium at irreducible water saturation in a 2-D domain. In the second step, the heterogeneously-distributed liquid contaminant residing in the pore space and its vapor was to be removed employing soil-vapor extraction under controlled conditions. CS_2 concentrations were measured in the extracted soil vapor of the flume to evaluate mass removal. In addition, the initial CS_2 distribution and the effect of SVE were visualized qualitatively. Proof of concept was thus based on parameters such as different porous media, spill types, and effective soil-gas velocities as well as contaminant removal observed during the remediation process.

4.3.2. Experimental set-up

The spill and remediation experiments were conducted in a 2-D flume. Figure 4.6 illustrates the experimental set-up consisting of the flume itself, the clean-gas inflow and soil-vapor extraction part, the saturation/drainage set-up, and concentration measurement.

The flume had dimensions of 1.00 x 0.70 x 0.12 m (see Fig. 4.6 and 4.7a). The bottom, the sides, and the back were made of stainless steel plates (1.4539). A 3 cm thick glass window allowing for visual observation during the experiments was pressed against an extruded PTFE tape (2 cm x 0.5 cm) fixed on a bearing area on the front side. The packing of the flume was carried out through the open top of the flume which could be sealed by means of a steel plate as described in Sec. 3.3. The back of the flume was equipped with 23 ports (either 6 mm or 8 mm compression fittings) which could be used to install tensiometers, horizontal wells or to pass tubings to the outside. Two vertical wells used for clean-gas inflow and soil-vapor extraction were installed at the left-hand (inflow) and right-hand (extraction) side of the flume. They were built from perforated metal rods (o.d. = 5 cm) covered by a 50 µm stainless steel mesh. The top and the bottom of these wells were connected via tubings leading to the inflow and extraction peripherals outside. Figure 4.7a shows a picture of the empty flume with the two wells installed on each side.

CS_2 distribution and remediation was investigated in two different porous media: fine glass beads and Geba fine sand (Tab. 3.2). Fine glass beads were characterized by a very uniform and narrow grain-size distribution ranging from 100 to 200 µm. Geba fine sand was defined by a wider distribution of 63 to 350 µm. Further information, capillary pressure–water saturation relationships, and description of packing procedure are given in Section 3.3 of Materials and Methods.

The flume was saturated and drained using the equipment introduced in Section 3.4.2. Two 30 cm long porous rods were embedded in the sand at 2 cm from the bottom of the flume before packing was continued (see Fig. 4.7b). They were connected via tubings through ports (#6 and #22) to the saturation and drainage set-up. Custom-built tensiometers, introduced in Sec. 3.4.2, were installed at ports number 2, 5, 7, 9, 12, 18, and 21 (Fig. 4.6). Tensiometer data recorded during drainage provided water-saturation profiles. Additionally, the static water saturation (initial condition) could be verified prior to each experiment. Moreover, water saturations were monitored during soil-vapor extraction.

Two different methods, single-port or multi-port injection, were applied for the demonstration of a liquid spill of CS_2 and for the observation of CS_2 migration and distribution in moist porous media. A constant, predefined mass flow was maintained by either a diaphragm pump (Stepdos 03, KNF Flodos AG, Sursee, Switzerland) or a syringe pump (PHD Ultra, Harvard Apparatus, Massachusetts, USA). The pumps were connected to a stainless steel transport vessel (V = 500 mL), filled with CS_2 covered with de-ionized water. CS_2 was dyed with hydrophobic Oil Red O ($C_{26}H_{24}N_4O$, CAS Number 1320-06-5, Sigma-Aldrich) for better visibility.

The single-port injection was conducted using a horizontal well (stainless steel, o.d. = 6 mm). It was perforated over the width of the flume (0.12 m) and was installed at port 8. The membrane pump injected water into the transport vessel, thereby injecting CS_2 into the porous medium.

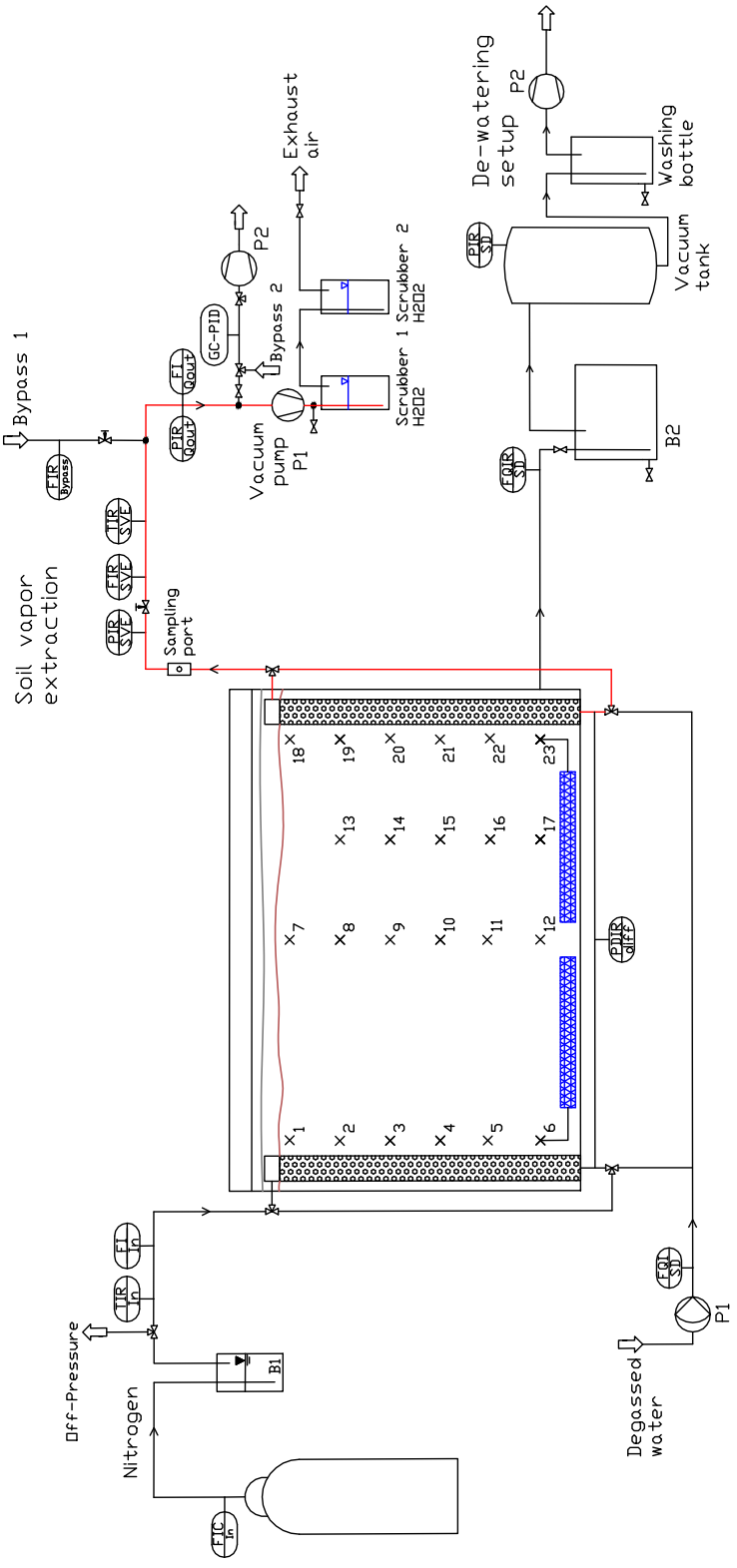

Figure 4.6. Flowchart of spill and remediation experiment, showing 2-D flume with peripheral devices.

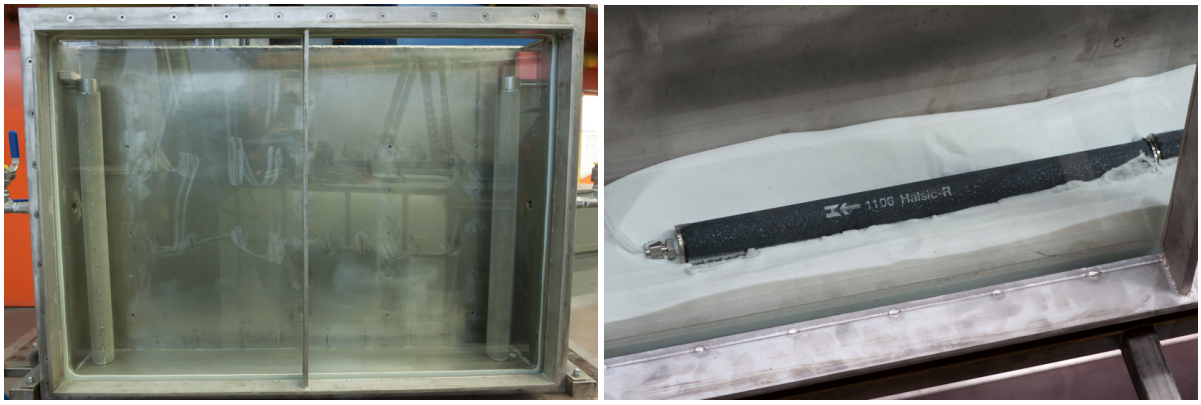

(a) Empty flume showing vertical wells used for clean-gas inflow (left-hand) and soil-vapor extraction (right-hand).

(b) Placement of porous rods on first layer of porous medium used for management of water saturation.

Figure 4.7. Pictures of the 2-D flume used for experiments.

Mass balance could be determined from the mass difference of the vessel, the known mass of water pumped into the vessel and the densities of both liquids. First results of single-port injections into fine glass beads (see Sec. 3.3) showed that CS_2 followed one preferential flow path to the bottom of the flume resulting in a wide-spread pool at the bottom of the flume, only leaving a residual trace along its pathway.

No visual observation of the spreading but only of the pooling was observed with the single-port injection. For this reason, the multi-port injection was developed to avoid the preferential downward migration of CS_2 and, instead of that, achieve a wide-spread residual distribution in the region of high relative permeability for gas. The multi-port injection was carried out by means of a stainless steel needle (L = 200 mm, o.d. = 1 mm) perforated over a length of 30 mm at its tip. The needle was inserted successively into ports 8, 9, 13, and 14 (labeled in Fig. 4.6) and a volume of 3 mL each was injected at three different positions, starting from the back, over the middle to the front side. The flow was controlled by means of the syringe pump. The syringe (V = 10 mL, VWR International GmbH, Darmstadt, Germany) was connected to the injection needle and the transport vessel via a T-union and the predefined volume of about 9 mL (7.126 g), injected into one port, could be directly withdrawn from the vessel. A tubing (L = 2 m, o.d. = 1/8 ") open to the surroundings was connected to the vessel to allow for the withdrawal of CS_2. Mass balance of CS_2 was determined by the mass difference of the vessel at the end of injection and verified by the volume dispensed by the syringe pump. This method resulted in a better controlled injection over width, thus spreading of liquid CS_2 could be observed on the window front. The spreading of CS_2 was recorded by a camera taking pictures of the front window at an interval of 2 min during the spill and 10 min after the spill until the start of extraction.

The spill of liquid CS_2 was to be remediated using soil-vapor extraction. The vertical wells were used for clean-gas inflow (left-hand side) and vapor extraction (right-hand side) establishing a horizontal gas flow field. Flow rates were determined manually from variable-area flow meters (see Sec. 4.3.3 Sampling and Monitoring). For safety reasons, nitrogen was provided

on the inflow side at a predefined flow rate to avoid the connection to the atmosphere and thus possible leakages of CS_2 from the flume. A drying-up of the moist porous medium was prevented by bubbling humidified nitrogen through a scrubber bottle. The total flow rate of the humidified nitrogen was set to always stay above the extraction flow rate. A pressure relief opening at 2 mbar was used to allow the excess volume to leave and thereby prevent an undesired pressurizing or active gas injection into the flume.

The extraction was achieved by means of a vacuum pump (MZ 2, vacuubrand GmbH, Wertheim, Germany). Total extraction flow rate could be adjusted by means of needle valves allowing additional gas inflow at the inlet of the pump (bypass). This was necessary to reduce the total flow rate to the defined soil-vapor extraction rate (Bypass 1) while keeping the absolute pressure of the system close to pressures measured during field applications. A second bypass (Bypass 2) was used to dilute the extracted vapor in order to decrease the CS_2 saturation concentrations thus allowing for the operation of the gas chromatograph. Strong deviations from atmospheric pressure could falsify analytical results due to compression or expansion of the gas phase in the sample loop of the gas chromatograph.

4.3.3. Sampling and monitoring

An extensive monitoring set-up and procedure was developed to measure CS_2 concentrations, flow rates, pressures, and temperatures during the experiments. The CS_2 mass balance was determined and evaluated based on these parameters.

The high volatility of liquid CS_2 was responsible for concentrations up to saturation concentration in the vapor extracted from the flume. These high concentrations in the outflow could last for at least 2 PV. The duration was mainly controlled by the distribution of liquid CS_2 in the porous medium. In this period, CS_2 concentrations could not be directly measured by the GC-PID. Hence, gas samples had to be taken manually at an interval of 5 min from a customized flow-through cell equipped with a septum installed at the outflow. This high frequency was necessary to accurately cover the period of high mass recovery and minimize mass balance errors resulting from sample deviation. Samples were taken by 100 µL or 500 µL gas-tight syringes for high or low concentrations, respectively, and subsequently injected into 20 mL headspace vials. The vials were analyzed by the GC-PID combined with the autosampler. CS_2 calibration ranged from 7 to 1210 $g\,m^{-3}$. Linearity of the GC-PID was tested and verified for concentrations up to 1560 $g\,m^{-3}$.

Manual sampling was replaced by the continuous concentration measurement with the GC-PID (Sec. 3.4.3) once concentrations decreased below 250 $g\,m^{-3}$. The sampling interval was then decreased to 10 min. Still, a dilution (Bypass 2, Fig. 4.6) was required to further decrease absolute concentration at the GC-PID sampling inflow. The GC-PID was calibrated with outflow gas samples analyzed with the autosampler. During the decrease of concentration, the dilution ratio had to be adapted and the GC-PID was re-calibrated with the autosampler. The GC-PID could be operated without dilution once outflow concentration dropped below 0.15 $g\,m^{-3}$. A single-point calibration ($C = 0.1\,g\,m^{-3}$) was utilized. The measurement interval was set to 10 min during operation with dilution and to 30 min once dilution had been shut off.

Gas inflow and outflow was read from variable-area flow meters. They were installed at the inflow (EW-32460-40, flow rate from 100 to 500 mL min^{-1}, Cole-Palmer), outflow (UNIFLUX 1/4 ", flow rate from 60 to 600 mL min^{-1}, Influx Measurements Ltd., Hampshire, UK), Bypass 2 (FAG D10A1197, flow rate from 46 to 1180 mL min^{-1}, ABB, Zürich, Switzerland), at the sample-in of the GC-PID (UNIFLUX 1/4 ", flow rate: 5 to 100 mL min^{-1}, Influx Measurements Ltd.), and Bypass 1. A camera took pictures of the flow meters installed at the outflow and Bypass 2 at a 15 min interval (FIR-SVE, FIR-Bypass). In addition, all flow meters were manually read when gas samples were taken.

Temperature and pressure are important parameters regarding vaporization of liquids and for the accurate calculation of volume fluxes of gases. The soil-vapor extraction set-up was equipped with two temperature sensors and three pressure transducers connected to the data acquisition system. Temperature sensors (Pt100) were installed in the inflow (TIR-In) and outflow (TIR-SVE) tubing. A differential pressure transducer (Sitrans-P DS3, full span 0.06 to 6.00 hPa, Siemens, Karlsruhe, Germany) was connected to the inlet and outlet of the flume for continuous measurement of pressure losses caused by the flow through the porous medium. On the extraction side of the flume, one relative pressure transducer was installed at the outflow and a second at the sampling location of the GC-PID. This ensuring a thorough monitoring of the vapor-extraction process.

4.3.4. Experimental procedure

Two series of experiments were conducted in the flume to observe the spill and distribution of liquid CS_2 and to investigate its remediation using soil-vapor extraction. In the first series fine glass beads were used and the second series was conducted with Geba fine sand. The experiments could be divided into several steps. Within one series the flume was not repacked but a saturation-and-drainage cycle was carried out prior to each experiment. This did not apply to Experiments 7 and 8 in order to maintain identical initial conditions as those of Experiment 6 to investigate the impact of different soil-gas velocities on remediation. The water saturation was monitored throughout the experiments. The porous medium at irreducible water saturation was flushed with humidified nitrogen, concluding the preparation of the initial conditions. In the first part of the experiments, the spill of liquid CS_2 was carried out and the spreading was observed at the window front of the flume. Two different injection methods, the single-port and the multi-port injection, introduced in Sec. 4.3.2, were used to observe different CS_2 distributions. Subsequently, the flume was left to equilibrate for 12 h to reach similar conditions.

Then the second part of the experiment was initiated by starting the remediation using soil-vapor extraction. This involved frequent manual sampling of the soil-vapor extraction during the first phase of high concentration before switching to the continuous concentration measurement. The soil-vapor extraction was shut down when CS_2 concentrations decreased below the defined threshold and was restarted after 24 h of equilibration to observe potential rebound effects. Finally, the experiments were terminated once no CS_2 could be measured in the extraction flow and the flume was flushed excessively with nitrogen prior to conducting the next experiment.

Summary

- Experiments in a 2-D flume were designed to observe the distribution of liquid CS_2 in moist porous media and investigate the in-situ remediation technique using soil-vapor extraction.
- The flume (1.00 x 0.70 x 0.12 m) was packed with fine glass beads or Geba fine sand.
- The moist porous media was obtained by means of saturation and subsequent drainage establishing static water-saturation profiles (initial conditions).
- Spills of liquid, dyed CS_2 were performed using either a single-port (continuous) or a multi-port (interrupted) injection and the distributions were observed at the window front.
- Two vertical wells were used for clean-gas inflow (left-hand side) and vapor extraction (right-hand side) establishing a horizontal gas flow field.
- CS_2 concentrations, extraction flow rates, temperatures, and pressures were recorded to quantify the mass removal.
- The impact of different porous media, mean soil-gas velocities (extraction rates), and inflow temperatures on the remediation performance was investigated.

5. Results and discussion

5.1. Density-driven vapor migration

5.1.1. Large-scale column experiments

Two types of column experiments were conducted to explore density-driven vapor migration in dry porous media. These differed in the boundary conditions for CS_2-vapor injection thus allowing for a clear differentiation of density-driven advection from dispersion. The continuous injection helped describe the porous media and the experimental system. The slug injection was realized to observe migration of the established plume only controlled by the density difference at the prevailing boundary conditions.

The experiments were characterized by the variations of the permeability (porous media) and the type of injection. The total number of experiments was determined by a combination of the variables plus one repetition for each of them. In general, the experimental/boundary conditions (injection type, CS_2 mass flux, and top/bottom outlet pressure) were kept constant as far as technically feasible. CS_2 mass flux was influenced by nitrogen flow rate and temperature of the water bath containing the gas scrubber (Fig. 4.1). It slightly deviated between experiments due to technically-induced temperature changes of the water bath affecting CS_2-vapor saturation concentration.

Comparability between experiments was ensured by a constant nitrogen flow rate of about $25\,mL\,min^{-1}$. This flow rate was chosen based on the continuous-injection experiments, taking into account porosity, pore volume and permeabilities of the column packings. In the following paragraphs, one selected experiment with continuous and one with slug injection is described in detail before summarized results are discussed. Time data is related to the start of injection.

Continuous-injection experiment

Continuous CS_2-injection experiments were conducted to characterize the general behavior of density-driven vapor migration. They provided fundamental parameters about the porous media and the observations helped to decide on an injection flow rate and injection duration (for the total injected CS_2 mass) later applied in the slug-injection experiments. The boundary conditions of these experiments were characterized by the constant-pressure boundary at the bottom and top outlets and the continuous injection (q_{CS2} = const.) throughout the experiment. Table 5.1 summarizes the experimental conditions.

Table 5.1. Experimental conditions of the vapor-migration experiments with continuous injection.

Series	Glass beads Coarse		Glass beads Medium	
Experiment	1	2	3	4
CDS mass flow, $g\,h^{-1}$	3.02	3.02	2.77	2.84
Absolute pressure, hPa	974	952	980	950
Ambient temperature, °C	20.7	21.7	21.7	20.8
Bath temperature, °C	18.4	19.0	18.0	18.1

Exemplary description Figure 5.1 shows the CS_2 breakthrough at the sampling ports of the column and temperature recordings as a function of time for Experiment 1 in coarse material. The upper part of the graph shows concentrations of the ports above and the lower part of the ports below the injection section. Same graph colors represent equidistant sampling ports from the injection section. The maximum of the y-axis of these graphs show in opposite directions and the origin represents the location of injection. The lowermost part shows temperature recordings of the water bath and temperature of the surroundings close to the column and near the bottles connected to the column outlets.

Gas samples were taken from the sampling ports at predefined intervals (Sec. 4.1.3). The injection concentration of CS_2 was sampled four times with an average of $1343.1 \pm 33.8\,g\,m^{-3}$ during the experiment (samples are depicted in the first graph of Fig. 5.1 as crosses). After starting the injection, concentrations increased steadily at the sampling ports around the injection section. A downward migration of CS_2 vapor due to the density difference compared to nitrogen was clearly observed after around one hour of continuous injection. CS_2 was measured only as far as the fourth sampling port (90 cm) above the injection section (Port +4) reaching there a maximum at around 1.75 h. CS_2 concentration measured at the sampling ports below the injection location reached a maximum concentration after around 3 h. Breakthrough at the column bottom was around 2.5 h, indicated with "circle" symbols in the lower graph (samples of bottom outlet bottle). The bottle sampling procedure is described in Section 4.1.3. The density induced downward migration of the entire gas phase in the system resulted in a siphoning of air into the column through the top opening. This caused a dilution of the injection concentration observed as a decrease in Figure 5.1. Steady state was reached after around 5 h.

Figure 5.2 shows concentration profiles over column length for selected time steps. The injected CS_2 vapor spread around the injection section at $t = 0.3$ h and, subsequently, the front propagated downward. After approximately 1.0 h, maximum concentrations were reached just underneath the injection section. This concentration front migrated downward for approx. 2.5 to 3.0 h. Then, the just described dilution process resulted in the reduced concentrations. Steady state was reached when the effect of the air inflow finally reached the bottom of the column after around 5.0 h.

CS_2 mass balance is summarized in Figure 5.3 showing mass fraction of CS_2 over time. The cumulative injected mass was calculated from the mass flow determined by the mass balance

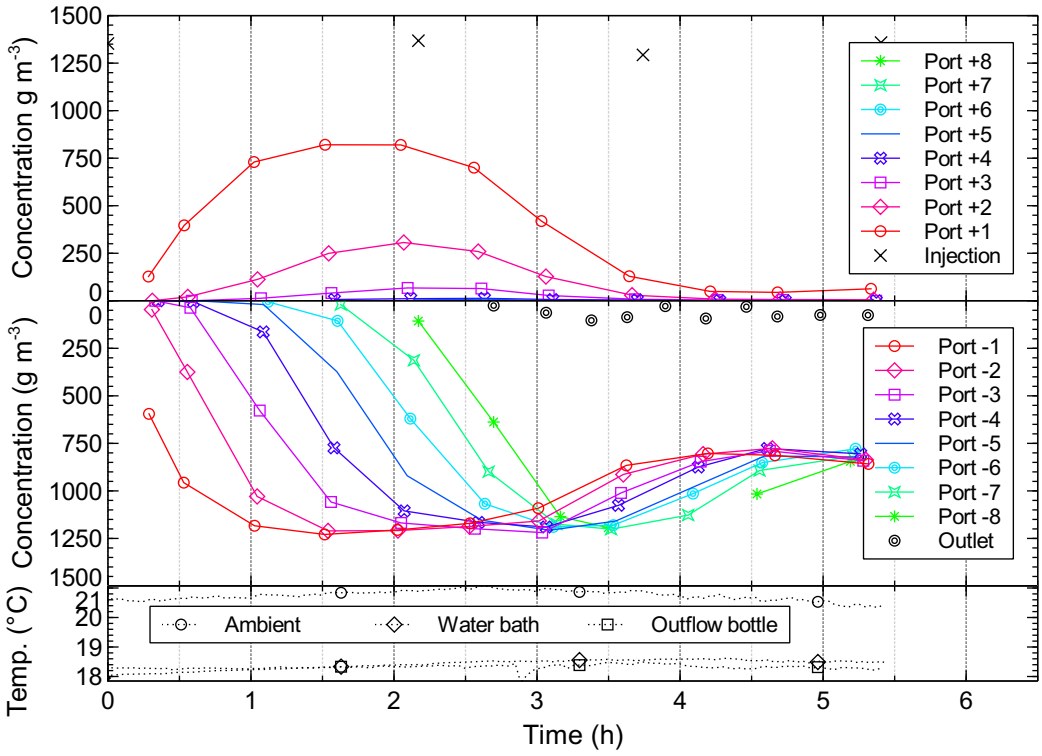

Figure 5.1. Breakthrough curves and temperature recordings of continuous-injection experiment (Exp. 1) in coarse material.

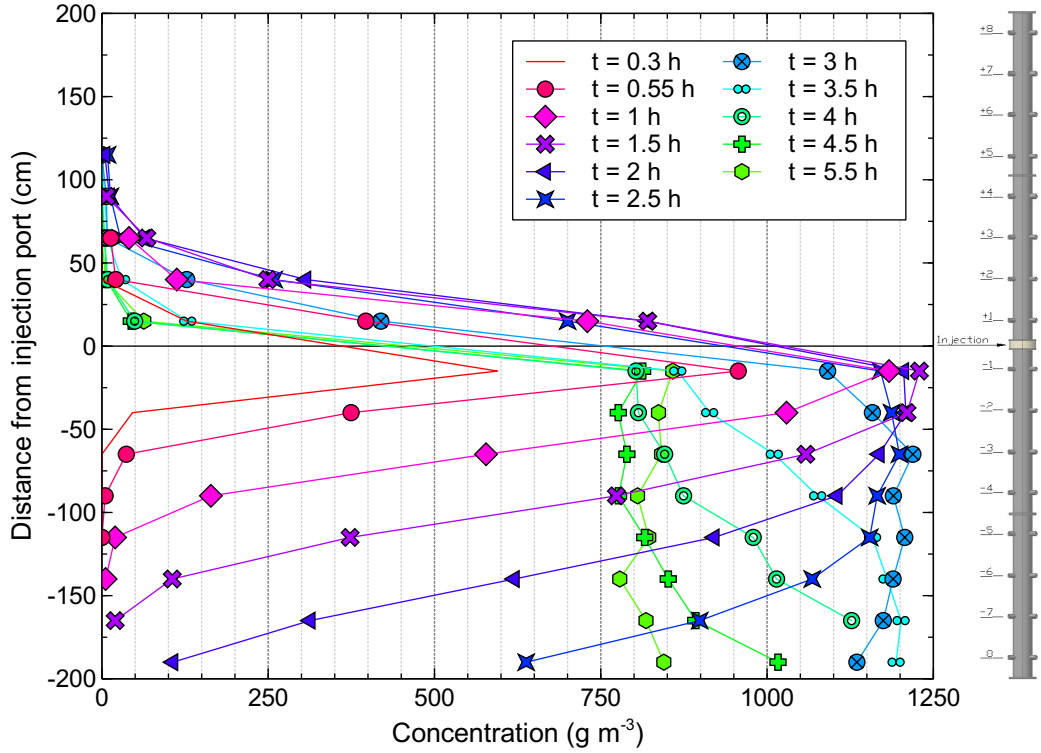

Figure 5.2. Concentration profiles in the column at different points in time of continuous-injection experiment (Exp. 1) in coarse material.

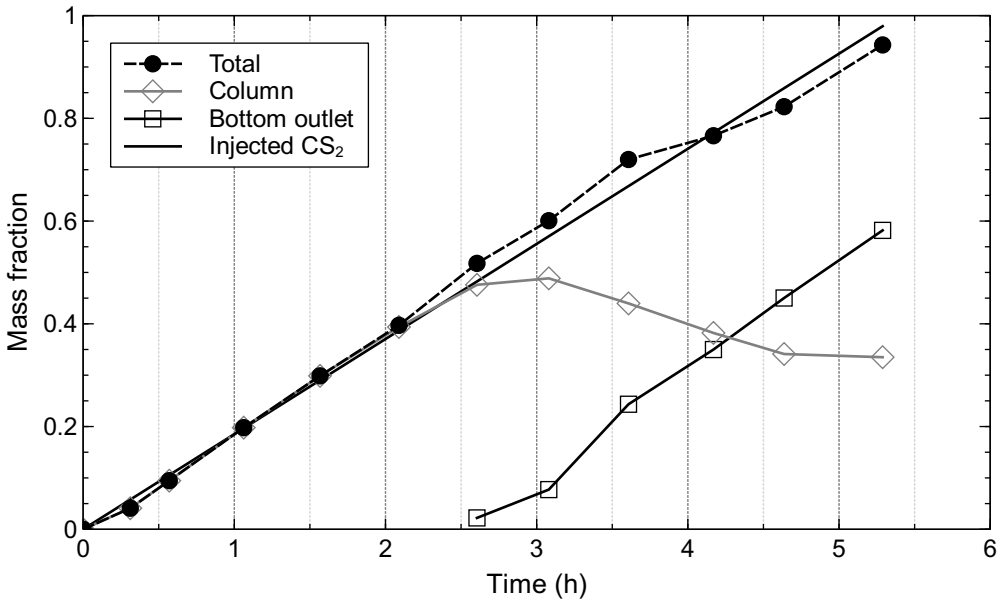

Figure 5.3. CS_2 mass balance (cumulative injected mass, mass residing in column, cumulative collected mass in bottom outlet bottles, and total mass of experiment) of the continuous-injection experiment (Exp. 1) in coarse material.

of the CS_2 gas scrubber (see Sec. 4.1.2). The sum of the mass residing in the column (calculated from samples and pore volume of the column) and the cumulative mass collected in the bottom outlet bottles yielded the total CS_2 mass in the experiment. A deviation of 5 % between the total CS_2 mass from measurements and cumulative injected mass is considered satisfactory taking into account the inaccuracy of gas sampling and the open boundaries. A total CS_2 mass of 16.32 g was injected as vapor. At steady state, 5.47 g (36 %) still resided inside the pore space of the column and 9.92 g (0.64 %) were recovered from the bottom-outlet bottles.

The flow of the CS_2 vapor was controlled by the constant mass flux and by gravity depending on the total vapor mass in the column. This is illustrated in Figure 5.2 showing the concentration profiles. The higher the amount of mass residing inside the porous medium, the higher the potential for the downward migration. The maximum mass in the column was measured after 3.1 h of continuous injection, see Figure 5.3. This state was responsible for the high potential for downward migration resulting in the air siphon eventually reducing the steady-state concentrations.

Summarized results In total four experiments, two in coarse and two in medium material, were performed. Table 5.1 shows the experimental conditions of the experiments with continuous injection in dry porous media.

The measured concentrations over time were evaluated by fitting the breakthrough curves with the advection-dispersion equation (Eq. 2.20) using the CXTFIT 2.0 excel plugin described in Section 3.5.1. The breakthrough curves show that the injected CS_2 vapor accelerated, which

complicated the aim of a single fit including all BTCs (illustrated in Fig. 3.4). Therefore, the BTCs were fitted separately between two ports at a time to avoid these difficulties and thus allowed for evaluating the transient behavior. Figure 5.4 shows migration velocity and dispersivity over distance from the injection section of the column. Results of the experiments in coarse glass beads are shown on the left-hand side and the plots for the medium ones on the right-hand side. The migration of the injected CS_2 vapor and the resulting concentration breakthrough at the ports were determined by the constant injection mass flux and were additionally driven by gravity. A constant mass flux into porous media with similar porosities results in a similar front propagation. However, an average velocity of about $62\,cm\,h^{-1}$ in coarse and $50\,cm\,h^{-1}$ in medium glass beads was observed. This could be explained by the additional migration due to gravity depending on permeability while the mass flux was constant. The acceleration was apparent from the velocity increase with distance from the location of injection occurring in both series. Dispersivity ranged from 2 to 4 cm in both materials. Similar dispersivity values were expected due to the same porosity and the uniform grain-size distribution of the glass beads.

A comparison of the unidirectional velocity of about $80\,cm\,h^{-1}$ with the velocities calculated from the breakthrough curve fits revealed that the CXTfit tool was not directly applicable. This was due to the different initial conditions as compared to tracer tests in groundwater flow. The experiments were characterized by a superposition of flow induced by the boundary conditions and flow due to gravity (density difference). The gas phase in the column was initially at rest and the injected CS_2 vapor could flow upward and downward from the injection section. Once a critical mass was exceeded, the vapor started the density-driven downward migration. This caused a change in the upper constant-head boundary condition eventually siphoning air responsible for the dilution and reduced concentration at steady state. Typically, a tracer is injected into an already-existent groundwater flow and does not itself induce migration; however forced tracer tests exist dealing with similar challenges regarding data evaluation as seen in this case. Consequently, the results from CXTfit were used to understand the system and its boundary conditions but the obtained parameters could not be taken as final values. Furthermore, the adapted evaluation to only fit between two breakthrough curves, instead of a single fit including all BTCS, increased the parameter uncertainty.

The experiments conducted with continuous injection showed clearly that gravity controlled the transport of the heavier CS_2 vapor. Moreover, it depended on the total injected vapor mass in the column. These experiments were crucial for defining the initial and boundary conditions of the slug-injection experiments. Based on the results, an injection duration of 1.25 h with a similar mass flux was selected for the experiments with slug injection. This ensured reaching a critical total CS_2 mass required to start density-driven migration while remaining in a time frame where it could still be considered a pulse.

Slug-injection experiment

Slug type of injection in the vapor-migration experiments was carried out to extend the knowledge gained in the previous experiments and to characterize density-driven migration of a finite vapor plume. The boundary conditions of these experiments were constant pressure at the

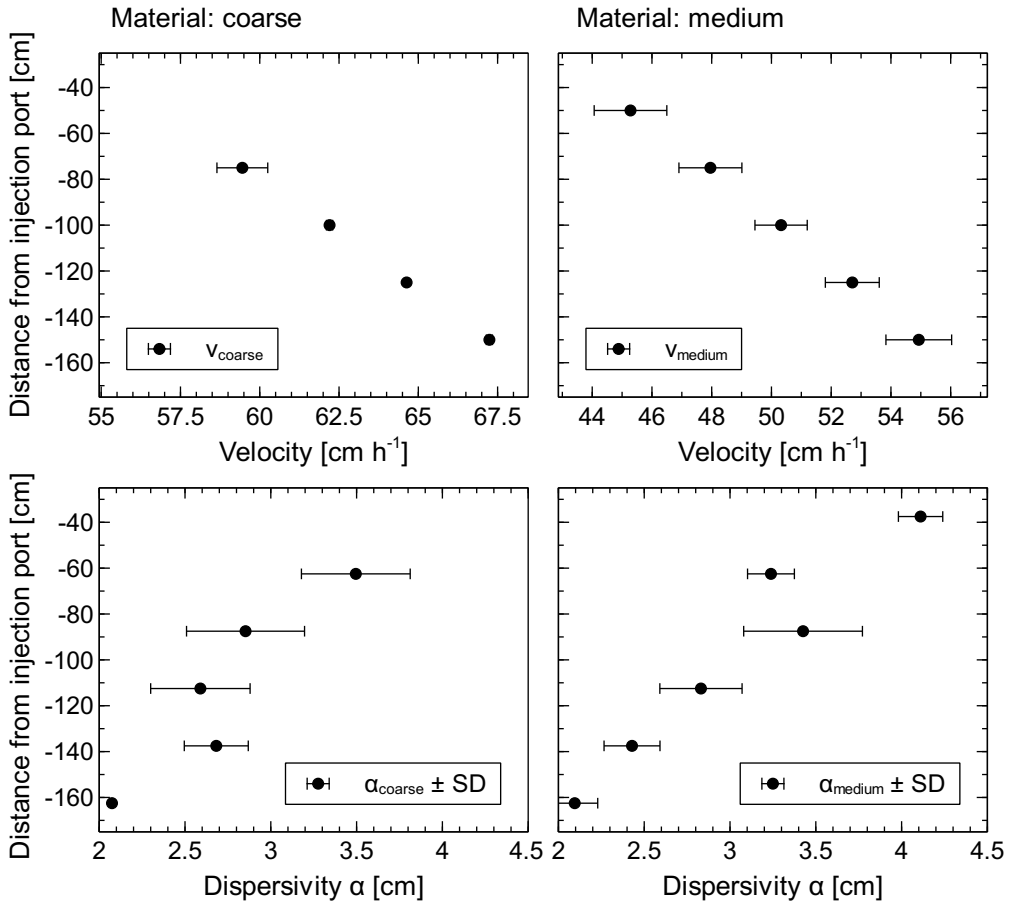

Figure 5.4. Summarized results of continuous-injection experiments in coarse (left-hand) and medium (right-hand) material obtained from CXTFIT; migration velocity and dispersivity over distance from injection location.

Table 5.2. Experimental conditions of the vapor-migration experiments with slug injection.

Series	Glass beads Coarse		Glass beads Medium			Glass beads Fine	
Experiment	1	2	3	4	5	6	7
CS_2 mass flow, $g\,h^{-1}$	3.02	3.14	3.27	2.80	2.92	3.13	3.02
Absolute pressure, hPa	970	960	974	968	964	959	959
Ambient temperature, °C	18.7	21.8	21.3	23.1	23.3	21.3	24.8
Bath temperature, °C	17.7	19.3	20.5	17.9	18.2	20.0	20.0

bottom and top outlets and the slug injection (q_{CS2} = const. for the duration of the slug). After shutdown of the slug injection, the vapor migration was controlled by the pressure distribution in the system and the constant-pressure boundaries. Table 5.2 summarizes the experimental conditions of these experiments.

Exemplary description Figure 5.5 shows CS_2 concentrations measured at the sampling ports and temperatures over time of Experiment 5 in medium material. A detailed explanation of the graph designs is given in the previous part of this section. Average injection concentration was about $1408.9 \pm 34.9\,g\,m^{-3}$, measured at the beginning and end of the injection. During CS_2 injection, a concentration rise was observed at the three ports above and below the injection section until the end of the injection. The difference of CS_2 distribution after the first 1.25 h in Fig. 5.1 (continuous injection) and Fig. 5.5 (slug injection) is related to the different materials (coarse and medium glass beads). For equal injected mass, the CS_2 vapor could migrate faster in coarse than in medium glass beads due to the higher permeability. The distribution around the injection location already showed a slightly-preferred downward movement. This was caused by the experimental set-up with the different lengths of the top and bottom tubing. The shutdown of the injection ($q_{CS2} = 0$) after 1.25 h indicated by the vertical black line marked the beginning of the first stage of migration. It was characterized by the purely gravity-driven advection as compared to driven by gravity and the constant injection mass flux. The downward migration and concurrent spreading of the injected vapor due to gravity was observed throughout the entire experiment. First breakthrough at the bottom of the column was detected after 4 h. The experiment was terminated after the peak of the CS_2 concentration profile passed the bottom of the column. After around 15 h, sufficiently accurate fittings of measured concentration profiles with Gaussian curves could no longer be guaranteed.

The migration of the CS_2-vapor distribution was measured in a temporal resolution sufficient to observe influences from advection and dispersion on the overall process. Figure 5.6 shows the location of the peak of the vapor distribution tracked over the entire duration of the experiment. From the graph it becomes evident that the vapor distribution matches the shape of a Gaussian curve as predicted from the advection-dispersion equation.

The mass balance was closed with a recovery deviation of about 7 % (Fig. 5.7). A total mass of 3.92 g was injected. When the experiment was terminated, about 0.52 g (13 %) remained in the column and about 3.40 g (87 %) were collected in the bottom-outlet bottles.

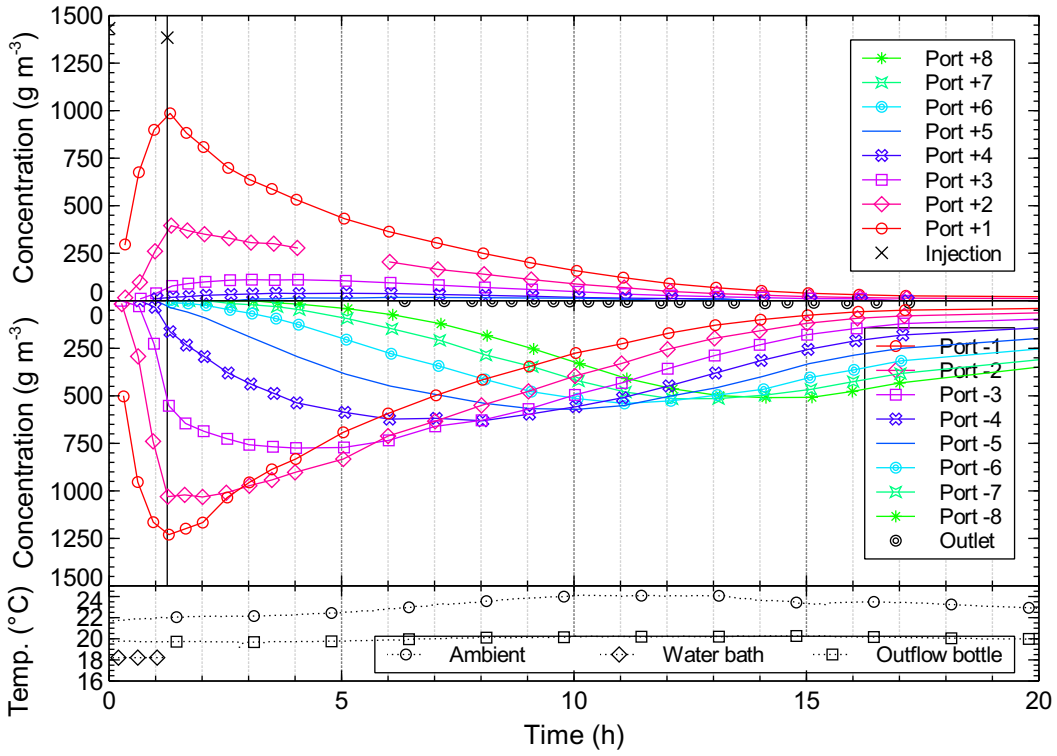

Figure 5.5. Breakthrough curves and temperature recordings of slug-injection experiment (Exp. 5) in medium material.

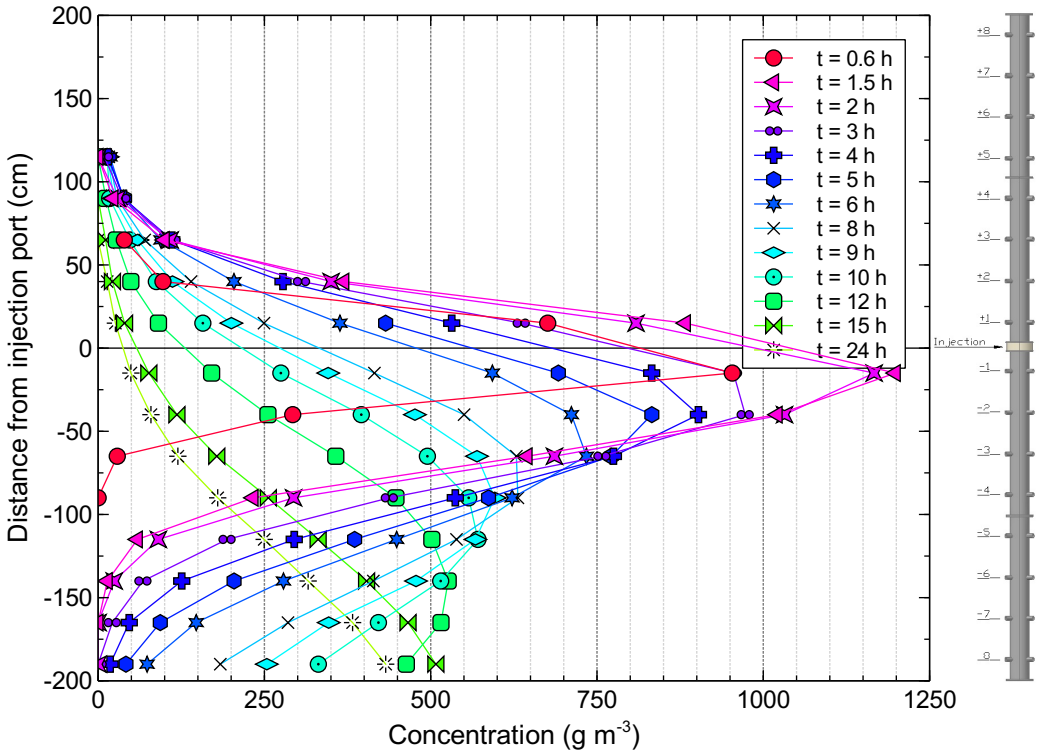

Figure 5.6. Concentration profiles in the column at different points in time of the slug-injection experiment (Exp. 5) in medium material.

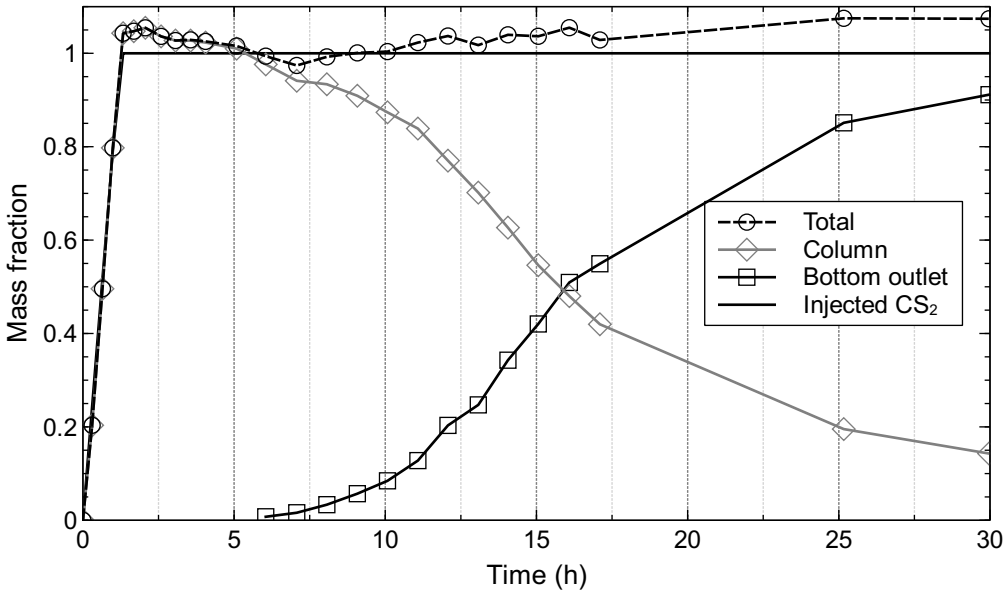

Figure 5.7. CS_2 mass balance (cumulative injected mass, mass residing in column, cumulative collected mass in bottom-outlet bottles, and total mass of experiment) of the slug-injection experiment (Exp. 5) in medium material.

Summarized results In total seven experiments, two in coarse, three in medium, and two in fine glass beads were performed using the same nitrogen flow rate and injection duration. Table 5.2 summarizes the experimental conditions of the experiments with slug injection in dry porous media.

Figure 5.6 shows the concentration profiles of the CS_2-vapor distribution measured in medium material (Exp. 5) at different times. The vertical axis of the graph represents the distance from injection section and the horizontal axis shows CS_2 concentrations. The first profile (t = 0.6 h) was measured during the injection and shows CS_2 vapor distributing around the injection section. The profile indicates a slight tendency toward the lower part of the column. Comparison of the profile peaks after injection shutdown (at t = 1.25 h) reveals a clear downward migration of the injected vapor. The widening of the plume with a constant decrease in maximum concentration with time shows the dispersion of migrating vapor in the pore space. Each profile shape depicts an approximate Gaussian curve as estimated from the 1-D advection-dispersion equation (ADE, Eq. 2.21).

Figure 5.8 illustrates the results obtained from fitting the Gaussian curve to each profile (concentration measurement) over time. It shows peak location (upper left) and CS_2 concentration (upper right) as well as half-width-at-half-maximum (HWHM; lower left)). HWHM describes the width of a mathematical function with a maximum and is used to quantify a peak widening related in this case to dispersion. The dispersion coefficient (lower right) of each concentration profile was calculated by comparing standard deviations of the Gaussian curves with the ADE. Mean values are based on repetitions in the same material; deviations from the mean are shown as error bars in the graph. A constant downward migration was observed in Stage 1

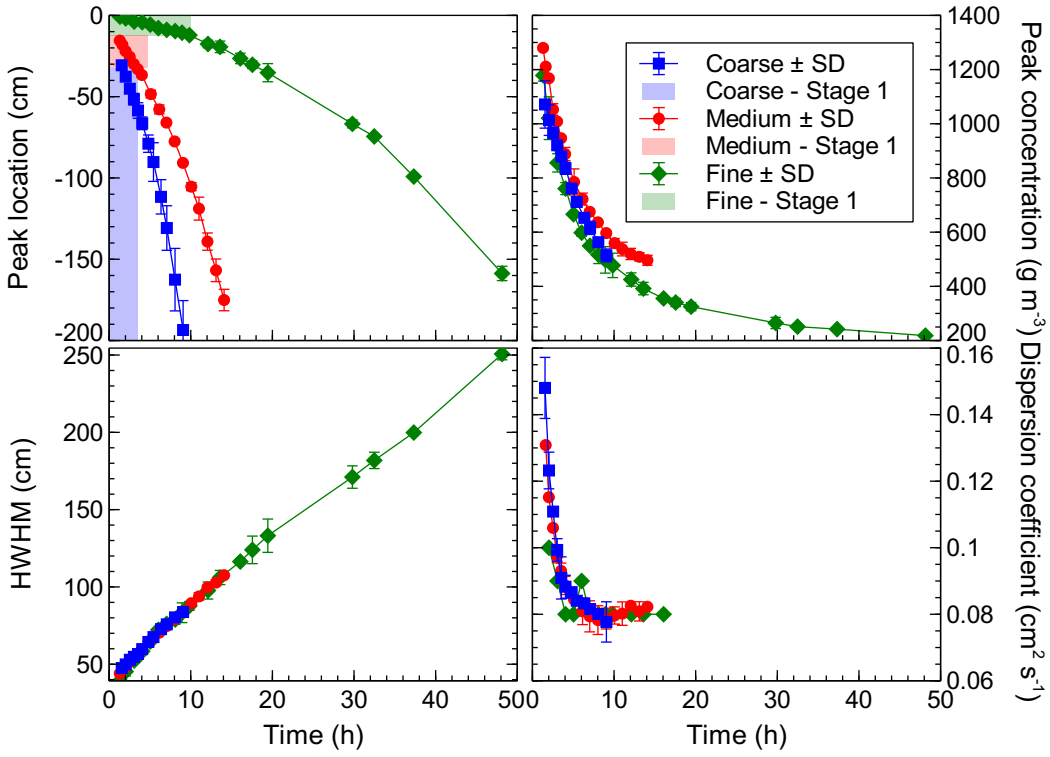

Figure 5.8. Summarized results of coarse (blue, square), medium (red, circle) and fine (green, diamond) series obtained from Gaussian-curve fits and evaluation of advection-dispersion equation (Eq. 2.21). Shaded regions mark the constant-migration part (Stage 1) of the experiments.

of the experiments with a velocity depending on the system permeability. This is shown by the linear part (colored area) of the peak-location curve (Fig. 5.8, upper left). The total injected mass spread over a certain height (H) in the column was responsible for the gravity-induced downward migration. Of course due to continuity, if the CS_2 vapor moves within the porous medium, the entire gas phase in the system migrates. In other words, the downward-migrating gas phase in the system was siphoning fresh air from the surroundings through the open top boundary.

It is important to note that a change in migration behavior was observed coinciding with CS_2 vapor entering and filling the tubing connected to the bottom outlet of the column (Fig. 4.1). This provoked a change in the bottom-boundary condition of the system. A quasi-instantaneous filling occurred due to the small volume of the tubing (volume = 44 mL, length = 3.5 m) compared to the pore volume of the porous medium. The sudden enlargement of the effective height filled with heavy CS_2 vapor (column plus tubing) resulted in an increased pressure gradient. This triggered an acceleration, starting Stage 2 of the experiment at around 3.5 h in coarse, 4.5 h in medium and 10 h in fine experiments, respectively. The curved part of the peak-location graph (Fig. 5.8, upper left) shows this acceleration. The parameter HWHM (Fig. 5.8, lower left) showed a similar behavior in all experiments. This was expected due to the uniformity of the glass beads and the similar porosities of the packings. Dispersion coefficient (Fig. 5.8, lower right) decreased rapidly to approximately 0.08 $cm^3\,s^{-1}$ in all experiments.

Figure 5.9 shows migration velocities over time for all three experiment series. They were determined from peak-location data (Fig. 5.8, upper left) by using the traveled distance of the peak between two sampling intervals (Point-Point) and by time derivatives of the fitted linear regression (Stage 1) or time derivatives of the fifth-order polynomial (Stage 2). The choice for a fifth-order polynomial was made after the comparison with first results from numerical simulations, discussed in Section 5.1.2. The coefficient of determination was calculated to estimate the quality of the linear regression and the fifth-order-polynomial fits. It was calculated to 0.954 (linear reg.) and 0.985 (fifth-order poly.) in coarse, 0.994 and 0.998 in medium and 0.962 and 0.998 in fine material, respectively. Figure 5.9 illustrates the two stages of the experiments. The comparison of constant migration velocities between experiment series (different glass beads) revealed a fairly small difference (linear reg. [dashed, symbol] in Fig. 5.9). This suggests that migration not only depends on the permeability of the porous media but also on the boundary installations. Therefore, the harmonic-average permeability (Table 4.2) of the entire system was determined, taking into account the porous media (Table 4.1) and pressure-loss measurements of the boundary installations. The correlation between constant migration velocity and harmonic-average permeability of the system yielded a coefficient of determination (R^2) of about 0.9997. The distinct linear relationship between these two parameters confirmed the dependency of density-driven vapor migration on the system permeability and proved the correct consideration of the boundary conditions. The different porous media showed similar porosity due to the uniform and narrow grain size distribution of the glass beads. This resulted in similar diffusion in the different porous media.

The Rayleigh number (Eq. 3.3), the ratio between advection and diffusion, was determined for each series of experiments (Table 5.3). It was calculated based on the experimental conditions at injection shutdown using the corresponding vertical spread (H) and mean vapor density

Table 5.3. Rayleigh number (Eq. 3.3) and comparison of theoretical velocities (Eq. 3.4) with observations in Stage 1.

Parameter Parameter	Glass beads Coarse	Glass beads Medium	Glass beads Fine
Rayleigh number (Ra)	247	143	25
Theoretical velocity, cm h^{-1}	39.0	23.2	6.4
Experimental velocity (Stage 1), cm h^{-1}	13.6	8.3	1.4

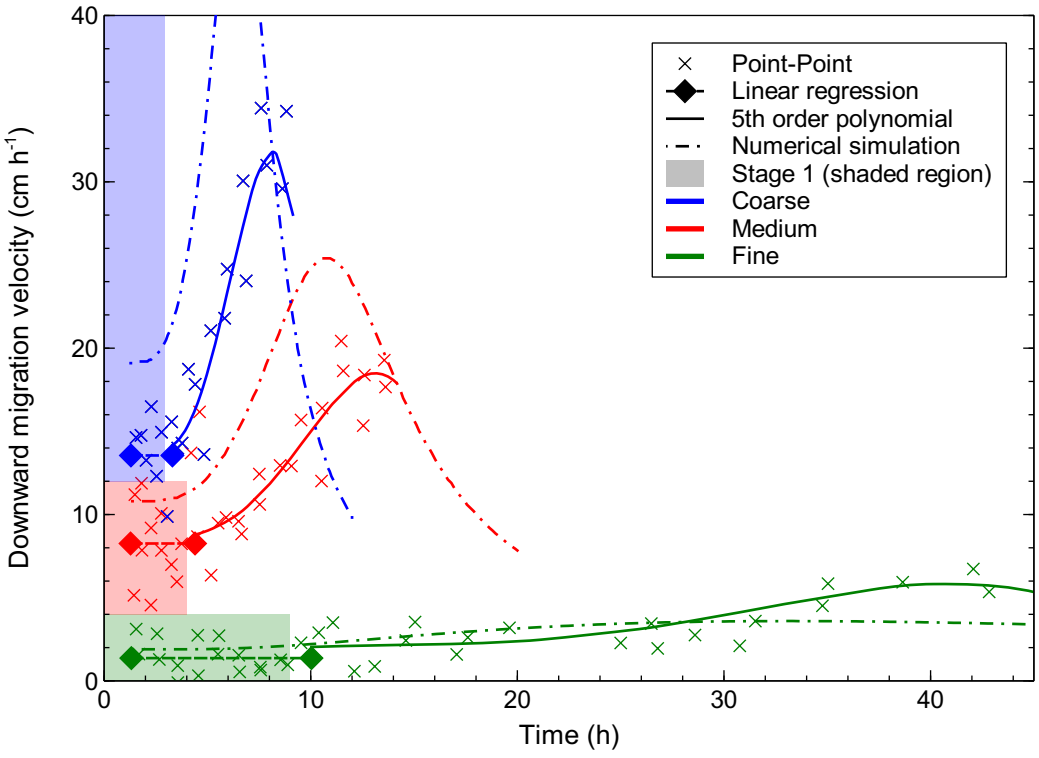

Figure 5.9. Downward-migration velocities over time observed in large-scale column experiments in coarse (blue), medium (red) and fine (green) porous media. Velocities were determined from measurement points (cross), linear regression (dashed, symbol) and fifth-order polynomial (line). Shaded regions mark the constant-migration part (Stage 1) of the experiments.

(ρ_c) of the CS_2 distribution. All experiments showed an advection-dominated behavior and Rayleigh numbers $Ra > 10$, thus confirming *Seely et al.* (1994) who found this threshold value for density-driven migration. The modified form of Darcy's law (Eq. 3.4), when applied to estimate constant downward-migration velocities during Stage 1, overestimated them compared to observations. This could be due to the fact that minor pressure gradients might have affected migration and/or minor pressure losses were not accounted for when calculating system permeability from gas-permeameter experiments. In this investigation it was seen how a vapor plume migrates due to gravity on a large scale in dry porous media. Furthermore, the impact of the boundary conditions on the migration could be delineated thus helping to provide a thorough understanding of density-driven vapor migration. The findings argue in support of comparing the large-scale column experiments with numerical simulations for additional evaluation and interpretation.

5.1.2. Numerical simulation

Simulating vapor migration

The first objective was to gain a fundamental process understanding of density-driven vapor migration. Consequently, the influence of the total injected CS_2 mass and the resulting vapor concentrations on the migration was investigated. This was achieved by performing simulations with different total injected CS_2 mass. The reference run was carried out with the original input parameters. Then the total injected mass was reduced to 80, 60, 40, and 20 % of the reference mass. In addition, two different simulations were performed for each total mass series. The total mass was defined by the parameters mass flux and injection duration. In the first simulation, a CS_2 mass flux at a lower rate was applied and the injection duration was kept constant. In the second simulation, this parameter combination was applied vice versa. Hence, this showed density-driven vapor migration for the same total injected mass but different absolute CS_2-vapor concentrations due to the two methods applied. Table 5.4 shows the parameter combinations used in these simulation runs. For these simulations, the introduced model at an early development stage without the tubing domains was employed.

Figure 5.10 shows downward velocities over distance from the injection section of all runs and the impact of the variations on migration. It can be easily seen that migration velocity is a function of the total injected mass by comparing the reference run with the 80, 60, 40, and 20 % mass runs. The higher the mass the higher the potential for migration, i.e. the higher the downward velocity. Furthermore, absolute concentrations had no effect on migration which becomes evident when comparing one simulation pair with the same mass injected. An example for this is R60-t and R60-$\dot{m}$ where the same mass was injected. The reduced injection time resulted in higher absolute concentrations as compared to the simulation run where the reduced mass flux was applied. Hence, migration was only controlled by the total injected mass residing in the porous medium. This basic understanding helped with the numerical model.

The second objective of the numerical simulation was to develop the final model taking into account the tubing domains as introduced in Sec. 4.1.5 and to simulate the vapor-migration

Table 5.4. Parameter combinations for investigating influence of total injected mass and absolute vapor concentration on migration behavior.

Series	1	2		3		4		5	
Factor	100 %	80 %		60 %		40 %		20 %	
Label	Ref	R80-t	R80-$\dot{m}$	R60-t	R60-$\dot{m}$	R40-t	R40-$\dot{m}$	R20-t	R20-$\dot{m}$
Injection time	1.0	0.8	1.0	0.6	1.0	0.4	1.0	0.2	1.0
Mass flux	1.0	1.0	0.8	1.0	0.6	1.0	0.4	1.0	0.2

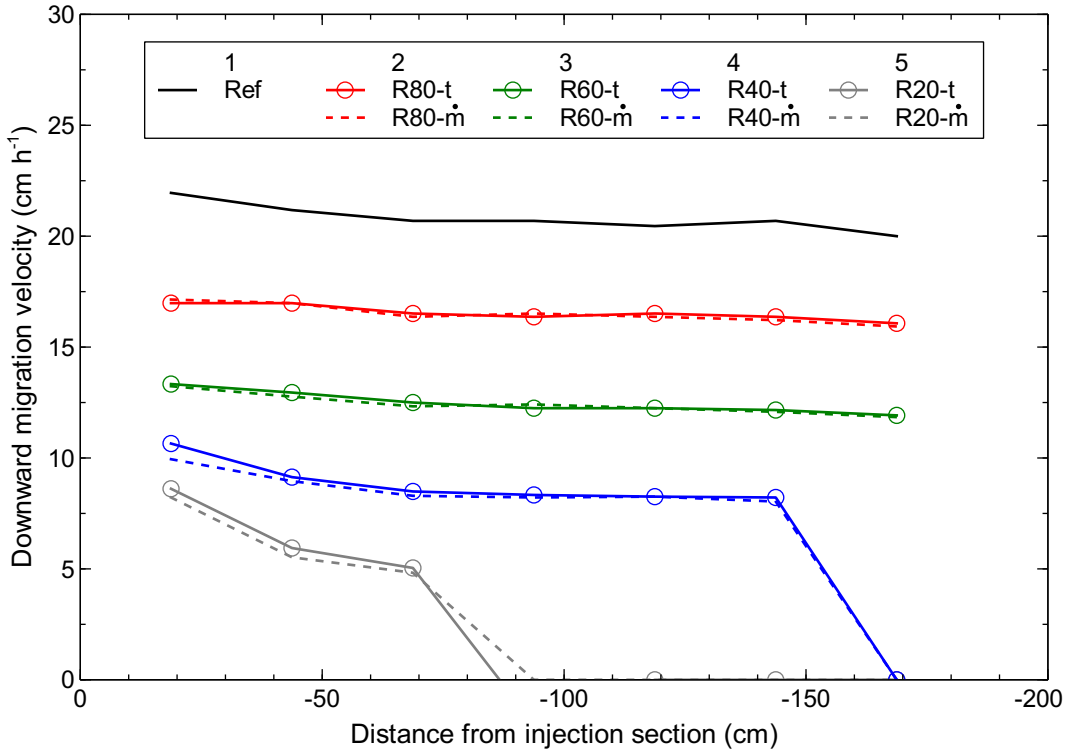

Figure 5.10. Dependency of downward-migration velocity on injected total CS_2 mass in numerical simulation.

experiments with slug injection described in Section 5.1.1. Recalling the experiments, the results showed a constant migration velocity in Stage 1, followed by an acceleration of the vapor plume in Stage 2. These two stages of migration were addressed in this second part. Figure 5.9 shows downward-migration velocities measured in the experiments and obtained by the numerical simulations (dashed-dotted). While results from simulations suggested higher migration velocities than observed in the experiments, the overall migration, including the constant velocities in Stage 1 as well as the acceleration in Stage 2, were reproduced in good accordance with the experiments. This maximum velocity is followed by a deceleration determined by the last concentration measurement. In the simulations, the plume migration could be estimated over a longer period, showing first the acceleration reaching a maximum downward velocity and second a deceleration. This deceleration is due to CS_2 mass leaving the bottom of the model domain resulting in a reduced pressure gradient driving migration.

The results prove that the numerical model was able to reproduce the migration observed in the experiments as well as the correct implementation of the boundary installations and their pseudo-permeabilities. They suggest that the total mass of a CS_2 spill controls the migration of a vapor plume in the unsaturated zone. However, it is clear that this is only valid for the chosen conditions when the contaminant resides in the gas phase or presupposes an instantaneous vaporization of the liquid, respectively. In a real-life scenario, the spill and spreading of the liquid contaminant and its vaporization controlled by the specific interfacial area will affect the density-driven vapor migration. Therefore, different spills and distributions of liquid CS_2 were investigated in detail in the spill and remediation experiments (SRE) and their results are discussed in Section 5.3.

Sensitivity analysis

The model developed and discussed in the previous section was used to explore the impact of specific input parameters on the vapor migration with the objective of gaining a better understanding of the process itself and the experimental set-up. A detailed description of the sensitivity analysis is given in Section 4.1.5. A set of input parameters used for simulating the vapor-migration experiments was defined and two sensitivity analyses were carried out. First, a general analysis was conducted to gain a basic understanding of the importance of the particular parameters. This was done by applying the same variation range to all parameters. Second, an adapted variant was conducted taking into account specific uncertainties assessed from experimental measurement methods and experience. In other words a sensitivity analysis with weighted parameters. Dynamo/MoReS was used for the sensitivity analysis due to its extensive multi-run tools and the possibility to vary the model domain size between runs. Figure 5.11 shows the results of the general sensitivity analyses discussed in the following paragraphs.

General sensitivity of input parameters The input parameters introduced in Sec. 4.1.5 were varied within a range of 0.5 to 1.5 by means of multipliers (or factors). Figure 5.11a illustrates the impact of these input parameters on the simulation output and helps to select the

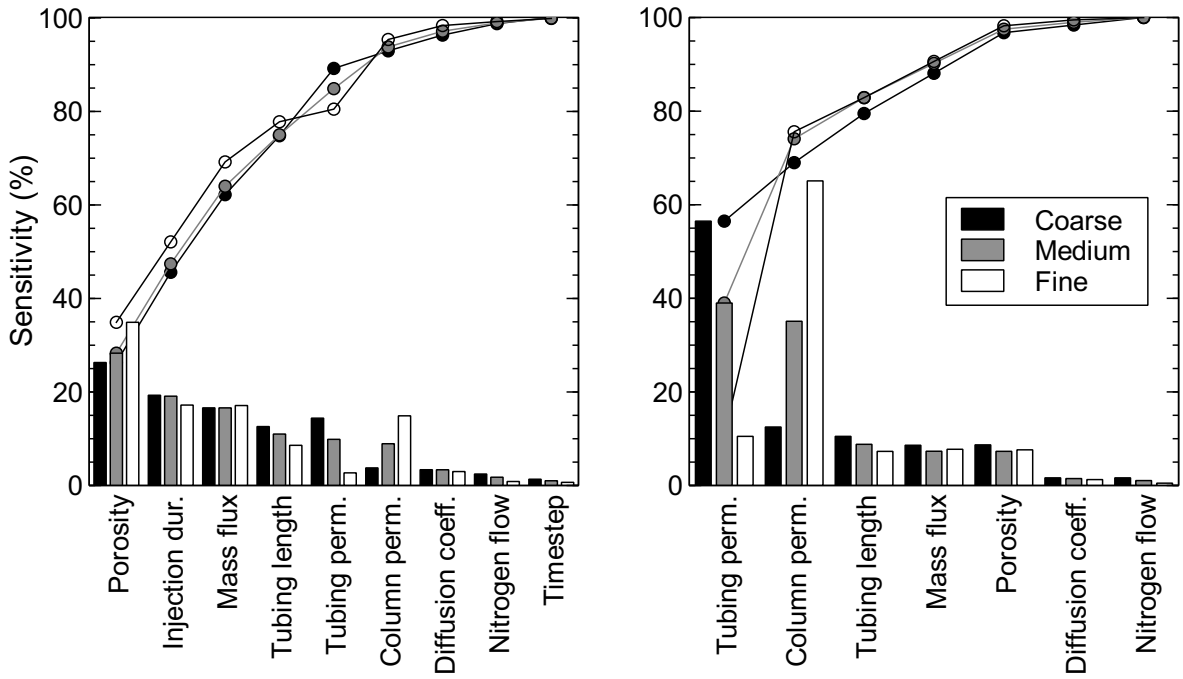

(a) Equal Parameter Uncertainty (b) Adapted Parameter Uncertainty

Figure 5.11. Pareto plot showing the sensitivity of the simulation output to the input parameters of vapor migration (slug injection): relative contribution (bars) of the input parameters to sensitivity and the cumulative total (line).

most significant parameters. The relative contribution of each input parameter is shown in descending order by the bars and the cumulative total is displayed by the line. Dynamo/MoReS determined these results by comparing the output with the observation data set containing the experimental vapor-migration velocities.

In all three materials, coarse (black), medium (grey) and fine (white) material, the input parameters porosity, injection duration, and mass flux showed the greatest impact on the simulation output. Porosity of the porous media is a measure of the void space available for the injected CS_2-vapor phase, hence, a change in porosity highly affected the initial spreading around the injection section as well as the overall migration. Injection duration and mass flux were the parameters controlling the total amount of mass, thus affecting migration velocities. They showed very similar relative contributions from 16 to 19 % in all three materials. Except for the coarse material, the length of the bottom tubing had the fourth-biggest impact, being the main parameter controlling acceleration by determining the vertical spread of the heavy vapor.

Permeability of the column (porous medium) and of the tubing domains controlled the velocity of the entire gas phase in the system as well as the acceleration. The system permeability (Table 4.2) depended, as discussed in Section 4.1.2, on the porous medium (column) and the tubing domain taking into account the length of the domains and their particular permeability. The same boundary installations (same tubing permeability) were used and only the porous medium changed (column permeability) between the series. In medium material, the pressure loss due to flow in the tubing was of the same order as the losses due to the porous medium,

thus they had a similar impact on the vapor migration. In coarse and fine material, their relative contributions were negatively correlated. Since the coarse material has a higher permeability than the tubing domains, the parameter significance was shifted toward the latter and vice versa in fine material. Diffusion coefficient and nitrogen flow (injected vapor consisted of a mixture defined by CS_2 mass rate and nitrogen flow rate) had only a minor influence on the simulation output. Time step size had the lowest influence on vapor migration, hence, effects like numerical diffusion could be disregarded. These results demonstrate the parameters controlling density-driven vapor migration in the simulated vapor-migration experiments.

Uncertainty-adapted variation range sensitivity The general sensitivity analysis showed the parameters controlling vapor migration in the large-scale column experiments. In the next step, variation ranges were adapted according to uncertainty estimates of the respective parameter. The objective of this step was to determine the most significant parameters for density-driven vapor migration in the experiments later employed in the history matching task. Input values of the parameters were determined from the experiments and the set-up. It is apparent that different uncertainties apply to parameters resulting from different measurement methods. An example for this is permeability where a higher uncertainty applies due to inaccuracies in flow and differential-pressure measurements in comparison to porosity or injection time. Spatial variations of the porosity could occur due to inaccuracies during the column packing whereas injection time measured with a stopwatch was considered a zero-uncertainty parameter. The variation ranges of the parameters were set to: permeability (0.5 to 1.5), tubing length (0.9 to 1.1), mass flux, diffusion coefficient, and nitrogen flow (0.95 to 1.05), and porosity (0.975 to 1.025). Injection duration and time step were not considered in this part. A possible variation of the injection duration in the experiments could be ruled out and results of the general sensitivity analysis (Fig. 5.11a) showed that simulation output was insensitive to the size of time steps. After defining uncertainties for all parameters, Tornado runs were executed applying these variation ranges.

Figure 5.11b shows the sensitivity of the simulation output to the input parameters for the adapted parameter uncertainties. The sensitivity tendency of both column and tubing-domain permeability, previously observed in the equal parameter uncertainty, was also reflected by this adapted analysis; however its relative contribution was greatly increased. It is evident that permeability was the main parameter controlling migration. This could mainly be ascribed to the relatively high variation range used for the permeability parameters based on experimental experience. The parameters porosity, mass flux, and tubing length showed similar impacts on the simulation output as compared to results from equal parameter uncertainty. The contribution of porosity was greatly reduced due to the chosen variation range. Diffusion coefficient and nitrogen flow were not significant compared to the other parameters.

History matching

Based on the knowledge gained from the sensitivity analyses, history matching (see Sec. 4.1.5) was carried out. This method was used to validate and calibrate the numerical model developed to simulate vapor migration observed in the large-scale column experiments. Velocities

and concentrations from experiments were used as observations and were compared with the simulation output to evaluate the initial guess of the input parameters and find best-match solutions. Therefore, selected input parameters were varied within a predefined range. These included permeability, porosity, and mass flux of CS_2. The choice fell on these parameters as they showed the highest impact on density-driven migration of the vapor in the sensitivity analyses. System permeability was used rather than column or tubing domain permeabilities. History matching was conducted for the slug-injection experiments in all materials. It is a complex and sensitive task and multiple solutions may exist. In addition, the initial definition of parameter variation ranges could influence best-match solutions. Thus, the results have to be interpreted thoroughly and with respect to the parameters varied and to the observation data sets available.

Two cases of history matching were conducted. The first case C1 was performed for all three materials and employed only the parameter system permeability to match the downward-migration velocities implemented as observations. This case was carried out to benchmark the history matching and to see whether the observed vapor migration could be matched with the most significant parameter. Since the vapor migration observed in the experiments followed Darcy's law, system permeability was most likely to match advective observations (downward-migration velocities). The second case C2 was only performed for medium material and employed the parameters system permeability, porosity and mass flux of CS_2. This case was divided into two sub-cases, case C2a used only velocities as observations whereas case C2b used velocities plus the concentration data of four sampling ports. The additional concentration data included in case C2b improved history matching by providing observations which factor in diffusive flow. The purpose of the case C2 was to exemplarily evaluate best-match results and their quality when increasing the number of observations while matching them with several, strongly-correlated parameters.

Table 5.5 summarizes the input and output parameters of all history-matching cases. The columns list the conducted cases (C1, C2a, and C2b), the material of the porous medium, the lower and upper boundary (LB/UB) of the variation range applied to the input values of the parameters, the best-match values that are the factors with which the input value has to be multiplied to obtain the best-match solution, the calculated total sensitivity, the marginal standard deviation (M), and the ratio between marginal and conditional standard deviation (C/M) which is considered a measure of parameter independence. For further information on these parameters see *Finsterle* (2007).

For all three materials in case C1, the variation range (multiplier) was set to 0.5 as the lower boundary (LB) and 1.5 as the upper boundary (UB) of the input value (see Table 4.2). A mean best-match value of 0.740 ± 0.019 was found. This demand to reduce system permeability in all three materials suggested that a part of the experiment set-up causing pressure losses was not considered in the model or that permeability measurements were imprecise. The complexity of the set-up required to simplify implementations or to disregard minor experimental parts (valves or outflow bottles) possibly affecting vapor migration in the experiments. Figure 5.12a (left) compares downward-migration velocities of the experiments (line, diamond) with simulations employing input values determined from the experiments ($DuMu^x$; dashed line) and best match values of history-matching case C1 ($DuMu^x$ HM - C1; dotted line, circles).

Table 5.5. History matching results: history-matching case, material, lower/upper boundary (LB/UB) of variation parameter, best-match value, total sensitivity, marginal standard deviation (M), and measure of parameter independence (C/M; ratio between marginal and conditional estimation uncertainty).

Case	Material	Parameter	Input	Output			
			LB/UB	Best match	Sensitivity	M	C/M
C1	Coarse	System perm.	0.50/1.50	0.718	53.4	1.93×10^{-3}	1.0
	Medium	System perm.	0.50/1.50	0.755	53.2	2.60×10^{-3}	1.0
	Fine	System perm.	0.50/1.50	0.746	20.8	6.88×10^{-2}	1.0
C2a	Medium	System perm.	0.50/1.50	0.885	45.3	6.91×10^{-3}	0.078
		Porosity	0.95/1.05	1.039	48.6	7.02×10^{-2}	0.025
		Mass flux CS_2	0.75/1.25	0.895	44.1	6.58×10^{-7}	0.023
C2b	Medium	System perm.	0.50/1.50	0.766	163.1	9.39×10^{-3}	0.437
		Porosity	0.95/1.05	1.039	236.0	1.23×10^{-7}	0.300
		Mass flux CS_2	0.75/1.25	1.059	154.1	4.58×10^{-3}	0.218

Table 5.6. Matrix of direct correlation of the history-matching cases C2a and C2b.

Medium glass beads		System perm.	Porosity	Mass flux CS_2
C2a	System perm.	1.000	0.996	−1.000
	Porosity	0.996	1.000	0.997
	Mass flux CS_2	−1.000	0.997	1.000
C2b	System perm.	1.000	0.856	−0.703
	Porosity	0.856	1.000	0.935
	Mass flux CS_2	−0.703	0.935	1.000

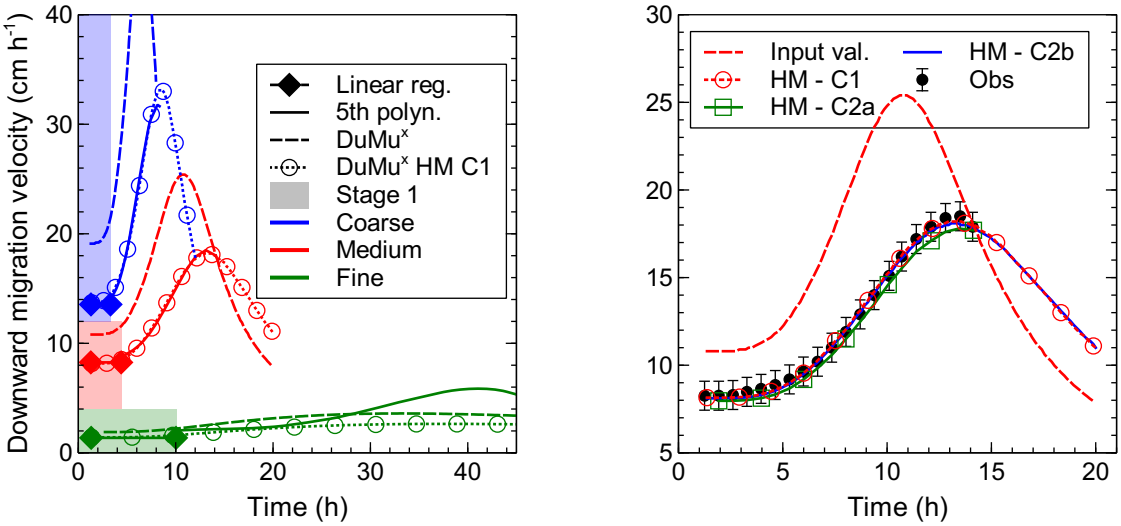

(a) Simulations with input values and best match values from case C1).

(b) Simulations with input values and best match values from cases C1, C2a and C2b for medium material.

Figure 5.12. History-matching results: Comparison of downward-migration velocities of numerical simulations with experiments.

The simulations with input values overestimated migration velocities as discussed earlier. The simulations applying best-match values from case C1 could reproduce the constant migration velocities of Stage 1 for all three materials. The acceleration in Stage 2 was well matched in coarse (blue) and medium (red) material, only slightly overshooting the maximum velocity in coarse material. In fine (green) material, the model was not able to reproduce velocities at a later stage and strongly deviated from the velocity observations (that was obtained from the time derivative of the fifth-order polynomial fit of the concentration peak over time (see Sec. 3.5.1 for further information on experimental data evaluation). The experiment suggested an ongoing acceleration until the duration of 40 h was reached which DuMu^x was not able to capture while still matching the constant migration velocity of Stage 1.

The second case C2 employed the parameters system permeability, porosity and mass flux of CS_2. The variation ranges were set to 0.5/1.5 (LB/UB) for system permeability, 0.95/1.05

for porosity, and 0.75/1.25 for mass flux of CS_2. Table 5.5 shows detailed results of history-matching case C2a and C2b in medium material. Both matches demanded a reduction of system permeability, 0.885 in C2a and 0.766 in C2b to capture downward-migration-velocity observations. Porosity had to be increased by a factor of 1.039 in both cases. Mass flux of CS_2 had to be decreased by 0.895 in C2a but had to be increased by 1.059 in C2b. The difference between the two matches resulted from the available observation data sets. Recalling that case C2b additionally utilized concentration data, this match also accounted for diffusive spreading of CS_2 in comparison to case C2a where only velocity observations were used. Hence, in case C2a a greater number of parameter combinations was possible since only the advective flow had to be matched. This became evident by the strong correlation between the parameters reflected by the output parameter C/M in Table 5.5 and the matrix of direct correlation shown in Table 5.6. The physical explanation for the strong correlation between the parameters is that the overall downward migration was controlled by permeability and injected mass of CS_2. These two parameters were negatively correlated thus a reduction of permeability can be counterbalanced by an increase of mass flux i.e. total mass inside the porous medium and vice versa. Porosity affected the spreading of CS_2 during injection as well as while migrating downward and was positively correlated with permeability and mass flux. A reduced porosity led to an earlier arrival of the heavy vapor at the bottom tubing which could be compensated by a reduced permeability or mass flux. The sensitivity of the simulation output to the individual input parameters was similar for all three parameters of the history-matching case C2a. In case C2b, the simulation was more sensitive to the porosity than to the system permeability and the mass flux. This was due to the concentration observations additionally used together with the velocity observations.

Figure 5.12b compares downward-migration velocities obtained from simulations with input and best-match values with observations. Results from case C1 and C2a were almost identically matching the observations. It is obvious that an increase in degree of freedom (parameters) with the same set of observations yielded similar results. Velocities of Case C2b slightly deviated from the observations during the acceleration. Figure 5.13 illustrates concentrations of CS_2 (different y-axis range) over time of the four sampling ports which were used as observations in case C2b. The concentration obtained by the simulation with input values (original parameters) deviated significantly from the measured concentrations. Concentrations of case C1 were in good agreement with the concentration observations (at the four selected sampling ports) though iTOUGH2 did not utilize concentration data for matching. Case C2a predicted overall lower concentrations due to the reduced mass flux of CS_2 (0.895). The mass flux defined the total injected mass, thereby controlling migration velocities. The dependency of migration on total injected CS_2 mass was discussed in Section 5.1.2. Concentrations of case C2b resulted only in marginally better matches compared to case C1. Hence, the additional computational effort due to an increase of parameters to be varied for history matching and additional observations did not pay off in this case. However, Table 5.6 shows that the additional concentration observations improved the strong direct correlation between these parameters. Hence, additional observation sets of a different type should be included whenever correlated parameters are used for history matching. History matching helped with understanding the experimental set-up, interpreting the experimental observations, and adapting the input parameters to obtain good matches.

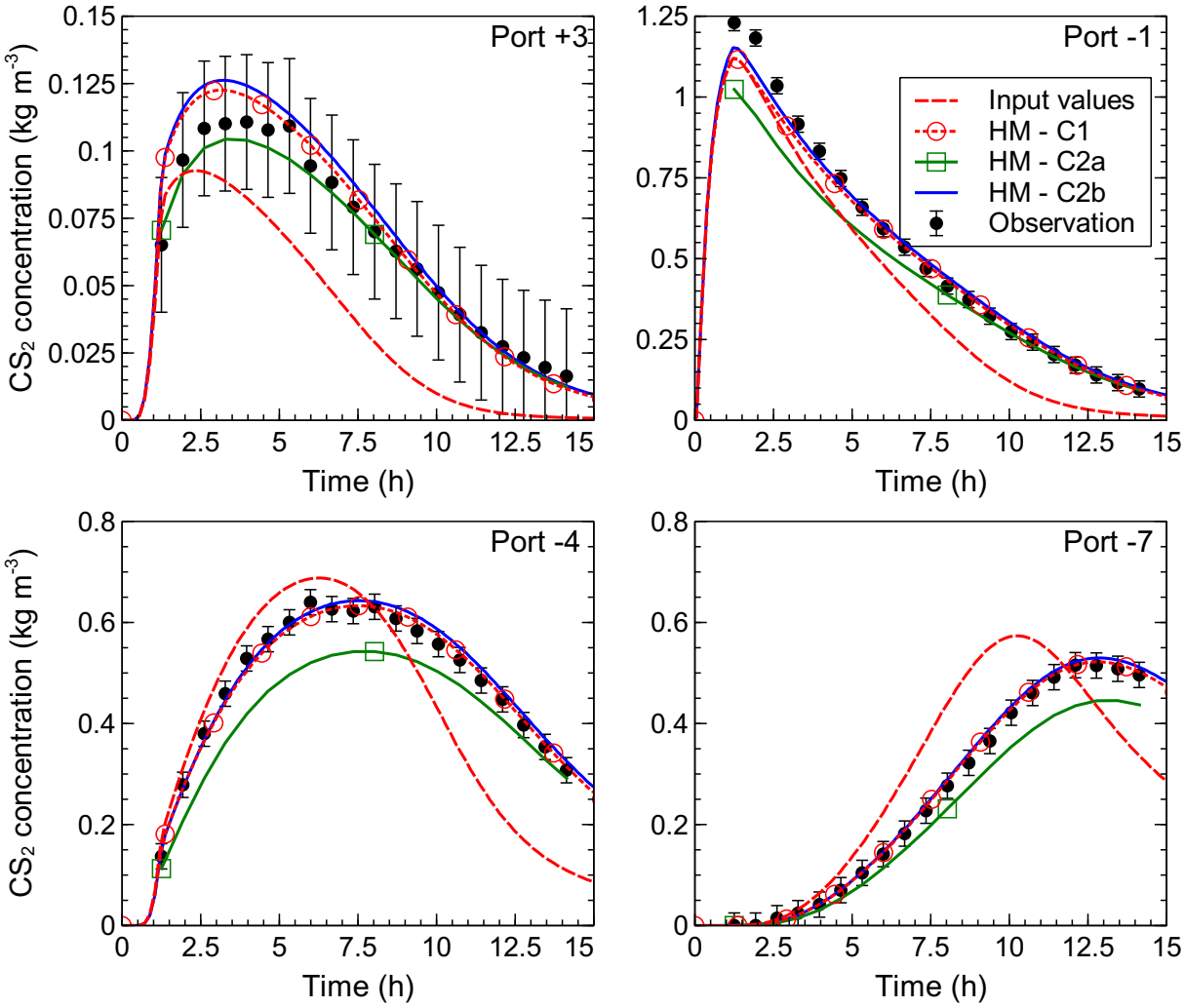

Figure 5.13. Comparison of CS_2 concentrations from simulations with experiments at four locations (Port +3, -1, -4, and -7) in medium material.

5.1.3. Summarized results

Experiments were conducted in 4 m long, vertical columns packed with a dry porous medium to describe and quantify density-driven migration of a heavy CS_2-vapor plume. Three different types of glass beads (coarse, medium and fine) were used to observe the influence of permeability on migration. Tubes connected to the top and bottom outlet ended at the same elevation. The boundaries were open to the atmosphere and hence considered constant-pressure boundaries. This allowed for an unhindered migration of the heavy CS_2 vapor injected into the middle section of the column. Gas samples were taken along the column throughout the experiment to quantify time-and-space-dependent vapor migration.

First, experiments were conducted with a continuous injection of CS_2vapor until steady state was reached. The injected heavy vapor triggered a downward migration of the entire gas phase in the system. This caused a change in the upper boundary condition eventually siphoning air responsible for the observed dilution of steady-state concentrations. The concentration breakthrough curves measured at the sampling ports along the column were fitted to an advection-dispersion equation using CXTfit to quantify the migration. This procedure was complicated by the transient behavior of the gas phase due to gravity additionally driving migration. The findings of these experiments were required to define the initial and boundary conditions of the experiments with slug injection.

Second, experiments with slug injection of heavy CS_2 vapor were performed to characterize density-driven migration of a finite vapor plume. They were based on the experiments with continuous injection which revealed that a critical CS_2 mass is required to start migration. This resulted in a injection duration of 1.25 h at the given CS_2 mass flux. After shutdown of injection, the migration of the CS_2-vapor plume was induced only by gravity. The concentration profiles determined from gas sampling were fitted to Gaussian curves to quantify the migration. Two stages of migration were observed as a result of a change in the bottom-boundary condition. In the first stage, a constant downward migration as a function of the permeability of the porous medium and the injected CS_2 mass was observed. Migration velocities of 13.6, 8.3, and 1.4 $cm\,h^{-1}$ were measured in coarse, medium, and fine glass beads, respectively. The perfect correlation between the migration velocities and the harmonic-average permeabilities of the entire system confirmed the dependency of the migration on the system permeability. The second stage was characterized by an acceleration of the migrating gas phase coinciding with CS_2 entering and accumulating the tubing connected to the bottom outlet. The dimensionless Rayleigh number was determined to estimate the importance of density-driven migration competing with gas diffusion. For all three materials, a Rayleigh number greater than 10 was calculated, thus confirming the advection-dominated behavior observed in the experiments.

The numerical model was used to simulate the vapor-migration experiments with the correct boundary conditions and to compare the results with the observed migration. The simulations were carried out with DuMu^x and Dynamo/MoReS. First results showed that for this particular system the downward migration was controlled by the total injected CS_2 mass and was independent of the absolute concentrations in the gas phase. The model was able to reproduce the migration behavior in good agreement with the experiments but suggested slightly higher velocities. The sensitivity analyses showed that the permeability of the porous medium (col-

umn) and the pseudo-permeability of the top and bottom tubing, the mass flux of CS_2, and the porosity of the porous medium were the main parameters controlling the migration.

History matching of the slug-injection experiments was performed employing the most-significant parameters according to the sensitivity analyses. The permeabilities of the domains (column and tubing) were combined into the single parameter system permeability to avoid arbitrary best-match solutions as a result of their strong correlation. Two cases of history matching were carried out. In the first case C1, system permeability was able to accurately capture the experimental migration velocities used as observations. The results suggested a mean best-match value (factor) of 0.740, hence a reduction of permeability for all three materials. From this follows that simplified implementations of the experimental set-up in the model neglected minor parts responsible for additional pressure losses. In the second case C2, the three most significant parameters were enabled for variation and the history-matching performance was evaluated based on two sub-cases in medium material. The first sub-case C2a used migration velocities only while the second sub-case C2b utilized velocities plus selected concentration data as observations. The negative correlation of system permeability and mass flux however favored the ambiguity of history match results regarding these two parameters as observed in case C2a. This could be avoided by introducing additional observations of a different type (concentration data), thereby improving the direct correlation between the parameters. History matching proved to be a very effective and reliable method for benchmarking the numerical model and for understanding the process of vapor migration.

Key findings

- Density-driven vapor migration was quantified in large-scale column experiments packed with different dry porous media.
- The novel set-up allowed for observing the unhindered migration of a heavy CS_2-vapor plume.
- The numerical model showed that the total injected CS_2 mass controlled the migration in this particular system.
- The simulations satisfactorily reproduced the migration behavior, only suggesting slightly higher velocities than observed in the experiments.
- Sensitivity analyses determined permeability, porosity, and mass flux of CS_2 to be the most-significant parameters controlling migration.
- History matching confirmed that the model reproduced the experimental set-up and that it covered all relevant processes describing downward vapor migration.
- The results showed similar best-match values of system permeability in all three materials.
- Different types of observations (in this case velocities and concentration data) are required to reduce the direct correlations of strongly-correlated parameters employed for history matching.

5.2. Vapor retardation

Column experiments were conducted with dry and moist porous media to characterize retardation of CS_2 vapor. Table 5.7 shows the experimental conditions of each series performed in fine glass beads and Geba fine sand. Several series of experiments were performed in each porous medium to quantify retardation. Series 1 refers to the experiments conducted in dry porous media while Series 2 to 4 refer to the experiments in moist conditions. A saturation-and-drainage cycle was performed prior to each moist series. A slug of 3.5 PV of the gas mixture was injected ensuring, even for high flow rates, a sufficient residence time to reach equilibrium in the 2 m long column. Different seepage velocities (25, 50, 100, and 200 cm h^{-1}) were applied, similar to the velocities observed in the experiments investigating density-driven vapor migration discussed in the previous section. Breakthrough curves under the prevailing experimental conditions were determined from concentration measurements at the column outlet. The temporal-moment analysis was applied to the breakthrough curves (BTC) to quantify retardation and to characterize diffusion/dispersion as a function of the porous media, the water saturation, and the flow conditions. A detailed summary of all experiments (experimental conditions, injected mass, and mass recovery) is given in Table A.2 in the appendix of this work.

Table 5.7. Experimental conditions of vapor-retardation experiments in fine glass beads and Geba fine sand in dry and moist conditions (series).

Series	1	2	3	4
Condition	dry	moist	moist	moist
	Fine glass beads			
Porosity (ϕ)	0.40	0.40	0.40	0.40
Mean water saturation (S_w)	0.0	0.088	0.154	0.073
Eff. pore volume, L	7.72	7.04	6.53	7.16
	Geba fine sand			
Porosity (ϕ)	0.40	0.40	0.40	-
Mean water saturation (S_w)	0.0	0.162	0.150	-
Eff. pore volume, L	7.58	6.35	6.45	-

5.2.1. Water saturations

The moist porous medium required for this investigation was obtained by saturation and subsequent drainage, as introduced in Section 3.4.2 of Materials and Methods. The suction applied at the bottom of the column during drainage was responsible for the observed water-saturation profiles. The capillary pressure was measured with the tensiometers installed at the column ports to derive water saturations along the column (P_c–S_w, Fig. 3.1). Mean water saturations of the moist series are given in Table 5.7.

Figure 5.14a shows the initial water-saturation profiles along the column measured in fine glass beads (only Series 4) and Geba fine sand (Series 2 and 3). Unfortunately, no tensiometer measurement data was available for Series 2 and 3 in fine glass beads. However, the available profile of Series 4 revealed a uniform saturation along the column, only slightly increasing toward the bottom from $S_w = 0.07$ to 0.14. The very narrow and uniform grain-size distribution of the fine glass beads was responsible for a sharp transition from full to irreducible saturation (see P_c–S_w curve in Fig. 3.1), thus favoring a uniform saturation profile. In Geba fine sand, a constant water saturation of $S_w = 0.15$ above a column height of 70 cm was measured. However, both profiles showed a pronounced increase in the water saturation toward the bottom of the column, apparently reaching fully-saturated conditions according to the P_c–S_w relationship of Geba fine sand (Fig. 3.1). Still, capillary pressures of $P_c = 55$ and $65\,\mathrm{hPa}$ were measured at the lowest port. The suction applied via the porous plate was limited by its air entry pressure. A further decrease of pressure would have resulted in a breakthrough of air (continuous gas phase). Thus, in future experiments a different suction plate characterized by a higher air entry pressure to allow for a higher suction has to be used. The mean water saturation (Tab. 5.7) but also the observed profiles were expected to have an impact on the retardation behavior of CS_2, as discussed in Sec. 5.2.3.

Figure 5.14b shows an exemplary progression of water saturations measured in Experiment 28 of Series 2 with Geba fine sand (Tab. A.2). The saturations were based on tensiometers along the column during the injection of the slug and the subsequent nitrogen chase. The tensiometers suggested an apparent change in water saturation during active gas flow through the porous medium. This was most likely provoked by the pressure increase due to the injection and the gas flow around the tensiometer. It is important to note that the tensiometers measured the suction at a very spatially-limited location in the porous medium due to the small size of their tips (o.d. = 6 mm, length = 8 mm). In addition, the pressure transducers of the tensiometers showed periodic fluctuations as a result of daily temperature changes in the laboratory hall and due to varying ambient pressure. However, a drying-out of the porous medium was prevented by the humidification of all gases (slug and chase) prior to injection. This was confirmed by the water mass balance by means of the continuous weight measurement of the entire column throughout all experiments conducted within a series. Hence, the initial water-saturation profile could be maintained throughout the experiments. These experiments allowed for the characterization of transport behavior under different initial and controlled boundary conditions.

5.2.2. Impact of velocity on breakthrough

The impact of the seepage velocity on the concentration breakthroughs of argon and CS_2 was investigated. Thus different velocities were applied to characterize the transport. Figure 5.15 and 5.16 show breakthrough curves of CS_2 and argon as a function of pore volume for different flow conditions (velocities) in moist fine glass beads and Geba fine sand. The breakthrough curves were adapted to the actual gas-effective pore volume determined from the mean breakthrough arrival time τ_{Ar} (Eq. 3.6) of the conservative tracer argon. Seepage velocities of about 25, 50, 100, and 200 cm h^{-1} (residence time of about 8, 4, 2, and 1 h) were applied successively in the same column and under similar initial conditions. The lines represent measured concentrations (c/c_{ss}) normalized to steady-state concentration. The graphs are split and the right-hand

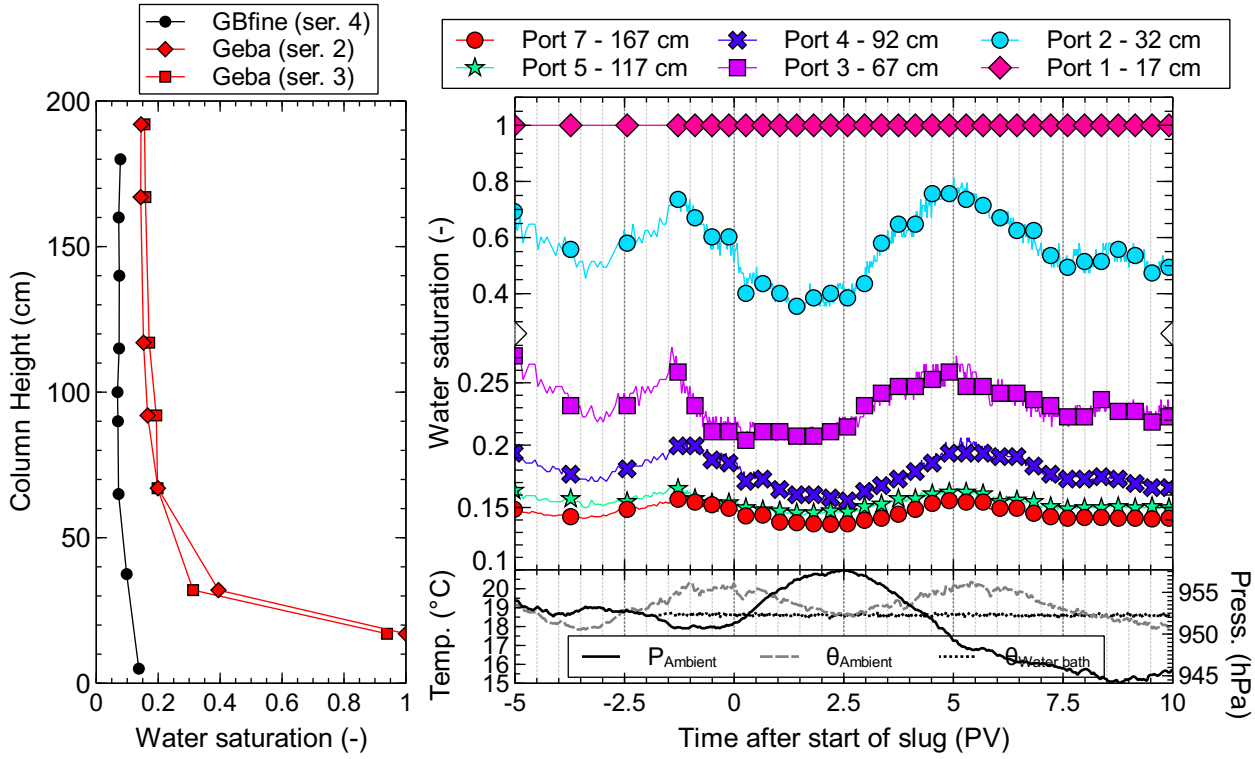

(a) Initial water saturation.

(b) Development of water saturation in experiment with Geba fine sand (Series 2).

Figure 5.14. Initial water saturation in vapor-migration experiments and exemplary graph showing the development of water saturation during the slug injection and subsequent chase in Geba fine sand (Series 2).

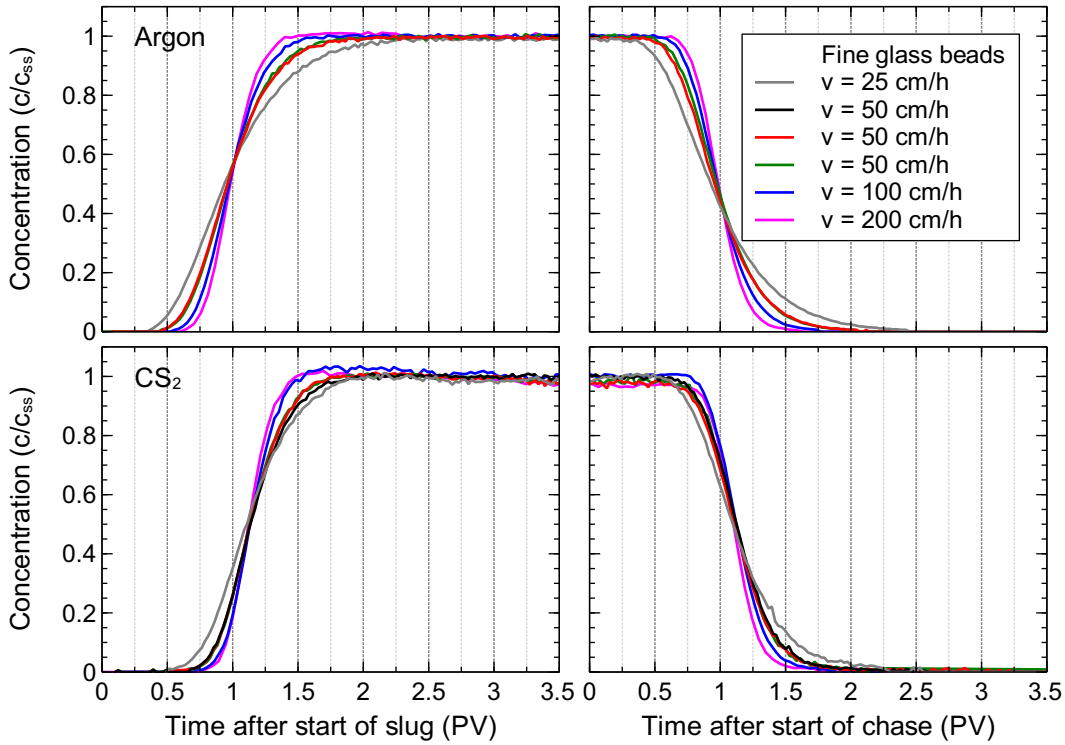

Figure 5.15. Breakthrough curves of CS_2 and Ar in moist fine glass beads ($S_w = 0.088$) for different velocities.

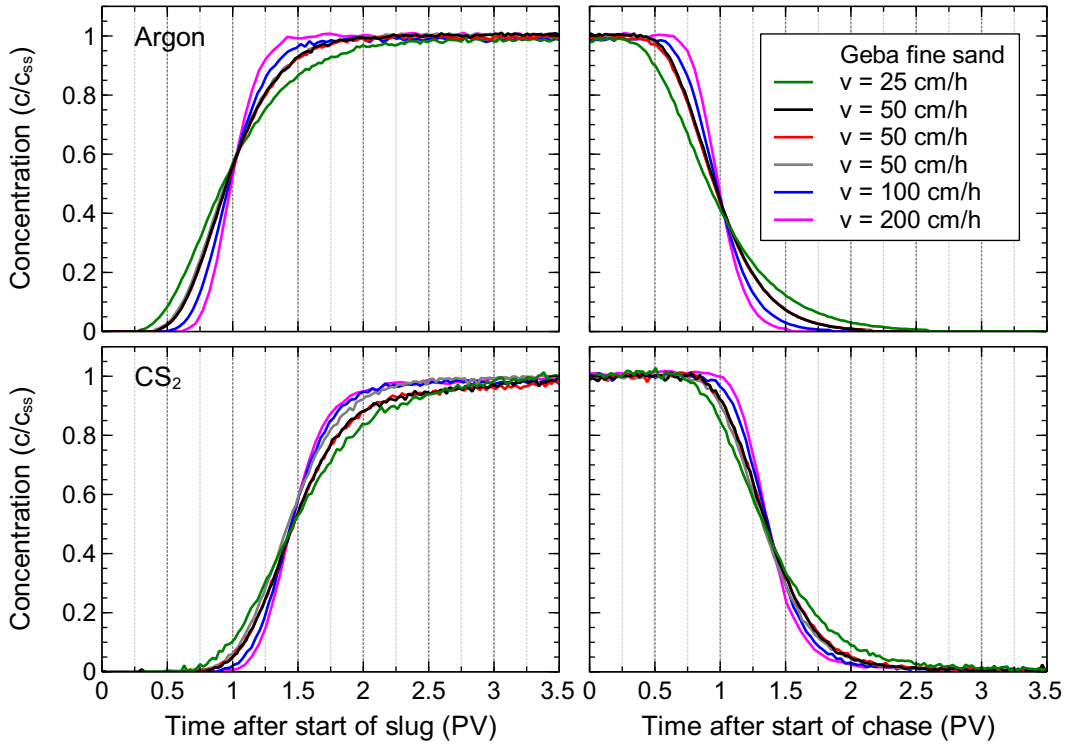

Figure 5.16. Breakthrough curves of CS_2 and Ar in moist Geba fine sand ($S_w = 0.154$) for different velocities.

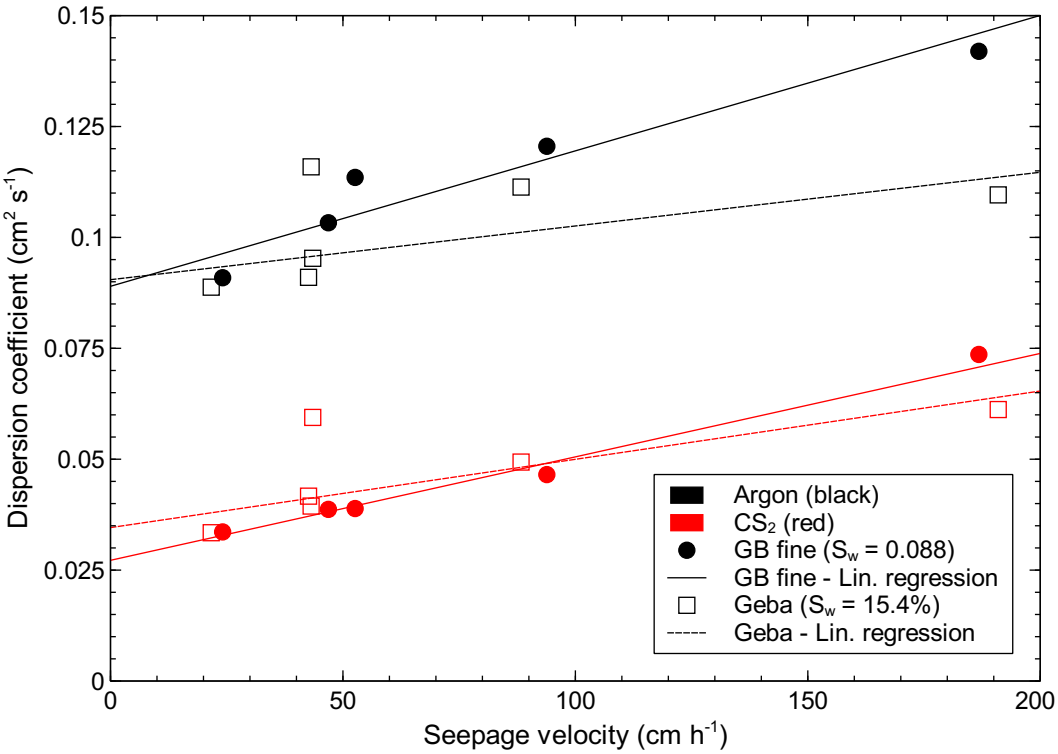

Figure 5.17. Dispersion coefficients of CS_2 and Ar determined from TMA as a function of velocity. Experiments were conducted in fine glass beads ($S_w = 0.088$, Series 2) and Geba fine sand ($S_w = 0.154$, Series 2).

side shows the outflow concentrations after the injection was switched from the gas-mixture slug to the N_2 chase. Thus, these experiments allowed for the individual evaluation of the slug and of the N_2 chase breakthroughs. The skewness of a BTC is a result of the longitudinal molecular diffusion and the mechanical mixing (often referred to as hydrodynamic dispersion in the field of groundwater flow). The molecular diffusion gains importance with decreasing seepage velocity due to longer residence times in the porous media while mechanical mixing increases with increasing velocity. The BTCs of argon and CS_2 shown in the graphs revealed that the skewness increased with decreasing seepage velocity as a result of increased diffusion during the longer residence time. Since argon was used as a conservative tracer, its breakthrough was a function of the seepage velocity only. CS_2 was additionally affected by retardation, hence its breakthrough depended on seepage velocity as well as water saturation. The retardation of CS_2 is discussed in detail in the following Section 5.2.3. The repetitions with a velocity of about $50\,cm\,h^{-1}$ proved that equilibrium was reached and they showed good reproducibility of the experiments.

The BTCs were evaluated with the temporal-moment analysis (TMA) to obtain dispersion coefficients (Eq. 3.9) of argon and CS_2 for different flow conditions. Figure 5.17 shows dispersion coefficients as a function of velocity of these experiments in moist, fine porous media. Dispersion coefficients of argon and CS_2 increased from $D_{Ar} = 0.089$ to $0.142\,cm^2\,s^{-1}$ and $D_{CS_2} = 0.033$ to $0.074\,cm^2\,s^{-1}$ as a function of the seepage velocity and the porous medium. The dispersion

Table 5.8. Theoretical and experimental effective binary diffusion coefficient D^* of argon and CS_2, dispersivity α, and coefficient of determination R^2 of linear regression determined from experiments in moist porous media (Series 2).

Porous medium		Fine glass beads	Geba fine sand
Water saturation S_w		0.088	0.154
Tortuosity τ		0.220	0.161
Argon	D_t^*, $cm^2\,s^{-1}$	0.0386	0.0284
	D^*, $cm^2\,s^{-1}$	0.0909	0.0966
	α, cm	1.029	0.313
	R^2 (lin. regression)	0.919	0.254
CS_2	D_t^*, $cm^2\,s^{-1}$	0.0213	0.0157
	D^*, $cm^2\,s^{-1}$	0.0263	0.0332
	α, cm	0.888	0.552
	R^2 (lin. regression)	0.987	0.952

coefficient is defined as $D = D^* + \alpha v$ (see Eq. 2.17). Under static conditions ($v = 0\,cm\,h^{-1}$), the effective binary diffusion coefficients D^* in porous media should apply. D^* is defined as the product of the binary diffusion coefficient (Eq. 2.11) of the component in nitrogen and a tortuosity factor τ (Eq. 2.14). In the case of flow, the dispersion coefficient increases due to hydrodynamic dispersion/mechanical mixing which is a measure of the heterogeneity of the porous medium or the flow region, respectively. It is defined as the product of the dispersivity α and the velocity.

The effective binary diffusion coefficients D^* and the dispersivity α were determined from the breakthrough curves of the experiments. Based on the equation above (Eq. 2.17), a linear regression was fitted to the dispersion coefficients as a function of the velocity for each porous medium. The y-intercepts of the regression lines represent the coefficient D^* and the slopes express dispersivity α of the respective porous medium. The theoretical coefficient D_t^* was determined according to the Chapman-Enskog theory and the approach by *Millington and Quirk* (1961) which accounts for tortuosity due to porous matrix and water saturation. Table 5.8 compares theoretical with experimental effective binary diffusion coefficients of CS_2 and argon in fine glass beads and Geba fine sand under the given experimental conditions (water saturation S_w and tortuosity tau). In fine glass beads, effective binary diffusion coefficients of argon were $D^*_{Ar} = 0.0909\,cm^2\,s^{-1}$ compared to $D^*_{t,Ar} = 0.0386\,cm^2\,s^{-1}$ and of CS_2 were $D^*_{CS_2} = 0.0263\,cm^2\,s^{-1}$ compared to $D^*_{t,CS_2} = 0.0213\,cm^2\,s^{-1}$. In Geba fine sand, coefficients of argon were $D^*_{Ar} = 0.0966\,cm^2\,s^{-1}$ compared to $D^*_{t,Ar} = 0.0284\,cm^2\,s^{-1}$ and of CS_2 were $D^*_{CS_2} = 0.0332\,cm^2\,s^{-1}$ compared to $D^*_{t,CS_2} = 0.0157\,cm^2\,s^{-1}$. The experimental coefficients D^* differed from the theoretical effective binary diffusion coefficient D_t^* calculated for the prevailing conditions. This could result from the choice of porous media, since both media were characterized by a uniform and narrow grain-size distribution, as well as the observed water-saturation profiles. *Werner et al.* (2004) reported that theoretical approaches are often sensitive since the majority of their parameters are raised to a high power and do not apply satisfactorily to a wide variety of soils. Furthermore, the theoretical approach does not take into account

material characteristics such as the pore-size distribution which may vary for similar porosities and hence affect the tortuosity factor. Dispersion coefficients shown in Figure 5.17 varied for a given velocity due to minor differences between the experiments and to variations arising from the temporal-moment analysis. The equation used to determine the dispersion coefficient (Eq. 3.9) from TMA raises the velocity to the power of three, thus minor deviations had a great impact on the final values.

The increase in the dispersion coefficient in Figure 5.17 from the effective binary diffusion coefficient (at $v = 0\,cm\,h^{-1}$) with increasing velocity resulted from mechanical mixing due to flow through the moist porous medium. This was observed in all experiments. The increase is determined by the slope of the linear regression representing the dispersivity α which should be a parameter of the porous medium only and should be independent of the components (gases) and flow conditions. A slight difference was found between CS_2 and argon for both materials, resulting in a mean dispersivity of $\alpha_{GBfine} = 0.958\,cm$ in fine glass beads and $\alpha_{Geba} = 0.432\,cm$ in Geba fine sand. The difference could be due to dispersivity transforming from a physical system to a lumped parameter, because of e.g. diffusional or nonequilibrium effects. This then results in a component-dependent dispersivity according to *Costanza-Robinson and Brusseau* (2002), who reported that dispersivity ranges from approx. 0.1 to 5 cm. Since argon is a conservative tracer and CS_2 is affected by retardation, greater reliability was attributed to the dispersivity α_{Ar} determined from BTCs of argon.

Popovičová and Brusseau (1997) showed in their column experiments that for gas velocities smaller than $1200\,cm\,h^{-1}$, breakthrough curves were affected by longitudinal diffusion only. Thus the experiments conducted in this study were predominantly characterized by longitudinal diffusion. Moreover, they were conducted at low inflow pressures (close to ambient pressure) and with fairly high permeabilities (see Tab. 3.2). Hence, effects such as slip flow or viscous flow which gain importance at higher pressures and lower permeabilities (approx. $1 \times 10^{-18}\,m^2$) could be ruled out (*Thorstenson and Pollock*, 1989; *Webb and Pruess*, 2003). The results of the experiments in this work demonstrate the impact of seepage velocities on the diffusion/dispersion of CS_2 vapor and of argon. Thus, an influence of the velocity on the retardation of CS_2 was expected.

5.2.3. Retardation of CS_2

Different series of experiments were conducted to quantify retardation of CS_2 as a function of water saturation and seepage velocity. Figure 5.18 and 5.19 compare breakthrough curves (BTC) of argon and CS_2 in dry (black) and moist (red) porous medium for the same seepage velocity ($v = 50\,cm\,h^{-1}$). Two to three repetitions of each run in dry and moist conditions, respectively, are shown. The graphs show normalized concentrations as a function of effective pore volume (total pore volume minus water content after drainage).

The BTCs of argon showed excellent reproducibility in repetition experiments in both materials at the same conditions ($v = 50\,cm\,h^{-1}$). In fine glass beads, argon showed very similar BTCs for dry and moist experiments. This thus confirmed that argon experiences no retardation and may be used as a conservative tracer and as a reference for CS_2. In Geba fine sand, a different skewness was observed between dry and moist conditions as a result of the reduced pore space

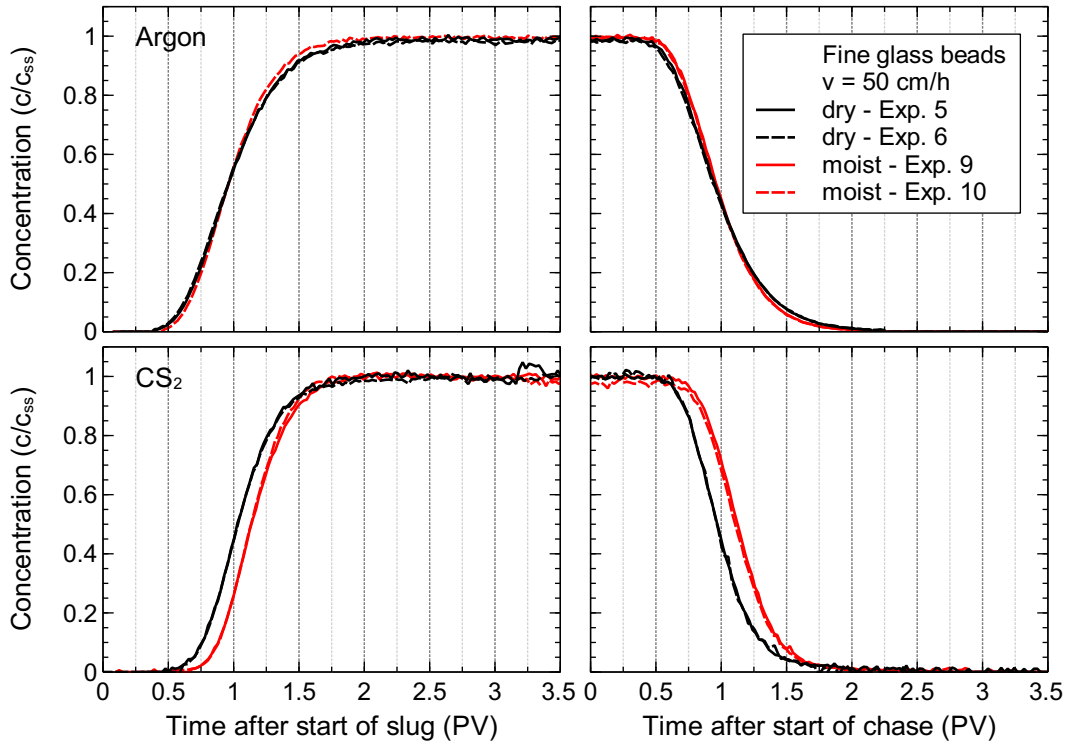

Figure 5.18. Breakthrough curves of CS_2 and Ar in dry and moist ($S_w = 0.088$) fine glass beads under identical slug and flow conditions ($v = 50\,cm\,h^{-1}$).

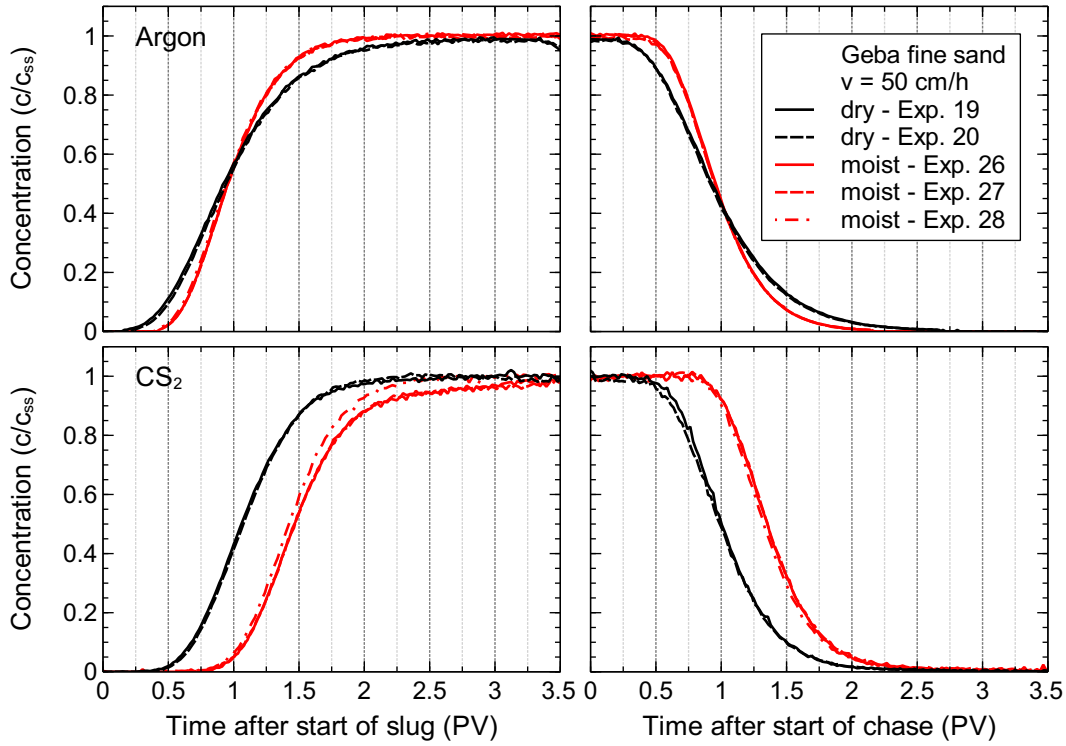

Figure 5.19. Breakthrough curves of CS_2 and Ar in dry and moist ($S_w = 0.154$) Geba fine sand under identical slug and flow conditions ($v = 50\,cm\,h^{-1}$).

in moist conditions. Hence, a comparison of the BTCs revealed that the effective-flow region in fine glass beads was similar in dry and moist conditions, whereas in Geba fine sand it was reduced in moist conditions. This resulted in BTCs which were less affected by diffusion due to a shorter residence time. Since the experiments were conducted with a constant-flow-rate boundary condition based on the calculated effective pore volume, a shorter residence time i.e. higher seepage velocity occurred when the actual effective pore volume available for gas flow is smaller than the calculated volume.

The BTCs of CS_2 showed, in general, good reproducibility for all experiments. In fine glass beads, a later breakthrough of CS_2 compared to argon can be observed in Figure 5.18, demonstrating the retardation of CS_2 due to partitioning into the water phase. The different effective pore volume due to the pore water and possible reduced residence time (actual vs. calculated PV) resulted in less skewed BTCs compared to the dry experiments. In Geba fine sand, a more pronounced retardation of CS_2 was observed compared to experiments in fine glass beads. The later breakthrough becomes evident when comparing BTCs in dry (black) with moist (red) conditions in Figure 5.19. This could be ascribed to the overall higher water saturation and the increase in saturation toward the bottom of the column. In two of the three BTCs in moist experiments (Fig. 5.19), CS_2 concentrations leveled at around $c/c_{ss} = 0.9$ followed by an increase to steady-state (plateau) concentrations toward the end of the slug. This behavior might be a consequence of the water saturation over column height (Fig. 5.14a) affecting the partitioning processes. The water-saturation profile was obtained by drainage via the suction plate installed into the bottom of the column which was used for the drainage. It showed an air entry pressure below the referenced pressure of 100 mbar thus the irreducible water saturations (see P_c–S_w, Fig. 3.1) along the entire column height in Geba fine sand could not be reached.

The retardation coefficients of CS_2 as a function of porous medium, water saturation, and seepage velocity were determined using the temporal-moment analysis (TMA) of the breakthrough curves (see Sec. 3.5.2). The coefficients were normalized with respect to the BTCs from dry porous medium. Thereby, errors due to set-up or other systematic errors could be eliminated and allowed for the comparison with theoretical values. Figure 5.20 shows retardation coefficients of CS_2 as a function of water saturation (upper) and seepage velocity (lower) in fine glass beads (black) and Geba fine sand (red). The coefficients of the slug (circle) and the chase (rectangle) are given and their size represents seepage velocity or water saturation. Note the broken x-axis (water saturation) between $S_w = 0.10$ and 0.13 in the upper graph indicated by the vertical, dashed lines. Detailed TMA results of all conducted vapor-retardation experiments are given in Tables A.3 and A.4 in the appendix.

In fine glass beads, a non-linear increase in the retardation coefficient from $R_{GBfine} = 1.09$ to 1.16 with increasing water saturation from $S_w = 0.075$ to 0.155 was observed. Of course, partitioning to the water phase is dependent on the gas-water interfacial area which should decrease with increasing water saturation. Thus an extrapolation of the retardation coefficient to higher water saturations might be difficult. The retardation of the slug and of the chase were different in fine glass beads, the chase being more prone to retardation than the slug. The breakthrough of the N_2 chase (removal of the CS_2 vapor) showed a higher retardation by a factor (average) of 1.05 compared to the breakthrough of the slug throughout all experiments in fine glass beads. This behavior can be also seen when comparing the BTCs of CS_2 in the upper graph of Figure 5.18.

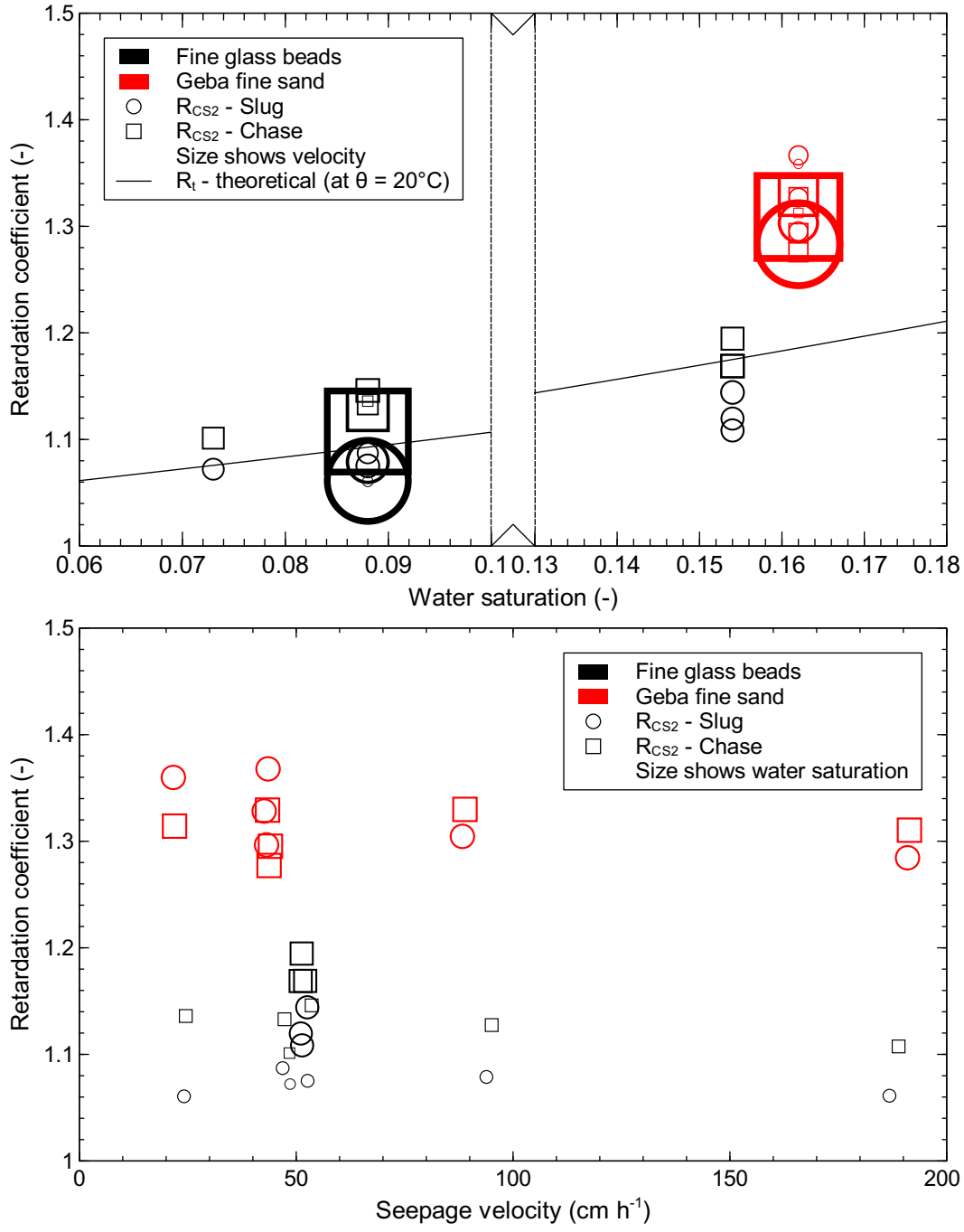

Figure 5.20. Retardation coefficients of CS_2 determined from experiments with different seepage velocities in fine glass beads and in Geba fine sand at different water saturations (evaluated with temporal-moment analysis).

In Geba fine sand, higher retardation coefficients compared to fine glass beads were measured in the experiments. These ranged between $R_{Geba} = 1.29$ and 1.34 at a mean water saturation of $S_w = 0.162$. This was due to the higher water saturation and its increase toward the bottom (discussed in Sec. 5.2.1), the different gas-water interfacial area, and the pore space available for gas flow. Unfortunately, Series 3 in Geba fine sand had to be excluded from these graphs due to mass balance issues discussed later. Hence, results were only available for one particular water saturation in Geba fine sand. The ratio between the retardation coefficient of the slug and that of the chase did not show a clear trend as observed in fine glass beads despite the differences seen in Figure 5.20.

The retardation coefficients gained from the experiments were compared to a theoretical approach. The adapted theoretical retardation coefficient (Eq. 3.11) is shown as a line in the upper graph. The theoretical coefficient is calculated taking into account the porosity of the porous medium, the water saturation, and the Henry coefficient. Hence, only one function is shown in the upper graph of Figure 5.20, since the porosities of the fine glass beads and the Geba fine sand used were similar. In fine glass beads, the theoretical coefficient compared very well with the values from the experiments. It slightly overpredicted the retardation of the slug while it underpredicted that of the chase, however it reproduced satisfactorily the mean retardation coefficient and its increase with water saturation. In Geba fine sand, the theoretical coefficient significantly underestimated the observed retardation. This could be due to the fairly simple theoretical approach only taking into account the porosity of the porous medium. It is obvious that the pore-size distribution depending on the grain-size distribution of the porous medium determines the gas-water interfacial area and thus has a significant impact on retardation. However, such material characteristics are not factored in by the theoretical coefficient. Moreover, the non-uniform water-saturation profile along the column height could be responsible for varying partitioning. Finally, deviations could occur due to adsorption processes or higher-order kinetics during partitioning which were neglected in the theoretical factor. These findings suggest that retardation may vary along the depth of the unsaturated zone due to spatially-varying water saturations and especially around the capillary fringe in the vicinity of the groundwater level.

The experiments were conducted with different seepage velocities to evaluate their impact on retardation. The lower graph in Figure 5.20 shows the retardation coefficients as a function of seepage velocity. A mean retardation coefficient of $R_{GBfine} = 1.1000 \pm 0.0096$ and $R_{Geba} = 1.3150 \pm 0.0152$ was measured in the experiments with fine glass beads ($S_w = 0.088$) and Geba fine sand ($S_w = 0.162$), respectively. In general, no significant change of the retardation behavior with increasing seepage velocity was observed. This confirmed that the mass transport rate was low enough and the residence time of the slug was sufficient for the partitioning processes to reach equilibrium. Concluding from the experiment with $v = 200\,cm\,h^{-1}$ it seems likely that there was a slight tendency toward a reduced retardation. In fact, retardation may reduce at higher seepage velocities due to limiting contaminant diffusion. If no equilibrium is reached in case of high velocities, the retardation coefficient reflects an apparent coefficient since in this case it is a function of the experimental system used (i.e. length of the column). Additional experimental repetitions would have been required to provide proof. However, this experimental investigation aimed at characterizing retardation of CS_2 in the range of seepage velocities observed during vapor-plume migration in the previous experimental investigation

($v \ll 200\,cm\,h^{-1}$). Hence, the focus laid on the velocities used and higher values were beyond the scope.

Mass balance analyses were performed to obtain mass recovery (r) from each breakthrough curve. Mass recovery was calculated from concentration and flow measurements and were normalized with respect to the injected mass. In general, mass recoveries of argon and CS_2 showed good results. The mean recovery of argon calculated from all vapor-retardation experiments conducted yielded $r_{Ar} = 0.995 \pm 0.007$ and confirmed complete mass recovery. The mean recovery of CS_2 was $r_{CS_2} = 0.981 \pm 0.084$ (without the experiments of Series 3), thus only suggesting slight mass losses. Mass recoveries of all experiments are given in Table A.2 in the appendix. The mass balance and complete recovery proved the reliability and quality of the results gained from these column experiments.

The results discussed above excluded Series 3 conducted in Geba fine sand. Series 3 was the second saturation and drainage cycle which was carried out to establish a different static water saturation than in Series 2. However, significant CS_2 mass losses became more pronounced with each experiment in this series, eventually leading to its exclusion from the results.

Recoveries of CS_2 decreased from $r_{CS_2} = 0.854$ in the first experiment of Series 3 down to $r_{CS_2} = 0.010$. This mass loss of CS_2 was caused by biodegradation which was confirmed by the smell of hydrogen sulfide in the column outflow. *Cox et al.* (2013) found carbonyl sulfide (COS) and hydrogen sulfide (H_2S) as by-products during CS_2 biodegradation in their experiments. The mass balance analysis of the experiments enabled for determining mean degradation rates of CS_2 which were calculated from the CS_2 mass rate and the recovery. The mean degradation rates ranged from 0.12 to $1.28\,mg\,h^{-1}$ depending on the respective seepage velocity applied in the experiments. The experiments showed that biodegradation may have a considerable potential for mitigating the contaminant mass transfer by vapor migration to the underlying aquifer. However, the quantification of biodegradation of CS_2 was beyond the scope of this work but should be addressed in future research.

5.2.4. Summarized results

Vapor-retardation experiments were conducted in large, 2 m long columns packed with fine glass beads or Geba fine sand in dry and moist conditions. This custom-built set-up allowed for characterizing the retardation behavior of CS_2 as a function of porous medium, water saturation, and seepage velocity. The concentration breakthrough curves were evaluated with the versatile temporal-moment method (TMA) to evaluate the transport and to quantify the retardation of CS_2 by relating its mean arrival time to that of the conservative tracer argon.

The moist porous media were obtained by saturation and subsequent drainage until finally reaching static water-saturation profiles (see Fig. 5.14a). A uniform profile at irreducible water saturation ($S_w = 0.07$) was observed in fine glass beads whereas a pronounced increase in saturation (from $S_w = 0.15$ to 1.00) toward the bottom was measured in Geba fine sand. This was due to the characteristics of the porous media and the suction applied during drainage which was limited by the air entry pressure of the porous plate (Sec. 3.4.2). Tensiometer measurements confirmed that the initial water-saturation profile could be maintained throughout

all experiments conducted within a series. The retardation of CS_2 was expected to be affected by the mean water saturation or the non-uniform water-saturation profiles in the case of Geba fine sand.

Different seepage velocities ranging from 25 to 200 cm h^{-1} were applied to characterize the vapor transport and to evaluate their impact on retardation. The range was chosen based on the velocities observed during the experimental investigation into density-driven vapor migration (Sec. 5.1). The experiments showed that the velocities affected diffusion/dispersion of the gases due to the corresponding residence time in the porous medium and due to mechanical mixing. This effect was illustrated by the skewness of the breakthrough curves shown in Figure 5.15 and 5.16. The skewness of the BTCs was negatively correlated to the seepage velocity. Dispersion coefficients as a function of seepage velocity were obtained from the temporal-moment analysis for experiments in moist conditions. These ranged from $D_{Ar} = 0.089$ to $0.142\,cm^2\,s^{-1}$ and $D_{CS_2} = 0.033$ to $0.074\,cm^2\,s^{-1}$ as a function of the seepage velocity and the porous medium.

Based on the graph of dispersion coefficients as a function of seepage velocity (Fig. 5.17), linear regressions were used to determine the effective binary diffusion coefficient of argon and CS_2 as well as the dispersivity of the two porous media. In fine glass beads, effective binary diffusion coefficients of argon were $D^*_{Ar} = 0.0909\,cm^2\,s^{-1}$ and of CS_2 were $D^*_{CS_2} = 0.0263\,cm^2\,s^{-1}$. In Geba fine sand, coefficients of argon were $D^*_{Ar} = 0.0966\,cm^2\,s^{-1}$ and of CS_2 were $D^*_{CS_2} = 0.0332\,cm^2\,s^{-1}$. The effective binary diffusion coefficients of the experiments were higher than those calculated from the theoretical approach (*Millington and Quirk*, 1961) given in Table 5.8. The higher experimental values could be a result of the porous media used in this work which were characterized by a uniform and narrow grain-size distribution. Furthermore, the theoretical approach takes into account the porosity only and neglects material characteristics such as grain-size or pore-size distribution which affect diffusion/dispersion. This confirms that theoretical approaches do not apply satisfactorily to a wide variety of materials. Dispersivity was obtained from the slope of the linear regression and differed slightly for argon and CS_2. A mean dispersivity of $\alpha_{GBfine} = 0.958$ cm in fine glass beads and $\alpha_{Geba} = 0.432$ cm in Geba fine sand was determined in moist conditions. Since CS_2 was affected by retardation, the dispersivity gained from the breakthrough curve of argon was considered more reliable.

The retardation of CS_2 was quantified based on the experiments in dry and moist porous media. The injection of a slug and subsequent chase allowed for the separate evaluation employing the temporal-moment analysis which has been adapted for step input. The breakthrough of CS_2 was first related to that of argon and second compared with breakthroughs in dry porous media. This ensured reproducible results and eliminated systematic errors or set-up related errors (Fig. 5.18 and 5.19). The experiments conducted showed a clear retardation of CS_2 in moist porous media as a function of water saturation (Fig. 5.20). In fine glass beads, the retardation coefficient increased from $R_{GBfine} = 1.09$ to 1.16 with water saturation increasing from $S_w = 0.075$ to 0.155. Retardation in fine glass beads compared very well with the theoretical retardation coefficient (Eq. 3.11) taking into account the partitioning into the aqueous phase. The results benefited from the uniform water-saturation profile in the column observed with fine glass beads. In all experiments, a slightly higher retardation of the chase by a factor of 1.05 compared to that of the slug was observed. Retardation in Geba fine sand was stronger than predicted by the theoretical coefficient which was believed to be influenced by the particular

water-saturation profile. A mean retardation coefficient of $R_{Geba} = 1.32$ was determined at a water saturation of $S_w = 0.162$. The pronounced increase in water saturation toward the bottom probably contributed to the retardation due to the higher reservoir available for dissolved CS_2 despite the smaller interfacial area. Retardation coefficients as a function of (seepage) velocity revealed only a minor dependency and suggested a slight tendency toward a reduced retardation at higher velocities. Further repetitions and experiments with higher velocities would be required to investigate this behavior.

Mass balance of argon and CS_2 confirmed complete mass removal. A mean recovery of argon yielded $r_{Ar} = 0.995 \pm 0.007$ and of CS_2 $r_{CS_2} = 0.981 \pm 0.084$. These high recovery values support the experimental results presented in this work. In the last series of vapor-migration experiments conducted in Geba fine sand, the mass balance revealed significant losses of CS_2 increasing with every experiment conducted. This series of experiments revealed biodegradation of CS_2 due to microbial growth after the last saturation-and-drainage cycle. This was confirmed by the smell of hydrogen sulfide in the column outflow which *Cox et al.* (2013) has reported to be a by-product of degradation in soils. Mean degradation rates up to $1.28\,mg\,h^{-1}$ were determined from mass balance analyses. These findings demonstrate the potential of biodegradation to reduce the total CS_2 mass in case of a contamination in the unsaturated zone and of migrating vapor plumes eventually threating the underlying aquifer.

The vapor-retardation experiments conducted in this work successfully allowed for quantifying the retardation of CS_2 vapor as a function of water saturation and seepage velocity in two different porous media. It was shown that the migrating CS_2 vapor was retarded due to partitioning into the aqueous phase. Retardation coefficients up to 1.20 and 1.36 were measured in fine glass beads ($S_w = 0.162$) and in Geba fine sand ($S_w = 0.162$), respectively. The breakthrough of the slug and of the chase was observed and evaluated, the latter demonstrating a complete removal of the gaseous CS_2 confirmed by mass balance analyses. This observation clearly promotes the remediation of a liquid CS_2 spill using soil-vapor extraction. SVE was investigated in detail in 2-D experiments and their results are discussed in the following section.

Key findings

- The retardation of CS_2 was quantified in column experiments for two porous media at different water saturations by comparison with the conservative tracer argon.
- The temporal-moment analysis (TMA) was successfully applied to quantify diffusion/dispersion of CS_2 and argon as well as retardation of CS_2 from concentration breakthrough curves.
- The effective binary diffusion coefficient at the given experimental conditions was found to be slightly higher than theoretical values based on the approach by *Millington and Quirk* (1961).
- The impact of different seepage velocities on the breakthrough curves and thus on the dispersion coefficient was observed.

- The retardation coefficient of CS_2 increased with increasing water saturation and compared very well with the theoretical approach for fine glass beads. A pronounced higher retardation was observed in Geba fine sand due to the different grain-size distribution and the particular water-saturation profile.
- Clear evidence of the biodegradation of CS_2 was found in the last series of experiments in Geba fine sand confirmed by the mass balance analysis.
- The experiments conducted clearly proved that a migrating CS_2-vapor plume in the unsaturated zone is retarded and that dissolved CS_2 is amenable to biodegradation.

5.3. Spill and remediation

A spill of liquid CS_2 into moist porous media was observed visually in 2-D flume experiments. Two different materials, fine glass beads and Geba fine sand, were used. The spreading strongly depended on the moisture content of the porous media and its capillary pressure–water saturation relationship (Fig. 3.1) and the type of spill.

The subsequent remediation of the liquid CS_2 spill employing soil-vapor extraction was performed successfully and proved an efficient contaminant removal. The extraction mass rate was confirmed to be dependent on the contaminant distribution in the moist porous media and the applied extraction flow rate. CS_2 residing as a micro pool on local heterogeneities was removed more slowly than CS_2 at residual saturation. The overall performance showed that soil-vapor extraction is the method of choice for the in-situ remediation of CS_2 from the unsaturated zone.

This chapter addresses the results and discusses CS_2 distribution and remediation behavior of the conducted spill and remediation experiments. The window front of the 2-D flume allowed for visual observation during injection. The performance of spill and remediation of each experiment was recorded and time-lapse movies were produced in order to visually demonstrate and support the results.

5.3.1. Initial water saturation

The spreading of liquid CS_2 after a spill was affected by the water saturation of the porous media. Thus, similar initial conditions were necessary to allow for the comparison of results from different experiments. The purpose of the saturation and drainage set-up, introduced in Sec. 3.4.2, was to establish similar water saturations in each porous medium. Table 5.9 shows mean water saturation determined from mass balance prior to each experiment. The difference in mean water saturation of fine glass beads ($S_w = 0.21$, 0.21, and 0.18) and Geba fine sand ($S_w = 0.41$ and 0.40) was due to the different grain-size distributions and capillary pressure–water saturation relationships (Fig. 3.1) of the respective porous medium.

Figure 5.21 shows static water-saturation profiles based on tensiometer measurements at different elevations in the flume prior to CS_2 injection. In fine glass beads, a water saturation of about $S_w = 0.07$ was measured above 18 cm of flume height. A strong increase to $S_w = 0.60$ was observed in the vicinity of the rods at the base of the flume. This abrupt change in saturation was clearly visible through the window. In Geba fine sand, the water saturation steadily increased from $S_w = 0.24$ at the top to approx. 0.55 toward the bottom. The suction applied via the porous rods for drainage was limited by the air entry pressure (approx. 100 mbar). Thus, a higher suction could not be established in order to obtain irreducible water saturations in Geba fine sand (see also Sec. 5.2.1). The water-saturation profiles of experiments with the same porous medium showed good reproducibility. Exemplary plots of tensiometer measurements during spill and remediation are given in the appendix (Fig. A.6a and b).

The water saturation greatly affected the distribution of the injected CS_2 which was characterized by a three-phase, three-component behavior (Liquid-Liquid-Gas) where water was considered the wetting fluid compared to CS_2 and the gas phase. Water filled the small pores

Table 5.9. Experimental parameters and conditions of the spill and remediation experiments.

Experiment	1	2	3	4	5	6	7	8
Material	Fine glass beads			Geba fine sand				
Mean water saturation	0.21	0.21	0.18	0.41	0.41	0.41	0.41	0.41
Effective pore volume, L	22.1	22.1	22.1	17.0	17.0	17.0	17.0	17.0
CS_2 injection method	Single-port			Multi-port				
CS_2 distribution type	Pool			Residual				
Spill (injection) rate, mL min^{-1}	2.0	n/a	n/a	0.5	0.5	1.0	1.0	1.0
Injected CS_2 mass, g	156.6	149.8	139.0	146.6	146.4	146.4	146.2	146.0
Injected CS_2 volume, mL	124.0	118.6	110.1	116.0	115.9	115.9	115.8	115.7
Mean effective soil-gas velocity, m h^{-1}	1.0	0.5	0.5	1.0	1.0	1.0	0.5	2.0
Mean inflow temperature, °C	26.0	20.7	20.4	18.7	19.4	21.7	21.3	21.4
Mean outflow temperature, °C	26.5	20.9	20.6	19.7	20.7	21.7	21.6	22.0
Extracted CS_2 mass, g	99.4	95.2	90.5	121.7	124.7	116.1	107.8	112.1
90 % of normalized recovery, PV	98	20	10	6.5	13	5	4	6
Mean CS_2 mass removal rate (at 90 % norm. recov.), g L^{-1}	0.04	0.20	0.34	0.87	0.49	1.31	1.38	1.02
Apparent total recovery	0.64	0.64	0.65	0.83	0.85	0.79	0.74	0.77
End of Phase 1, PV	3	10	10	14	16	7	6	9
End of Phase 2, PV	158	37	24	96	108	36	39	42
End of Phase 3, PV	230	70	79	156	352	98	90	138

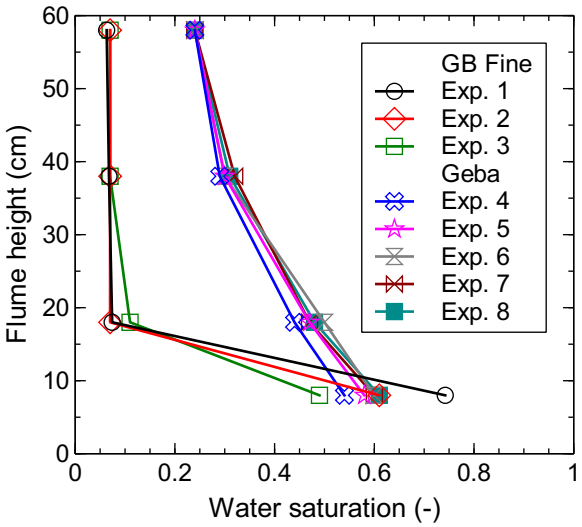

Figure 5.21. Static water saturation determined from tensiometer measurements.

while liquid CS_2 (non-wetting) had to spread into bigger pores. Lower capillary forces yielded a very limited retention of CS_2 around the point of injection. The different water saturations in fine glass beads and Geba fine sand additionally affected CS_2 spreading. The higher the water saturation the less space was available for the injected CS_2 which resulted in a larger horizontal spreading around the point of injection. Distribution of liquid CS_2 as a function of porous medium, water saturation, CS_2 mass and injection rate are discussed in the following section.

5.3.2. Spill and distribution of CS_2

The experiments visualized the spreading behavior of liquid, dyed CS_2 after a spill in fine glass beads and Geba fine sand at static water saturation. Different CS_2 distributions were observed as a result of the material characteristics (Fig. 3.1), water saturation, and single-port vs. multi-port injection method (Sec. 4.3.2), as they caused either a pool of CS_2 or a residual distribution. Figure 5.22 shows snapshots of selected spills (experiments) at the end of redistribution. Table 5.9 summarizes the applied injection method and total mass of CS_2 (ranging from 139 to 157 g) injected in each experiment.

Spill in fine glass beads Three experiments with spills of liquid CS_2 were performed in fine glass beads. In the first experiment a single-port injection was applied. The second and third experiment were conducted with multi-port injection. The final CS_2 distribution (Fig. 5.22) of Experiment 1 and 3 demonstrated the difference between the two injection methods.

In Experiment 1, the single-port injection at the upper part of the porous medium (port no. 7 in Fig. 4.6) produced a pool of liquid CS_2 at the bottom of the flume. Liquid CS_2 was injected at a constant rate into the horizontal, fully screened (over flume width) well. It penetrated the porous medium at the point of lowest resistance (entry pressure) and presumably followed a

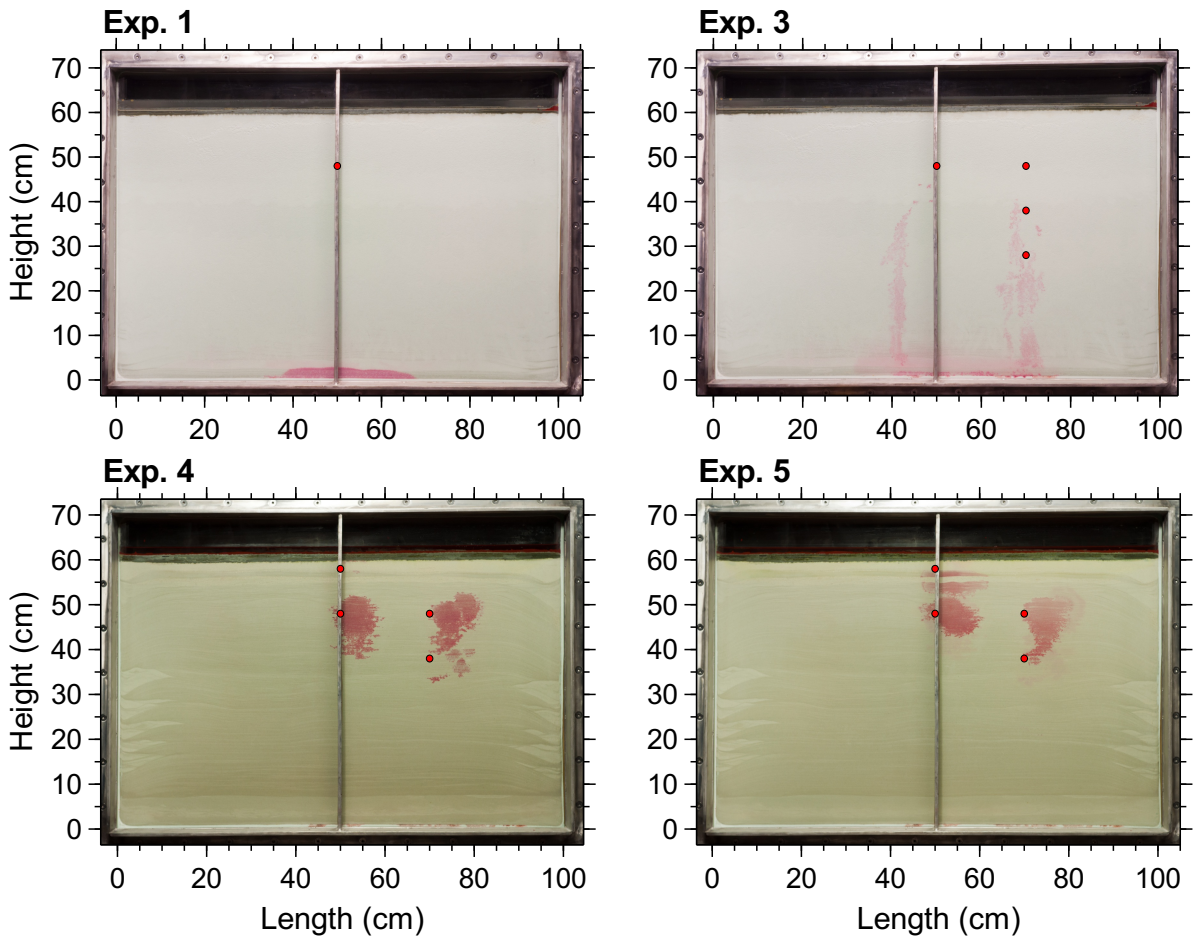

Figure 5.22. Pictures of liquid CS_2 spills into fine glass beads (Exp. 1 and 3) and Geba fine sand (Exp. 4 and 5) in a 2-D flume (red spots indicate points of injection).

preferential path as a continuous phase toward the bottom. CS_2 was first visible upon accumulating (pooling) at the bottom of the flume or at zones of higher water saturation near the suction rods around 30 min after the start of injection.

In Experiment 3, the multi-port injection was performed by means of a needle connected to a syringe. The method is illustrated in Figure A.5 in the appendix. The needle was introduced into the porous medium through the backside ports and CS_2 was injected at three different distances from the back to the front in each injection line. In total three lines with different horizontal angles were used, which resulted in a total of nine injection points per port. A volume of 3 mL was injected at each point. Injections were carried out into ports 7, 13, 14, and 15 (Fig. 4.6). Experiment 3 (Fig. 5.22) shows two flow paths of liquid CS_2 spreading downward in the vicinity of the window front. In contrast to the single-port injection, CS_2 formed a discontinuous phase due to the interrupted multi-port injection. The liquid phase thus started its downward migration from each single injection point and left every time a trace of residual CS_2 saturation due to snap-off effects. Since sufficient" CS_2 was injected, pooling at the bottom of the flume occurred. However, it took about 50 % longer for CS_2 to start accumulating at the bottom and the accumulated (pooled) mass was much smaller than in Experiment 1.

Spill in Geba fine sand Several experiments employing multi-port injection as described above were carried out in Geba fine sand. Compared to fine glass beads, Geba fine sand was characterized by a wider grain-size distribution including a higher fraction of small particles. Hence, a different distribution of CS_2 was expected. Port 7, 8, 13, and 14 were used for injection of CS_2 due to a rearrangement of tensiometers to different ports after packing with Geba fine sand. Figure 5.22 shows the final CS_2 distribution of Experiment 4 and 5. The pictures demonstrate the different spreading in fine glass beads compared to Geba fine sand. CS_2 spread uniformly around the point of injection showing a slight tendency toward a downward migration. Within 18 h (between stop of injection and start of remediation) the liquid phase migrated around 3 cm downward. The CS_2 distribution was additionally characterized by strong lateral spreading, induced by micro-heterogeneities, compared to the fine glass beads where a predominant vertical sinking was observed. The Geba fine sand characteristics formed smaller pores responsible for the higher retention ability.

Summarized results Different CS_2 distributions subsequent to the spills were observed in the experiments as a function of the injection methods, the porous media, and the initial water saturations (Fig. 5.22). Two different methods, a single-port (continuous) and a multi-port (interrupted) injection were used in fine glass beads. The continuous injection provoked a single flow path of a continuous CS_2 phase traveling through the pore space. This happened due to the accumulation of liquid CS_2 during injection eventually overcoming the entry pressure. The continuous method resulted in a pooling of liquid CS_2 at the bottom of the flume. The interrupted injection prevented a continuous phase and resulted in a more widespread distribution at residual saturation. However, the injected volume of liquid CS_2 was still sufficient for a pronounced downward migration even though multi-port (interrupted) injection was applied.

The porous media used had a strong impact on the spill behavior. Fine glass beads showed a poor ability to hold the injected liquid CS_2 in the vicinity of the injection point. The uniformity

of the glass beads facilitated the very fast downward migration toward the bottom of the flume within 30 to 45 min. This was observed with both continuous and interrupted injection. In Geba fine sand, the injected CS_2 was held by capillary forces around the points of injection. Only a slight downward migration of about 3 cm was observed over a period of 18 h. The higher water saturation in Geba fine sand compared to fine glass beads caused a wider distribution due to the smaller pore space available for CS_2.

The experiments demonstrated that the distribution of CS_2 in the unsaturated zone will be affected by the type of spill (or spill rate) and the characteristics of the porous medium. The findings are in good accordance with *Poulsen and Kueper* (1992), who reported similar observations in their investigations into spills of tetrachloroethene in an unsaturated porous medium. The experiments showed that a spill from a point source combined with a limited ability of the porous medium to hold the contaminant by capillary forces results in a severe percolation toward the underlying aquifer. Scattered contaminant spills, or higher capillary forces to hold the liquid contaminant may slow down percolation and reduce the threat of groundwater contamination. The different distributions of the liquid CS_2 observed in the experiments had a high impact on the remediation discussed in the following section.

5.3.3. Remediation of spill

This section addresses the investigation of soil-vapor extraction (SVE) for the remediation of liquid CS_2 in the unsaturated zone. The principal of a remediation with SVE is the extraction of contaminated soil air by means of blowers through wells installed in the subsurface. Thereby volatile compounds of a contamination can be efficiently removed from the unsaturated zone. This remediation technique was applied in the 2-D flume experiments. Table 5.9 summarizes for all experiments: mean water saturation (-), effective pore volume (L), CS_2 injection method, type of distribution, spill (injection) rate ($mL\,min^{-1}$), injected CS_2 mass (g) and volume (mL), mean effective soil-gas velocity ($m\,h^{-1}$), inflow and outflow temperatures (°C), and extracted CS_2 mass (g). Furthermore, the performance parameter defined as 90 % of normalized recovery (PV), mean CS_2 mass removal rate ($g\,L^{-1}$) calculated from total extracted mass divided by volume extracted at 90 % normalized recovery, and apparent total recovery are given. Since extraction flow rate (volume per time) is a function of geometry (dimensions of flume), porous medium, and water saturation; the mean soil-gas velocity (length per time) in the porous medium was used instead. It was calculated from the extraction flow rate and the effective pore volume. This facilitated interpretation and allows for comparison with field applications. Figures 5.23, 5.24, 5.26, and 5.28 show absolute CS_2 concentrations and normalized recovery for different time frames, a short term (left-hand side) and a long term (right-hand side) graph. The graphs are drawn as a function of effective pore volume (normalized time with respect to extraction) to allow for direct comparison between the experiments. The effective pore volume was determined from the dry pore volume and the initial water saturation of each experiment. Additional information is given in parenthesis in the legend of the graphs (soil-gas velocity [$m\,h^{-1}$], porous medium [GB = glass beads, FS = Geba fine sand], type of CS_2 distribution [pool or residual]). The injected mass of liquid CS_2 (139 to 157 g; Table 5.9) corresponded to a gas volume of about 70 to 79 L at standard conditions. This was equal to ap-

proximately 3.5 times the available pore volume of the fine glass beads packing and 4.5 times the pore volume of Geba fine sand.

Soil-vapor extraction was started about 12 h after the spill to ensure equilibrium regarding CS_2 distribution (liquid and gas/vapor) in the flume. The remediation progress was expected to be influenced by the CS_2 distribution in the porous medium, water saturation and mean effective soil-gas velocity (extraction flow rate). Residual CS_2 was expected to have a large liquid-gas interfacial area whereas a pool of CS_2 was expected to be rather characterized by a reduced area. The interfacial area between the liquid and the existing gas phase affects the vaporization process of liquid CS_2. From this consideration follows that the remediation of a residual distribution was expected to be faster and thus more efficient than of CS_2 residing as a pool. The water saturation of a porous medium determines the relative permeability for the gas phase. Figure 5.21 showed an increase in water saturation toward the bottom, hence a decrease of relative permeability. A slower removal of CS_2 was expected in the case of liquid CS_2 residing predominantly at the flume bottom. The soil-gas velocity was assumed to control remediation time. A slow velocity was expected to be more efficient but would result in a longer duration. High extraction concentrations may be reached due to a longer residence time of the extracted soil vapor. A high velocity was assumed to be less efficient but faster. However, due to limited vaporization or mass transfer, the CS_2 mass removal rate only increases to a certain point and thereafter decreases again.

In all experiments conducted, the remediation progress showed a similar behavior which was separated into three phases. Table 5.9 lists the end time (PV) of each phase. The first phase was determined by a high extraction mass rate of CS_2 (removal). Evaporated liquid CS_2 during the time period between injection and start of extraction filled the pore space available for gas with highly-concentrated vapor. The high interfacial area of liquid CS_2 or availability for vaporization during the first pore volumes extracted additionally increased mass removal. This was observed as initially high concentrations from the start of extraction which then continuously decreased over 2 to 4 extracted pore volumes. This phase was stretched over the first pore volumes as relative permeability for the gas phase (as a function of water saturation) and local heterogeneities promoted preferential, horizontal gas flow paths. Its end was marked by a strong concentration decline. In the second phase, the extraction mass flux was entirely controlled by the mass transfer rate from the liquid to the gas phase. The higher the specific surface or interfacial area of liquid CS_2 in this phase, the higher the vaporization rate and hence the soil-vapor concentration. Continuously decreasing CS_2 concentrations were observed during this long-lasting phase, ending with concentrations of less than $0.5\,g\,m^{-3}$. In the third phase, mass removal was controlled by diffusion of CS_2 toward the effective flow area. It lasted until extraction was shut off at concentrations below $0.05\,g\,m^{-3}$. One day (24 h) after shutdown and equilibration, soil-vapor extraction was restarted. This time was considered sufficient to reach chemical equilibrium due to re-partitioning and gas diffusion. Only minor concentration rebounds were measured, thus it could be concluded that the remediation was successful. The following paragraphs describe the remediation part of the experiments, first in fine glass beads and second in Geba fine sand, then the results are summarized and discussed.

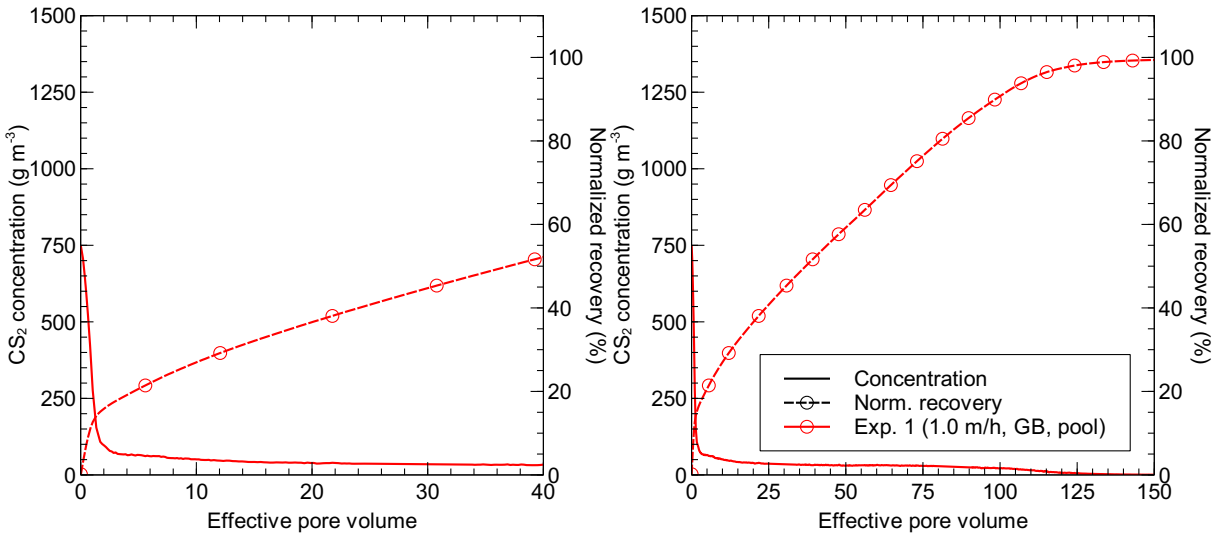

Figure 5.23. CS_2 extraction concentration and normalized recovery of the remediation of a CS_2 pool in fine glass beads (Experiment 1). The left graph focuses on the initial remediation.

Remediation in fine glass beads The first of three experiments conducted in fine glass beads aimed at the remediation of a CS_2 pool. The single-port (continuous) injection of CS_2 resulted in downward-migrating liquid CS_2 forming a pool at the bottom of the flume, thus an impact on the remediation was expected. The CS_2 distribution of Exp. 1 was discussed in the previous Section 5.3.2. The soil-vapor extraction led to a mean effective soil-gas velocity of about 1.0 m h^{-1}. Figure 5.23 shows CS_2 concentration in the extracted gas phase (line) and normalized recovery (line and marker) as a function of pore volume for Experiment 1. The left graph focuses on the first 40 PV.

In the first phase of Experiment 1, extracted soil-vapor concentrations started at around 750 g m^{-3} (approx. 60 % of saturation concentration) and declined within 2 PV to approximately 75 g m^{-3}. This was followed by the vaporization-limited second phase of remediation where concentrations continuously decreased to 0.5 g m^{-3} from 2 to 158 PV. Recalling the predominant CS_2 pool at the bottom of the flume, only a small mass fraction of CS_2 was residing in the region of high relative permeability for the gas phase. These circumstances resulted in low absolute concentrations not reaching saturation concentrations at the beginning of extraction and the earlier decline in the first phase. Furthermore, a re-distribution of water caused a layer of high saturation at the bottom of the flume due to the long time period (35 d) between end of drainage and injection of CS_2 as a result of technical issues. The liquid CS_2 pool at the bottom of the flume partly penetrated this water layer. The limited mass transfer rate of CS_2 into the gas phase as well as the reduced relative permeability in the zone of high CS_2 saturation were responsible for the long-lasting second phase. In the third phase, extraction was shut down after 230 PV when concentrations fell below 0.05 g m^{-3}. After one day (24 h) of equilibration, two rebound tests were performed with concentrations up to 2.7 g m^{-3} dropping back to 0.1 g m^{-3}. The rebound tests confirmed a successful remediation of the CS_2 pool; however a small mass was still residing in the water layer only slowly diffusing into the gas phase.

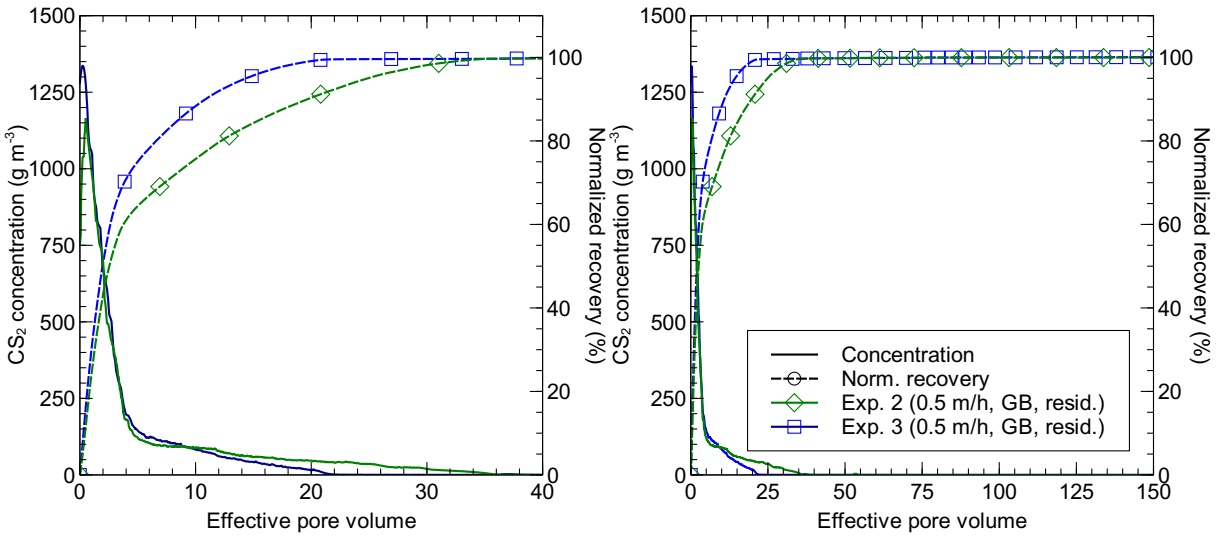

Figure 5.24. CS_2 extraction concentration and normalized recovery of the remediation of a residual CS_2 distribution in fine glass beads (Experiments 2 and 3). The left graph focuses on the initial remediation.

A total mass of 99.4 g was removed which corresponded to an apparent total recovery of 0.64. The rather poor recovery was caused by inaccuracies arising from manual gas sampling, analytics, and technical inaccuracy of flow meters and their manual reading. Mechanical deterioration of the autosampler's rotor seal of the injection valve led to reduced concentration measurements which further contributed to the lower apparent total recovery. These inaccuracies had a major impact on the total recovery, since the high concentrations measured in the first phase were responsible for a high percentage of mass removal. The performance parameter defined as 90 % normalized recovery, was reached after 98 PV. A mean CS_2 mass removal rate of 0.04 g L^{-1} was measured in Experiment 1.

The remediation of a residual CS_2 distribution showed an altogether different behavior which was addressed in Experiments 2 and 3. The residual distribution of liquid $CS_2$was a result of the multi-port (interrupted) injection method (Sec. 5.3.2) used in these experiments, hence a faster remediation was expected. Both experiments were conducted with a mean effective soil-gas velocity of 0.5 m h^{-1}. Figure 5.24 shows CS_2 concentration and normalized recovery as a function of pore volume. The left graph focuses again on the first 40 PV.

Concentrations reached saturation concentration at the beginning of the first phase which lasted for about 4 PV. Within 2 PV, concentrations decreased rapidly to around 100 g m^{-3} at the end of Phase 1. During the second phase, concentrations declined continuously to below 0.5 g m^{-3} after 37 and 24 PV in Experiments 2 and 3 respectively. In the third phase, extraction was shut down after 70 PV (Exp. 2) and 79 PV (Exp. 3) after concentrations of less than 0.05 g m^{-3} had been reached. Two rebound tests after 24 h of equilibration were performed in both experiments. In Exp. 2, concentration rebounds up to 0.4 and 0.12 g m^{-3} were measured. In Exp. 3, concentrations up to 2.5 and 0.4 g m^{-3} were observed following the extraction restart. In both experiments, concentrations fell below 0.05 g m^{-3} within 4 to 6 PV after SVE restart.

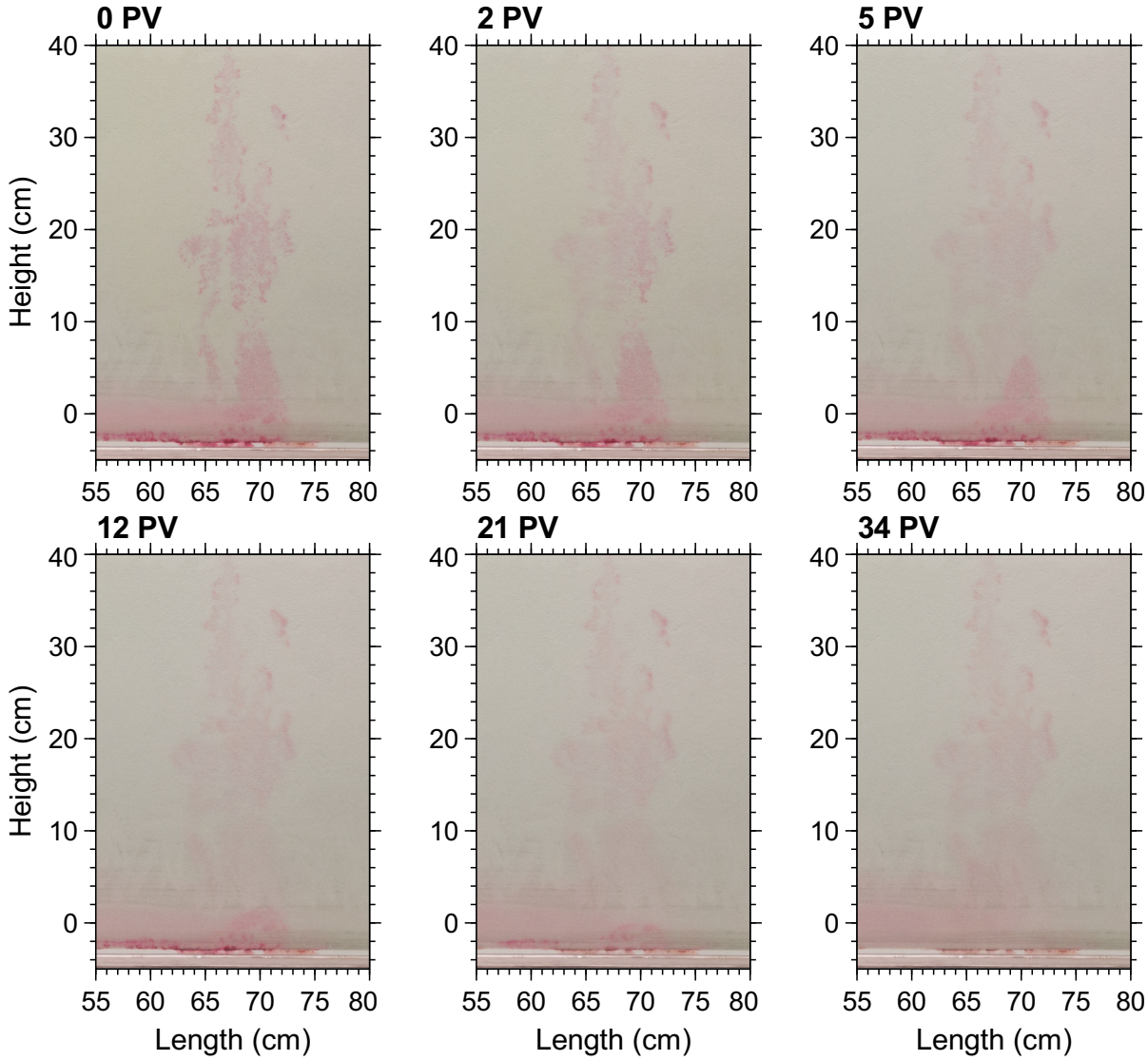

Figure 5.25. Experiment 2: Close-up view on CS_2 spill in fine glass beads at chosen extracted pore volumes during ongoing soil-vapor extraction.

A total mass of 95.5 and 90.5 g was removed in Experiment 2 and 3, respectively, corresponding to the apparent total recovery of 0.64 and 0.65. Again, the rather poor apparent total mass removals were caused by the sum of inaccuracies from manual gas sampling, analytics, and flow meters. However, the two rebound tests confirmed the nearly complete removal of CS_2 and thus successful remediation. Therefore, the actual total recovery was assumed to be closer to 1.00. The performance parameter was already reached after 20 and 10 PV and mean CS_2 mass removal rates of 0.20 and 0.34 g L^{-1} were measured in Exp. 2 and 3, respectively. This reflected the better remediation performance of a residual contaminant distribution compared to a pool.

Figure 5.25 shows close-up views of the spill over time during the remediation of Experiment 2.

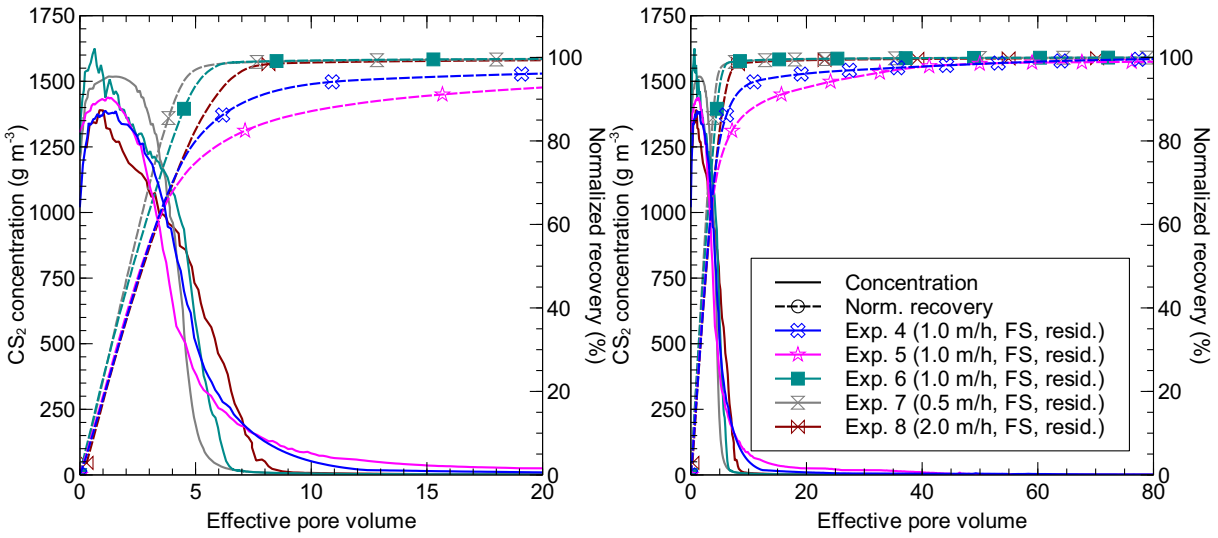

Figure 5.26. CS_2 extraction concentration and normalized recovery of the remediation of a residual CS_2 distribution in Geba fine sand (Experiment 4 through 8). The left graph focuses on the initial remediation.

What can be seen in the pictures is the vaporization process of the residually-distributed, dyed, liquid CS_2 phase in fine glass beads. This is visualized by the decreasing color intensity (attenuation). The residually-distributed phase (residual trace from top to bottom) was removed quickly. Clean gas entered the flume on the left-hand side gradually evaporating the liquid CS_2 while flowing through the porous medium. The accumulated part at the bottom kept vaporizing after the easily available part of the spill was removed from the upper region of the porous medium with high relative permeability and large interfacial area. The visual disappearance of the liquid phase coincided with the final decline of concentrations measured after 36 PV (Fig. 5.24). The reddish residues were dye (Oil Red O) adsorbed on the grains which stayed behind after the vaporization of CS_2.

Remediation in Geba fine sand Five experiments were performed to investigate the remediation of a residual CS_2 distribution in Geba fine sand as described in Sec. 5.3.2. Comparability between experiments was achieved by applying the same injection method and injected CS_2 mass (Table 5.9). Experiments 4 and 5 were conducted applying the same soil-gas velocity of $1.0\,m\,h^{-1}$ to test reproducibility in Geba fine sand. Moreover, they were compared to Exp. 6 to evaluate the impact of temperature on remediation. Finally, Experiments 6 to 8 were studied to quantify the influence of the soil-gas velocity on remediation. Figure 5.26 illustrates extraction concentration and normalized recovery as a function of effective pore volume (0 to 20 PV and 0 to 80 PV) of Experiment 4 to 8.

Experiments 4 and 5 showed satisfactory similarity regarding the concentration measurements and the remediation progress. High CS_2 concentrations up to saturation concentration were measured at the beginning of remediation until 3 PV. This was due to the large interfacial area of residually distributed, liquid CS_2 in the upper region of the flume with high relative per-

meability, thus permitting high extraction mass rates. At this point, already 50 % of the total recovered mass was removed in both experiments demonstrating a fast remediation. CS_2 concentration gradually decreased from saturation to below 100 g m^{-3} within 8 PV, marking the end of Phase 1. Significantly lower concentrations were measured during the second phase as a result of the remaining CS_2 residing in the lower part of the flume with lower relative permeability for gas. The second phase ended with concentrations below 0.5 g m^{-3} after approximately 96 PV (Exp. 4) and 108 PV (Exp. 5). The third phase lasted until the shutdown of extraction at 156 PV in Exp. 4 and 352 PV in Exp. 5. After one day (24 h) of equilibration, SVE was restarted to test for concentration rebounds. No rebound was measured in Experiment 4. In Experiment 5, a concentration rise from 0.07 to 0.4 g m^{-3} was measured after restart, decreasing again within 4 PV. The rebound tests confirmed nearly complete removal of CS_2 in both experiments. 90 % of normalized recovery was reached at around 6.5 PV (Exp. 4) and 13 PV (Exp. 5).

Figure 5.27 shows close-up views of the CS_2 spill during the remediation of Experiment 4. The pictures clearly show the vaporization of the liquid phase starting on the left-hand side followed by the right-hand side. Again, a slight delay of the lower part compared to the upper part was observed. This stemmed from the higher relative permeability for gas in the upper region of the porous medium due to the water-saturation profile (see Fig. 5.21). The vanishing of the liquid phase coincided with the steep concentration decline between 3 to 10 PV. This was already observed in the experiments performed with fine glass beads (Fig. 5.25).

The impact of temperature on the remediation performance could be determined comparing Experiments 4/5 to 6. Already minor changes in temperature had a significant impact on vaporization due to the low boiling point and high vapor pressure of CS_2. The experiments were conducted at different gas-inflow temperatures while applying the same mean effective soil-gas velocity of 1 m h^{-1}. Experiments 4 and 5 were conducted at a mean inflow temperature of 18.7 and 19.4 °C and Experiment 6 at 21.7 °C. These minor differences in temperature significantly influenced the remediation performance. In the first phase, lower absolute concentrations were measured in Exp. 4 and 5 compared to Exp. 6. Moreover, a significant difference in the concentration decline (tailing) was observed, shown in Fig. 5.26 (left-hand). Experiments 4 and 5 showed a more pronounced tailing compared to Exp. 6 where concentrations dropped considerably faster. The end of the decline marked the beginning of the second phase where concentration were determined by the availability of CS_2. The performance parameter (90 % of normalized recovery) was reached after 6.5 and 13 PV in Exp. 4 and 5 and after 5 PV in Exp. 6. Thus, the increase in temperature sped up the remediation in Experiment 6 by approximately 10 and 43 % K^{-1} compared to Exp. 4 and 5, respectively. The CS_2 mass removal rate increased from 0.87 g L^{-1} (Exp. 4) and 0.49 g L^{-1} (Exp. 5) to 1.38 g L^{-1} (Exp. 6) as a result of the higher temperature.

Experiments 6 to 8 were conducted to investigate remediation efficiency as a function of mean effective soil-gas velocity. Comparability was achieved by conducting these experiments at similar gas-inflow temperatures of about 21.47 ± 0.16 °C. No saturation-and-drainage cycle was performed in between the experiments and gas inflow was kept at 100 % humidity, thus same initial conditions were maintained. Concentration measurements of Experiments 6 to 8 in Figure 5.26 illustrate the influence of the soil-gas velocity on remediation. A slow velocity

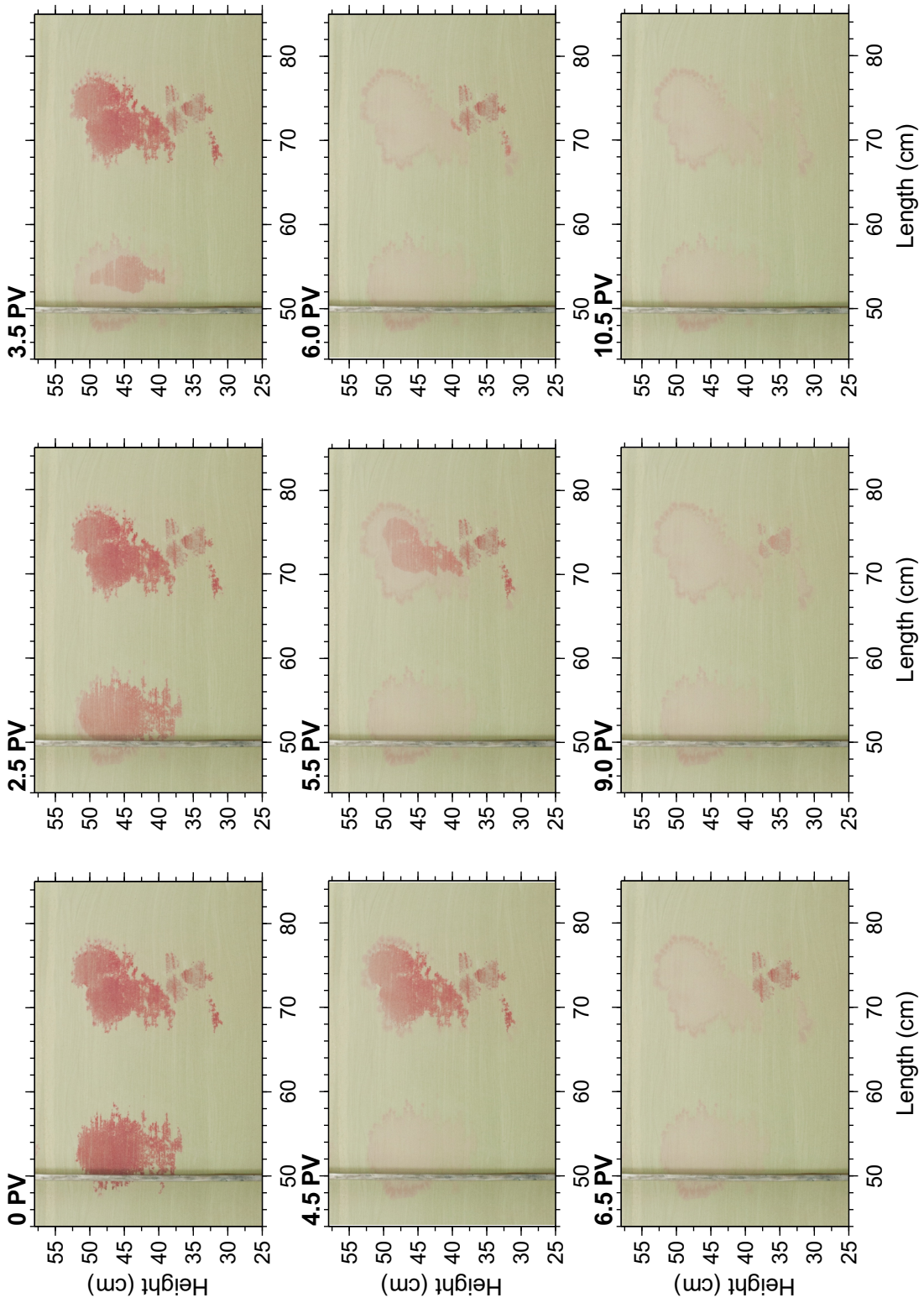

Figure 5.27. Experiment 4: Close-up view on CS_2 spill at chosen extracted pore volumes during ongoing soil-vapor extraction in Geba fine sand.

of about 0.5 m h^{-1} in Experiment 7 resulted in a longer-lasting first phase at high concentration with a steep decline ending at around 6 PV. This proved an efficient remediation of the residual CS_2 distribution residing in the region of high relative permeability. Faster soil-gas velocities of about 1.0 and 2.0 m h^{-1} in Experiments 6 and 8, respectively, revealed a shorter duration of high concentration as well as an earlier and flatter decline. The end of the concentration decline which marked the beginning of the second phase was measured at 7 and 9 PV. Hence, the availability of CS_2 was limiting its removal at higher soil-gas velocities. 90 % of normalized recovery was reached after 4, 5, and 6 PV in Experiments 7, 6, and 8, conducted with mean effective soil-gas velocities of 0.5, 1.0, and 2.0 m h^{-1}. The mean CS_2 mass removal rate was determined to be 1.38, 1.31, and 1.02 g L^{-1} for these soil-gas velocities (same order). The inference of these experiments is that the mass removal rate (i.e. contaminant load in SVE) is inversely correlated to the soil-gas velocity. Thus, slower soil-gas velocities increase the mass removal rate resulting in a more efficient contaminant removal. One has to keep in mind that these observations are related to mean effective soil-gas velocities or extracted pore volumes, hence lower extraction rates lead to a longer duration of operation and vice versa despite a higher contaminant load. This has to be considered when assessing the efficiency (mass removal vs. energy input) of a remediation design.

Table 5.9 shows the total extracted CS_2 mass and apparent total recovery (ranging between 0.74 and 0.83) in Experiments 4 to 8. Apparent CS_2 recovery reached satisfactory results considering the uncertainties and errors arising from flow rate measurements and the high volatility of CS_2. Moreover, minor rebounds followed by a fast concentration decline confirmed the successful remediations. Thus, the actual mass recovery was believed to be significantly higher, reaching nearly complete CS_2 removal.

5.3.4. Summarized results

Eight 2-D flume experiments were performed exploring CS_2 distributions from different type of spills and their remediation using soil-vapor extraction in two different moist porous media (fine glass beads and Geba fine sand). Spills were performed applying either the single-port (continuous) or multi-port (interrupted) injection method (see Sec. 4.3.2). CS_2 distribution (Fig. 5.3.2) was found to be highly dependent on the injection method and the material characteristics (grain-size distribution, capillary pressure–water saturation relationship). The uniformity of fine glass beads combined with the single-port injection (Exp. 1) resulted in a preferential flow path of the continuous phase and a pool of liquid CS_2 at the bottom of the flume. The multi-port injection method favored a residual distribution showing traces of downward-spreading CS_2 from points of injection in fine glass beads. The CS_2 was observed to quickly reach the bottom (within 30 to 45 min). Spills in Geba fine sand behaved differently compared to fine glass beads. This was mainly due to the wider grain-size distribution with a higher fraction of small particles favoring residual spreading around the points of injection. The downward migration of the liquid phase, continuing after injection had been finished, was also greatly reduced to a distance of about 1 to 3 cm from point of injection. Moreover, it showed a lateral spreading as a result of micro-heterogeneities (horizontal layering).

These different CS_2 distributions had a significant impact on the subsequent remediation em-

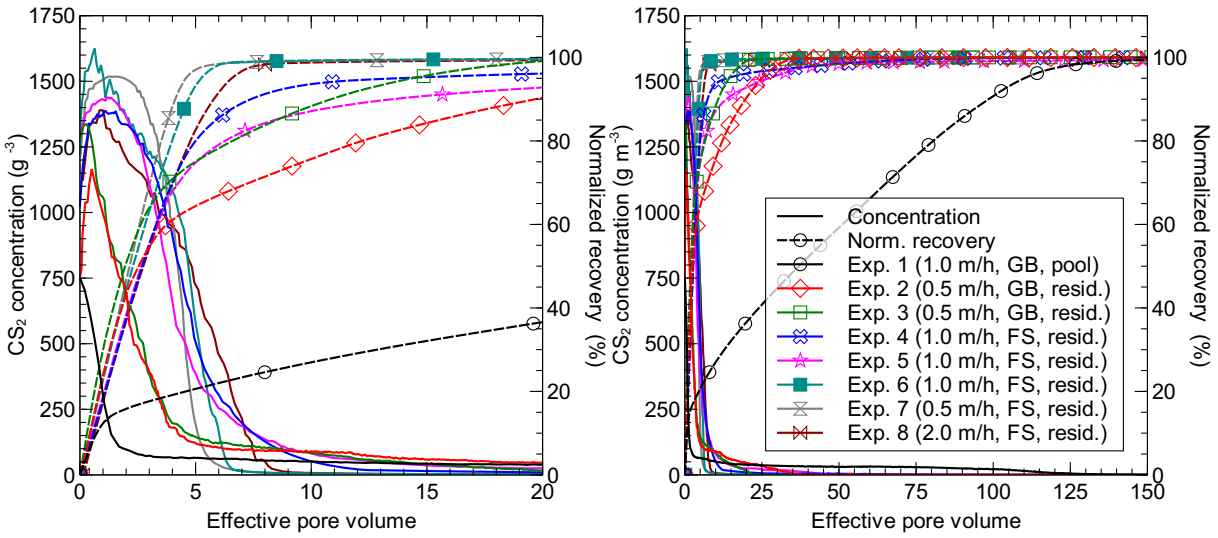

Figure 5.28. Comparison of extraction concentration and normalized recovery of all remediation experiments performed in 2-D flume. The left graph focuses on the initial remediation.

ploying soil-vapor extraction. Table 5.9 summarizes the experimental conditions. Figure 5.28 illustrates the extraction concentration and normalized recovery of all experiments showing the impact on remediation provoked by the porous medium, the injection method and the mean effective soil-gas velocity.

A pronounced difference was observed between the remediation of a CS_2 pool (Exp. 1) and a residual CS_2 distribution (Exp. 4 and 5). The remediation of a pool required significantly more time than that of a residual distribution. The single-port injection method applied in Exp. 1 caused a pool of liquid CS_2 at the bottom of the flume that partially penetrated the water layer. Thus, most of the CS_2 mass resided in the region of high water content resulting in a significantly reduced gas-liquid interfacial area with a concurrently low relative gas permeability. This was the reason for lower soil-vapor concentrations and an early concentration decline in the first phase of extraction. Furthermore, it prolonged the overall duration of the remediation due to long-lasting low concentrations and limited mass removal rates in the second phase. These observations are in agreement with *Illangasekare et al.* (2014) who reported that source zones with high water content and trapped NAPL have lower mass loading rates into the vadose zone.

The remediation of a residual CS_2 distribution was characterized by a faster and more efficient mass removal. The major fraction of CS_2 mass was distributed and held by capillary forces in the upper region of the flume at low water saturation, and thus high relative permeability. This allowed for high concentrations at the beginning of the remediation followed by a steep concentration decline to low concentrations after CS_2 removal from the area with high relative permeability. Hence, mass removal rates were considerably higher compared to a CS_2 pool illustrated by the normalized recovery as a function of pore volume in Figure 5.28.

These experimental observations will apply to a CS_2 contamination in the unsaturated zone. However, this work was based on a scenario with a large depth of the unsaturated zone and a deep groundwater level (100 m below the ground level). Thus, the experimental investigations were directed toward the remediation of residual CS_2 rather than pooled.

The remediation of a residual CS_2 distribution as a function of porous medium was evaluated by comparing Experiments 2 and 3 in fine glass beads with 4 and 5 in Geba fine sand. Different mean effective soil-gas velocities of $0.5\,m\,h^{-1}$ and $1.0\,m\,h^{-1}$ were applied (Table 5.9). The main difference observed during remediation stemmed from the different material characteristics responsible for the observed water-saturation profile and the CS_2 distribution. The lower ability of fine glass beads to hold fluids by capillary forces was responsible for a lower water saturation and for the downward migration of liquid CS_2 from the area of irreducible to higher water saturation (lower relative gas permeability). In contrast, in Geba fine sand CS_2 stayed around the points of injection despite higher water saturation. These circumstances were responsible for the observed behavior during remediation. In fine glass beads Exp. 2 and 3, concentrations lower than saturation concentration were measured in Phase 1 at the beginning of the extraction followed by an early and gradual decline. In Geba fine sand (Exp. 4 and 5), concentrations up to saturation concentration were observed which lasted two to three times longer due to the amount of residual CS_2 residing in the region of high relative permeability. The decline at the end of the first phase leveled at higher concentrations in fine glass beads compared to Geba fine sand. Recalling the slower soil-gas velocity in fine glass beads, similar velocities in Geba fine sand would have resulted in a longer period of high absolute concentrations, and hence a more efficient remediation. In conclusion, the type of porous medium affects the remediation indirectly by its material characteristics controlling water saturation and relative permeability for gas as well as contaminant distribution.

The influence of temperature on remediation was quantified by comparing the experiments with different mean inflow temperatures (Exp. 4/5 to 6). Already a temperature increase from 19.1 to 21.7 °C affected the remediation behavior due to the high vapor pressure and low boiling point of CS_2. Lower absolute concentrations were measured in the first phase of experiments at lower temperatures (Exp. 4 and 5) compared to higher inflow temperatures (Exp. 6). This also affected the concentration decline (tailing) shown in Fig. 5.26 (left-hand). Experiments 4 and 5 showed a more pronounced tailing while concentrations in the warmer Exp. 6 dropped significantly faster. Thus, the increase in temperature sped up the remediation by approximately 10 and $43\,\%\,K^{-1}$ when comparing Exp. 6 to 4 and 5. These results indicate possible ways for optimizing a remediation application such as the injection of warm exhaust air from technical equipment into the unsaturated zone with the aim of heating up the ground, and thereby increasing the vaporization rate of CS_2.

The impact of the mean effective soil-gas velocity on the remediation of a residual CS_2 distribution was analyzed in Geba fine sand (Exp. 6 to 8). A slow soil-gas velocity of $0.5\,m\,h^{-1}$ resulted in a longer-lasting first phase at high concentrations followed by a fast decline. The high extraction mass rate proved an efficient remediation of the residual CS_2 distribution residing in the region of high relative permeability. Faster velocities of 1.0 and $2.0\,m\,h^{-1}$ shortened Phase 1 or even reduced maximum concentrations while leading to a slower concentration decrease and a later beginning of Phase 2. Hence, the availability of CS_2 was limiting its removal at higher soil-

gas velocities. Smaller velocities lead to higher contaminant loads in the soil-vapor extraction but a longer absolute remediation duration. In contrast, high velocities reduce the contaminant load and speed up the overall duration in case of a large interfacial area of the contaminant. Reducing the soil-gas velocity sped up remediation in each case by around 20 % with respect to the extracted pore volume determined from the performance parameter defined as 90 % of normalized CS_2 mass recovery. This means that lower extraction rates lead to a longer duration of operation and vice versa despite of higher contaminant loads in the soil-vapor extraction. Thus, the choice of soil-gas velocity will affect the global efficiency of a remediation.

90 % of normalized recovery was reached no later than after 20 PV in all experiments with residual CS_2 distribution, demonstrating the efficient and fast remediation of residual CS_2 in the unsaturated zone. Soil-vapor extraction was shut down when CS_2 concentration fell below $0.05\,g\,m^{-3}$. It was restarted after one day (24 h) of equilibration to test for concentration rebounds which would occur in case of a persisting, liquid CS_2 source in the porous medium. None or only minor concentration rebounds were observed falling back to concentrations below $0.05\,g\,m^{-3}$ within 4 to 6 PV.

Apparent total recovery in fine glass beads (0.64, 0.64, and 0.65) ranked below that of Geba fine sand (0.83, 0.85, 0.79, 0.74, and 0.77). This was caused by technical issues of the lab equipment which were resolved prior to the experiments in Geba fine sand (Exp. 4). However, the rather poor apparent total recovery values were ascribed to the sum of errors and inaccuracies arising from calibration of analytical equipment, concentration measurements, manual gas sampling, technical inaccuracy of the flow meters (minimum ±4.5 %fs), and manual reading of flow rates. Higher measurement errors from flow meter readings had to be taken into account, since they were not operated at full scale. Values of error increase in the lower measurement ranges of variable-area flow meter according to *VDI/VDE 3513 Blatt 2:2008-08* (2008). These errors easily add up to 20 % of losses in the mass balance. Hence, the measurement errors suggested a higher recovery and the concentration rebound tests confirmed a nearly complete removal of the CS_2 contamination.

Key findings

- The distribution and percolation of liquid CS_2 depended on the porous medium and its characteristics as well as the type of spill (injection method).
- Both residually trapped CS_2 in the vicinity of the spill location and a pronounced downward migration and pooling of CS_2 were observed.
- The experiments proved that cold soil-vapor extraction is an applicable and efficient technique for the remediation of a CS_2 spill and emanating vapors in the unsaturated zone. The technique greatly benefited from the low boiling point and high vapor pressure of CS_2 responsible for a fast vaporization.
- The experimental results demonstrated that higher temperatures and lower soil-gas velocities will improve the remediation progress.
- In case of a CS_2 spill, a fast response time is advantageous to minimize the risk of groundwater contamination.

6. Final remarks

6.1. Summary and conclusions

This work focused on density-driven vapor migration and retardation of carbon disulfide (CS_2) vapor plumes in unsaturated porous media and aimed at providing the required understanding of fate and transport to assess the risk for underlying aquifers. In addition, it explored the feasibility of soil-vapor extraction as a remediation technique for a spill of liquid CS_2. The investigations were conducted in 1-D (column) and 2-D (flume) experiments and results were compared with theoretical approaches or numerical simulations. In the introduction of this dissertation, four central questions were posed which were addressed in the following chapters. This part revisits those questions and provides answers based on the results and conclusions which were gained from the conducted experimental investigations.

How does a CS_2-vapor plume migrate in the unsaturated zone and what influence do the contaminant's properties have on its behavior?

Vapor plumes migrate easily in the unsaturated zone as a result of their low viscosity and density compared to liquids. A driving force to trigger migration can be gravity. This occurs in case of a density difference between the contaminant vapor and the ambient soil air. The contaminant CS_2 used in this work is characterized by a gaseous density of 1.6 relative to air. Thus, being the heavier component, a preferential downward migration is expected.

Large-scale column experiments were conducted to describe and quantify density-driven migration of a heavy CS_2-vapor plume. The vapor-migration experiments were carried out in 4 m long, vertical columns packed with a dry porous medium. Three different types of glass beads (coarse, medium and fine) were used to observe the influence of permeability on migration. The porous medium was kept dry to avoid partitioning effects into pore water. Tubes connected to the top and bottom outlet ended at the same elevation. The upper and lower boundaries were open to the atmosphere and hence considered constant-pressure boundaries. This novel set-up allowed for an unhindered migration of the heavy vapor plume injected into the middle section of the column. Gas samples were taken along the column throughout the experiment to quantify time-and-space-dependent vapor migration.

The experiments confirmed the density-driven migration of the heavy CS_2 vapor in dry porous media. The design of the long columns enabled the observation of the migration of a vapor plume established in a porous medium. Very small pressure differences controlled the vapor migration. Two stages of migration were observed. After shutdown of injection in Stage 1, the injected vapor plume migrated downward at a constant velocity. The downward-migrating

gas phase established a siphon sucking in air through the open top boundary. A change in migration behavior was observed, coinciding with CS_2 vapor entering and filling the tubing connected to the bottom outlet of the column. The sudden enlargement of the effective height filled with heavy CS_2 vapor (column plus tubing) resulted in a sudden increase in negative head thus provoking an acceleration of the downward-migrating vapor in Stage 2.

Experiments were compared with numerical simulations employing a 1-D, two-phase, two-component, isothermal model. The numerical model satisfactorily reproduced the overall migration behavior observed in the experiments but suggested slightly higher velocities. The implementation of the boundary installations ensured correct boundary conditions in the model, thereby obtaining a good reproduction of the two stages of migration observed in the experiments. Simulations showed that total advective (downward) migration was controlled only by the total injected mass residing in the porous medium. Hence, the total mass of a CS_2 spill determines advection of a dense vapor plume in the unsaturated zone, while vapor concentration (gradient) controls the distribution of mass within and the spatial extent of the vapor plume (diffusion). Two cases of history matching were performed. In the first case, the parameter system permeability was used to match for experimental downward-migration velocities employed as observations. History matching using the system permeability was performed for all three materials. The constant migration (Stage 1) as well as the acceleration, except for the fine material, was captured accurately. In the second case, the parameters system permeability, porosity, and mass flux of CS_2 were used and migration velocities plus concentration data was employed as observations. The usage of additional observations reduced direct correlations between the strongly-correlated parameters. Hence, different type of observations are required when using multiple parameters for history matching to avoid arbitrary best-match solutions.

The experiments conducted allowed for the first time the examination of a gravity-driven vapor plume migrating in a long column. Both the experiments and the numerical simulations demonstrated that vapors migrate due to density difference, hence posing a threat to underlying aquifers. The greater the density difference, the greater the driving force and the faster the vapor-plume migration. The density is determined by the molecular mass of the contaminant, hence upward or downward migration can occur. The spatial extent of vapor plumes emanating from a liquid source is controlled mainly by its boiling point and vapor pressure. Thus, highly volatile liquids rapidly form vapor plumes and spread further in the same period of time.

Do physical processes (e.g. partitioning) affect migration in porous media and what influence does water saturation have on the overall behavior?

The first experimental investigation proved that density differences trigger and control the migration of contaminant-vapor plumes in the unsaturated zone. The experiments were conducted in dry porous media to allow for the observation of vapor migration under controlled boundary conditions without any side effects. However, in case of contaminant mass transport as a vapor plume, it is expected to be affected by pore water in the unsaturated zone. Hence, partitioning processes have an impact on the vapor-plume migration and thus the total contaminant mass flux potentially threatening the underlying aquifer. The question regarding the

significance of such processes and their dependence on the water saturation was addressed in a second experimental investigation.

Vapor-retardation experiments explored the retardation behavior of CS_2 vapor in dry and moist porous media under controlled boundary conditions. The experiments were carried out in a specifically designed set-up consisting of 2 m long, vertical columns packed with a porous medium. Two different types of porous media (fine glass beads and Geba fine sand) were used to investigate the retardation of CS_2 in similar materials as used in the density-driven migration experiments. The moist porous media were obtained by saturation with water and subsequent drainage under controlled conditions. Thereby, static water-saturation profiles could be established and capillary pressures were measured by tensiometers throughout the experiments. A slug of gaseous CS_2 and tracer argon was injected via an injection section at the bottom of the column. The slug was followed by a nitrogen chase to investigate the removal of the injected CS_2 vapor. Different seepage velocities were applied to characterize the vapor transport and to evaluate their impact on retardation. The range was chosen based on the velocities observed in density-driven vapor-migration experiments. Concentrations of CS_2 and argon were measured online at the top outlet of the column using two gas chromatographs. Hence, the bottom of the column was realized as a constant-mass-flux boundary while the top was open to the surroundings, hence at constant pressure.

The concentration measurements yielded breakthrough curves (BTC) of CS_2 and argon under the prevailing conditions. The temporal-moment analysis (TMA) for step-input was employed to evaluate the BTCs. Dispersion coefficients as a function of seepage velocity were obtained from the temporal-moment analysis in moist conditions. In addition, the experimental data was evaluated to obtain effective binary diffusion coefficients and dispersivities of the porous media used. The injection of the slug and the subsequent chase allowed for a separate evaluation. Relating the breakthrough of CS_2 to that of argon and comparing it with breakthroughs in dry porous media showed a clear retardation of CS_2 in moist porous media as a function of the porous medium and the water saturation. Retardation in fine glass beads compared very well with the theoretical retardation coefficient taking into account the partitioning into the aqueous phase. In fine glass beads, a slightly higher retardation of the chase compared to that of the slug was observed. Retardation in Geba fine sand was stronger than predicted by the theoretical coefficient which could be attributed to the impact of the particular water-saturation profile. The pronounced increase of water saturation toward the bottom of the column yielded higher retardation values. In both materials, the nitrogen chase completely removed the CS_2 vapor thus proving that the partitioning process was fully reversible. Retardation coefficients as a function of (seepage) velocity revealed only a minor dependency and suggested a slight tendency toward a reduced retardation at the highest velocity tested.

The experiments demonstrated that partitioning into the aqueous phase during vapor migration is responsible for the retardation of a migrating CS_2-vapor plume. An increase of the retardation coefficient with increasing water saturation was observed as suggested by the theoretical approach. However, above a given water saturation, retardation decreases with further increasing water saturation due to the decrease of the gas-water interfacial area. In conclusion, a downward-migrating vapor plume in the unsaturated zone is retarded by partitioning processes and a certain contaminant mass dissolves into the pore water.

Does migration of vapor from a liquid CS_2 spill in the unsaturated zone pose a potential threat to underlying aquifers?

Density-driven vapor-plume migration has to be considered when assessing the threat of a CS_2 contamination in the unsaturated zone to the underlying aquifer. Vapor-plume migration was observed in the large-scale column experiments. In reality, velocities as high as measured in the experiments are not expected due to the generally lower permeability of the subsoil. However, vertical fractures, faults or layers of high permeability in the unsaturated zone may provide preferential flow paths. In addition, they could cause a rapid change in boundary conditions which may lead to an acceleration of migrating heavy vapor plumes. Such an acceleration was observed in the experiments as a result of the sudden change of the bottom boundary condition due to the experimental set-up.

While migrating downward in the unsaturated zone, vapor plumes are affected by partitioning processes. Vapor-retardation experiments showed that migrating CS_2 vapor is retarded as a result of partitioning into the aqueous phase. The retardation helps to reduce the mass transfer to the underlying aquifer. Moreover, CS_2 which is dissolved in the pore water is amenable to biodegradation. First evidence of CS_2 decay by biodegradation was found in the experiments. However, these processes do not prevent the CS_2-vapor plume from reaching and eventually contaminating the underlying aquifer. Thus, a significant risk of contamination of the groundwater resource persists which demands a fast response and an efficient remediation technique.

Which remediation technique can be applied in the unsaturated zone to mitigate potential dangers to the environment due to migrating vapors and to remove a liquid spill?

The experimental investigations into density-driven vapor migration and vapor retardation highlighted the danger of a migrating CS_2-vapor plume contaminating an underlying aquifer. Hence, a remediation technique allowing for a fast response and an efficient removal is required to prevent a contamination of the groundwater. The technique in demand has to ensure the removal of the migrating vapor plume and of the liquid CS_2 spill residing in the unsaturated zone. Based on the scenario and the physicochemical properties of CS_2, soil-vapor extraction was shown to be the most efficient in-situ remediation technique.

2-D flume experiments were conducted to first observe the spill and subsequent distribution of liquid CS_2 in moist porous media and then to investigate its remediation using soil-vapor extraction. The experiments aimed at delineating the impact of different porous media, water saturation, CS_2 distribution, temperature, and soil-gas velocity on the remediation behavior. The flume (1.00 x 0.70 x 0.12 m) was packed with a porous medium. Two different types, fine glass beads and Geba fine sand, were used to investigate the influence of material characteristics and different water saturations. A special set-up for saturation and drainage ensured static water saturations, hence similar initial conditions in each experiment. Different types of spills using a single-port (continuous) or a multi-port (interrupted) injection in the upper part of the flume resulted in preferential pooling or a residual contaminant distribution, respectively. The spills and CS_2 distributions were observed and recorded through the front window of the

flume. Two vertical wells used for clean-gas inflow and soil-vapor extraction were installed at the left-hand (inflow) and right-hand (extraction) side of the flume. Humidified nitrogen was provided at the inflow to avoid a drying up of the porous medium. Concentrations of CS_2, gas flow rates, pressures, and temperatures were measured and recorded to quantify the contaminant removal.

CS_2 distribution was found to be highly dependent on the injection method and the material characteristics (grain-size distribution, capillary pressure–water saturation relationship) determining its potential for retention by capillary forces. The uniformity of fine glass beads combined with the single-port injection resulted in a preferential flow path of the continuous phase and a pool of liquid CS_2 at the bottom of the flume. The multi-port injection method favored a residual distribution showing traces of downward-spreading CS_2 from points of injection in fine glass beads. Spills in Geba fine sand behaved differently compared to spills in fine glass beads. This was mainly due to its wider grain-size distribution with a higher fraction of small particles responsible for a capillary-driven spreading and residual saturation around the injection points. The observations of CS_2 spills in the experiments demonstrated the different distributions which may occur in the unsaturated zone depending on the material characteristics. Thus, the remediation technique had to be tested for two extreme cases; a severe percolation in the unsaturated zone which may form contaminant pools or a preferentially residual distribution close to the location of the spill.

A pronounced difference was observed between the remediation of a CS_2 pool and a residual CS_2 distribution. The remediation of a pool required significantly more time than that of a residual distribution and was characterized by low concentrations in the extracted gas phase. In case of a pool, most of the CS_2 mass resided in the region of low relative permeability for gas or, worse, was enclosed by water, resulting in a significantly reduced gas-liquid interfacial area. The remediation of a residual CS_2 distribution was characterized by a faster and more efficient mass removal due to concentrations up to saturation concentration. The major fraction of CS_2 mass was distributed and held by capillary forces in the upper region of the flume with a lower water saturation and, thus higher relative gas permeability. Hence, mass removal rates were considerably higher for the remediation of a residual CS_2 distribution compared to a pool.

The experiments clearly showed that the remediation was affected by the different porous media due to their material characteristics determining water saturation and relative permeability for gas and by the contaminant distribution. The influence of the temperature on remediation was quantified from comparison of experiments with different mean inflow temperatures. Already a minor temperature increase had a strong impact on the remediation behavior due to the high vapor pressure and low boiling point of CS_2. The increase of temperature sped up the remediation, thus indicating possible ways to optimize a field application. The impact of the mean effective soil-gas velocity on the remediation of a residual CS_2 distribution was analyzed in another set of experiments. A slow soil-gas velocity resulted in longer-lasting high vapor concentrations followed by a fast decline. This was responsible for a high extraction mass rate proving an efficient remediation of the residual CS_2 distribution which resided in the region of high relative permeability. Faster velocities shortened the duration of high concentrations or even reduced maximum concentrations which led to a slower concentration decrease. The availability of CS_2 was limiting its removal at higher soil-gas velocities. Hence, low velocities

lead to higher contaminant loads in soil-vapor extraction but a longer absolute remediation duration. In contrast, high velocities reduce the contaminant load and speed up overall duration in case of a large interfacial area of the contaminant. Thus, the choice of soil-gas velocity affects the global efficiency of a remediation.

Soil-vapor extraction was shut down and restarted after one day (24 h) to test for concentration rebounds which are to be expected in case of a persisting, liquid CS_2 source in the porous medium. None or only minor temporary rebounds were observed confirming a complete removal of the CS_2 contamination.

In conclusion, the remediation experiments for varying CS_2 distributions in partially water-saturated porous media proved that soil-vapor extraction is the method of choice for the remediation of a CS_2 spill in the unsaturated zone. The technique benefits from the low boiling point and high vapor pressure of CS_2 responsible for a fast vaporization. While for contaminants with lower vapor pressures additional energy (heat) is required for their remediation, these flume experiments demonstrated that cold soil-vapor extraction is an efficient and sufficient technique for the removal of CS_2 in field applications. The distribution of liquid CS_2 depended on the porous medium. Both a pronounced downward migration and pooling of CS_2 and residually trapped CS_2 in the vicinity of the spill location were observed. Thus, in the case of a CS_2 spill a fast response time is advantageous to minimize the risk of groundwater contamination. The experimental results showed that higher temperatures and lower soil-gas velocities improve the remediation progress. A thermally-enhanced soil-vapor extraction is not required, however, it might improve the remediation in areas of higher water saturation or in the case of a pool, since it speeds up the vaporization of CS_2. Warm exhaust air of the technical equipment could be injected to heat the subsurface, and thereby enhance the efficiency. This could also improve the global energy balance of a remediation application.

6.2. Outlook

The goal of this work was to contribute to the knowledge regarding the behavior of vapor plumes in the unsaturated zone and to characterize the principal processes affecting their fate and transport. In addition, proof of concept was provided for applying soil-vapor extraction as an efficient remediation technique for a spill of liquid CS_2. It is obvious that the experimental investigations were conducted under well-defined boundary conditions in the laboratory which aimed at providing a basic understanding. The conclusions drawn in the previous section give answers to the central questions posed in this work; however they also raise further questions on these topics.

First of all, the experimental investigations conducted in this work disregarded the vaporization process of the liquid contaminant. Both types of column experiments were conducted with already vaporized CS_2 to be able to clearly delineate the density-driven migration and retardation and avoid any superposition of processes. However, the low boiling temperature and high vapor pressure of CS_2 suggest a very fast vaporization resulting in a strong volume expansion (one liter of liquid fills about one cubic meter of gas). Thus, the fast spreading of CS_2 vapor due to vaporization could induce a contamination of the underlying aquifer. For this reason,

contaminant vaporization in porous media must not be neglected when assessing the threat of groundwater contamination. This process should be addressed in future research to gain insight about the spatial extent of vapor plumes and their spreading driven by vaporization.

Secondly, the column experiments on density-driven vapor migration and vapor retardation were conducted on a 1-D scale and under defined boundary conditions. These experiments demonstrated how CS_2 vapor migrates in dry porous media due to the density difference compared to ambient soil air and also showed the impact of partitioning processes on transport in moist porous media. Both investigations were conducted separately to allow for a clear differentiation of the processes. The next step would be to combine these investigations and transfer them to a larger scale and 3-D. Large tank or field experiments are needed to examine the effect of density differences on vapor-plume transport in moist porous media, the impact of partitioning processes responsible for retardation, and to quantify the effective contaminant mass transfer into the groundwater. The column experiments already showed the difficulties of controlling the boundary conditions and pointed out that upscaling requires a thorough planning to cope with the complexities that may emerge.

Thirdly, this work provided proof of concept that soil-vapor extraction is a suitable and efficient technique to remediate a CS_2 contamination in the unsaturated zone. The experiments showed the impact of different porous media, soil-vapor extraction velocity (rates), and temperature on mass removal and indicated possible ways for optimization. Since the experiments were conducted in a 2-D flume, 3-D applications are required to quantify the mass removal in a radial flow field and confirm applicability and efficiency in the field. *Soga et al.* (2004) reported a significant uncertainty of mass removal in upscaling from laboratory to field conditions and therefore suggested to evaluate the remediation efficiency by the risk reduction achieved by the application instead of mass removal. It was mentioned before that warm exhaust air of technical field devices could be used to thermally enhance the soil-vapor extraction by injection into the subsurface. This could have a high potential due to the low boiling point of CS_2. Such scenarios require a thorough calculation of the global energy balance and could pave the way toward a sustainable remediation technique.

Finally, the investigation into biodegradation of CS_2 in moist porous media was beyond the scope of this work. The experiments showed that CS_2, partitioned into the water phase, is amenable to biodegradation. Clear evidence was found in the last series of vapor-retardation experiments with Geba fine sand. Significant losses of CS_2 in the mass balance and the odor of hydrogen sulfide at the column outlet suggested the activity of microbes. *Cox et al.* (2013) found carbonyl sulfide (COS) and hydrogen sulfide (H_2S) as by-products during CS_2 biodegradation. Hence, biodegradation could help to mitigate the danger of contamination from migrating vapor plumes and might promote enhanced natural attenuation to be considered as a possible remediation technique. Further detailed investigations are necessary to develop this technique and to confirm its applicability in the field.

In field experiments or applications, changes in atmospheric pressure and temperature have to be taken into account, as they cause soil breathing for example. These real-life conditions additionally affect the processes investigated and discussed in this work.

References

Abbas, R. R., and S. K. Al-Naseri (2008), Natural transport of volatile organic compounds due to annual variation of soil temperature, *Jordan Journal of Civil Engineering*, *2*(4), 355–362.

Ahmed, T. (2001), *Reservoir Engineering Handbook*, 2nd ed., 1211 pp., Gulf Professional Publishing.

Ahmed, T. (2007), *Equations of State and PVT Analysis - Applications for Improved Reservoir Modeling*, Gulf Publishing Company.

Ahrens, J., B. Geveci, and C. Law (2005), *ParaView: An End-User Tool for Large-Data Visualization*, p. 717, Elsevier.

Altevogt, A. S., D. E. Rolston, and R. T. Venterea (2003), Density and pressure effects on the transport of gas phase chemicals in unsaturated porous media, *Water Resources Research*, *39*(3), doi:10.1029/2002WR001338.

Auer, L., N. Rosenberg, K. Birdsell, and E. Whitney (1996), The effects of barometric pumping on contaminant transport, *Journal of Contaminant Hydrology*, *24*(2), 145–166, doi:10.1016/S0169-7722(96)00010-1.

Barber, C., and G. B. Davis (1991), Fugacity model to assess the importance of factors controlling the movement of volatile organics from soil to ground water, in *Proceedings of a Workshop on Modelling the Fate of Chemicals in the Environment*, pp. 67–73, The Australian National University, Centre for Resource and Environmental Studies, Water Research Foundation of Australia.

Bastian, P., M. Blatt, A. Dedner, C. Engwer, R. Klöfkorn, M. Ohlberger, and O. Sander (2008a), A generic grid interface for parallel and adaptive scientific computing. Part I: abstract framework, *Computing*, *82*(2–3), 103–119, doi:10.1007/s00607-008-0003-x.

Bastian, P., M. Blatt, A. Dedner, C. Engwer, R. Klöfkorn, R. Kornhuber, M. Ohlberger, and O. Sander (2008b), A generic grid interface for parallel and adaptive scientific computing. Part II: implementation and tests in DUNE, *Computing*, *82*(2–3), 121–138, doi:10.1007/s00607-008-0004-9.

Bastian, P., et al. (2011), DUNE Web page, http://www.dune-project.org.

Bear, J. (1972), *Dynamics of fluids in porous media*, Elsevier, New York.

Bird, R. B., W. E. Stewart, and E. N. Lightfoot (1960), *Transport phenomena*, Wiley, New York.

Bohy, M., L. Dridi, G. Schäfer, and O. Razakarisoa (2006), Transport of a mixture of chlorinated solvent vapors in the vadose zone of a sandy aquifer, *Vadose Zone Journal*, *5*(2), 539–553, doi:10.2136/vzj2005.0079.

Brinkman, H. C. (1949), A calculation of the viscous force exerted by a flowing fluid on a dense swarm of particles, *Applied Scientific Research*, *1*(1), 27–34, doi:10.1007/BF02120313.

Brusseau, M. L., J. Popovičová, and J. A. K. Silva (1997), Characterizing gas-water interfacial and bulk-water partitioning for gas-phase transport of organic contaminants in unsaturated porous media, *Environmental Science & Technology*, *31*(6), 1645–1649, doi:10.1021/es960475j.

Brusseau, M. L., V. Rohay, and M. J. Truex (2010), Analysis of soil vapor extraction data to evaluate mass-transfer constraints and estimate source-zone mass flux, *Ground Water Monitoring & Remediation*, *30*(3), 57–64, doi:10.1111/j.1745-6592.2010.01286.x.

Budavari, S. (Ed.) (1996), *The Merck index: an encyclopedia of chemicals, drugs, and biologicals*, 12. ed., Merck, Whitehouse Station, NJ.

Cabbar, H., and A. Bostanci (2001), Moisture effect on the transport of organic vapors in sand, *Journal of Hazardous Materials*, *82*(3), 313–322, doi:10.1016/S0304-3894(01)00177-7.

Carroll, K. C., M. Oostrom, M. J. Truex, V. J. Rohay, and M. L. Brusseau (2012), Assessing performance and closure for soil vapor extraction: integrating vapor discharge and impact to groundwater quality, *Journal of Contaminant Hydrology*, *128*(1–4), 71–82, doi:10.1016/j.jconhyd.2011.10.003.

Choi, J.-W., F. D. Tillman, and J. A. Smith (2002), Relative importance of gas-phase diffusive and advective trichloroethene (TCE) fluxes in the unsaturated zone under natural conditions, *Environmental Science & Technology*, *36*(14), 3157–3164, doi:10.1021/es011348c.

Cirpka, O. A., and P. K. Kitanidis (2000), Characterization of mixing and dilution in heterogeneous aquifers by means of local temporal moments, *Water Resources Research*, *36*(5), 1221–1236, doi:10.1029/1999WR900354.

Class, H., and R. Helmig (2002), Numerical simulation of non-isothermal multiphase multicomponent processes in porous media.: 2. applications for the injection of steam and air, *Advances in Water Resources*, *25*(5), 551 – 564, doi:10.1016/S0309-1708(02)00015-5.

Class, H., R. Helmig, and P. Bastian (2002), Numerical simulation of non-isothermal multiphase multicomponent processes in porous media.: 1. an efficient solution technique, *Advances in Water Resources*, *25*(5), 533–550, doi:10.1016/S0309-1708(02)00014-3.

Class, H., R. Helmig, and I. Neuweiler (2008), Sequential coupling of models for contaminant spreading in the vadose zone, *Vadose Zone Journal*, *7*, 721–731, doi:10.2136/vzj2007.0056.

Conant, B. H., R. W. Gillham, and C. A. Mendoza (1996), Vapor transport of trichloroethylene in the unsaturated zone: field and numerical modeling investigations, *Water Resources Research*, *32*(1), 9–22, doi:10.1029/95WR02965.

Corley, T. L., J. Farrell, B. Hong, and M. H. Conklin (1996), VOC accumulation and pore filling in unsaturated porous media, *Environmental Science & Technology*, *30*(10), 2884–2891, doi:10.1021/es950644k.

Costanza-Robinson, M. S., and M. L. Brusseau (2002), Gas phase advection and dispersion in unsaturated porous media, *Water Resources Research*, *38*(4), 7–1–7–9, doi:10.1029/2001WR000895.

Cotel, S., G. Schäfer, V. Barthesa, and P. Baussand (2011), Effect of density-driven advection on trichloroethylene vapor diffusion in a porous medium, *Vadose Zone Journal*, *10*, 565–581, doi:10.2136/vzj2010.0032.

Cox, S. F., J. D. McKinley, A. S. Ferguson, G. O'Sullivan, and R. M. Kalin (2013), Degradation of carbon disulphide (CS2) in soils and groundwater from a CS2-contaminated site, *Environmental Earth Sciences*, *68*(7), 1935–1944, doi:10.1007/s12665-012-1881-y.

Daubinger, P. (2014), Aufbau und Verifizierung einer Gasmischanlage basierend auf einem neuartigen Mikroverdampfer, Bachelor's thesis, Universität Stuttgart.

Davarzani, H., K. Smits, R. M. Tolene, and T. H. Illangasekare (2014), Study of the effect of wind speed on evaporation from soil through integrated modeling of the atmospheric boundary layer and shallow subsurface, *Water Resources Research*, *50*(1), 661–680, doi:10.1002/2013WR013952.

Davis, E. (1997), How heat can enhance in situ soil and aquifer remediation: important chemical properties and guidance on choosing the appropriate technique, *Tech. rep.*, United States Environmental Protection Agency.

Davis, G., B. Patterson, and M. Trefry (2009), Evidence for instantaneous oxygen-limited biodegradation of petroleum hydrocarbon vapors in the subsurface, *Ground water monitoring & remediation*, *29*(1), 126–137, doi:10.1111/j.1745-6592.2008.01221.x.

Davis, G. B., J. L. Rayner, M. G. Trefry, S. J. Fisher, and B. M. Patterson (2005), Measurement and modeling of temporal variations in hydrocarbon vapor behavior in a layered soil profile, *Vadose Zone Journal*, *4*(2), 225–239, doi:10.2136/vzj2004.0029.

De Bruyn, W. J., E. Swartz, J. H. Hu, J. A. Shorter, P. Davidovits, D. R. Worsnop, M. S. Zahniser, and C. E. Kolb (1995), Henry's law solubilities and Setchenow coefficients for biogenic reduced sulfur species obtained from gas-liquid uptake measurements, *Journal of Geophysical Research*, *100*(D4), 7245–7251, doi:10.1029/95JD00217.

Falta, I., R. W.and Javandel, K. Pruess, and P. A. Witherspoon (1989), Density-driven flow of gas in the unsaturated zone due to the evaporation of volatile organic compounds, *Water Resources Research*, *25*, 2159–2169, doi:10.1029/WR025i010p02159.

Fernàndez-Garcia, D., T. H. Illangasekare, and H. Rajaram (2005), Differences in the scale-dependence of dispersivity estimated from temporal and spatial moments in chemically and physically heterogeneous porous media, *Advances in Water Resources*, *28*(7), 745 – 759, doi:10.1016/j.advwatres.2004.12.011.

Finsterle, S. (2007), *iTOUGH2 User's Guide*, Lawrence Berkeley National Laboratory, Berkeley, California, report lbnl-40040 ed.

Finsterle, S., and Y. Zhang (2011), Solving iTOUGH2 simulation and optimization problems using the PEST protocol, *Environmental Modelling & Software*, *26*(7), 959 – 968, doi:10.1016/j.envsoft.2011.02.008.

Flemisch, B., et al. (2011), DuMu^x: DUNE for multi-phase, component, scale, physics, ... flow and transport in porous media, *Advances in Water Resources*, *34*(9), 1102 – 1112, doi:10.1016/j.advwatres.2011.03.007.

Flemisch, B., et al. (2015), DuMu^x 2.7.0., doi:10.5281/zenodo.16722.

Gibson, T. L., A. S. Abdul, W. A. Glasson, C. C. Ang, and D. W. Gatlin (1993), Vapor extraction of volatile organic compounds from clay soil: a long-term field pilot study, *Ground Water*, *31*(4), 616–626, doi:10.1111/j.1745-6584.1993.tb00595.x.

Helmig, R., and R. Huber (1998), Comparison of galerkin-type discretization techniques for two-phase flow in heterogeneous porous media, *Advances in Water Resources*, *21*(8), 697 – 711, doi:10.1016/S0309-1708(97)00023-7.

Ho, C. K., and S. W. Webb (Eds.) (2006), *Gas Transport in Porous Media*, Theory and Applications of Transport in Porous Media Vol. 20, 444 pp., Springer, Dordrecht.

Hoff, J. T., R. Gillham, D. Mackay, and W. Y. Shiu (1993), Sorption of organic vapors at the air-water interface in a sandy aquifer material, *Environmental Science & Technology*, *27*(13), 2789–2794, doi:10.1021/es00049a018.

Höhener, P., N. Dakhel, M. Christophersen, M. Broholm, and P. Kjeldsen (2006), Biodegradation of hydrocarbons vapors: comparison of laboratory studies and field investigations in the vadose zone at the emplaced fuel source experiment, Airbase Værløse, Denmark, *Journal of Contaminant Hydrology*, *88*(3–4), 337–358, doi:10.1016/j.jconhyd.2006.07.007.

Illangasekare, T. H., J. L. Ramsey, Jr., K. H. Jensen, and M. B. Butts (1995a), Experimental study of movement and distribution of dense organic contaminants in heterogeneous aquifers, *Journal of Contaminant Hydrology*, *20*(1–2), 1–25, doi:10.1016/0169-7722(95)00045-W.

Illangasekare, T. H., E. Armbruster III, and D. Yates (1995b), Non-aqueous-phase fluids in heterogeneous aquifers - experimental study, *Journal of Environmental Engineering*, *121*(8), 571–579, doi:10.1061/(ASCE)0733-9372(1995)121:8(571).

Illangasekare, T. H., et al. (2014), Vapor intrusion from entrapped NAPL sources and groundwater plumes: process understanding and improved modeling tools for pathway assessment, *Tech. rep.*, Colorado School of Mines.

Jang, W., and M. Aral (2007), Density-driven transport of volatile organic compounds and its impact on contaminated groundwater plume evolution, *Transport in Porous Media*, *67*(3), 353–374, doi:10.1007/s11242-006-9029-8.

Jellali, S., H. Benremita, P. Muntzer, O. Razakarisoa, and G. Schäfer (2003), A large-scale experiment on mass transfer of trichloroethylene from the unsaturated zone of a sandy aquifer to its interfaces, *Journal of Contaminant Hydrology*, *60*(1-2), 31–53, doi:10.1016/S0169-7722(02)00062-1.

Kechavarzi, C., K. Soga, and T. Illangasekare (2005), Two-dimensional laboratory simulation of LNAPL infiltration and redistribution in the vadose zone, *Journal of Contaminant Hydrology*, *76*(3–4), 211 – 233, doi:10.1016/j.jconhyd.2004.09.001.

Kechavarzi, C., K. Soga, T. H. Illangasekare, and P. Nikolopoulos (2008), Laboratory study of immiscible contaminant flow in unsaturated layered sands, *Vadose Zone Journal*, *7*(1), 1–9, doi:10.2136/vzj2006.0177.

Kim, H., P. S. C. Rao, and M. D. Annable (1997), Determination of effective air-water interfacial area in partially saturated porous media using surfactant adsorption, *Water Resources Research*, *33*(12), 2705–2711, doi:10.1029/97WR02227.

Kim, H., M. D. Annable, and P. S. C. Rao (1998), Influence of air-water interfacial adsorption and gas-phase partitioning on the transport of organic chemicals in unsaturated porous media, *Environmental Science & Technology*, *32*(9), 1253–1259, doi:10.1021/es970868y.

Kim, H., M. D. Annable, and P. S. C. Rao (2001), Gaseous transport of volatile organic chemicals in unsaturated porous media: effect of water-partitioning and air-water interfacial adsorption, *Environmental Science & Technology*, *35*(22), 4457–4462, doi:10.1021/es001965l.

Kim, H., S. Lee, J.-W. Moon, and P. S. C. Rao (2005), Gas transport of volatile organic compounds in unsaturated soils, *Soil Science Society of America Journal*, *69*(4), 990–995, doi:10.2136/sssaj2003.0208.

Lagioia, R., A. Sanzeni, and F. Colleselli (2006), Air, water and vacuum pluviation of sand specimens for the triaxial apparatus, *Soils And Foundations*, *46*(1), 61–67, doi:10.3208/sandf.46.61.

Lenhard, R., M. Oostrom, C. Simmons, and M. White (1995), Investigation of density-dependent gas advection of trichloroethylene: experiment and a model validation exercise, *Journal of Contaminant Hydrology*, *19*, 47–67, doi:10.1016/0169-7722(94)00055-M.

Leube, P. C., W. Nowak, and G. Schneider (2012), Temporal moments revisited: why there is no better way for physically based model reduction in time, *Water Resources Research*, *48*(11), doi:10.1029/2012WR011973, w11527.

Liu, M., A. Bárdossy, J. Li, and Y. Jiang (2012), Physically-based modeling of topographic effects on spatial evapotranspiration and soil moisture patterns through radiation and wind, *Hydrology and Earth System Sciences*, *16*(2), 357–373, doi:10.5194/hess-16-357-2012.

Luo, J., O. A. Cirpka, and P. K. Kitanidis (2006), Temporal-moment matching for truncated breakthrough curves for step or step-pulse injection, *Advances in Water Resources*, *29*(9), 1306–1313, doi:10.1016/j.advwatres.2005.10.005.

Maxfield, B. T., D. M. Ginosar, R. D. McMurtrey, H. W. Rollins, and G. M. Shook (2005), The effect of moisture content on retention of fluorocarbon tracers on sand, *Geothermics*, *34*(1), 47–60, doi:10.1016/j.geothermics.2004.06.003.

Mayes, M., P. Jardine, T. Mehlhorn, B. Bjornstad, J. Ladd, and J. Zachara (2003), Transport of multiple tracers in variably saturated humid region structured soils and semi-arid region laminated sediments, *Journal of Hydrology*, *275*(3-4), 141–161, doi:10.1016/S0022-1694(03)00039-8.

McGarry, J. (1983), Correlation and prediction of the vapor pressures of pure liquids over large pressure ranges, *Industrial & Engineering Chemistry Process Design and Development*, *22*(2), 313–322, doi:10.1021/i200021a023.

McGeough, K. L., R. M. Kalin, and P. Myles (2007), Carbon disulfide removal by zero valent iron, *Environmental Science & Technology*, *41*(13), 4607–4612, doi:10.1021/es062936z.

Mendoza, C. A., and E. O. Frind (1990a), Advective-dispersive transport of dense organic vapors in the unsaturated zone - 1. model development, *Water Resources Research*, *26*, 379–387, doi:10.1029/WR026i003p00379.

Mendoza, C. A., and E. O. Frind (1990b), Advective-dispersive transport of dense organic vapors in the unsaturated zone - 2. sensitivity analysis, *Water Resources Research*, *26*, 388–398, doi:10.1029/WR026i003p00388.

Mercer, J. W., and R. M. Cohen (1990), A review of immiscible fluids in the subsurface: properties, models, characterization and remediation, *Journal of Contaminant Hydrology*, *6*(2), 107–163, doi:10.1016/0169-7722(90)90043-G.

Miguel, A. F., and A. Serrenho (2007), On the experimental evaluation of permeability in porous media using a gas flow method, *Journal of Physics D: Applied Physics*, *40*(21), 6824, doi:10.1088/0022-3727/40/21/050.

Millington, R. J., and J. P. Quirk (1961), Permeability of porous solids, *Transactions of the Faraday Society*, *57*, 1200–1207, doi:10.1039/TF9615701200.

Neuweiler, I., A. Papafotiou, H. Class, and R. Helmig (2011), Estimation of effective parameters for a two-phase flow problem in non-Gaussian heterogeneous porous media, *Journal of Contaminant Hydrology*, *120-21*, 141–156, doi:10.1016/j.jconhyd.2010.08.001.

Ochs, S. O., H. Class, A. Färber, and R. Helmig (2010), Methods for predicting the spreading of steam below the water table during subsurface remediation, *Water Resources Research*, *46*(5), W05,520–, doi:10.1029/2007WR006401.

Oostrom, M., C. Hofstee, R. Lenhard, and T. Wietsma (2003), Flow behavior and residual saturation formation of liquid carbon tetrachloride in unsaturated heterogeneous porous media, *Journal of Contaminant Hydrology*, *64*(1–2), 93–112, doi:10.1016/S0169-7722(02)00107-9.

Popovičová, J., and M. L. Brusseau (1997), Dispersion and transport of gas-phase contaminants in dry porous media: effect of heterogeneity and gas velocity, *Journal of Contaminant Hydrology*, *28*(1–2), 157–169, doi:10.1016/S0169-7722(97)00014-4.

Popovičová, J., and M. L. Brusseau (1998), Contaminant mass transfer during gas-phase transport in unsaturated porous media, *Water Resources Research*, *34*(1), 83–92, doi:10.1029/97WR02945.

Por, G. J., P. Boerrigter, J. G. Maas, and A. de Vries (1989), A fractured reservoir simulator capable of modeling block-block interaction, in *Society of Petroleum Engineers Ann. Tech. Conf. and Exhibition*, Society of Petroleum Engineers, doi:10.2118/19807-MS.

Poulsen, M. M., and B. H. Kueper (1992), A field experiment to study the behavior of tetrachloroethylene in unsaturated porous media, *Environmental Science & Technology*, *26*(5), 889–895, doi:10.1021/es00029a003.

Rad, N., and M. Tumay (1987), Factors affecting sand specimen fabrication by raining, *Geotechnical Testing Journal*, *10*(1), 31–37, doi:10.1520/GTJ10136J.

Riddick, J. A., W. B. Bunger, and T. K. Sakano (1986), *Organic Solvents: Physical Properties And Methods Of Purification*, vol. XV, 4th ed., 1325 pp., Wiley, New York.

Rivett, M. O., G. P. Wealthall, R. A. Dearden, and T. A. McAlary (2011), Review of unsaturated-zone transport and attenuation of volatile organic compound (VOC) plumes leached from shallow source zones, *Journal of Contaminant Hydrology*, *123*(3-4), 130–156, doi:10.1016/j.jconhyd.2010.12.013.

Schulze-Makuch, D. (2005), Longitudinal dispersivity data and implications for scaling behavior, *Ground Water*, *43*(3), 443–456, doi:10.1111/j.1745-6584.2005.0051.x.

Schwille, F., W. Bertsch, R. Linke, W. Reif, and S. Zauter (1988), *Dense Chlorinated Solvents in Porous and Fractured Media: Model Experiments, translated from German by J. F. Pankow*, 146 pp., Lewis Publishers.

Seely, G. E., R. W. Falta, and J. R. Hunt (1994), Buoyant advection of gases in unsaturated soil, *Journal of Environmental Engineering*, *120*, 1230–1247, doi:10.1061/(ASCE)0733-9372(1994)120:5(1230).

Shen, R., K. G. Pennell, and E. M. Suuberg (2012), A numerical investigation of vapor intrusion - the dynamic response of contaminant vapors to rainfall events, *Science of the Total Environment*, *437*(0), 110–120, doi:10.1016/j.scitotenv.2012.07.054.

Soga, K., J. W. E. Page, and T. H. Illangasekare (2004), A review of NAPL source zone remediation efficiency and the mass flux approach, *Journal of Hazardous Materials*, *110*(1-3), 13–27, doi:10.1016/j.jhazmat.2004.02.034.

Tang, G., M. A. Mayes, J. C. Parker, and P. M. Jardine (2010), CXTFIT/Excel - a modular adaptable code for parameter estimation, sensitivity analysis and uncertainty analysis for laboratory or field tracer experiments, *Computers & Geosciences*, *36*(9), 1200–1209, doi:10.1016/j.cageo.2010.01.013.

Thorstenson, D. C., and D. W. Pollock (1989), Gas transport in unsaturated porous media: the adequacy of Fick's law, *Reviews of Geophysics*, *27*(1), 61–78, doi:10.1029/RG027i001p00061.

Tidwell, V. (2006), Air permeability measurements in porous media, in *Gas Transport in Porous Media*, edited by C. Ho and S. Webb, Theory and Applications of Transport in Porous Media Vol. 20, pp. 273–278, Springer Netherlands, doi:10.1007/1-4020-3962-X_15.

Toride, N., F. Leij, and M. van Genuchten (1995), The CXTFIT code for estimating transport parameters from laboratory or field tracer experiments - version 2.0., *Research Report 137*, U.S. Salinity Laboratory, Agricultural Research Services, U.S. Department of Agriculture.

Toride, N., M. Inoue, and F. J. Leij (2003), Hydrodynamic dispersion in an unsaturated dune sand, *Soil Science Society of America Journal*, *67*(3), 703–712, doi:10.2136/sssaj2003.0703.

van Genuchten, M. T. (1980), A closed-form equation for predicting the hydraulic conductivity of unsaturated soils, *Soil Science Society of America Journal*, *44*, 892–898, doi:10.2136/sssaj1980.03615995004400050002x.

VDI/VDE 3513 Blatt 2:2008-08 (2008), *Variable-area flowmeters - Maximum permissible errors, G, of the system*, Verein Deutscher Ingenieure.

Webb, S. W., and K. Pruess (2003), The use of Fick's law for modeling trace gas diffusion in porous media, *Transport in Porous Media*, *51*, 327–341, doi:10.1023/A:1022379016613.

Werner, D., P. Grathwohl, and P. Höhener (2004), Review of field methods for the determination of the tortuosity and effective gas-phase diffusivity in the vadose zone, *Vadose Zone Journal*, *3*, 1240–1248, doi:10.2136/vzj2004.1240.

Yeten, B., A. Castellini, B. Guyaguler, and W. Chen (2005), A comparison study on experimental design and response surface methodologies, in *SPE Reservoir Simulation Symposium*, Society of Petroleum Engineers, doi:10.2118/93347-MS.

Yu, C., A. W. Warrick, and M. H. Conklin (1999), A moment method for analyzing breakthrough curves of step inputs, *Water Resources Research*, *35*(11), 3567–3572, doi:10.1029/1999WR900225.

A. Appendix

A.1. Fundamentals

Constants of Peng-Robinson equation of state

$$a = 0.45724 \frac{R^2 T_c^2}{P_c} \tag{A.1}$$

$$b = 0.07780 \frac{R T_c}{P_c} \tag{A.2}$$

$$\alpha = \left(1 + (0.37464 + 1.54226\omega - 0.26992\omega^2)\left(1 - \sqrt{\frac{T}{T_c}}\right)\right)^2 \tag{A.3}$$

with critical temperature T_c (K), critical pressure P_c (MPa), and accentric factor ω (dimensionless).

A.2. Materials and methods

Porous media

Transport and retardation of fluids in porous media are among others dependent on porosity, i.e. the void space that is available. However, not the entire pore space is necessarily available for advective transport due to e.g. dead-end pores or intraparticle porosity. Fluids may only reach these regions by diffusive transport. Examining the shape and structure of sand grains provide an important insight for estimating the occurrence of this porous media artifacts. Therefore, the grains of fine and medium glass beads, as well as Geba fine sand were examined with a scanning electron microscope (EVO LS 15, Carl Zeiss Microscopy GmbH, Jena, Germany).

The shape and size of the grains are shown in Figure A.1, A.2, and A.3. The medium glass beads showed an almost perfect circular shape and a homogeneous grain-size distribution. Small Dents and craters could be seen at a greater magnification but are of negligible size to affect transport behavior. The fine glass beads were also of circular shape, however the pictures revealed consolidations of several particles allowing for different shapes. The surface of the grains was smooth and homogeneous. The grains of the Geba fine sand showed a rather rock-like shape partly affected by grinding or other manufacturing processes. Significant surface

Table A.1. Wagner equation: constants and critical properties of components taken from (*McGarry*, 1983).

Component	A	B	C	D	P_c	T_c
Argon (Ar)	−5.905 01	1.126 27	−0.767 869	−1.627 21	4857.99	150.651
Water (H_2O)	−7.764 51	1.458 38	−2.775 80	−1.233 03	22 122.3	647.35
Carbon disulfide (CS_2)	−6.638 96	1.203 95	−0.376 534	−4.328 20	7903.4	552.0

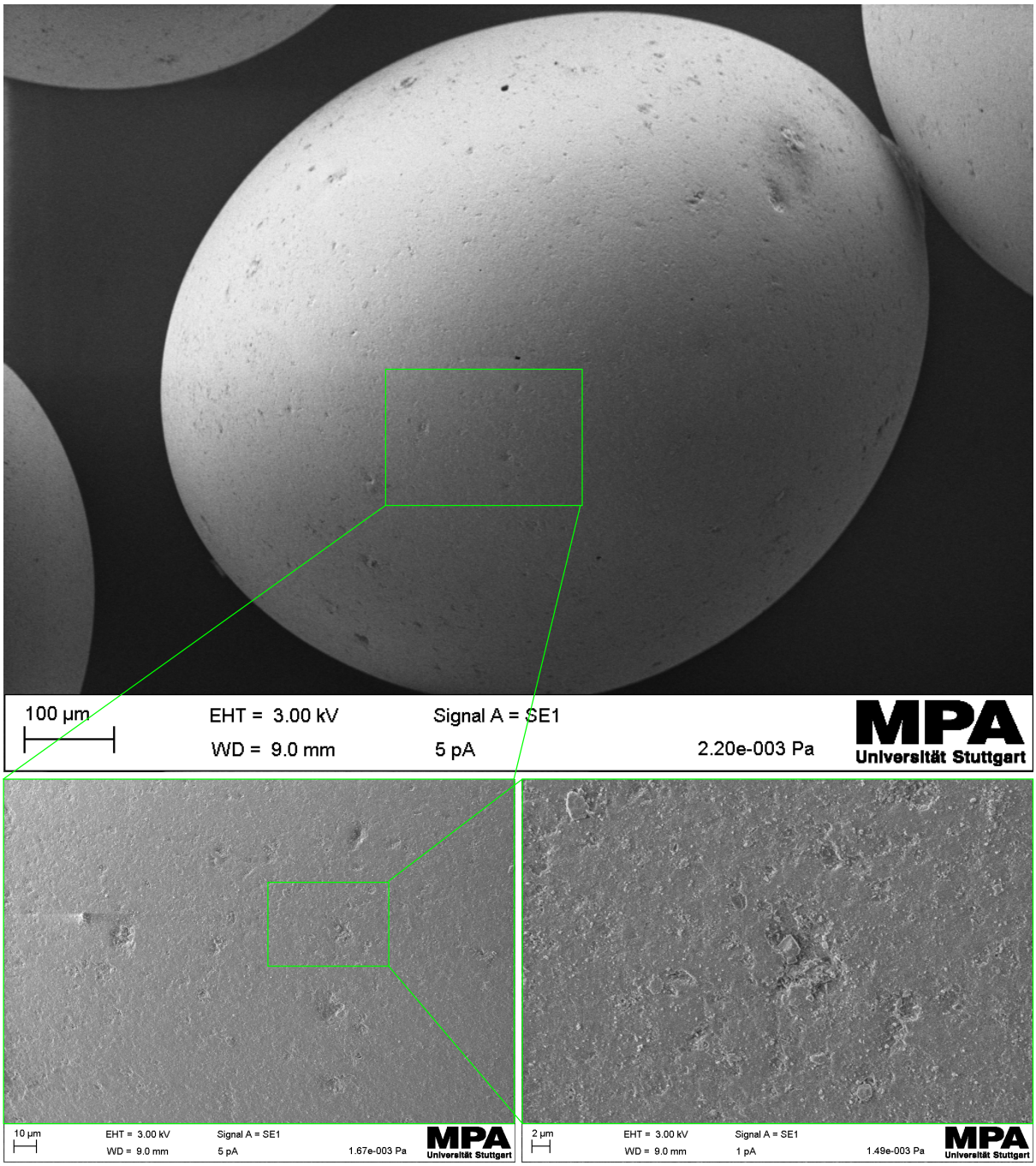

Figure A.1. SEM pictures of medium glass beads.

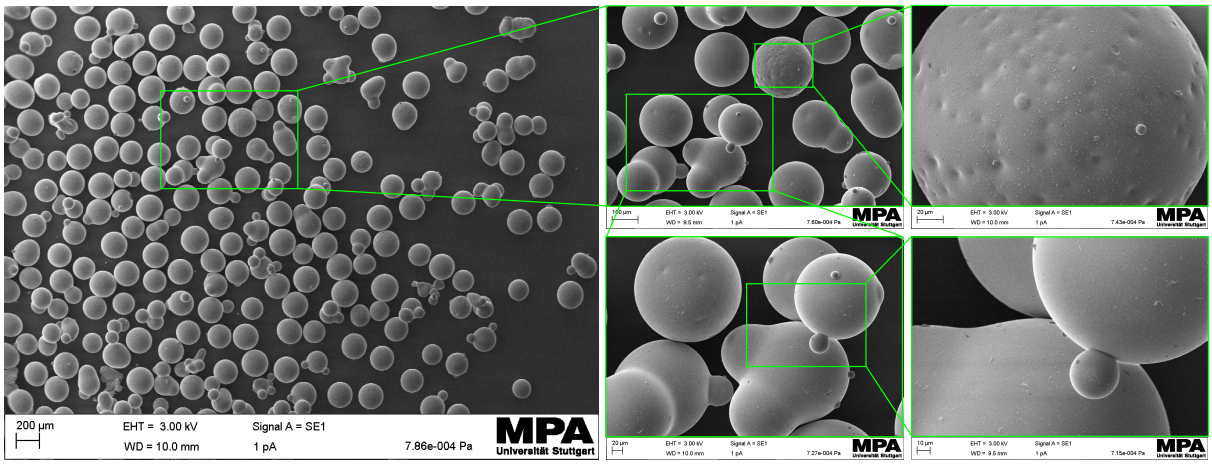

Figure A.2. SEM pictures of fine glass beads.

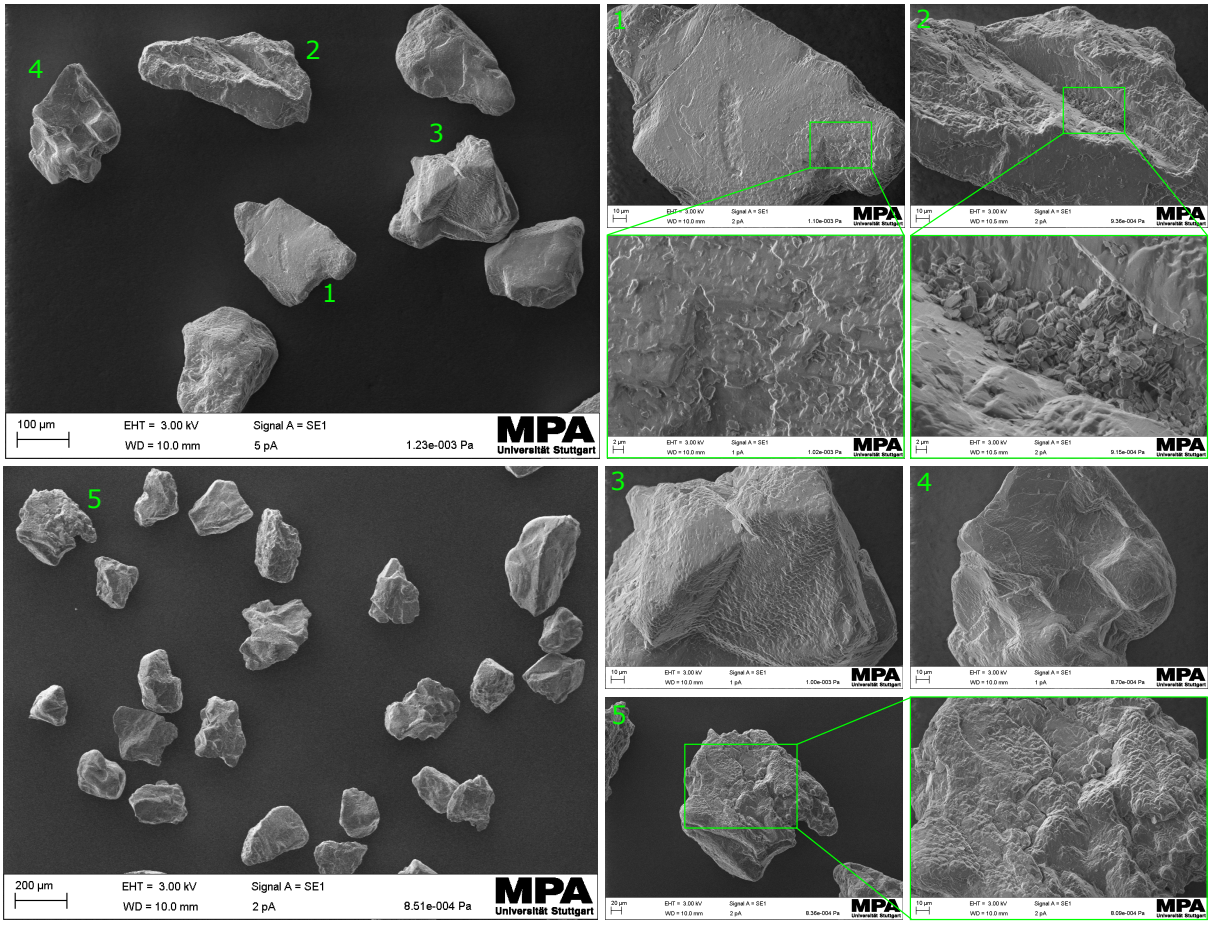

Figure A.3. SEM pictures of Geba fine sand.

structures or irregularities which could favor dead-end pores or intraparticle porosity were not observed. The grain's size were well distributed within the assumed distribution. The pictures of the sand grains obtained with the scanning electron microscope emphasize that the physical processes addressed in this thesis were not affected by dead-end pores or intraparticle porosity. Hence, a consideration of mobile and immobile regions with respect to transport can be excluded from the evaluation and discussion of the experiments.

Miniature vaporizer

The vapor-retardation experiments (see Sec. 4.2) explored the transport behavior of CS_2 in dry and moist porous media. The nitrogen chase as well as the CS_2 vapor injected into the column had to be water-saturated (100 % relative humidity) to prevent a drying-out of the moist porous media. The saturation of nitrogen was achieved by bubbling through ultra-pure water using a gas scrubber. In case of CS_2, this procedure could not be used since a defined mass flux was required in the experiments and a bubbling through water would have resulted in a mass sink. Therefore, a miniature vaporizer was used to water-saturate the CS_2 vapor. The miniature vaporizer was a special customization for this particular application developed by the Institute of Chemical Process Engineering (ICVT) of the University Stuttgart in collaboration with VEGAS. Prototyping, testing and developing the control software was performed within a bachelor thesis with the purpose of optimizing its operation in the VRE set-up (*Daubinger*, 2014). The vaporizer unit included the vaporizer itself, an ultra-low flow rate pump (M6, Valco Instruments Company Incorporated, Houston, TX, USA) to dose the to-be vaporized liquid and a power supply to control the temperature at the vaporizer tip. This unit was implemented in the gas-flow regulation unit consisting of several mass flow controllers used for the experiments of this work. Thereby, the required mass flux of ultra-pure water was vaporized and injected into the CS_2 vapor flow to obtain 100 % relative humidity prior to the injection into the column. This mass flux was calculated for the prevailing experimental conditions (temperature and pressure) employing the ideal gas law. Relative humidity in the vapor flow was checked manually by means of a moisture measuring device.

A.3. Experiments

Vapor retardation

Table A.2 shows the theoretical migration velocity, the injection duration (slug), the injected mass, and the normalized recovery of the components CS_2 and argon. The table is divided with respect to the used porous media and lists all experiments in order according to the conducted series.

Table A.3 and A.4 summarize the results obtained from the temporal-moment analysis of vapor-retardation experiments in dry and moist porous media, i.e. fine glass beads and Geba fine sand. The tables list all conducted experiments and the TMA results of the slug and the chase. The TMA results include the calculated migration velocities, the mean arrival time of the BTC, the retardation coefficient, and the dispersion coefficients.

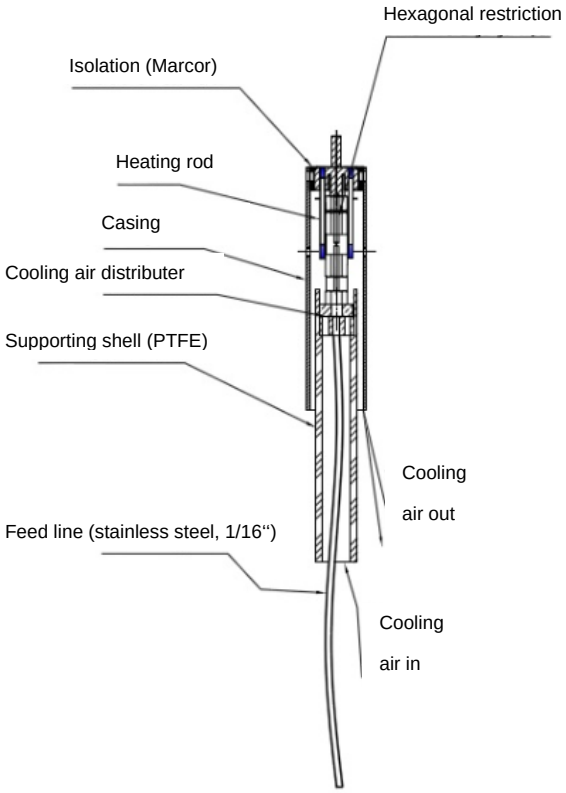

Figure A.4. Set-up of the miniature vaporizer (taken from ICVT, University of Stuttgart).

Table A.2. Experimental conditions of vapor-retardation experiments: series, experiment, theoretical seepage velocity, injection duration, and injected mass and recovery of CS_2 and argon.

Series #	Exp. #	v $cm\,h^{-1}$	t_{inj} h	m_{Ar} mg	m_{CS2} mg	r_{Ar} -	r_{CS2} -
Fine glass beads							
1	1	25	27.80	667.8	2671.4	0.994	1.123
	2	50	13.92	677.7	2710.9	1.011	1.066
	3	50	14.10	675.9	2703.5	0.996	1.005
	4	50	13.65	677.7	542.2	0.992	1.033
	5	50	14.29	690.3	13.8	0.988	0.822
	6	50	14.07	687.0	13.7	0.984	0.753
	7	50	13.82	673.3	13.5	0.987	0.770
2	8	25	28.35	619.9	12.4	0.989	1.022
	9	50	14.40	617.8	12.4	0.993	0.983
	10	50	12.83	615.2	12.3	0.997	1.010
	11	100	7.22	620.8	12.4	1.000	0.941
	12	200	3.56	617.1	12.3	0.998	0.941
3	13	50	14.38	635.0	12.7	0.995	1.054
	14	50	14.22	634.0	12.7	1.000	1.032
	15	50	14.43	635.4	12.7	0.989	1.013
4	16	50	14.06	626.0	12.5	0.994	1.039
Geba fine sand							
1	17	25	28.71	673.9	13.5	0.982	0.964
	18	25	40.97	944.5	18.9	0.992	0.942
	19	50	14.30	599.2	12.0	0.985	1.006
	20	50	14.31	597.5	12.0	0.983	0.970
	21	100	7.20	664.8	13.3	0.999	0.994
	22	100	7.32	665.9	13.3	0.999	1.062
	23	200	3.83	706.2	14.1	1.000	0.994
	24	200	3.54	657.7	13.2	0.995	0.962
2	25	25	41.17	795.7	15.9	0.984	1.009
	26	50	14.33	552.8	11.1	1.000	0.955
	27	50	20.28	767.3	15.3	0.992	1.115
	28	50	20.62	799.5	16.0	0.997	0.973
	29	100	10.12	797.6	16.0	0.987	0.965
	30	200	4.67	800.8	16.0	1.000	1.013
3	31	50	20.54	815.8	16.3	0.994	0.854
	32	50	24.04	955.8	19.1	0.998	0.684
	33	100	11.02	864.1	17.3	1.000	0.534
	34	200	5.16	782.9	15.7	1.008	0.689
	35	25	49.26	957.3	19.1	1.012	0.010
	36	100	10.28	793.0	15.9	1.000	0.174
	37	50	23.81	944.0	18.9	0.996	0.016

Table A.3. Detailed results from temporal-moment analysis of breakthrough curves measured in vapor-retardation experiments with fine glass beads.

Exp.	Slug							Chase							
#	v_{Ar} cm h^{-1}	v_{CS2} cm h^{-1}	τ_{Ar} h	τ_{CS2} h	R -	D_{Ar} cm^2 s^{-1}	D_{CS2} cm^2 s^{-1}	v_{Ar} cm h^{-1}	v_{CS2} cm h^{-1}	τ_{Ar} h	τ_{CS2} h	R -	D_{Ar} cm^2 s^{-1}	D_{CS2} cm^2 s^{-1}	S_w %
Fine glass beads															
1	23.9	22.1	8.56	9.30	1.09	0.125	0.074	23.5	23.9	8.72	8.59	0.99	0.118	0.057	0.0
2	48.2	42.7	4.26	4.80	1.13	0.130	0.113	46.9	43.1	4.37	4.75	1.09	0.127	−0.034	0.0
3	48.1	44.4	4.27	4.62	1.08	0.109	0.101	47.1	46.5	4.35	4.41	1.01	0.118	0.031	0.0
4	49.1	48.0	4.17	4.28	1.03	0.128	0.059	49.1	48.1	4.18	4.26	1.02	0.137	0.113	0.0
5	48.0	45.5	4.27	4.50	1.06	0.119	0.065	48.2	47.6	4.26	4.31	1.01	0.129	0.114	0.0
6	48.2	44.7	4.25	4.58	1.08	0.138	0.094	47.9	48.1	4.28	4.26	1.00	0.127	0.085	0.0
7	48.4	46.5	4.23	4.41	1.04	0.130	0.064	48.4	48.4	4.24	4.24	1.00	0.124	0.081	0.0
8	24.3	21.5	8.43	9.54	1.13	0.084	0.034	24.5	21.5	8.36	9.52	1.14	0.101	0.050	8.8
9	46.9	40.7	4.37	5.03	1.15	0.103	0.039	47.3	41.6	4.33	4.92	1.14	0.101	0.065	8.8
10	52.6	46.2	3.90	4.43	1.14	0.114	0.039	53.6	46.6	3.83	4.40	1.15	0.126	0.050	8.8
11	93.9	82.2	2.18	2.49	1.14	0.121	0.047	95.1	84.1	2.16	2.44	1.13	0.116	0.070	8.8
12	186.8	166.4	1.10	1.23	1.12	0.142	0.074	188.9	170.1	1.09	1.21	1.11	0.131	0.118	8.8
13	51.3	43.8	3.99	4.68	1.17	0.104	0.044	52.1	44.4	3.94	4.62	1.17	0.117	0.074	15.4
14	52.5	43.4	3.90	4.72	1.21	0.101	0.060	51.0	43.5	4.02	4.71	1.17	0.106	0.081	15.4
15	51.1	43.1	4.02	4.76	1.19	0.112	0.035	51.3	42.8	4.00	4.79	1.20	0.113	0.077	15.4
16	48.6	42.8	4.22	4.79	1.13	0.097	0.048	48.4	43.9	4.23	4.67	1.10	0.097	0.056	7.3

Table A.4. Detailed results from temporal-moment analysis of breakthrough curves measured in vapor-retardation experiments with Geba fine sand.

Exp.	Slug							Chase							
#	v_{Ar} cm h^{-1}	v_{CS2} cm h^{-1}	τ_{Ar} h	τ_{CS2} h	R -	D_{Ar} cm^2 s^{-1}	D_{CS2} cm^2 s^{-1}	v_{Ar} cm h^{-1}	v_{CS2} cm h^{-1}	τ_{Ar} h	τ_{CS2} h	R -	D_{Ar} cm^2 s^{-1}	D_{CS2} cm^2 s^{-1}	S_w %
Geba fine sand															
17	18.8	17.3	10.92	11.88	1.09	0.074	0.039	17.9	17.6	11.46	11.67	1.02	0.078	0.052	0.0
18	18.6	16.6	11.04	12.32	1.12	0.089	0.048	18.7	18.0	10.98	11.36	1.03	0.109	0.075	0.0
19	34.1	31.5	6.02	6.50	1.08	0.122	0.063	34.7	33.4	5.92	6.14	1.04	0.120	0.054	0.0
20	34.8	32.1	5.90	6.39	1.08	0.110	0.055	34.7	33.4	5.92	6.13	1.04	0.112	0.067	0.0
21	77.5	72.4	2.64	2.83	1.07	0.124	0.073	77.5	74.6	2.65	2.75	1.04	0.121	0.057	0.0
22	75.3	69.1	2.72	2.97	1.09	0.093	0.069	75.4	72.3	2.72	2.83	1.04	0.118	0.070	0.0
23	155.9	149.8	1.32	1.37	1.04	0.104	0.081	158.1	153.4	1.30	1.34	1.03	0.132	0.094	0.0
24	158.6	147.4	1.29	1.39	1.08	0.145	0.086	158.9	152.1	1.29	1.35	1.05	0.115	0.084	0.0
25	21.7	14.8	9.46	13.89	1.47	0.089	0.033	21.9	16.2	9.35	12.67	1.36	0.088	0.039	16.2
26	43.5	29.5	4.71	6.96	1.48	0.095	0.059	43.7	33.2	4.69	6.18	1.32	0.097	0.030	16.2
27	42.6	29.7	4.81	6.90	1.43	0.091	0.042	43.4	31.6	4.72	6.48	1.37	0.098	0.018	16.2
28	43.2	30.8	4.75	6.65	1.40	0.116	0.039	44.1	33.0	4.65	6.22	1.34	0.098	0.052	16.2
29	88.3	62.7	2.32	3.27	1.41	0.111	0.049	88.9	64.8	2.31	3.16	1.37	0.099	0.079	16.2
30	191.0	137.7	1.07	1.49	1.39	0.110	0.061	191.4	141.6	1.07	1.45	1.35	0.114	0.172	16.2
31	44.3	29.6	4.63	6.91	1.49	0.086	0.097	45.0	34.4	4.56	5.95	1.31	0.089	0.059	15.4
32	44.8	n/a	4.58	n/a	n/a	0.077	n/a	45.0	n/a	n/a	4.56	n/a	n/a	0.094	15.4
33	88.3	n/a	2.32	n/a	n/a	0.092	n/a	87.7	n/a	n/a	2.34	n/a	n/a	0.087	15.4
34	170.3	n/a	1.20	n/a	n/a	0.068	n/a	170.1	n/a	n/a	1.21	n/a	n/a	0.096	15.4
35	22.1	n/a	9.29	n/a	n/a	0.088	n/a	21.7	n/a	n/a	9.43	n/a	n/a	0.090	15.4
36	86.8	n/a	2.36	n/a	n/a	0.091	n/a	87.5	n/a	n/a	2.34	n/a	n/a	0.122	15.4
37	44.2	n/a	4.64	n/a	n/a	0.099	n/a	44.8	n/a	n/a	4.57	n/a	n/a	0.102	15.4

Spill and remediation

Figure A.5 illustrates the multi-port injection method applied in the experiments.

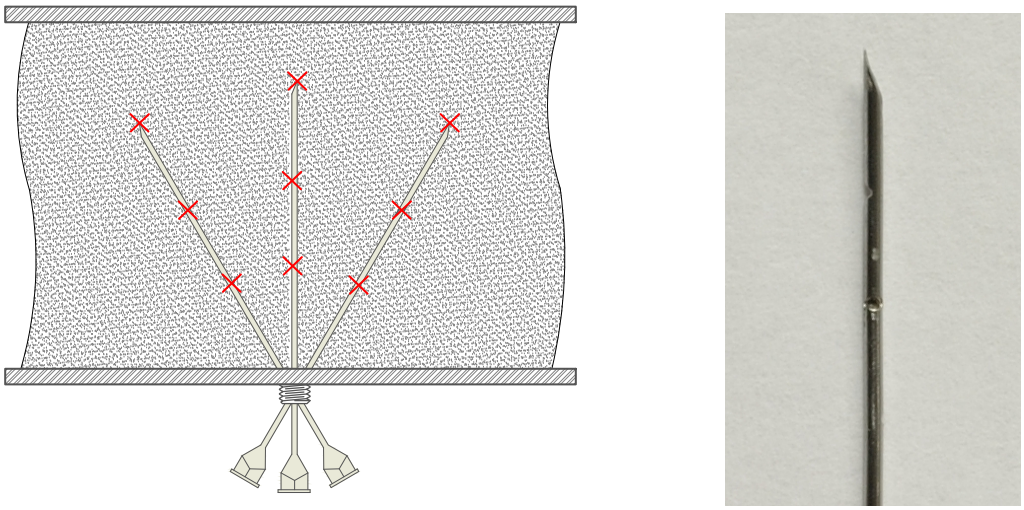

(a) Sketch of multi-port injection method (not drawn to scale). (b) Tip of customized injection needle.

Figure A.5. Multi-port injection of liquid CS_2 using a modified needle and syringe pump.

Figure A.6 shows water saturation from tensiometer measurements during spill performance and remediation with soil-vapor extraction. The tensiometer measurements showed great impacts in fine glass beads (Fig. A.6a) during spill of liquid CS_2 which was provoked by the downward-migrating liquid phase which could either have directly passed or pushed water to the tips of the tensiometers. Slight influences from the injection were also observed in Geba fine sand (Fig. A.6b). The pressure transducers of the tensiometers responded to the pressure increase in the closed flume caused by the vaporization of injected CS_2 until equilibrium was reached. The remediation slightly affected the tensiometer close to the bottom of the flume in fine glass beads. However no significant influence was observed in Geba fine sand.

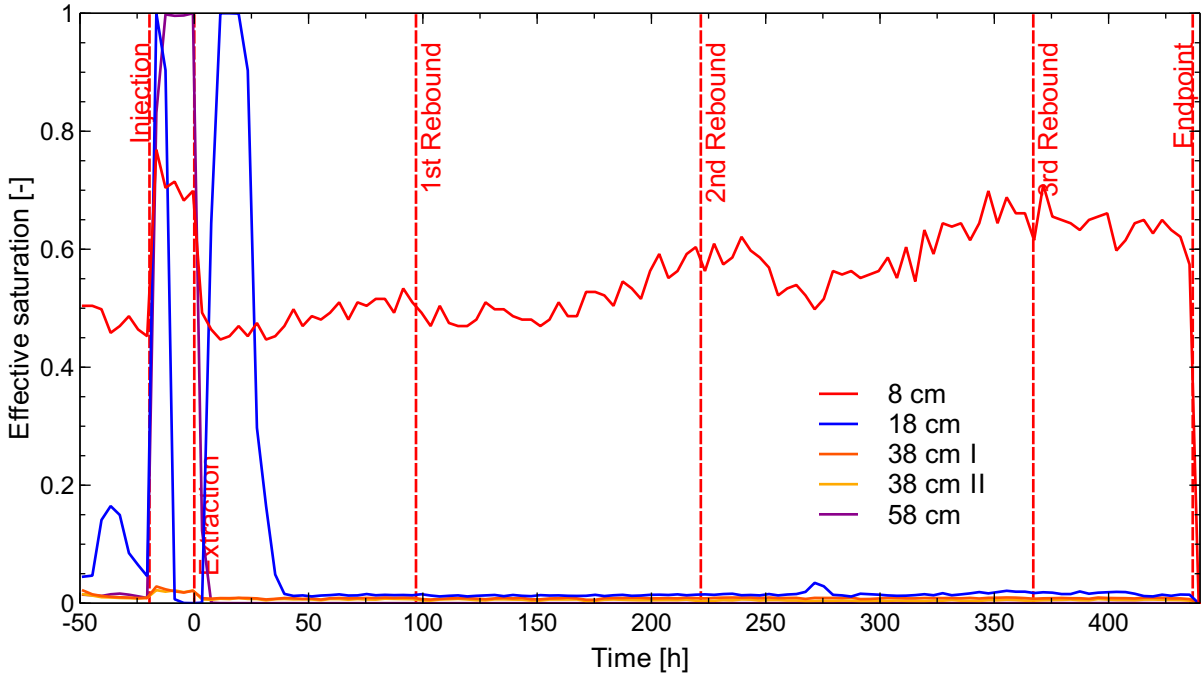

(a) Exp. 3 in fine glass beads.

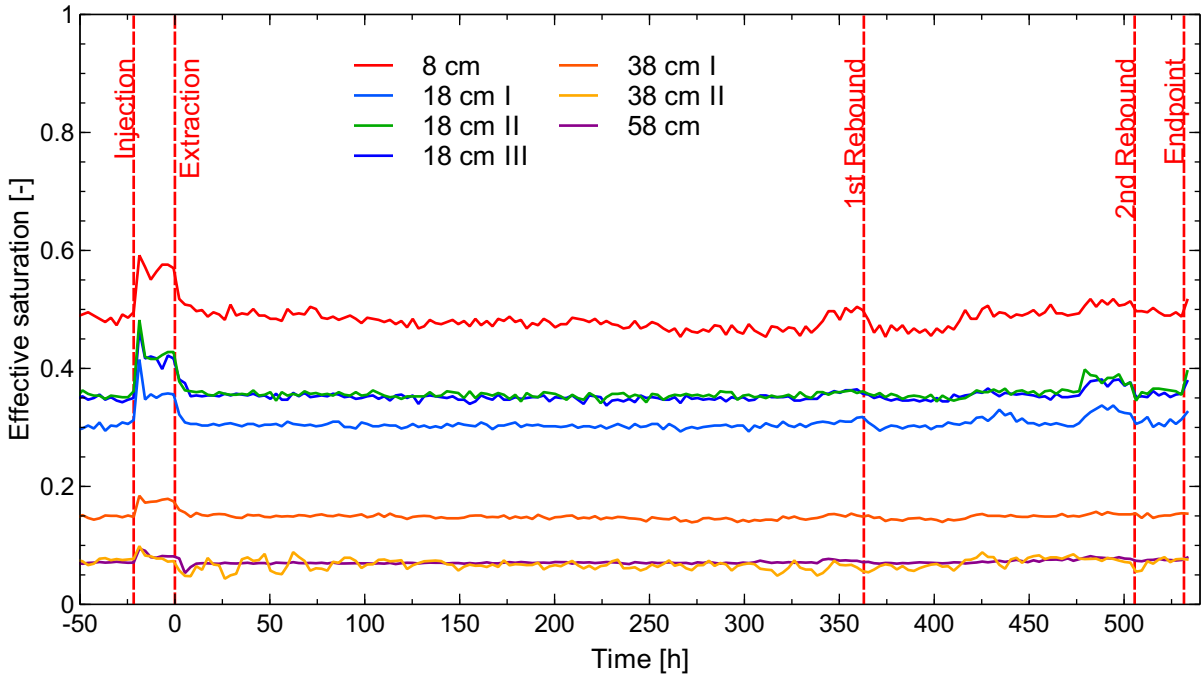

(b) Exp. 5 in Geba fine sand.

Figure A.6. Water saturation from tensiometer measurements (label denotes distance from bottom of flume) over time during spill and subsequent remediation.

Institut für Wasser- und Umweltsystemmodellierung
Universität Stuttgart

Pfaffenwaldring 61
70569 Stuttgart (Vaihingen)
Telefon (0711) 685 - 64717/64749/64752/64679
Telefax (0711) 685 - 67020 o. 64746 o. 64681
E-Mail: iws@iws.uni-stuttgart.de
http://www.iws.uni-stuttgart.de

Verzeichnis der Mitteilungshefte

Petrikat, Kurt: *Möglichkeiten und Grenzen des wasserbaulichen Versuchswesens*, 1966

5 Plate, Erich: *Beitrag zur Bestimmung der Windgeschwindigkeitsverteilung in der durch eine Wand gestörten bodennahen Luftschicht*,
und
Röhnisch, Arthur; Marotz, Günter: *Neue Baustoffe und Bauausführungen für den Schutz der Böschungen und der Sohle von Kanälen, Flüssen und Häfen; Gestehungskosten und jeweilige Vorteile*, sowie
Unny, T.E.: *Schwingungsuntersuchungen am Kegelstrahlschieber*, 1967

6 Seiler, Erich: *Die Ermittlung des Anlagenwertes der bundeseigenen Binnenschiffahrtsstraßen und Talsperren und des Anteils der Binnenschiffahrt an diesem Wert*, 1967

7 *Sonderheft anläßlich des 65. Geburtstages von Prof. Arthur Röhnisch mit Beiträgen von* Benk, Dieter; Breitling, J.; Gurr, Siegfried; Haberhauer, Robert; Honekamp, Hermann; Kuz, Klaus Dieter; Marotz, Günter; Mayer-Vorfelder, Hans-Jörg; Miller, Rudolf; Plate, Erich J.; Radomski, Helge; Schwarz, Helmut; Vollmer, Ernst; Wildenhahn, Eberhard; 1967

8 Jumikis, Alfred: *Beitrag zur experimentellen Untersuchung des Wassernachschubs in einem gefrierenden Boden und die Beurteilung der Ergebnisse*, 1968

9 Marotz, Günter: *Technische Grundlagen einer Wasserspeicherung im natürlichen Untergrund*, 1968

10 Radomski, Helge: *Untersuchungen über den Einfluß der Querschnittsform wellenförmiger Spundwände auf die statischen und rammtechnischen Eigenschaften*, 1968

11 Schwarz, Helmut: *Die Grenztragfähigkeit des Baugrundes bei Einwirkung vertikal gezogener Ankerplatten als zweidimensionales Bruchproblem*, 1969

12 Erbel, Klaus: *Ein Beitrag zur Untersuchung der Metamorphose von Mittelgebirgsschneedecken unter besonderer Berücksichtigung eines Verfahrens zur Bestimmung der thermischen Schneequalität*, 1969

13 Westhaus, Karl-Heinz: *Der Strukturwandel in der Binnenschiffahrt und sein Einfluß auf den Ausbau der Binnenschiffskanäle*, 1969

14 Mayer-Vorfelder, Hans-Jörg: *Ein Beitrag zur Berechnung des Erdwiderstandes unter Ansatz der logarithmischen Spirale als Gleitflächenfunktion*, 1970

15 Schulz, Manfred: *Berechnung des räumlichen Erddruckes auf die Wandung kreiszylindrischer Körper*, 1970

16 Mobasseri, Manoutschehr: *Die Rippenstützmauer. Konstruktion und Grenzen ihrer Standsicherheit*, 1970

17 Benk, Dieter: *Ein Beitrag zum Betrieb und zur Bemessung von Hochwasserrück-*

haltebecken, 1970

18 Gàl, Attila: *Bestimmung der mitschwingenden Wassermasse bei überströmten Fischbauchklappen mit kreiszylindrischem Staublech*, 1971, vergriffen

19 Kuz, Klaus Dieter: *Ein Beitrag zur Frage des Einsetzens von Kavitationserscheinungen in einer Düsenströmung bei Berücksichtigung der im Wasser gelösten Gase*, 1971, vergriffen

20 Schaak, Hartmut: *Verteilleitungen von Wasserkraftanlagen*, 1971

21 *Sonderheft zur Eröffnung der neuen Versuchsanstalt des Instituts für Wasserbau der Universität Stuttgart mit Beiträgen von* Brombach, Hansjörg; Dirksen, Wolfram; Gàl, Attila; Gerlach, Reinhard; Giesecke, Jürgen; Holthoff, Franz-Josef; Kuz, Klaus Dieter; Marotz, Günter; Minor, Hans-Erwin; Petrikat, Kurt; Röhnisch, Arthur; Rueff, Helge; Schwarz, Helmut; Vollmer, Ernst; Wildenhahn, Eberhard; 1972

22 Wang, Chung-su: *Ein Beitrag zur Berechnung der Schwingungen an Kegelstrahlschiebern*, 1972

23 Mayer-Vorfelder, Hans-Jörg: *Erdwiderstandsbeiwerte nach dem Ohde-Variationsverfahren*, 1972

24 Minor, Hans-Erwin: *Beitrag zur Bestimmung der Schwingungsanfachungsfunktionen überströmter Stauklappen*, 1972, vergriffen

25 Brombach, Hansjörg: *Untersuchung strömungsmechanischer Elemente (Fluidik) und die Möglichkeit der Anwendung von Wirbelkammerelementen im Wasserbau*, 1972, vergriffen

26 Wildenhahn, Eberhard: *Beitrag zur Berechnung von Horizontalfilterbrunnen*, 1972

27 Steinlein, Helmut: *Die Eliminierung der Schwebstoffe aus Flußwasser zum Zweck der unterirdischen Wasserspeicherung, gezeigt am Beispiel der Iller*, 1972

28 Holthoff, Franz Josef: *Die Überwindung großer Hubhöhen in der Binnenschiffahrt durch Schwimmerhebewerke*, 1973

29 Röder, Karl: *Einwirkungen aus Baugrundbewegungen auf trog- und kastenförmige Konstruktionen des Wasser- und Tunnelbaues*, 1973

30 Kretschmer, Heinz: *Die Bemessung von Bogenstaumauern in Abhängigkeit von der Talform*, 1973

31 Honekamp, Hermann: *Beitrag zur Berechnung der Montage von Unterwasserpipelines*, 1973

32 Giesecke, Jürgen: *Die Wirbelkammertriode als neuartiges Steuerorgan im Wasserbau*, und
Brombach, Hansjörg: *Entwicklung, Bauformen, Wirkungsweise und Steuereigenschaften von Wirbelkammerverstärkern*, 1974

33 Rueff, Helge: *Untersuchung der schwingungserregenden Kräfte an zwei hintereinander angeordneten Tiefschützen unter besonderer Berücksichtigung von Kavitation*, 1974

34 Röhnisch, Arthur: *Einpreßversuche mit Zementmörtel für Spannbeton - Vergleich der Ergebnisse von Modellversuchen mit Ausführungen in Hüllwellrohren*, 1975

35 *Sonderheft anläßlich des 65. Geburtstages von Prof. Dr.-Ing. Kurt Petrikat mit Beiträgen von*: Brombach, Hansjörg; Erbel, Klaus; Flinspach, Dieter; Fischer jr., Richard; Gàl, Attila; Gerlach, Reinhard; Giesecke, Jürgen; Haberhauer, Robert; Hafner Edzard; Hausenblas, Bernhard; Horlacher, Hans-Burkhard; Hutarew, Andreas; Knoll, Manfred; Krummet, Ralph; Marotz, Günter; Merkle, Theodor; Miller, Christoph; Minor, Hans-Erwin; Neumayer, Hans; Rao, Syamala; Rath, Paul; Rueff, Helge; Ruppert, Jürgen; Schwarz, Wolfgang; Topal-Gökceli, Mehmet; Vollmer, Ernst; Wang, Chung-su; Weber, Hans-Georg; 1975

36 Berger, Jochum: *Beitrag zur Berechnung des Spannungszustandes in rotationssymmetrisch belasteten Kugelschalen veränderlicher Wandstärke unter Gas- und Flüssigkeitsdruck durch Integration schwach singulärer Differentialgleichungen*, 1975

37 Dirksen, Wolfram: *Berechnung instationärer Abflußvorgänge in gestauten Gerinnen mittels Differenzenverfahren und die Anwendung auf Hochwasserrückhaltebecken*, 1976

38 Horlacher, Hans-Burkhard: *Berechnung instationärer Temperatur- und Wärmespannungsfelder in langen mehrschichtigen Hohlzylindern*, 1976

39 Hafner, Edzard: *Untersuchung der hydrodynamischen Kräfte auf Baukörper im Tiefwasserbereich des Meeres*, 1977, ISBN 3-921694-39-6

40 Ruppert, Jürgen: *Über den Axialwirbelkammerverstärker für den Einsatz im Wasserbau*, 1977, ISBN 3-921694-40-X

41 Hutarew, Andreas: *Beitrag zur Beeinflußbarkeit des Sauerstoffgehalts in Fließgewässern an Abstürzen und Wehren*, 1977, ISBN 3-921694-41-8, vergriffen

42 Miller, Christoph: *Ein Beitrag zur Bestimmung der schwingungserregenden Kräfte an unterströmten Wehren*, 1977, ISBN 3-921694-42-6

43 Schwarz, Wolfgang: *Druckstoßberechnung unter Berücksichtigung der Radial- und Längsverschiebungen der Rohrwandung*, 1978, ISBN 3-921694-43-4

44 Kinzelbach, Wolfgang: *Numerische Untersuchungen über den optimalen Einsatz variabler Kühlsysteme einer Kraftwerkskette am Beispiel Oberrhein*, 1978, ISBN 3-921694-44-2

45 Barczewski, Baldur: *Neue Meßmethoden für Wasser-Luftgemische und deren Anwendung auf zweiphasige Auftriebsstrahlen*, 1979, ISBN 3-921694-45-0

46 Neumayer, Hans: *Untersuchung der Strömungsvorgänge in radialen Wirbelkammerverstärkern*, 1979, ISBN 3-921694-46-9

47 Elalfy, Youssef-Elhassan: *Untersuchung der Strömungsvorgänge in Wirbelkammerdioden und -drosseln*, 1979, ISBN 3-921694-47-7

48 Brombach, Hansjörg: *Automatisierung der Bewirtschaftung von Wasserspeichern*, 1981, ISBN 3-921694-48-5

49 Geldner, Peter: *Deterministische und stochastische Methoden zur Bestimmung der Selbstdichtung von Gewässern*, 1981, ISBN 3-921694-49-3, vergriffen

50 Mehlhorn, Hans: *Temperaturveränderungen im Grundwasser durch Brauchwassereinleitungen*, 1982, ISBN 3-921694-50-7, vergriffen

51 Hafner, Edzard: *Rohrleitungen und Behälter im Meer*, 1983, ISBN 3-921694-51-5

52 Rinnert, Bernd: *Hydrodynamische Dispersion in porösen Medien: Einfluß von Dichteunterschieden auf die Vertikalvermischung in horizontaler Strömung*, 1983, ISBN 3-921694-52-3, vergriffen

53 Lindner, Wulf: *Steuerung von Grundwasserentnahmen unter Einhaltung ökologischer Kriterien*, 1983, ISBN 3-921694-53-1, vergriffen

54 Herr, Michael; Herzer, Jörg; Kinzelbach, Wolfgang; Kobus, Helmut; Rinnert, Bernd: *Methoden zur rechnerischen Erfassung und hydraulischen Sanierung von Grundwasserkontaminationen*, 1983, ISBN 3-921694-54-X

55 Schmitt, Paul: *Wege zur Automatisierung der Niederschlagsermittlung*, 1984, ISBN 3-921694-55-8, vergriffen

56 Müller, Peter: *Transport und selektive Sedimentation von Schwebstoffen bei gestautem Abfluß*, 1985, ISBN 3-921694-56-6

57 El-Qawasmeh, Fuad: *Möglichkeiten und Grenzen der Tropfbewässerung unter besonderer Berücksichtigung der Verstopfungsanfälligkeit der Tropfelemente*, 1985, ISBN 3-921694-57-4, vergriffen

58 Kirchenbaur, Klaus: *Mikroprozessorgesteuerte Erfassung instationärer Druckfelder am Beispiel seegangsbelasteter Baukörper*, 1985, ISBN 3-921694-58-2

59 Kobus, Helmut (Hrsg.): *Modellierung des großräumigen Wärme- und Schadstofftransports im Grundwasser*, Tätigkeitsbericht 1984/85 (DFG-Forschergruppe an den Universitäten Hohenheim, Karlsruhe und Stuttgart), 1985, ISBN 3-921694-59-0, vergriffen

60 Spitz, Karlheinz: *Dispersion in porösen Medien: Einfluß von Inhomogenitäten und Dichteunterschieden*, 1985, ISBN 3-921694-60-4, vergriffen

61 Kobus, Helmut: *An Introduction to Air-Water Flows in Hydraulics*, 1985, ISBN 3-921694-61-2

62 Kaleris, Vassilios: *Erfassung des Austausches von Oberflächen- und Grundwasser in horizontalebenen Grundwassermodellen*, 1986, ISBN 3-921694-62-0

63 Herr, Michael: *Grundlagen der hydraulischen Sanierung verunreinigter Porengrundwasserleiter*, 1987, ISBN 3-921694-63-9

64 Marx, Walter: *Berechnung von Temperatur und Spannung in Massenbeton infolge Hydratation*, 1987, ISBN 3-921694-64-7

65 Koschitzky, Hans-Peter: *Dimensionierungskonzept für Sohlbelüfter in Schußrinnen zur Vermeidung von Kavitationsschäden*, 1987, ISBN 3-921694-65-5

66 Kobus, Helmut (Hrsg.): *Modellierung des großräumigen Wärme- und Schadstofftransports im Grundwasser*, Tätigkeitsbericht 1986/87 (DFG-Forschergruppe an den Universitäten Hohenheim, Karlsruhe und Stuttgart) 1987, ISBN 3-921694-66-3

67 Söll, Thomas: *Berechnungsverfahren zur Abschätzung anthropogener Temperaturanomalien im Grundwasser*, 1988, ISBN 3-921694-67-1

68 Dittrich, Andreas; Westrich, Bernd: *Bodenseeufererosion, Bestandsaufnahme und Bewertung*, 1988, ISBN 3-921694-68-X, vergriffen

69 Huwe, Bernd; van der Ploeg, Rienk R.: *Modelle zur Simulation des Stickstoffhaushaltes von Standorten mit unterschiedlicher landwirtschaftlicher Nutzung*, 1988, ISBN 3-921694-69-8, vergriffen

70 Stephan, Karl: *Integration elliptischer Funktionen*, 1988, ISBN 3-921694-70-1

71 Kobus, Helmut; Zilliox, Lothaire (Hrsg.): *Nitratbelastung des Grundwassers, Auswirkungen der Landwirtschaft auf die Grundwasser- und Rohwasserbeschaffenheit und Maßnahmen zum Schutz des Grundwassers*. Vorträge des deutsch-französischen Kolloquiums am 6. Oktober 1988, Universitäten Stuttgart und Louis Pasteur Strasbourg (Vorträge in deutsch oder französisch, Kurzfassungen zweisprachig), 1988, ISBN 3-921694-71-X

72 Soyeaux, Renald: *Unterströmung von Stauanlagen auf klüftigem Untergrund unter Berücksichtigung laminarer und turbulenter Fließzustände*,1991, ISBN 3-921694-72-8

73 Kohane, Roberto: *Berechnungsmethoden für Hochwasserabfluß in Fließgewässern mit überströmten Vorländern*, 1991, ISBN 3-921694-73-6

74 Hassinger, Reinhard: *Beitrag zur Hydraulik und Bemessung von Blocksteinrampen in flexibler Bauweise*, 1991, ISBN 3-921694-74-4, vergriffen

75 Schäfer, Gerhard: *Einfluß von Schichtenstrukturen und lokalen Einlagerungen auf die Längsdispersion in Porengrundwasserleitern*, 1991, ISBN 3-921694-75-2

76 Giesecke, Jürgen: *Vorträge, Wasserwirtschaft in stark besiedelten Regionen; Umweltforschung mit Schwerpunkt Wasserwirtschaft*, 1991, ISBN 3-921694-76-0

77 Huwe, Bernd: *Deterministische und stochastische Ansätze zur Modellierung des Stickstoffhaushalts landwirtschaftlich genutzter Flächen auf unterschiedlichem Skalenniveau*, 1992, ISBN 3-921694-77-9, vergriffen

78 Rommel, Michael: *Verwendung von Kluftdaten zur realitätsnahen Generierung von Kluftnetzen mit anschließender laminar-turbulenter Strömungsberechnung*, 1993, ISBN 3-92 1694-78-7

79 Marschall, Paul: *Die Ermittlung lokaler Stofffrachten im Grundwasser mit Hilfe von Einbohrloch-Meßverfahren*, 1993, ISBN 3-921694-79-5, vergriffen

80 Ptak, Thomas: *Stofftransport in heterogenen Porenaquiferen: Felduntersuchungen und stochastische Modellierung*, 1993, ISBN 3-921694-80-9, vergriffen

81 Haakh, Frieder: *Transientes Strömungsverhalten in Wirbelkammern,* 1993, ISBN 3-921694-81-7

82 Kobus, Helmut; Cirpka, Olaf; Barczewski, Baldur; Koschitzky, Hans-Peter: *Versucheinrichtung zur Grundwasser und Altlastensanierung VEGAS, Konzeption und Programmrahmen*, 1993, ISBN 3-921694-82-5

83 Zang, Weidong: *Optimaler Echtzeit-Betrieb eines Speichers mit aktueller Abflußregenerierung*, 1994, ISBN 3-921694-83-3, vergriffen

84 Franke, Hans-Jörg: *Stochastische Modellierung eines flächenhaften Stoffeintrages und Transports in Grundwasser am Beispiel der Pflanzenschutzmittelproblematik*, 1995, ISBN 3-921694-84-1

85 Lang, Ulrich: *Simulation regionaler Strömungs- und Transportvorgänge in Karstaquiferen mit Hilfe des Doppelkontinuum-Ansatzes: Methodenentwicklung und Parameteridentifikation*, 1995, ISBN 3-921694-85-X, vergriffen

86 Helmig, Rainer: *Einführung in die Numerischen Methoden der Hydromechanik*, 1996, ISBN 3-921694-86-8, vergriffen

87 Cirpka, Olaf: *CONTRACT: A Numerical Tool for Contaminant Transport and Chemical Transformations - Theory and Program Documentation* -, 1996, ISBN 3-921694-87-6

88 Haberlandt, Uwe: *Stochastische Synthese und Regionalisierung des Niederschlages für Schmutzfrachtberechnungen*, 1996, ISBN 3-921694-88-4

89 Croisé, Jean: *Extraktion von flüchtigen Chemikalien aus natürlichen Lockergesteinen mittels erzwungener Luftströmung*, 1996, ISBN 3-921694-89-2, vergriffen

90 Jorde, Klaus: *Ökologisch begründete, dynamische Mindestwasserregelungen bei Ausleitungskraftwerken*, 1997, ISBN 3-921694-90-6, vergriffen

91 Helmig, Rainer: *Gekoppelte Strömungs- und Transportprozesse im Untergrund - Ein Beitrag zur Hydrosystemmodellierung*-, 1998, ISBN 3-921694-91-4, vergriffen

92 Emmert, Martin: *Numerische Modellierung nichtisothermer Gas-Wasser Systeme in porösen Medien,* 1997, ISBN 3-921694-92-2

93 Kern, Ulrich: *Transport von Schweb- und Schadstoffen in staugeregelten Fließgewässern am Beispiel des Neckars*, 1997, ISBN 3-921694-93-0, vergriffen

94 Förster, Georg: *Druckstoßdämpfung durch große Luftblasen in Hochpunkten von Rohrleitungen 1997*, ISBN 3-921694-94-9

95 Cirpka, Olaf: *Numerische Methoden zur Simulation des reaktiven Mehrkomponententransports im Grundwasser*, 1997, ISBN 3-921694-95-7, vergriffen

96 Färber, Arne: *Wärmetransport in der ungesättigten Bodenzone: Entwicklung einer thermischen In-situ-Sanierungstechnologie*, 1997, ISBN 3-921694-96-5

97 Betz, Christoph: *Wasserdampfdestillation von Schadstoffen im porösen Medium: Entwicklung einer thermischen In-situ-Sanierungstechnologie*, 1998, ISBN 3-921694-97-3

98 Xu, Yichun: *Numerical Modeling of Suspended Sediment Transport in Rivers*, 1998, ISBN 3-921694-98-1, vergriffen

99 Wüst, Wolfgang: *Geochemische Untersuchungen zur Sanierung CKW-kontaminierter Aquifere mit Fe(0)-Reaktionswänden,* 2000, ISBN 3-933761-02-2

100 Sheta, Hussam: *Simulation von Mehrphasenvorgängen in porösen Medien unter Einbeziehung von Hysterese-Effekten*, 2000, ISBN 3-933761-03-4

101 Ayros, Edwin: *Regionalisierung extremer Abflüsse auf der Grundlage statistischer Verfahren*, 2000, ISBN 3-933761-04-2, vergriffen

102 Huber, Ralf: *Compositional Multiphase Flow and Transport in Heterogeneous Porous Media*, 2000, ISBN 3-933761-05-0

103 Braun, Christopherus: *Ein Upscaling-Verfahren für Mehrphasenströmungen in porösen Medien*, 2000, ISBN 3-933761-06-9

104 Hofmann, Bernd: *Entwicklung eines rechnergestützten Managementsystems zur Beurteilung von Grundwasserschadensfällen*, 2000, ISBN 3-933761-07-7

105 Class, Holger: *Theorie und numerische Modellierung nichtisothermer Mehrphasenprozesse in NAPL-kontaminierten porösen Medien,* 2001, ISBN 3-933761-08-5

106 Schmidt, Reinhard: *Wasserdampf- und Heißluftinjektion zur thermischen Sanierung kontaminierter Standorte*, 2001, ISBN 3-933761-09-3

107 Josef, Reinhold:, *Schadstoffextraktion mit hydraulischen Sanierungsverfahren unter Anwendung von grenzflächenaktiven Stoffen*, 2001, ISBN 3-933761-10-7

108 Schneider, Matthias: *Habitat- und Abflussmodellierung für Fließgewässer mit unscharfen Berechnungsansätzen*, 2001, ISBN 3-933761-11-5

109 Rathgeb, Andreas: *Hydrodynamische Bemessungsgrundlagen für Lockerdeckwerke an überströmbaren Erddämmen*, 2001, ISBN 3-933761-12-3

110 Lang, Stefan: *Parallele numerische Simulation instätionärer Probleme mit adaptiven Methoden auf unstrukturierten Gittern*, 2001, ISBN 3-933761-13-1

111 Appt, Jochen; Stumpp Simone: *Die Bodensee-Messkampagne 2001, IWS/CWR Lake Constance Measurement Program 2001*, 2002, ISBN 3-933761-14-X

112 Heimerl, Stephan: *Systematische Beurteilung von Wasserkraftprojekten,* 2002, ISBN 3-933761-15-8, vergriffen

113 Iqbal, Amin: *On the Management and Salinity Control of Drip Irrigation,* 2002, ISBN 3-933761-16-6

114 Silberhorn-Hemminger, Annette: *Modellierung von Kluftaquifersystemen: Geostatistische Analyse und deterministisch-stochastische Kluftgenerierung,* 2002, ISBN 3-933761-17-4

115 Winkler, Angela: *Prozesse des Wärme- und Stofftransports bei der In-situ-Sanierung mit festen Wärmequellen,* 2003, ISBN 3-933761-18-2

116 Marx, Walter: *Wasserkraft, Bewässerung, Umwelt - Planungs- und Bewertungsschwerpunkte der Wasserbewirtschaftung,* 2003, ISBN 3-933761-19-0

117 Hinkelmann, Reinhard: *Efficient Numerical Methods and Information-Processing Techniques in Environment Water,* 2003, ISBN 3-933761-20-4

118 Samaniego-Eguiguren, Luis Eduardo: *Hydrological Consequences of Land Use / Land Cover and Climatic Changes in Mesoscale Catchments*, 2003, ISBN 3-933761-21-2

119 Neunhäuserer, Lina: *Diskretisierungsansätze zur Modellierung von Strömungs- und Transportprozessen in geklüftet-porösen Medien*, 2003, ISBN 3-933761-22-0

120 Paul, Maren: *Simulation of Two-Phase Flow in Heterogeneous Poros Media with Adaptive Methods*, 2003, ISBN 3-933761-23-9

121 Ehret, Uwe: *Rainfall and Flood Nowcasting in Small Catchments using Weather Radar*, 2003, ISBN 3-933761-24-7

122 Haag, Ingo: *Der Sauerstoffhaushalt staugeregelter Flüsse am Beispiel des Neckars - Analysen, Experimente, Simulationen -,* 2003, ISBN 3-933761-25-5

123 Appt, Jochen: *Analysis of Basin-Scale Internal Waves in Upper Lake Constance,* 2003, ISBN 3-933761-26-3

124 Hrsg.: Schrenk, Volker; Batereau, Katrin; Barczewski, Baldur; Weber, Karolin und Koschitzky, Hans-Peter: *Symposium Ressource Fläche und VEGAS - Statuskolloquium 2003, 30. September und 1. Oktober 2003,* 2003, ISBN 3-933761-27-1

125 Omar Khalil Ouda: *Optimisation of Agricultural Water Use: A Decision Support System for the Gaza Strip,* 2003, ISBN 3-933761-28-0

126 Batereau, Katrin: *Sensorbasierte Bodenluftmessung zur Vor-Ort-Erkundung von Schadensherden im Untergrund*, 2004, ISBN 3-933761-29-8

127 Witt, Oliver: *Erosionsstabilität von Gewässersedimenten mit Auswirkung auf den Stofftransport bei Hochwasser am Beispiel ausgewählter Stauhaltungen des Oberrheins*, 2004, ISBN 3-933761-30-1

128 Jakobs, Hartmut: *Simulation nicht-isothermer Gas-Wasser-Prozesse in komplexen Kluft-Matrix-Systemen*, 2004, ISBN 3-933761-31-X

129 Li, Chen-Chien: *Deterministisch-stochastisches Berechnungskonzept zur Beurteilung der Auswirkungen erosiver Hochwasserereignisse in Flussstauhaltungen,* 2004, ISBN 3-933761-32-8

130 Reichenberger, Volker; Helmig, Rainer; Jakobs, Hartmut; Bastian, Peter; Niessner, Jennifer: *Complex Gas-Water Processes in Discrete Fracture-Matrix Systems: Upscaling, Mass-Conservative Discretization and Efficient Multilevel Solution,* 2004, ISBN 3-933761-33-6

131 Hrsg.: Barczewski, Baldur; Koschitzky, Hans-Peter; Weber, Karolin; Wege, Ralf: *VEGAS - Statuskolloquium 2004,* Tagungsband zur Veranstaltung am 05. Oktober 2004 an der Universität Stuttgart, Campus Stuttgart-Vaihingen, 2004, ISBN 3-933761-34-4

132 Asie, Kemal Jabir: *Finite Volume Models for Multiphase Multicomponent Flow through Porous Media*. 2005, ISBN 3-933761-35-2

133 Jacoub, George: *Development of a 2-D Numerical Module for Particulate Contaminant Transport in Flood Retention Reservoirs and Impounded Rivers,* 2004, ISBN 3-933761-36-0

134 Nowak, Wolfgang: *Geostatistical Methods for the Identification of Flow and Transport Parameters in the Subsurface,* 2005, ISBN 3-933761-37-9

135 Süß, Mia: *Analysis of the influence of structures and boundaries on flow and transport processes in fractured porous media*, 2005, ISBN 3-933761-38-7

136 Jose, Surabhin Chackiath: *Experimental Investigations on Longitudinal Dispersive Mixing in Heterogeneous Aquifers,* 2005, ISBN: 3-933761-39-5

137 Filiz, Fulya: *Linking Large-Scale Meteorological Conditions to Floods in Mesoscale Catchments,* 2005, ISBN 3-933761-40-9

138 Qin, Minghao: *Wirklichkeitsnahe und recheneffiziente Ermittlung von Temperatur und Spannungen bei großen RCC-Staumauern*, 2005, ISBN 3-933761-41-7

139 Kobayashi, Kenichiro: *Optimization Methods for Multiphase Systems in the Subsurface - Application to Methane Migration in Coal Mining Areas*, 2005, ISBN 3-933761-42-5

140 Rahman, Md. Arifur: *Experimental Investigations on Transverse Dispersive Mixing in Heterogeneous Porous Media,* 2005, ISBN 3-933761-43-3

141 Schrenk, Volker: *Ökobilanzen zur Bewertung von Altlastensanierungsmaßnahmen,* 2005, ISBN 3-933761-44-1

142 Hundecha, Hirpa Yeshewatesfa: *Regionalization of Parameters of a Conceptual Rainfall-Runoff Model*, 2005, ISBN: 3-933761-45-X

143 Wege, Ralf: *Untersuchungs- und Überwachungsmethoden für die Beurteilung natürlicher Selbstreinigungsprozesse im Grundwasser,* 2005, ISBN 3-933761-46-8

144 Breiting, Thomas: *Techniken und Methoden der Hydroinformatik - Modellierung von komplexen Hydrosystemen im Untergrund*, 2006, 3-933761-47-6

145 Hrsg.: Braun, Jürgen; Koschitzky, Hans-Peter; Müller, Martin: *Ressource Untergrund: 10 Jahre VEGAS: Forschung und Technologieentwicklung zum Schutz von Grundwasser und Boden,* Tagungsband zur Veranstaltung am 28. und 29. September 2005 an der Universität Stuttgart, Campus Stuttgart-Vaihingen, 2005, ISBN 3-933761-48-4

146 Rojanschi, Vlad: *Abflusskonzentration in mesoskaligen Einzugsgebieten unter Berücksichtigung des Sickerraumes,* 2006, ISBN 3-933761-49-2

147 Winkler, Nina Simone: *Optimierung der Steuerung von Hochwasserrückhaltebecken-systemen,* 2006, ISBN 3-933761-50-6

148 Wolf, Jens: *Räumlich differenzierte Modellierung der Grundwasserströmung alluvialer Aquifere für mesoskalige Einzugsgebiete*, 2006, ISBN: 3-933761-51-4

149 Kohler, Beate: *Externe Effekte der Laufwasserkraftnutzung*, 2006, ISBN 3-933761-52-2

150 Hrsg.: Braun, Jürgen; Koschitzky, Hans-Peter; Stuhrmann, Matthias: *VEGAS-Statuskolloquium 2006,* Tagungsband zur Veranstaltung am 28. September 2006 an der Universität Stuttgart, Campus Stuttgart-Vaihingen, 2006, ISBN 3-933761-53-0

151 Niessner, Jennifer: *Multi-Scale Modeling of Multi-Phase - Multi-Component Processes in Heterogeneous Porous Media*, 2006, ISBN 3-933761-54-9

152 Fischer, Markus: *Beanspruchung eingeerdeter Rohrleitungen infolge Austrocknung bindiger Böden,* 2006, ISBN 3-933761-55-7

153 Schneck, Alexander: *Optimierung der Grundwasserbewirtschaftung unter Berücksichtigung der Belange der Wasserversorgung, der Landwirtschaft und des Naturschutzes*, 2006, ISBN 3-933761-56-5

154 Das, Tapash: *The Impact of Spatial Variability of Precipitation on the Predictive Uncertainty of Hydrological Models,* 2006, ISBN 3-933761-57-3

155 Bielinski, Andreas: *Numerical Simulation of CO_2 sequestration in geological formations*, 2007, ISBN 3-933761-58-1

156 Mödinger, Jens: *Entwicklung eines Bewertungs- und Entscheidungsunterstützungssystems für eine nachhaltige regionale Grundwasserbewirtschaftung*, 2006, ISBN 3-933761-60-3

157 Manthey, Sabine: *Two-phase flow processes with dynamic effects in porous media - parameter estimation and simulation,* 2007, ISBN 3-933761-61-1

158 Pozos Estrada, Oscar: *Investigation on the Effects of Entrained Air in Pipelines,* 2007, ISBN 3-933761-62-X

159 Ochs, Steffen Oliver: *Steam injection into saturated porous media – process analysis including experimental and numerical investigations*, 2007, ISBN 3-933761-63-8

160 Marx, Andreas: *Einsatz gekoppelter Modelle und Wetterradar zur Abschätzung von Niederschlagsintensitäten und zur Abflussvorhersage, 2007,* ISBN 3-933761-64-6

161 Hartmann, Gabriele Maria: *Investigation of Evapotranspiration Concepts in Hydrological Modelling for Climate Change Impact Assessment*, 2007, ISBN 3-933761-65-4

162 Kebede Gurmessa, Tesfaye: *Numerical Investigation on Flow and Transport Characteristics to Improve Long-Term Simulation of Reservoir Sedimentation*, 2007, ISBN 3-933761-66-2

163 Trifković, Aleksandar: *Multi-objective and Risk-based Modelling Methodology for Planning, Design and Operation of Water Supply Systems*, 2007, ISBN 3-933761-67-0

164 Götzinger, Jens: *Distributed Conceptual Hydrological Modelling - Simulation of Climate, Land Use Change Impact and Uncertainty Analysis*, 2007, ISBN 3-933761-68-9

165 Hrsg.: Braun, Jürgen; Koschitzky, Hans-Peter; Stuhrmann, Matthias: *VEGAS – Kolloquium 2007,* Tagungsband zur Veranstaltung am 26. September 2007 an der Universität Stuttgart, Campus Stuttgart-Vaihingen, 2007, ISBN 3-933761-69-7

166 Freeman, Beau: *Modernization Criteria Assessment for Water Resources Planning; Klamath Irrigation Project, U.S.*, 2008, ISBN 3-933761-70-0

167 Dreher, Thomas: *Selektive Sedimentation von Feinstschwebstoffen in Wechselwirkung mit wandnahen turbulenten Strömungsbedingungen*, 2008, ISBN 3-933761-71-9

168 Yang, Wei: *Discrete-Continuous Downscaling Model for Generating Daily Precipitation Time Series*, 2008, ISBN 3-933761-72-7

169 Kopecki, Ianina: *Calculational Approach to FST-Hemispheres for Multiparametrical Benthos Habitat Modelling,* 2008*,* ISBN 3-933761-73-5

170 Brommundt, Jürgen: *Stochastische Generierung räumlich zusammenhängender Niederschlagszeitreihen*, 2008, ISBN 3-933761-74-3

171 Papafotiou, *Alexandros: Numerical Investigations of the Role of Hysteresis in Heterogeneous Two-Phase Flow Systems*, 2008, ISBN 3-933761-75-1

172 He, Yi: *Application of a Non-Parametric Classification Scheme to Catchment Hydrology*, 2008, ISBN 978-3-933761-76-7

173 Wagner, Sven: *Water Balance in a Poorly Gauged Basin in West Africa Using Atmospheric Modelling and Remote Sensing Information*, 2008, ISBN 978-3-933761-77-4

174 Hrsg.: Braun, Jürgen; Koschitzky, Hans-Peter; Stuhrmann, Matthias; Schrenk, Volker: *VEGAS-Kolloquium 2008 Ressource Fläche III*, Tagungsband zur Veranstaltung am 01. Oktober 2008 an der Universität Stuttgart, Campus Stuttgart-Vaihingen, 2008, ISBN 978-3-933761-78-1

175 Patil, Sachin: *Regionalization of an Event Based Nash Cascade Model for Flood Predictions in Ungauged Basins*, 2008, ISBN 978-3-933761-79-8

176 Assteerawatt, Anongnart: *Flow and Transport Modelling of Fractured Aquifers based on a Geostatistical Approach,* 2008, ISBN 978-3-933761-80-4

177 Karnahl, Joachim Alexander: *2D numerische Modellierung von multifraktionalem Schwebstoff- und Schadstofftransport in Flüssen*, 2008, ISBN 978-3-933761-81-1

178 Hiester, Uwe: *Technologieentwicklung zur In-situ-Sanierung der ungesättigten Bodenzone mit festen Wärmequellen,* 2009, ISBN 978-3-933761-82-8

179 Laux, Patrick: *Statistical Modeling of Precipitation for Agricultural Planning in the Volta Basin of West Africa,* 2009, ISBN 978-3-933761-83-5

180 Ehsan, Saqib: *Evaluation of Life Safety Risks Related to Severe Flooding,* 2009, ISBN 978-3-933761-84-2

181 Prohaska, Sandra: *Development and Application of a 1D Multi-Strip Fine Sediment Transport Model for Regulated Rivers,* 2009, ISBN 978-3-933761-85-9

182 Kopp, Andreas: *Evaluation of CO_2 Injection Processes in Geological Formations for Site Screening,* 2009, ISBN 978-3-933761-86-6

183 Ebigbo, Anozie: *Modelling of biofilm growth and its influence on CO_2 and water (two-phase) flow in porous media,* 2009, ISBN 978-3-933761-87-3

184 Freiboth, Sandra: *A phenomenological model for the numerical simulation of multiphase multicomponent processes considering structural alterations of porous media*, 2009, ISBN 978-3-933761-88-0

185 Zöllner, Frank: *Implementierung und Anwendung netzfreier Methoden im Konstruktiven Wasserbau und in der Hydromechanik*, 2009, ISBN 978-3-933761-89-7

186 Vasin, Milos: *Influence of the soil structure and property contrast on flow and transport in the unsaturated zone*, 2010, ISBN 978-3-933761-90-3

187 Li, Jing: *Application of Copulas as a New Geostatistical Tool*, 2010, ISBN 978-3-933761-91-0

188 AghaKouchak, Amir: *Simulation of Remotely Sensed Rainfall Fields Using Copulas*, 2010, ISBN 978-3-933761-92-7

189 Thapa, Pawan Kumar: *Physically-based spatially distributed rainfall runoff modelling for soil erosion estimation*, 2010, ISBN 978-3-933761-93-4

190 Wurms, Sven: *Numerische Modellierung der Sedimentationsprozesse in Retentionsanlagen zur Steuerung von Stoffströmen bei extremen Hochwasserabflussereignissen*, 2011, ISBN 978-3-933761-94-1

191 Merkel, Uwe: *Unsicherheitsanalyse hydraulischer Einwirkungen auf Hochwasserschutzdeiche und Steigerung der Leistungsfähigkeit durch adaptive Strömungsmodellierung*, 2011, ISBN 978-3-933761-95-8

192 Fritz, Jochen: *A Decoupled Model for Compositional Non-Isothermal Multiphase Flow in Porous Media and Multiphysics Approaches for Two-Phase Flow*, 2010, ISBN 978-3-933761-96-5

193 Weber, Karolin (Hrsg.): *12. Treffen junger WissenschaftlerInnen an Wasserbauinstituten*, 2010, ISBN 978-3-933761-97-2

194 Bliefernicht, Jan-Geert: *Probability Forecasts of Daily Areal Precipitation for Small River Basins,* 2011, ISBN 978-3-933761-98-9

195 Hrsg.: Koschitzky, Hans-Peter; Braun, Jürgen: *VEGAS-Kolloquium 2010 In-situ-Sanierung - Stand und Entwicklung Nano und ISCO -,* Tagungsband zur Veranstaltung am 07. Oktober 2010 an der Universität Stuttgart, Campus Stuttgart-Vaihingen*,* 2010*,* ISBN 978-3-933761-99-6

196 Gafurov, Abror: *Water Balance Modeling Using Remote Sensing Information - Focus on Central Asia,* 2010, ISBN 978-3-942036-00-9

197 Mackenberg, Sylvia: *Die Quellstärke in der Sickerwasserprognose: Möglichkeiten und Grenzen von Labor- und Freilanduntersuchungen,* 2010, ISBN 978-3-942036-01-6

198 Singh, Shailesh Kumar: *Robust Parameter Estimation in Gauged and Ungauged Basins,* 2010, ISBN 978-3-942036-02-3

199 Doğan, Mehmet Onur: *Coupling of porous media flow with pipe flow,* 2011, ISBN 978-3-942036-03-0

200 Liu, Min: *Study of Topographic Effects on Hydrological Patterns and the Implication on Hydrological Modeling and Data Interpolation,* 2011, ISBN 978-3-942036-04-7

201 Geleta, Habtamu Itefa: *Watershed Sediment Yield Modeling for Data Scarce Areas,* 2011, ISBN 978-3-942036-05-4

202 Franke, Jörg: *Einfluss der Überwachung auf die Versagenswahrscheinlichkeit von Staustufen,* 2011, ISBN 978-3-942036-06-1

203 Bakimchandra, Oinam: *Integrated Fuzzy-GIS approach for assessing regional soil erosion risks,* 2011, ISBN 978-3-942036-07-8

204 Alam, Muhammad Mahboob: *Statistical Downscaling of Extremes of Precipitation in Mesoscale Catchments from Different RCMs and Their Effects on Local Hydrology,* 2011, ISBN 978-3-942036-08-5

205 Hrsg.: Koschitzky, Hans-Peter; Braun, Jürgen: *VEGAS-Kolloquium 2011 Flache Geothermie - Perspektiven und Risiken,* Tagungsband zur Veranstaltung am 06. Oktober 2011 an der Universität Stuttgart, Campus Stuttgart-Vaihingen, 2011, ISBN 978-3-933761-09-2

206 Haslauer, Claus: *Analysis of Real-World Spatial Dependence of Subsurface Hydraulic Properties Using Copulas with a Focus on Solute Transport Behaviour,* 2011, ISBN 978-3-942036-10-8

207 Dung, Nguyen Viet: *Multi-objective automatic calibration of hydrodynamic models – development of the concept and an application in the Mekong Delta,* 2011, ISBN 978-3-942036-11-5

208 Hung, Nguyen Nghia: *Sediment dynamics in the floodplain of the Mekong Delta, Vietnam,* 2011, ISBN 978-3-942036-12-2

209 Kuhlmann, Anna: *Influence of soil structure and root water uptake on flow in the unsaturated zone,* 2012, ISBN 978-3-942036-13-9

210 Tuhtan, Jeffrey Andrew: *Including the Second Law Inequality in Aquatic Ecodynamics: A Modeling Approach for Alpine Rivers Impacted by Hydropeaking,* 2012, ISBN 978-3-942036-14-6

211 Tolossa, Habtamu: *Sediment Transport Computation Using a Data-Driven Adaptive Neuro-Fuzzy Modelling Approach,* 2012, ISBN 978-3-942036-15-3

212 Tatomir, Alexandru-Bodgan: *From Discrete to Continuum Concepts of Flow in Fractured Porous Media,* 2012, ISBN 978-3-942036-16-0

213 Erbertseder, Karin: *A Multi-Scale Model for Describing Cancer-Therapeutic Transport in the Human Lung,* 2012, ISBN 978-3-942036-17-7

214 Noack, Markus: *Modelling Approach for Interstitial Sediment Dynamics and Reproduction of Gravel Spawning Fish,* 2012, ISBN 978-3-942036-18-4

215 De Boer, Cjestmir Volkert: *Transport of Nano Sized Zero Valent Iron Colloids during Injection into the Subsurface*, 2012, ISBN 978-3-942036-19-1

216 Pfaff, Thomas: *Processing and Analysis of Weather Radar Data for Use in Hydrology*, 2013, ISBN 978-3-942036-20-7

217 Lebrenz, Hans-Henning: *Addressing the Input Uncertainty for Hydrological Modeling by a New Geostatistical Method*, 2013, ISBN 978-3-942036-21-4

218 Darcis, Melanie Yvonne: *Coupling Models of Different Complexity for the Simulation of CO_2 Storage in Deep Saline Aquifers*, 2013, ISBN 978-3-942036-22-1

219 Beck, Ferdinand: *Generation of Spatially Correlated Synthetic Rainfall Time Series in High Temporal Resolution - A Data Driven Approach*, 2013, ISBN 978-3-942036-23-8

220 Guthke, Philipp: *Non-multi-Gaussian spatial structures: Process-driven natural genesis, manifestation, modeling approaches, and influences on dependent processes*, 2013, ISBN 978-3-942036-24-5

221 Walter, Lena: *Uncertainty studies and risk assessment for CO_2 storage in geological formations*, 2013, ISBN 978-3-942036-25-2

222 Wolff, Markus: *Multi-scale modeling of two-phase flow in porous media including capillary pressure effects,* 2013, ISBN 978-3-942036-26-9

223 Mosthaf, Klaus Roland: *Modeling and analysis of coupled porous-medium and free flow with application to evaporation processes,* 2014, ISBN 978-3-942036-27-6

224 Leube, Philipp Christoph: *Methods for Physically-Based Model Reduction in Time: Analysis, Comparison of Methods and Application*, 2013, ISBN 978-3-942036-28-3

225 Rodríguez Fernández, Jhan Ignacio: *High Order Interactions among environmental variables: Diagnostics and initial steps towards modeling*, 2013, ISBN 978-3-942036-29-0

226 Eder, Maria Magdalena: *Climate Sensitivity of a Large Lake*, 2013, ISBN 978-3-942036-30-6

227 Greiner, Philipp: *Alkoholinjektion zur In-situ-Sanierung von CKW Schadensherden in Grundwasserleitern: Charakterisierung der relevanten Prozesse auf unterschiedlichen Skalen*, 2014, ISBN 978-3-942036-31-3

228 Lauser, Andreas: *Theory and Numerical Applications of Compositional Multi-Phase Flow in Porous Media*, 2014, ISBN 978-3-942036-32-0

229 Enzenhöfer, Rainer: *Risk Quantification and Management in Water Production and Supply Systems*, 2014, ISBN 978-3-942036-33-7

230 Faigle, Benjamin: *Adaptive modelling of compositional multi-phase flow with capillary pressure*, 2014, ISBN 978-3-942036-34-4

231 Oladyshkin, Sergey: *Efficient modeling of environmental systems in the face of complexity and uncertainty*, 2014, ISBN 978-3-942036-35-1

232 Sugimoto, Takayuki: *Copula based Stochastic Analysis of Discharge Time Series*, 2014, ISBN 978-3-942036-36-8

233 Koch, Jonas: *Simulation, Identification and Characterization of Contaminant Source Architectures in the Subsurface*, 2014, ISBN 978-3-942036-37-5

234 Zhang, Jin: *Investigations on Urban River Regulation and Ecological Rehabilitation Measures, Case of Shenzhen in China*, 2014, ISBN 978-3-942036-38-2

235 Siebel, Rüdiger: *Experimentelle Untersuchungen zur hydrodynamischen Belastung und Standsicherheit von Deckwerken an überströmbaren Erddämmen,* 2014, ISBN 978-3-942036-39-9

236 Baber, Katherina: *Coupling free flow and flow in porous media in biological and technical applications: From a simple to a complex interface description,* 2014, ISBN 978-3-942036-40-5

237 Nuske, Klaus Philipp: *Beyond Local Equilibrium — Relaxing local equilibrium assumptions in multiphase flow in porous media,* 2014, ISBN 978-3-942036-41-2

238 Geiges, Andreas: *Efficient concepts for optimal experimental design in nonlinear environmental systems*, 2014, ISBN 978-3-942036-42-9

239 Schwenck, Nicolas: *An XFEM-Based Model for Fluid Flow in Fractured Porous Media*, 2014, ISBN 978-3-942036-43-6

240 Chamorro Chávez, Alejandro: *Stochastic and hydrological modelling for climate change prediction in the Lima region, Peru*, 2015, ISBN 978-3-942036-44-3

241 Yulizar: *Investigation of Changes in Hydro-Meteorological Time Series Using a Depth-Based Approach*, 2015, ISBN 978-3-942036-45-0

242 Kretschmer, Nicole: *Impacts of the existing water allocation scheme on the Limarí watershed – Chile, an integrative approach*, 2015, ISBN 978-3-942036-46-7

243 Kramer, Matthias: *Luftbedarf von Freistrahlturbinen im Gegendruckbetrieb*, 2015, ISBN 978-3-942036-47-4

244 Hommel, Johannes: *Modeling biogeochemical and mass transport processes in the subsurface: Investigation of microbially induced calcite precipitation*, 2016, ISBN 978-3-942036-48-1

245 Germer, Kai: *Wasserinfiltration in die ungesättigte Zone eines makroporösen Hanges und deren Einfluss auf die Hangstabilität*, 2016, ISBN 978-3-942036-49-8

246 Hörning, Sebastian: *Process-oriented modeling of spatial random fields using copulas*, 2016, ISBN 978-3-942036-50-4

247 Jambhekar, Vishal: *Numerical modeling and analysis of evaporative salinization in a coupled free-flow porous-media system, 2016, ISBN* 978-3-942036-51-1

248 Huang, Yingchun: *Study on the spatial and temporal transferability of conceptual hydrological models*, 2016, ISBN 978-3-942036-52-8

249 Kleinknecht, Simon Matthias: *Migration and retention of a heavy NAPL vapor and remediation of the unsaturated zone*, 2016, ISBN 978-3-942036-53-5

Die Mitteilungshefte ab der Nr. 134 (Jg. 2005) stehen als pdf-Datei über die Homepage des Instituts: www.iws.uni-stuttgart.de zur Verfügung.